UTS UNIVERSITY OF TECHNOLOGY SYDNEY

DISTRIBUTED COOPERATIVE CONTROL FOR AUTONOMOUS MICROGRIDS

by Mahmuda Begum

Thesis submitted in fulfilment of the requirements for the degree of

Doctor of Philosophy

under the supervision of A/Prof. Li Li (Principal Supervisor) and Prof. Jianguo Zhu (Co-Supervisor)

University of Technology Sydney
Faculty of Engineering and IT

August 2021

Certificate of Original Authorship

I, *Mahmuda Begum* declare that this thesis, is submitted in fulfilment of the requirements for the award of *Doctor of Philosophy*, in the *Faculty of Engineering and IT* at the University of Technology Sydney.

This thesis is wholly my own work unless otherwise referenced or acknowledged. In addition, I certify that all information sources and literature used are indicated in the thesis.

This document has not been submitted for qualifications at any other academic institution.

This research is supported by the Australian Government Research Training Program.

Production Note:
Signature removed prior to publication.

Signature of Student:

Date: 15/08/2021

Keywords

Active Power Sharing, Autonomous Microgrid, Consensus Control, Cost Function, Distributed Control, Eigenvalue Analysis, Frequency Restoration, Fuzzy-Control, Hierarchical Control, Microgrid Control, Particle Swarm Optimisation, Reactive Power Sharing, Secondary Control, Small-Signal Model, Stability Analysis, Voltage Restoration, SoC Balancing, Power Sharing, Secondary Control.

Abstract

Distributed control for microgrids (MGs) is the current development due to its numerous benefits compared to traditional central control systems, such as system reliability, reducing its sensitivity to failures, and eliminating the requirement for central computing and communication structure. Although many research works have been accomplished on the design of MG control, distributed secondary control (DSC) needs more attention. There is still a lack of appropriate DSC design for islanded AC MGs which can restore the frequency and voltage along with precise power-sharing with detailed stability analysis. Another concern is the simplicity of DSC system design. Moreover, very little research addressed the DSC for distributed energy storage units (DESUs) for MGs considering state of charge (SoC) balancing along with frequency and voltage restoration with precise power-sharing.

This thesis proposes MG control that addresses frequency and voltage restoration with precise power-sharing, and optimises the control parameters by utilising intelligent controller and SoC balancing for DESUs in a single control strategy with detailed stability analysis. The significant contributions of this thesis are to: (1) design a DSC for MGs which covers all the control aspects in a single control strategy; (2) model the MGs for the proposed DSC in a systematic way and perform a detailed stability analysis; (3) verify the presented control with several case studies; (4) consider SoC balancing along with other control aspects in designing DSC for DESUs; (5) propose intelligent control methods to find the optimal control parameters for stability enhancement of MGs and verify their effectiveness with different case studies.

Firstly, a novel DSC with an incremental cost-based droop controller is proposed. The parameters of the proposed DSC are designed utilising the particle swarm optimization (PSO) method. A linearised small-signal state-space model considering DSC with stability studies of an islanded AC MG is also presented. The dynamic response of DSC initiates additional oscillatory modes, which affects the damping performance of the system. To enhance the system stability with DSC, a fuzzy logic based intelligent controller is also offered for tuning the secondary control parameters for the best functioning of the offered DSC. This research also introduces a new DSC system for DESUs in an islanded AC MG. By applying the suggested methodology, all the DESUs achieve exactly the same SoC with the power proportional to their capacity at the steady state, and hence the uneven degradation of DESUs is avoided.

Acknowledgement

Firstly, thanks to my Almighty lord Allah, for giving me his blessing to finish this thesis. I would like to express my sincere gratitude to my principal supervisor, A/Prof. Li Li, for giving me the opportunity to do the research. It would not have been possible to finish this thesis without his inspiration, direction and constant support throughout my entire research period. I am tremendously thankful to him for doing my PhD under his supervision and sharing his opinions and advice during my PhD study. His patience, understanding, experience and vision continuously encouraged me to follow the exact track. I would also like to thank my research co-supervisor, Prof. Jianguo Zhu, for his supervision, understanding, patience as well as support during my study.

I would also like to give my acknowledgement to the University of Technology Sydney (UTS) for the financial support by providing me the UTS FEIT Strategic Scholarship (PhD Scholarship for research study). I would also like to thank all the staff from IT, UTS, who have always been helpful in providing in installing or updating software and any other associated technical issues. I am thankful to all my colleagues at UTS for their support and discussion at times during my research.

Finally, I would like to thank all my family members, especially my parents, for their love, endless motivation and support in every aspect. I am also grateful to my husband, Md Eusuf Iqbal for his care, understanding and constant support throughout my PhD tenure. Last but not least, thanks to my little daughter, Ishya Iqbal who has brought limitless joy and happiness to me.

Table of Contents

List of Figures

List of Tables

List of Abbreviations

AC-Alternating Current

ADM-Active Demand Management

DC-Direct Current

DER-Distributed Energy Resources

DG-Distributed Generation

DQ-Direct Quadrature

DSC-Distributed Secondary Controller

DSFC-Distributed Secondary Frequency Controller

DSM-Demand Side Management

DSVC-Distributed Secondary Voltage Controller

ED-Economic Dispatch

EES-Electrical Energy Storage

GPS-Global Positioning Control

ILC-Interlinking Converter

LC-Inductor-Capacitor

LCL-Inductor-Capacitor-Inductor

(*P-f*) Droop-(Active Power-Frequency) Droop

PI-Proportional-Integral

PV- Photovoltaic

PCC-Point of Common Coupling

PSO-Particle Swarm Optimisation

PWM-Pulse Width Modulation

RL-Resistor-Inductor

RC-Resistor-Capacitor

RLC-Resistor-Inductor-Capacitor

MAS-Multi-Agent System

MATLAB-Matrix Laboratory

MG-Microgrid

MCC-Microgrid Central Controller

MPC-Model Predictive Control

SoC- State of Charge

(Q-v) Droop- (Reactive Power-Voltage) Droop

VSI-Voltage Source Inverter

List of Publications

Journal Papers:

1. **Begum, M.,** Li, L. & Zhu, J. 2021, 'Fuzzy-Based Distributed Cooperative Secondary Control with Stability Analysis for Microgrids', *Electronics, vol 10, issue 4.*

Conference Papers:

2. **Begum, M.**, Li, L. & Zhu, J. 2020, 'Distributed Secondary Control of Energy Storage Units for SoC balancing in AC Microgrid', *IEEE Innovative Smart Grid Technologies (ISGT-North America)*, Washington DC, USA.

3. **Begum, M.**, Li, L. & Zhu, J. 2019, 'PSO-based Secondary Frequency Control and Active Power Sharing', *IEEE Innovative Smart Grid Technologies (ISGT-Asia)*, Chengdu, China.

4. **Begum, M.**, Li, L. & Zhu, J. 2018, 'State-Space Modelling and Stability Analysis for Microgrids with Distributed Secondary Control'-, *The 27th IEEE International Symposium on Industrial Electronics (ISIE)*, Cairns, Australia.

5. **Begum, M.**, Li, L. & Zhu, J. 2017, 'Distributed Control Techniques for Autonomous AC Microgrids-A brief Review', *The 5th International Conference on IEEE Region 10 Humanitarian Technology Conference (R10HTC)*, Dhaka, Bangladesh.

6. **Begum, M.**, Li, L. & Zhu, J. 2017, 'Distributed Secondary Voltage Regulation for Autonomous Microgrid', *20th IEEE International Conference on Electrical Machines and Systems (ICEMS)*, Sydney, Australia.

7. Abuhilaleh, M., Li, L. & Zhu, J., **Begum, M.** 2017, 'Power Management and Control Strategy for Hybrid AC/DC Microgrids in Autonomous Operation Mode', *20th IEEE International Conference on Electrical Machines and Systems (ICEMS)*, Sydney, Australia.

Chapter 1: Introduction

1.1 BACKGROUND

1.1.1 Renewable Energy Resources into Power System

In recent years, the fast development of countries has greatly stimulated the electricity demand. Traditional energy resources like coal, diesel, gas, etc., are unable to fulfil the power demands. Also, fossil fuels have destructive effects on the environment. As a result, researchers/experts are seeking the best way to convert the existing conventional energy resources-based power system to renewable-energy-based systems to supply the energy demands. Therefore, the integration and acceptance of renewable energy resources (RERs) is growing. To integrate the RERs into the power networks successfully, more and more advanced technologies need to be developed and investigated [1].

Fig.1.1 depicts the percentage of power generation by several RERs in 2021 by International Renewable Energy Agency (ARENA), Australia [2]. Fig. 1.2 represents the renewable power capacity growth, and Fig. 1.3 shows the renewable share of annual power capacity expansion respectively. From these graphical representations, it can be seen that the global renewable generation capacity was increased to 2799 GW at the end of 2020. According to the statistics shown in Fig. 1.1, hydropower shared the largest amount of the global total, with a capacity of 1211 GW. Wind and solar energy accounted for the same shares of the remainder, with capacities of 733 GW and 714 GW, respectively. Other renewables comprised 127 GW of bioenergy and 14 GW of geothermal, plus 500 MW of marine energy.

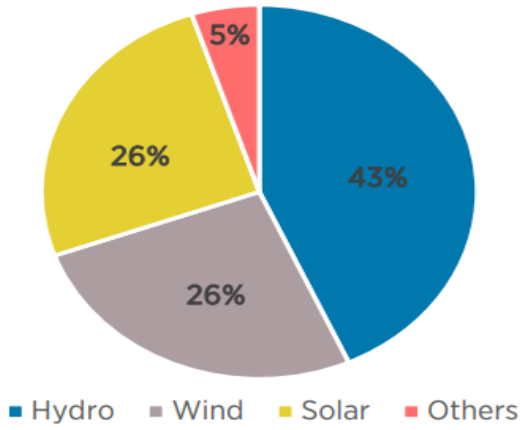

Fig. 1.1 Renewable generation capacity by energy source [2]

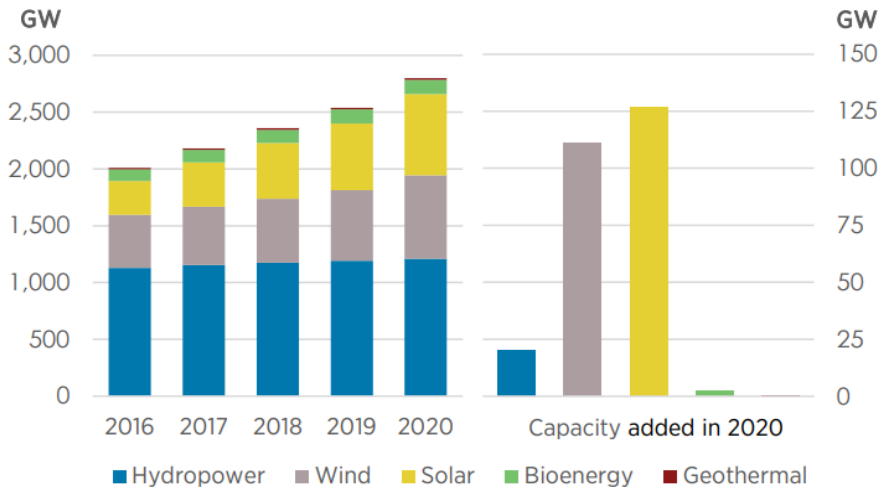

Fig. 1.2 Renewable power capacity growth [2]

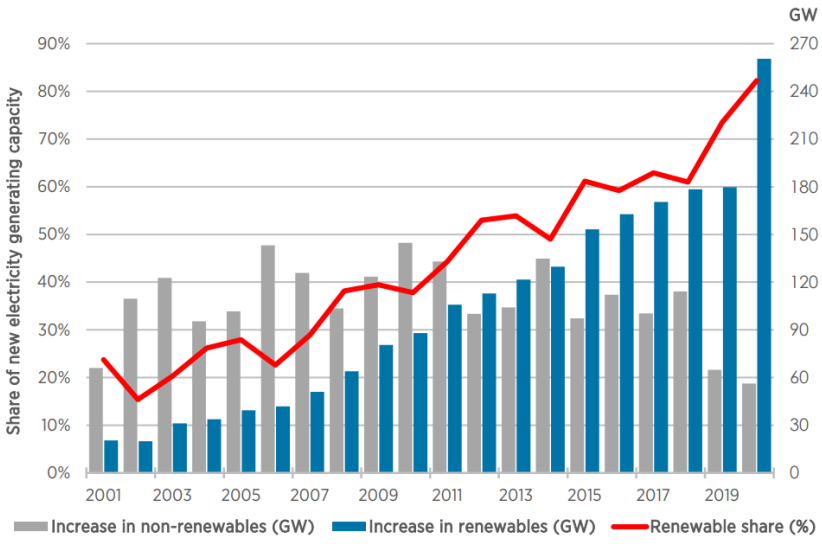

Fig. 1.3 Renewable share of annual power capacity expansion [2]

From the statistics mentioned above, it can be declared that solar and wind energy continued to lead the renewable capacity expansion, jointly accounting for 91% of all net renewable additions in 2020. Along with the resumed development of hydropower, this remarkable evolution in wind and solar led to the highest annual growth in renewable generating capacity ever seen.

1.1.2 Microgrid Concept

Electric Power Systems (EPS) have been designed as one-way power flow systems with centralised generation sources, long-distance transmission systems, distribution systems and power demand. Centralised power generation, power flow in a one-way direction, passive nature of electricity distribution network as well as demand-driven operation are thoughts originated more than a century old [3]. However, traditional ways for one-way power flow analysis will soon be inefficient in controlling renewable generations integrated into the network; innovative control approaches are necessary to assist the bidirectional power flow incurred by the power generation of the distributed energy resource (DER) units. The transition of energy networks from centralised to

decentralised generation will necessitate intelligent distribution automation using decentralised/distributed control techniques to actualize smart grid modernization. In the past decades, contemporary solutions, namely distributed generation (DG), predominantly in accordance with renewable energies, distributed energy storage units (DESUs), resilient Alternating Current (AC) transmission structures, active demand management (ADM), microgrids (MGs) networks, and smart control and management as control of information and communication technologies (ICTs), have prepared it likely to design new prospects for traditional power systems. Therefore, thorough research works should still be performed to build such advanced systems a reality today.

The idea of MG has been developed, seeing an effective resolution in the new decentralised paradigm of power systems for the local management of generation and demand in sub-sections of the network. MGs have been employed globally to develop the reliability as well as resiliency of networks, facilitate the integration of renewable resources, defer network investments, and meet the wide-ranging needs of different communities from large metropolitan areas to rural and remote regions. MGs offer a flexible structure allowing to incorporate various technologies, accommodate a wide selection of architectures, and be used for different applications [4]. In general, MG comprises various DGs commonly interfaced to the grid via power electronics inverters. One of the attractive features of MG is the capability of working in both grid-connected and islanded operating modes. For the islanding operation of AC MGs, two important tasks are sharing load demand amongst multiple parallel-connected inverters proportionally in addition to maintaining the voltage and frequency stabilities. Appropriate regulation of internal components is essential for an MG to gain such functionality. These requirements introduce a hierarchical control structure [5] to reduce the complex control structure of MG and address individual requirements at every control level. In MGs, the hierarchical control structure comprises primary, secondary, and tertiary layers. MGs are becoming a key idea for the integration of DGs [3, 4, 6, 7]. The need for small-scale power generation and local control has been distinguished from different viewpoints. Development of the technical action of an MG is done in the following aspects.

- Power loss reduction of power lines.
- Synchronisation of reactive power control along with controlled active power dispatch to improve the voltage regulation.
- Release of peak loading of constrained network devices over specific scheduling of adjacent DG outputs.
- Improvement of supply reliability through partial or full islanding throughout loss of main grid.
- Smaller architectures to reduce the construction times and lower investment costs.

1.1.3 MG Structure and Challenges

A. General MG Structure

MG has different structures depending on how the AC and direct current (DC) sources are connected to the loads and the grid. There are three main structures [8-10], (a) the DC MG, (b) the AC MG, (c) the hybrid AC/DC MG, where some of the DGs and DESUs are linked to a DC bus and others linked to an AC bus. In the hybrid AC/DC MG, these DC and AC buses are linked by interlinking converters (ILCs) to transfer power from one sub-grid to another. While conventional AC systems are still the prevalent choice for most MG projects, the specific characteristics of MGs make them an attractive option for DC reticulation. Since most DERs (such as batteries, PV panels, and fuel cells) and many loads (including electronic devices, electric vehicles, washers,

dryers and air-conditioning systems equipped with variable speed drives) operate with DC voltage, the required AC-DC and DC-AC stages can sum up to losses of between 5% and 15% of generated electricity [11]. These losses can be largely mitigated by using DC reticulation. In addition, DC systems do not have reactive power control, power factor correction and synchronisation issues associated with AC control and reticulation making their overall control and operation simpler. Conversely, the complexity of protection systems, the lack of zero crossing (current zero) point during the breaker operation, grounding and corrosion issues are the main drawbacks of DC systems [9]. In addition, new standards dealing with DC systems and DC equipment are needed.

B. Inverter-Based MG Structure

The majority of existing grid networks and loads are in the form of AC due to historical reasons, and AC voltage levels can be efficiently stepped up and stepped down by a transformer [7]. As part of the distribution system, AC MGs interface with the utility grid at the point of common coupling (PCC) with the ability to switch between the grid-connected and islanded modes. DC DGs such as photovoltaic (PV) generators require DC-AC converters linked to an AC bus. Generally, a voltage source inverter (VSI) - based DG unit contains a DC/AC inverter bridge, a primary DC power supply, an inductor-capacitor (LC) filter and a resistor-inductor (RL) at output connection [3], as represented in Fig.1.4. AC MG is probably the most common form of the existing MGs because of its advantageous features, such as easy-to-integrate with existing power systems and load.

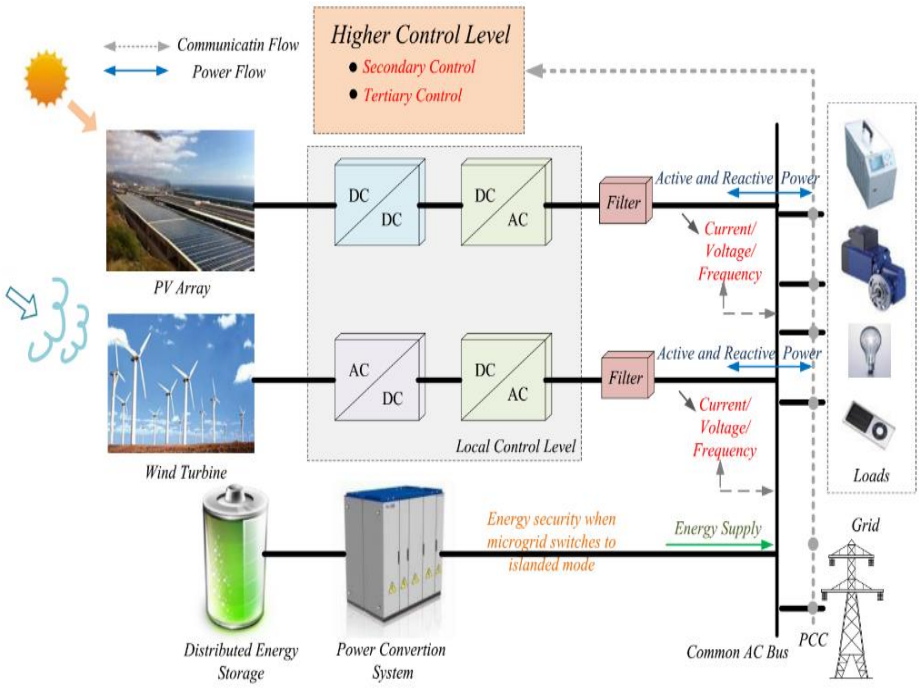

Fig. 1.4 A simple form of AC MG structure

C. Mode of Operation

Two operational modes of MG are as below:

1. Grid-connected mode [12] or
2. Autonomous mode [13, 14]

In the grid-connected mode, the main grid maintains the frequency and voltage, whereas DG units deliver the power to the entire load or part of it. For that, it acts as a regulated load or power supply through either receiving power from or delivering power to the main grid based on the overall generation and overall load in the MG. In the autonomous mode, DG units control the frequency and voltage while sharing the total active and reactive power of the loads. An MG sometimes separates all DG units on purpose and runs in the autonomous mode during the fault conditions of the main grid. This mode of operation is also beneficial even when the overall generation of DG units is not adequate, and they can be isolated without major effect on the system by using appropriate control strategies. The grid-connected MG is believed to be more reliable, but the standalone microgrid can be more sustainable and environmentally friendly. With an appropriate design of the control system, standalone MG can have better reliability and be a viable option for sustainability [15-17]. However, it is very difficult to control the power of integrated multiple DG sources within the MG [18].

D. MG Control

MG control is always challenging due to the diverse technologies, architectures, and operational modes. Advanced control strategies are necessary for converters interfaced with DERs and MGs to control the output voltage and current to achieve the desired active and reactive power set points. If the MG is connected to a strong distribution network, the voltage and frequency will generally have only small variations and MG stability is maintained by the main distribution network. In this case, converters act as "grid-feeding" converters by inserting active and reactive power into the network and the DER unit can, therefore, be seen as a current source whose power flow can be adjusted by varying the issued set points. The control approach in islanded mode is more difficult since the voltage and frequency of MG along with the balance between the loads and generation must be retained by the MG itself. A "grid forming" converter performs like a voltage source and controls the voltage and frequency in the absence of the main grid. The key functionalities of the MG controller can be summarised as follows [19-21]:

- Capability of smooth switching throughout the islanded and grid-connected operation.
- Voltage and frequency regulation considering every operational condition.
- Active and reactive power regulation to preserve precise power-sharing.
- Capability to reduce oscillations and retain the stable operation condition of the MG.
- Energy management and economic dispatch of the MG for getting the maximum benefits.

It is crucial that the inverters-based DERs should be able to handle frequency and voltage regulations and load sharing in the MG under disturbances without producing high circulating var [22] due to the high penetration of RERs. High circulating var is an unwanted consequence of parallel inverter operation. To fix the limitations, several control strategies have been offered and have afterward been combined into a hierarchical control architecture [15-17, 22-26], which includes three levels with different responsibilities, namely, primary, secondary and tertiary control. The objectives of MG control can be achieved using these three control levels. This hierarchical framework includes primary, secondary, and tertiary control stages which are accountable for different control actions and operate at different time scales. The control at these levels can be realised using various control methods. The detailed description of these three control levels is explained in Chapter 2.

E. Communication Architectures for MGs

Several MG elements, such as DERs and loads, are equipped with information and communication abilities which permit them to receive and send data over communication links. This concept provides growth of intelligent electronic devices (IEDs) [27] which are linked with each other and also communicate with the central controller for transferring operational data and performing control actions. Communication infrastructure plays an important role in the control and management of the MG. The MG communication network establishes bidirectional connectivity among MG elements and promises its safe and optimal operation. Many MGs still depend on legacy communication technologies. Different efforts such as standards and protocols are in progress to address the irreplaceable challenges of MGs.

Traditional electricity networks mostly rely on centralised communication architectures where a central controller communicates with the components and makes choices. Such frameworks are realised using SCADA (supervisory control and data acquisition) systems. SCADA systems work based on the EPA (enhanced performance architecture) model which contains only three of seven layers (layers 1, 2, and 7) defined in the OSI model. The use of only three layers reduces functionality. The low data rate, asynchronous data transfer, and use of direct communication links (no internet) are among other features of these systems [27]. Various protocols are traditionally used in power systems, including MODBUS, DNP3, PROFIBUS, and CANBUS.

F. Necessity of the Communication for MGs

The exclusive features of smart grids in general and MGs explicitly necessitate new standards and protocols for communication. For DERs, their dispersed geographical positions, the much higher data traffic, and the real-time monitoring and control are among their unique characteristics. Any communication network requires to fulfil the performance obligations for each MG application, such as protection, monitoring, control, synchronisation and demand response. These conditions need different bandwidths and acceptable time delays [27]. Data transmission requirements for MG functions are based on the IEEE, IEC, and ETSI standards. Some of the available standards which address MG communications and network needs are IEC 61850, IEC 61968, IEEE 1547.x, and IEEE 1646. The detailed specifications of these standards are described in [27].

G. The communication area networks

The communication network can be organised into different area networks based on the operation levels, including home area network (HAN), building area network (BAN), industrial area network (IAN), field/ neighbourhood area network (FAN/NAN), and wide area network (WAN). HAN, BAN, and IAN are local area networks (LAN) used by customers. HAN is used for interconnecting smart appliances and PV and storage systems inside the home and can be used for home energy management systems. BAN and IAN are more complex networks that connect various devices and are used for automation as well as energy management tasks of buildings and industrial plants. FAN and NAN work at the secondary substation level and establish the communication between customer networks and the WAN. They manage different tasks such as the transmission of smart meter data, load management, and distribution automation. WAN covers a wide geographical area and handles long-distance data transmissions with many communication nodes using high bandwidth communication networks.

A communication link can be accomplished based on different technologies by means of wired or wireless communication media. Wired technologies offer high reliability and security but have higher costs and are less

flexible to network amendments. Power line communication (PLC) systems operate by sending the modulated carrier signals on the available power lines. This is a cost-effective resolution; however, it faces various technical challenges owing to the propagation natures of power system elements. Instead of using PLC systems, dedicated wireline networks can be used for constructing the communication system, including technologies in particular synchronous optical networking/synchronous digital hierarchy (SONET/ SDH), Ethernet, digital subscriber line (DSL), and coaxial cables. SONET/SDH networks use optical fibers for transmitting very high data rates. Ethernet is a promising technology for MGs since it can offer decentralised communications in a reliable manner [27]. Wireless technologies are prone to environmental interference and transmission attenuation. On the other hand, they are economically viable, scalable, and more versatile than wired mediums. Recent developments in wireless technologies in terms of data rate and security make them an attractive option for communication networks in some parts of MGs. Various wireless technologies have been introduced, including Wi-Fi (IEEE802.11), WiMAX (IEEE802.16), Bluetooth (IEEE 802.15.1), ZigBee (IEEE 802.15.4), and cellular network communication such as 3/4/5 G networks [28]. Each of the wired and wireless technologies may be more suitable for the implementation at different control levels or area networks.

H. Cyber Attack in Stand-alone MG

In recent years, MGs have acquired considerable attention as a consequence of their possible advantages with regard to reducing greenhouse gases, the closeness of energy resources to loads, accelerating the usage of RESs, and reducing power losses. MGs are considered as small-scale power grids that include DERs, energy storage systems (ESSs), electric vehicles (EVs), and domestic loads. They have been effectively employed in hospitals, data centres, universities, ships, government organisations and remote areas. The steady action of a MG is self-sufficiently administered through a MG control centre (MGCC) that profoundly depends on sensor measurements through communication networks (cyber layer); hence, an entire MG system is usually regarded as a cyber-physical system [29]. MG frequency stability is administered through the capability of the MG to regain steady-state frequency operation after some unexpected disturbances. Dissimilar to large power grids or grid-connected MGs, stand-alone MGs have faced low-inertia problems [17]. The hierarchical control structure of the MG can be classified into local or primary control, secondary control, and tertiary control which will be discussed in Chapter 2 in detail. The primary control scheme, usually a droop control mechanism, is a local control that does not require communication links for operation and is intended to function at nominal operating points. The secondary control, typically applied at the MGCC, complements the primary frequency control by coordinating the parallel operation of multiple micro-sources, keeping the frequency in operating boundaries. The use of communication networks for secondary operation causes the MG network vulnerable to cyberattacks that can be a threat to security and lead to MG instability or breakdown. Cyberattacks could be one of many occasions: a time-delay attack where the attacker delays the measure signals for a period in time to ill-time control operations; a denial-of-service attack where the attacker blocks the measurement from being sent to the MGCC, disturbing the real-time control decision; and a false data injection (FDI) attack [29].

1.2 RESEARCH MOTIVATION AND SIGNIFICANCE

MGs has two operational modes: grid-connected or islanded modes. A hierarchical control method is familiarized to fulfil the operational purposes in the islanded MGs. This hierarchical structure includes the

primary control level, secondary control (SC) level or MG central control (MGCC) level, and tertiary/global control level [26, 30, 31]. The primary control layer contains three core control loops: current control, voltage control, and droop control loops. While the droop control technique guarantees (active) power-sharing, it exhibits errors in the voltage amplitude and frequency during the steady-state condition. The SC of the MG is initiated to recover the frequency and voltage amplitude to the reference values with proportional power-sharing within DGs [3], [4]. Centralised, distributed, and decentralised are three widely used control architectures for the SC employment. The basic idea of the centralised SC is relied on the point-to-point communication amongst all DGUs and experiences a single point of failure, leading the system to poorly reliable operation [8].

As DGs in the MG are spatially distributed and heterogeneous in nature, distributed control architecture is attracting solutions to increase the MG reliability. In comparison to the centralised architecture, distributed SC structure delivers higher reliability and better scalability by putting on a sparse CN. Among all the distributed control, consensus control is one of the main distributed SC architectures. Regarding consensus-based SC techniques, the CN is lessened more by transmitting the essential information only amongst the neighbour DGUs. Stability and robustness of this control method is verified in [9], [11], [15], [21]. Nevertheless, the dynamic response of the MG considering distributed secondary control (DSC) could be unexpected regarding the system oscillation, reaction time, stability margins [10] and steady-state behaviour. Despite several advantages of distributed control, the limitations mentioned above are taken as key challenges for an islanded MG with DSC. Moreover, the impact assessment of DSC parameters based on the dynamic model, the requirement of fine-tuning of DSC parameters for stability enhancement, and the corresponding suitable solution (i.e., fuzzy-based controller) for that are still needed to be researched. The MG control system design should address these drawbacks in a proper way to maintain the stability and resilience of the whole network. In addition to that fewer research works have been done on frequency and voltage restoration simultaneously with accurate active and reactive power-sharing. A proper DSC is still needed that considers all the drawbacks in a single control strategy.

One of the main motivations behind using MGs is that they can manage and coordinate DGs, storages, and loads in a more decentralised way, reducing the need for the centralised coordination and management. Hence, the optimisation of the MG operations is particularly important in order to cost-efficiently manage its energy resources. In this scenario, new modelling requirements are needed, e.g., storage modelling must be incorporated into the operation planning problem in order to coordinate storage use with DER generation and energy prices and address the complexity of the charging/discharging schedule. It is important to notice that there are no current modelling tools to include controllable loads and energy storage modelling in a smart grid environment.

The purpose of this thesis is to establish MG control that can address frequency and voltage restoration with precise power-sharing, optimise the control parameters by utilising intelligent controller and SoC balancing for DESUs in a single control strategy. The proposed controls are applicable for DGs and DESUs with different capacities for islanded modes of operation. The fundamental motivation behind this effort is to model the MG networks and present a systematic way of performing stability analysis in detail. The controller responses are examined in the Matlab/Simulink software, and their mathematical representations are developed in the time domain. In this thesis, detailed stability analysis is done using mathematical models developed for both linear and non-linear systems. To get the eigenvalues, the non-linear equations are linearised at a stable operating point.

These linearised equations form the small-signal state-space representation of the MG network. Then the linearised model is verified by detailed stability analysis. For DESUs, the detailed stability analysis is done using non-linear equations.

1.3 RESEARCH GAPS

Many research works have been accomplished on the design of autonomous MG control systems over the last decade. In the latest research trends, the concept of MG control has been shifting to distributed control to lessen the computational and communication requirement due to the high penetration of DGs. The main purpose of this thesis is to perform a literature review on the existing distributed control techniques mentioned in the literature so far for autonomous AC MGs with DGs and ESUs and categorises them with a comparison based on their design approach and viewpoint. Then it is aimed to identify the research gap from the studied literature review and address those gaps by designing appropriate control systems for islanded AC MG networks.

Low inertia, uncertainties, dynamic modelling and stability, along with bidirectional power flow problems, are identified as the most relevant challenges in MGs control and protection. MG Control is one of the key enabling technologies for the deployment of future power systems. Current efforts are mostly being put into the design of more effective control strategies and special protection schemes in different control levels that ensure stable, reliable, secure and economical operation of MGs in either grid-connected or islanded operation mode.

Various control loops must be used to improve the MG's stability and performance. The current, voltage/amplitude, frequency/angle, and active and reactive power are the main feedback variables used in the existing MG control loops in both grid-connected and islanded operation modes. Like conventional power grids, the MG has a hierarchical control structure with different operation layers. The hierarchical control structure of MGs is responsible for providing proper load sharing and DGs coordination, voltage/frequency regulation in both operating modes.

Three major gaps in the literature are identified:

The first gap is the lack of proper DSC for islanded AC MG network which can address the frequency and voltage regulation along with accurate power-sharing with appropriate stability analysis.

The second gap is the simplicity in DSC system design where an intelligent control system, i.e., Fuzzy logic controller, is utilised to tune the DSC parameters to enhance the stability.

The third gap is the lack of DSC for energy storage units in islanded AC MG networks where DSC addresses SoC balancing along with all others mentioned in the first gap.

Though existing literature addresses some of the above gaps by proposing different control strategies, but it is still missing to address all the gaps in a single framework, which needs to be considered.

1.4 RESEARCH AIMS AND OBJECTIVES

1.4.1 Aims

This thesis aims at representing a systematic methodology as well as mathematical description to develop a small-signal dynamic representation of an MG that consists of renewable energy sources (DERs) and a non-linear dynamic model that comprises DESUs in addition to DERs. The effectively designed control system can assure stable and high-quality power supply even with disturbances and instabilities.

The aims of this research are highlighted as follows:

- To design a distributed controller at the upper control level for frequency and voltage restoration and accurate power-sharing simultaneously and identify the control signals for stabilisation of MG under study.
- To optimise the controller parameters for delivering desired damping profile.
- To perform the time-domain simulations to evaluate the usefulness of the suggested controller for enhancing stability.
- To consider the MG system under both linear and non-linear environments to do detailed stability analysis under different proposed control strategies.

1.4.2 Objectives

The primary objective of this dissertation is to develop and demonstrate distributed cooperative control techniques that focus on integrating modelling, analysing and stabilising MGs to meet the requirements outlined in the previous section. Work has been conducted in three major areas to support these objectives which are summarised below:

A. Objective 1-Distributed cooperative control

This research work seeks to develop DSC frameworks based on the consensus control technique for MGs to address some limitations of the current strategies with the objectives below:

- Develop a frequency and voltage control scheme to restore their values to their reference level as well as maintaining the steady operation of an islanded MG containing electronically-interfaced DER elements.
- Improve the control strategy in order that DER units can maintain the output PCC voltage.
- Enhance both active and reactive power-sharing among the DER units,
- Increase the ability of plug-and-play operation of renewable energy resources along with energy storage units by developing a backup control in the event of communication failure and offer robustness against fault occurrences.

The main objective plan here is to increase the performance of the upper-level control in MGs by conducting MG modelling and analysis through advanced analytical techniques.

B. Objective 2-Stability Assessment

The main objectives of this part of the research are:

• Develop incorporated small-signal dynamic representation of the MG considering DSFC and DSVC for the lossy-line networks.

• Conduct a thorough stability study of the MG on the basis of its small-signal dynamic representation to uncover the mechanism of unwanted dynamic response and probable oscillations introduced over the DSC.

• Design a distributed optimal controller for stability enhancement of the MG and develop the system to achieve desired performance in terms of fast response, appropriate damping and satisfactory stability margin.

C. Objective 3- State of Charge (SoC) balancing for DESUs along with power sharing and stability analysis

The main objectives of this part of the research are:

• Develop a novel control strategy to balance SoC for DESUs at the secondary control level in a distributed way.

• Performed the detailed stability analysis for the non-linear dynamic model in a systematic way

• Verify the proposed DSC method with time-domain simulation under several case studies which include plug-and-play capability, different communication methods and applying PV data.

1.5 RESEARCH NOVELTY AND CONTRIBUTION

Decentralised controller has recently been proposed as an alternative solution of traditional centralised controllers to boost the effectiveness, reliability and power quality of DERs. The implementation of decentralised or DSCs was restricted to the voltage/frequency control. Besides, the literature deficits an uncomplicated design of distributed controllers considering energy storage components in MGs through inadequate information trade-off among batteries. Due to this fact, this dissertation builds a unique distributed cooperative control for inverter-based DGs and energy storage devices with bounded information shared among DGs and energy storage devices. The current technical publications concerning the DSC especially emphasise the realisation of the stable control goals, e.g., (i) recovery of the system frequency, (ii) control of DG unit's voltages on the AC side or critical bus voltage, and (iii) precise reactive power sharing amidst DG units.

On the other hand, the dynamic behaviour of the MG over the DSC could be unwanted regarding the damping of the system, response time, stability margin, etc. In addition to that, the DSC could establish additional less damped modes to the network directing the whole network to oscillatory responses. Even though there are few scientific publications implementing small signal stability analysis for the DSC, a detailed assessment of the mechanism of unwanted dynamic responses and the likely oscillations produced by the DSC has been stated in very limited research works earlier. Moreover, although several techniques have been studied to improve the stability of the primary control, to the best of our awareness, the equivalent stability improvement methods to increase the dynamic behaviour of the DSC utilising an intelligent controller have not been described before. The relevant stability enhancement techniques must be capable to realise the synchronisation of all the DG units because of their contribution to the oscillations.This thesis contains the following major contributions:

- Provide a brief overview on the literature review for distributed control strategies applied to control islanded AC MG networks with DERs and DESUs. Current trends and various research practices employed to date in three control layers (Primary, Secondary and Tertiary) are distinctly stated.

- Propose a novel voltage control which can keep accurate reactive power sharing after voltage restoration.
- Propose a novel frequency control which can keep accurate active power-sharing after frequency restoration; minimise the operation cost by applying the optimal active power sharing using the equal-cost increment values of DG units; utilise the optimisation technique, Particle Swarm Optimisation (PSO), to choose the optimal control parameters to improve the damping of less damped modes.
- Introduces a systematic process of establishing a fully dynamic linearised small-signal state-space representation considering DSC considering also the line resistance in the model.
- The eigenvalue study is conducted to assist in distinguishing the interrelation between the system stability and controller variables. A comprehensive evaluation of the impact of the distributed controllers on the MG dominant oscillatory modes based on the small-signal dynamic representation is shown.
- Propose a novel DSC to restore frequency and voltage simultaneously while accurate active and reactive power-sharing. Unlike the existing consensus methods, the proposed method utilises a proportional-integral (PI) controller at the output voltage of the inverter. Thus, voltage mismatches are reduced to a great extent.
- The small-signal stability analysis for the proposed DSC for the networked MG model is carried out in detail. Note that eigenvalue analysis for parallel-connected DGs in the MG was previously studied in many studies, but very few studies have addressed the small-signal stability analysis for a networked MG model considering DSC.
- In most of the previous related works, other tuning methods/optimal controllers are used for finding DSC parameters. Utilising the intelligent fuzzy logic (FL) parameter-tuner in accordance with small-signal stability analysis for the networked MG model has been presented as a new solution. The fuzzy logic controller (FLC) not only improves the performance of the suggested DSC but also lessens the complexity of the DSC design.
- Consensus-based DSC is proposed for DESUs in AC islanded MG system to recover the frequency and voltage to the reference values within a finite time. The proposed control is responsible for SoC balancing in the case of batteries with different initial SoC as well as sharing the active and reactive power with hierarchical control architecture applying simplified dynamic design.
- Present detailed stability analysis considering the underlying non-linear model with the help of Lyapounov stability criteria.
- In comparison with the existing DESUs, the proposed control is robust against load disturbances, different communication topologies and plug-and-play capabilities. The proposed DSC is verified with real-time PV data, which ensures the effectiveness of the proposed DSC.
- This thesis covers all the main aspects of MG control in a single control strategy which is one of the main contributions.

1.6 METHODOLOGY

In this thesis, DSC system design for islanded MG networks utilising consensus control theory has been addressed. We focus on designing such a DSC system which can restore system frequency and voltage to their reference values as well as share active and reactive power accurately by designing a secure framework applying

consensus control theory. To do so, we started reviewing background knowledge for the MG concept and identifying research aims and objectives. The motivation of the research is discussed, and research contributions have been presented. A thorough literature review on the MG control system has been discussed which includes the hierarchical control system. As the main focus is DSC for this thesis, current literature reviews on DSC for both DGs and DESUs have been discussed in detail. After doing a proper literature review, suitable MG models/networks have been developed for analysis. Mathematical models of those MG networks have been developed under both linear and non-linear environments to make the research more robust. Detailed stability analysis which includes eigen-value analysis for linear MG networks has been done. After confirming the stability of the models, fine-tuning of DSC parameters has been employed to enhance the stability of the system, which means the optimal value of the DSC parameters is chosen to get the best performance from the designed control system. The performance of the selected DSC parameters is then validated by the time-domain simulation to ensure the accuracy of the tuning process which includes applying fuzzy-logic based intelligent control. After verifying by the time-domain simulation, conclusions and recommendations for future research are made to continue the research in the proper direction. The methodology followed in this thesis has been represented in a flow chart in Fig. 1.5.

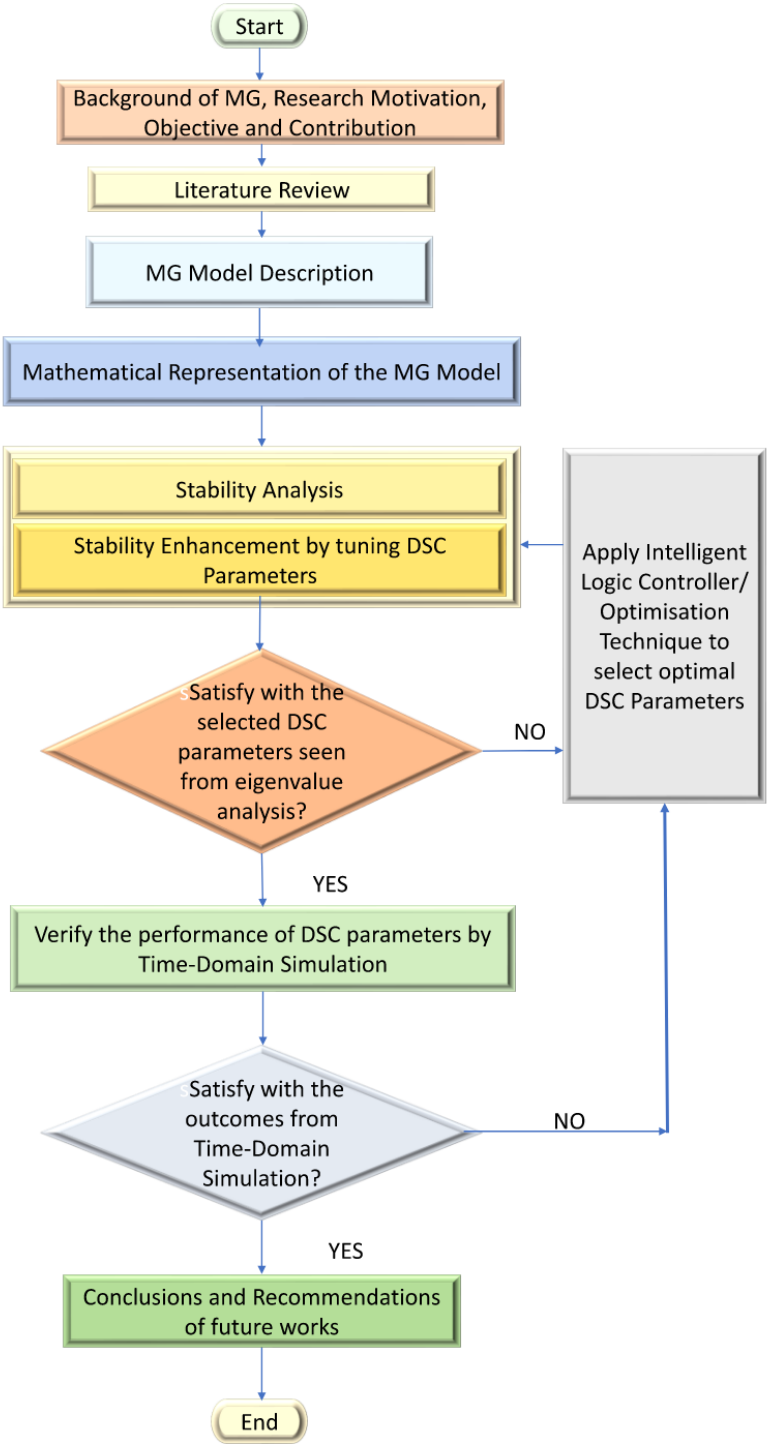

Fig. 1.5 Flow chart of research methodology

1.7 THESIS STRUCTURE

The organisation of the thesis is as follows:

In Chapter 2, the latest literature reviews on control system design for islanded AC MG are presented, focused on the secondary control level. DGs as well as DESUs are performing an increasingly significant part in

modern power systems. The main objective of this chapter is to provide a brief review of distributed control structures used so far to control an autonomous AC MG system. The distributed control for both grid-connected and autonomous MG is current development for their several advantages compared to conventional central control systems comprising the system trustworthiness, lessening its sensitivity to failures, and removing the necessity for a central computing and communication unit. The overall control architecture is divided into three basic control levels, such as primary, secondary and tertiary control levels, and control schemes are considered here for autonomous operation mode. Trends and different strategies used so far for MGs, including DGs and DESUs, in the above control levels are clearly stated for understanding a brief overview.

Chapter 3 presents a novel secondary control for restoring the system frequency in a distributed manner with incremental cost-based droop-controlled MGs. The proposed control ensures the frequency restoration and accurate active power-sharing in an optimal way simultaneously. Stability analysis with state-space modelling is completed with the proposed distributed secondary frequency controller (DSFC). The DSFC parameters are designed with the particle swarm optimization (PSO) technique where the selection of DSFC parameters is considered as an optimisation problem for enhancing the overall stability of the system. A test MG model in the MATLAB-based Simscape platform is taken for modelling and simulation. The outcomes from the simulation confirm that the proposed DSFC can simultaneously restore the frequencies and optimal active power-sharing while the optimal DSFC parameters reduce the overshoot and maintain better stability for the system.

Chapter 4 addresses the control problem of MGs and presents a DSC system for voltage regulation of an islanded MG with droop-controlled and inverter-based DGs. A consensus-based distributed control approach is proposed to restore the voltage and share the precise reactive power of the islanded MG for all DGs within a very short time. An integrated small-signal dynamic representation of the offered distributed secondary voltage controller, allowing the line resistance in the model. The proposed voltage controller can keep precise reactive power-sharing after voltage restoration. A thorough evaluation of the effect of distributed controllers on the MG dominant oscillatory modes constructed on that small-signal dynamic model. The proposed method is flexible to system topology variations, which aids the plug-and-play operation of MG. An autonomous MG test system consisting of four DGs is constructed in MATLAB using SimPowerSystem Toolbox to test the proposed design method, and the simulation results show the effectiveness of the proposed control strategy. The performance of the proposed controller is shown through several test case studies.

Chapter 5 suggests a novel distributed cooperative control methodology for the secondary controller in islanded MGs. The proposed control technique not only brings back the frequency/voltage to its reference values, also maintains precise active and reactive power-sharing among DG units by means of a sparse communication system. Because of the dynamic behaviour of DSC, stability issues are a great concern for a networked MG. To address this issue, the stability analysis is undertaken systematically, utilizing the small-signal state-space linearized model of considering DSC loops as well as parameters. As the dynamic behaviour of DSC creates new oscillatory modes, an intelligent fuzzy logic-based parameter-tuner is proposed for enhancing system stability. Accurate tuning of the DSC parameters can develop the functioning of the control system, which increases MG stability to a greater extent. Moreover, the performance of the offered control method is proved by conducting a widespread simulation considering several case scenarios in MATLAB/Simscape platform. The proposed control method addresses the dynamic nature of the MG by supporting the plug-and-play functionality,

as well as working even in fault conditions. Finally, the convergence as well as comparison study of the offered control system is shown.

Chapter 6 introduces a new DSC method for distributed energy storage units (DESUs) in islanded AC MGs. Dynamics of distributed storages (DSs) for the extended time duration are not considered in the traditional hierarchical control of MG. Thus, it is challenging to control the DESUs with various levels of stored energy represented by the state of charge (SoC). The storage units can utilise their full power capacity after converging to a common SOC to mitigate the generation and demand variations in the MG. Depletion of SoC with lower initial SoC occurs faster than with higher SoC by using *P-f* droop control, and then their capacities are no longer accessible. Furthermore, applying droop control to match the SoC of DESUs, causes the deviation of frequency and voltage from the reference values. However, restoration of the MG frequency and voltage using the conventional DSC disrupts SoC-balancing. With the proposed method, all the DESUs operate in the same state of charge (SoC) and the same powers, and thus the uneven degradation of DESUs is avoided. Under the distributed control architecture, the network resource can be saved since the control center just communicates with parts of ESUs. The proposed designs bring plug-and-play capability to the smart grid system. The proposed method is evaluated in the established Matlab/Simulink model, and the results validate the effectiveness of the proposed method.

Chapter 7 highlights the main contributions of this thesis and gives a summary of the overall thesis. This chapter also provides recommendations for the future direction of this research/thesis. The eventual goal of this research is to make the best use of the advantages of MG by addressing its technical challenges at the SC level and propose the possible solutions to further enable its capabilities from a control perspective.

Chapter 2: Literature Review

2.1 INTRODUCTION

MG is an emerging idea designed for future power distribution systems, which empowers renewable energy integration. It usually has various distributed generators that are generally interfaced with the main grid through power electronics converters [3]. One smart characteristic of MG is the ability to operate in both grid-connected and autonomous operating modes. In the case of the islanding operation of AC MGs, two significant functions are to share the load demand among various parallel-connected inverters and preserve the voltage and frequency stability. Proper coordination of internal elements is a key criterion for an MG to achieve such functionality. However, not all the research questions for the future power system have been resolved yet, so intensive research work should still be needed to make such advanced schemes an actuality.

Power systems can be a connection of several interrelated MGs where an individual MG is responsible for maintaining its own demand of energy with the neighbouring MGs in case of additional generation in the near future. Therefore, the future MG will be converted to a distributed system, in which the generation and consumption units can be regarded as distributed agents. This chapter reviews and classifies several methodologies of distributed control for an autonomous AC MG. Concurrently, some control systems are graphically shown. Finally, the future trends of MG control are presented. Several reviews on MG control have already been done; however, most of them [19, 32-34] do not consider the distributed control of an autonomous MG system specifically. One contribution of this chapter is to identify the recent trends in the distributed control for an autonomous AC MG system so that one can easily get a clear concept on this topic, not the overall control system of MG.

2.2 HIERARCHICAL CONTROL STRUCTURE

The traditional large-scale power system has a three-level hierarchical control architecture. Similarly, the hierarchical control structure of MG comprises three control levels, specifically, primary, secondary and tertiary control [21] as in Fig. 2.1. In the hierarchical control, the system state data passes from the primary level to the tertiary level, and the result indicators pass from the tertiary level to the primary level to gain overall action objectives. The primary control is responsible for power-sharing among distributed generators (DGs). The primary control is recognised regionally through the droop control technique at every DG terminal to preserve the voltage and frequency stability. Regardless of the distributed characteristics of droop control, it has a limitation of generating voltage and frequency deviations from their references. Hereafter, the SC stage is compulsory to cancel the deviations produced by primary droop control and to recover the voltage and frequency to their reference values. The SC system restores the voltage and frequency back to their nominal values. The

tertiary control stage acts on the optimisation of the operating cost and power flow of the MG. Tertiary control deals with the power flow between the MG and the main grid and is used to optimize the MG based on efficiency and economics.

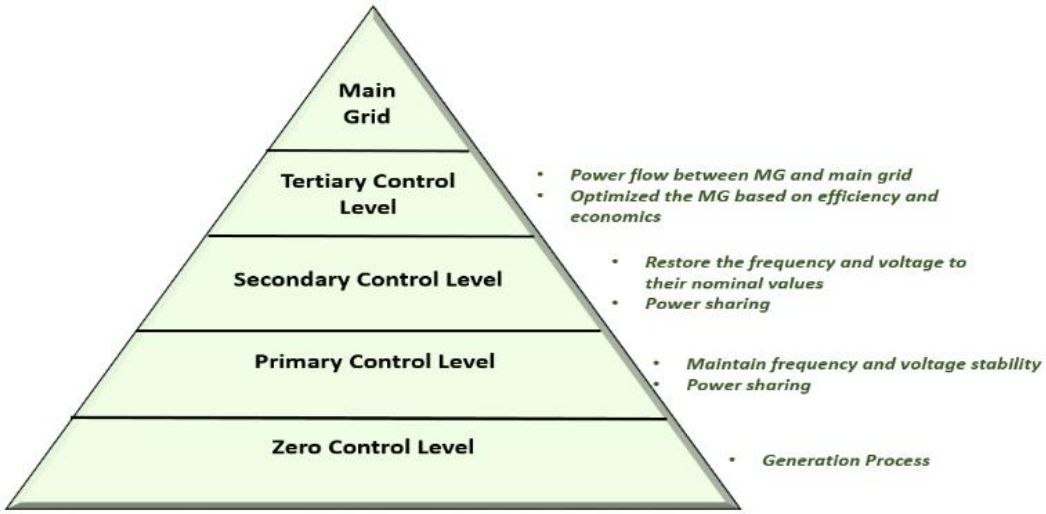

Fig. 2.1 Hierarchical control arrangement of an MG

In general, the overall control system of MG can be divided into three categories: centralised, decentralised and distributed. Fig. 2.2 shows the basic structure of a centralised, decentralised and distributed control system. A completely centralised control depends on the information collected in a dedicated central controller that accomplishes the necessary computations and decides the control acts for every unit at a particular point, requiring vast communication between the central controller and controlled units [32]. Alternatively, in completely decentralised control, each unit is controlled by its local controller, which only collects local data and is neither fully responsive to system-wide variables nor to other controllers' performances [35]. In distributed control, presented in Fig. 2.2 (c), the units (DGs) are not distantly dispatched. Instead, all the units cooperate to attain a collective decision in consistence with the objectives that have been fixed (i.e., by means of the grid operator or the consumer). Every controller requires to interact just with neighbouring units, and therefore, global data of the grid, e.g., the state of every unit, are not demanded for the purpose of determining the control rule. The main intention of a distributed coordination framework is to achieve a self-organised power grid that has the capability to handle efficiently the issues which might happen, employing only regional interactions and offering "plug-and-play" ability, amongst other benefits. Distributed structures can show a robust and resilient control of the distribution grid [36]. Furthermore, they can work with sparse communication and low bandwidth that are less affected after applying faults in the communication lines. All these potentials build them highly promising for smart grid applications. This research mainly focuses on the distributed control techniques used/proposed at the primary, secondary and tertiary control levels for autonomous AC MG in the literature.

(a)

Advantages:
- Easy to implement
- Easy to maintenance in the case of single point failure

Disadvantages:
- Computational burden
- Not easy to expand (so it is not suitable for smart grids)
- Single point of failure (highly unstable)
- Requires a high level of connectivity

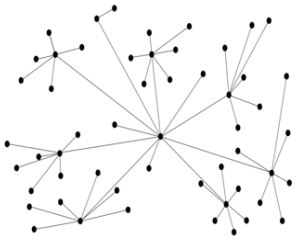

(b)

Advantages
- Local information only
- No need for a comprehensive two-way high-speed communication
- Without leaders, system still includes some control island-area
- Parallel computation

Disadvantages:
- Absence of communication links
- between agents restricts performance
- Moderate scalability

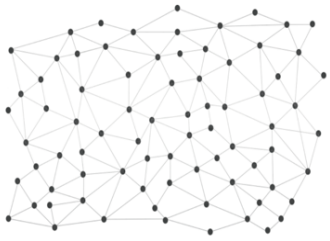

(c)

Advantages:
- Easy to expand (high scalability)
- Low computational cost (parallel computation)
- Avoids single point of failure
- Suitable for large-scale systems
- Not affected by changes in system topology.
- practical solution for plug and-play characteristic of smart grid

Disadvantages:
- Needs synchronization
- Convergence rates may be affected by the communication network topology
- Needs a two-way communication infrastructure

Fig. 2.2 (a) Centralised, (b) Decentralised and (c) Distributed control structure of an MG

2.3 DECENTRALISED/DISTRIBUTED CONTROL FOR MGS

The emphasis of this chapter is to build a SC system considering an islanded MG. The goal is to bring back the frequency/voltage to the required estimate and keep precise active/reactive power sharing among all distributed generator (DGs) units. Currently available SC strategies can be categorised into three groups: centralised [19, 21] , decentralised [19, 37-39] , and distributed control [20, 40-43]. The conventional centralised strategy needs central communication with complex computation elements to gather and manage huge data of all DGs. These necessities may reduce the entire system's reliability and experience from a single point of failure issue. Decentralised control technique may not be applicable to synchronise all existing capacities within the MG in an optimal way because of the insufficiency of broader accessible information [44].

Comparatively, DC is encouraged by means of the viewpoints of multi-agent network coordination founded on consensus algorithms [42, 45-47], which permits all DGs to accomplish a common target by applying the peer-to-peer communication protocol. Because of the readiness of renewable generators, MG's physical and communication topologies can be varied over time. To assist plug-and-play ability, the DC technique gives a robust SC framework that works successfully despite time-varying communication networks. Additionally, DC strategies support better scalability, manageable communication system, and quicker distributed data computing that can ease extremely resourceful data sharing and rulemaking.

2.4 OVERVIEW OF CURRENT DISTRIBUTED CONTROL TECHNIQUES FOR MGS

Due to the distributed nature of MGs, the distributed control architecture is a desirable as well as advantageous solution, especially for small and isolated MGs. The distributed control system mainly has a central

computer instead of a central controller to monitor the action of the whole process. This central computer can also run operations or download configuration settings to distributed controllers even in the period of system commissioning and maintenance. All kinds of control functions can easily be implemented on distributed controllers even in the disconnected mode [35]. Distributed control is very flexible which lets the incorporation of additional energy resources in the current MG without adverse impact on the structure. This characteristic supports the plug-and-play operation, which is essential for movable and remote MGs. Among the existing distributed control techniques, the consensus and cooperative control has drawn much more attention in the MG control community at the primary, secondary and tertiary control level [43]. Another popular distributed control is multi-agent-based cooperative control method. The multi-agent-based control system can accomplish system objectives cooperatively, which is difficult to reach by a single agent or centralised controller. There are many other techniques mentioned in the literature for decentralised/distributed control at all three levels, which are stated below:

2.4.1 Primary Control Level

Primary control, also known as local control or internal control, is the first level in the control hierarchy, giving the fastest response. Based entirely on local information, this control can perform the operation without any communication link. The primary concerns of this control level are to maintain the stability of output voltage and frequency as well as the control of power-sharing and balance. In conventional power systems, synchronous generators control the output voltage and power-sharing by the voltage controller, governor, and the inertia of the device. To pretend the inertia property of synchronous generators and offer suitable frequency regulation, voltage-source inverters (VSIs) necessitate a particularly designed control technique. According to that designed technique, VSI controllers consist of two controllers: one is the DG power-sharing controller, and the other is the inverter output controller [48]. Accurate sharing of active and reactive power is the main responsibility of power controllers, whereas consensus-based distributed control for MG proper regulation of output voltages and currents is the principal task of inverter output controllers. Inverter output control is composed of an outer loop for voltage regulation and an inner loop for current regulation. Active power-frequency and reactive power-voltage droop controllers are popular at this level to maintain power-sharing that emulates the droop characteristics of synchronous generators without using a communication network.

A. Droop Control

Droop control method is well known decentralised control at the primary control level of inverter-based MGs. The conventional *P/f* and *Q/V* droop approaches have been widely researched and examined in the past literature [25, 26, 49, 50]. The inverter output impedance in the conventional droop control is assumed to be purely inductive because of its high inductive line impedance and large inductor filter. Generally, in an MG system, every inverter interfaced DG comprises a primary constant dc power source, a voltage source inverter (VSI), an LCL filter (combining the LC filter with coupling inductor) and an output connector, as shown in Fig. 2.3. In the autonomous or islanded mode, VSIs are the key controllable elements with two major controlling phases. Every DG is associated with the load and linked with neighbouring DG through feeder lines. The power

controller (Fig. 2.3) permits DG units to share the active and reactive power requirement according to their maximum ratings based on the droop gain, i.e.,

$$\omega_i=\omega_{ref}\text{-}m_{pi}P_i \tag{2.1}$$

$$v_i=v_{ref}\text{-}n_{qi}Q_i \tag{2.2}$$

where, P_i and Q_i are the measured active and reactive power at the output of i^{th} DG units, respectively; m_{pi} and n_{qi} are the droop coefficient for frequency and voltage control of i^{th} DG units, respectively; ω_{ref} and v_{ref} are the reference angular frequency and reference voltage, respectively. The frequency and voltage droop coefficient are designed from (2.1) and (2.2), as follows:

$$m_{pi}=\frac{\Delta\omega}{P_{max}}$$

$$n_{qi}=\frac{\Delta v}{Q_{max}}$$

where $\Delta\omega$ and Δv are the maximum allowed deviation of frequency and voltage, respectively. P_{max} and Q_{max} are the nominal active and reactive power supplied by the system, respectively. The relationship between *f-P* and *v-Q* droop controllers is shown in Fig. 2.4

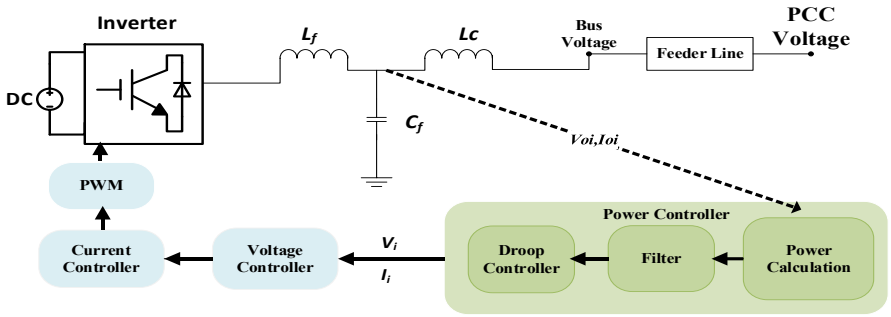

Fig. 2.3 Block diagram of an individual DG

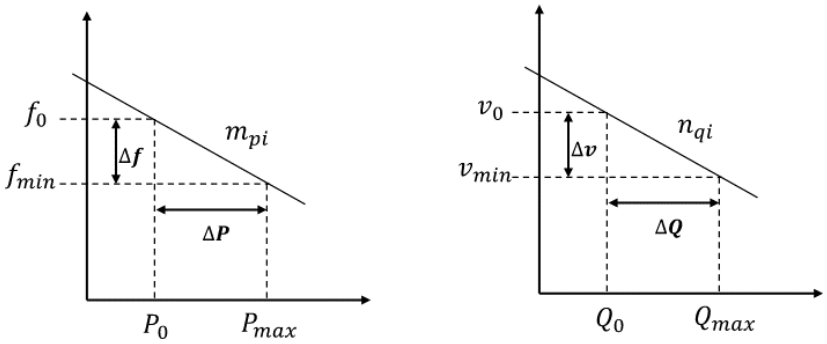

Fig. 2.4. The relationship between f-P and v-Q droop controllers

Although droop control retains many inherent benefits such as unnecessity of communication link, the conventional droop technique has several drawbacks, such as slow transient response, inherent trade-off between voltage regulation and load sharing, poor harmonic load sharing between parallel-connected inverters in the case of non-linear loads, line impedance mismatch between parallel-connected inverters that affect active and reactive power-sharing, and poor performance with renewable energy resources which are discussed in [38, 49, 51, 52] and need to be overcome. For this purpose, some improved and enhanced droop methods like virtual output impedance with droop control as well as distributed control like MAS based, consensus control techniques, model predictive control (MPC), etc. have emerged in the MG control [49, 51, 53-62] which are briefly summarized with advantages and disadvantages in Table 2.1.

B. Virtual impedance loop-based droop control

The conventional droop control cannot provide a balanced reactive power-sharing among parallel-connected inverters under line impedance mismatch. Therefore, the imbalance in reactive power-sharing is a serious problem in an AC microgrid. Several studies have achieved balanced reactive power-sharing by implementing virtual output impedance in the droop control method through a fast control loop which emulates the line impedance (Fig. 2.5) [63]. Thus, the reference voltage of each inverter can be modified as follows:

$$f_{refi} = f_n - k_{fi}P_i \tag{2.3}$$

$$\begin{cases} v_{drefi} = v_n - k_{vi}Q_i - R_{viri}i_{odi} + \omega_n L_{viri}i_{oqi} \\ v_{qrefi} = -R_{viri}i_{oqi} - \omega_n L_{viri}i_{odi} \end{cases} \tag{2.4}$$

where P_i and Q_i are the active and reactive powers of the i^{th} DG units, respectively, k_{fi} and k_{vi} are the frequency and voltage droop gains, respectively, f_n and v_n are the nominal frequency and voltage, respectively, v_{drefi} and v_{qrefi} are the reference values for the direct-quadratic (d-q) components of voltage magnitude in the synchronous reference frame, ω_n denotes the nominal angular frequency, R_{vir} and L_{vir} are embedded to model the virtual resistance and virtual inductance, respectively, v_{odi} *and* v_{oqi} are the *d-q* components of the inverters output voltage and i_{odi} and i_{oqi} are the *d–q* components of the inverters output current. Based on (2.3) and (2.4), the frequency and voltage excursions would be established in the autonomous MG due to load variations.

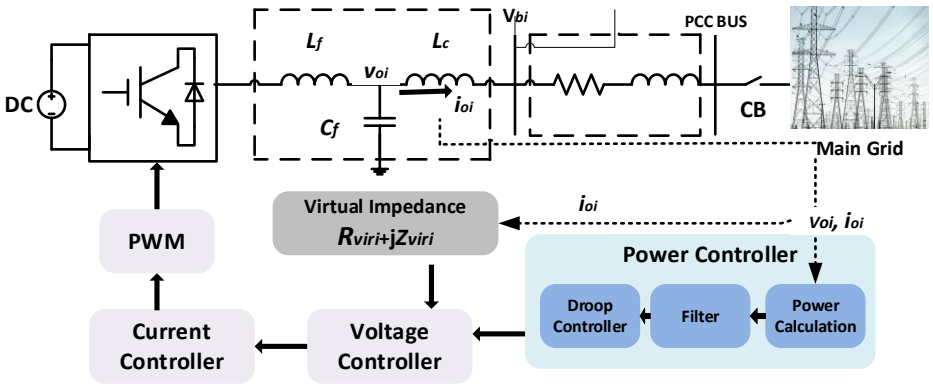

Fig. 2.5 Block diagram of an individual DG with virtual impedance

The virtual output impedance is generally selected to dominate line impedance. Thus, the virtual output impedance can be chosen through the summation approach, in which balanced reactive power sharing is achieved if the voltage drop from every inverter to the AC bus is as follows [64].

C. Consensus Control

The consensus algorithm has been researched for ages and has played an important role in computer science and the accomplishment associated to distributed computing. It has been researched and is being practiced in diverse areas, including underwater robotics [65], autonomous vehicles [66], telecommunications [67], car industries [68] and others [66, 69, 70]. In recent years, consensus-based control has also been investigated for smart grids. The areas researched in power systems include power-sharing between distributed generation inverters [71, 72], control of virtual synchronous generators [73-75], economic dispatch [76, 77] and control of energy storage systems [71, 78-80].

In consensus control, through autonomous control, several similar units or 'agents' work together to attain a specific 'consensus' to accomplish the anticipated system performance. Communications with only the directly connected neighbouring generators are necessary for the consensus-based algorithm to function, which leads to a very robust and reliable system subject to large load variations [69]. The consensus-based multi-agent control theory appears to be very promising and worth investigating. The DGs are of intermittent nature and can be physically located in wide-ranging locations, and consequently, a much more robust and reliable approach of distributed control and management is necessary to achieve the complete security, stability and scalability of the MG. The consensus-based algorithm is an outstanding resolution for the above challenges as it can straightforwardly drive all the generators in the MG to a global agreement of a particular parameter of the generators by means of just neighbour-to-neighbour communication among them.

Consensus-based *P-f* droop control is first suggested in [81]. Consensus-based distributed voltage controls (DVC) are suggested in [82, 83], which resolve the difficulty of reactive power control in inverter-based MGs but mainly for inductive power lines. Authors in [84] consider the consensus process for frequency control allowing for agents with system dynamics. As the communication among the agents in the consensus control follows the graph theory, a detailed explanation of graph theory is below.

Graph Theory:

A directed graph (digraph) $G = (N_G, E_G)$ with a set of N nodes, $N_G = \{1,2,3,4 \dots \dots . N\}$, a set of edges $E_G \subset N_G \times N_G$ and an adjacency matrix $A_G = \left(a_{ij} \geq 0\right) \in R^{N \times N}$ (where $a_{ij} = 1$ if there is a path from the i^{th} node to the j^{th} node and otherwise $a_{ij} = 0$) is considered here. An agent is represented by a node, and each edge (i, j) (pointing from j to i) indicates that the information flows from j to i related with a_{ij}. The neighbors of node i are represented as $N_i = \{j \in N_G : (i, j) \in E_G\}$. According to this, an agent/node i only has access to the data from its neighbours in N_i. If every agent (node) can be represented as a single-state system defined by $\dot{x_i} = u_i$ where u_i is the input as a function of the i^{th} agent's neighbouring state $x_j, j \in N_i$, the common form of consensus protocol is as below:

$$\dot{x}_i = u_i = -\sum_{j\in N_i} a_{ij}(x_i - x_j) \tag{2.5}$$

Based on (2.5), all are driven to the equilibrium by setting the derivative of x_i to be the consensus protocol $u_i = -\sum_{j\in N_i} a_{ij}(x_i - x_j)$. The objective of the work proposed in [85] is to have all $\frac{Q_i}{n_{qi}}$'s to be identical (in this way Q_i will be proportional to n_{qi}). Thus, a straightforward control design would be substituting the x_i in (2.5) to $\frac{Q_i}{n_{qi}}$. However, equation (2.5) requires x_i to be directly controllable, while Q_i cannot because the inverters are usually operating in *V-f* mode. Thus, a modification to (2.5) is made: the control protocol $u_i = -\sum_{j\in N_i} a_{ij}\left(\frac{Q_j}{n_{qj}} - \frac{Q_i}{n_{qi}}\right)$ is set to a controllable quantity $\dot{V}_i$ instead of $\frac{\dot{Q}_i}{n_{qi}}$. This yield the proposed algorithm is as below:

$$\dot{V}_i = -\sum_{j\in N_i} a_{ij}\left(\frac{Q_j}{n_{qj}} - \frac{Q_i}{n_{qi}}\right) \tag{2.6}$$

D. Model Predictive Control (MPC)

Separately from consensus-based algorithms, other distributed algorithms have also been studied, for example, the predictive control-based algorithms. The application of MPC for primary control of MG is presented in [86]. Power is predicted and regulated directly in predictive power control (PPC), which is another MPC-based control method mentioned in [87]. MPC technique is used to regulate the inverter output voltage in order to ensure power-sharing among the DG inverters. Using the MPC technique eliminates cascaded current and voltage control loops, which is shown is Fig. This results in a very fast dynamic response while ensuring almost zero steady-state operation. It can be seen that MPC consists of three main layers: extrapolation, predictive control and minimisation of the cost function. To use reference capacitor voltage in the cost function, v_c^* must be extrapolated to next sampling time. To do that, fourth-order Lagrange extrapolation technique can be used [86].

$$x^*(k+1) = 4x^*(k) - 6x^*(k-1) + 4x^*(k-2) - x^*(k-3) \tag{2.7}$$

The next step in the predictive control is obtaining the discrete-time model. The continuous-time model of the system can be defined as:

$$i_f = \frac{2}{3}\left(i_{fa} + \mathrm{a}\, i_{fb} + \mathrm{a}^2 i_{fc}\right)$$

$$v_c = \frac{2}{3}\left(v_{ca} + \mathrm{a}\, v_{cb} + \mathrm{a}^2 v_{cc}\right)$$

$$i_o = \frac{2}{3}\left(i_{oa} + \mathrm{a}\, i_{ob} + \mathrm{a}^2 i_{oc}\right)$$

where i_f is the filter current, v_c is the output voltage and i_o is the output current. The continuous-time model of *LC* filter voltage and current can be expressed by

$$L\,\frac{di_f}{dt} = v_i - v_c$$

$$C\,\frac{dv_c}{dt} = i_f - i_o$$

where L is the inductance and C is the capacitance of the LC filter. Fig. 2.6 shows the block diagram presentation of the MPC-based droop control proposed in [86].

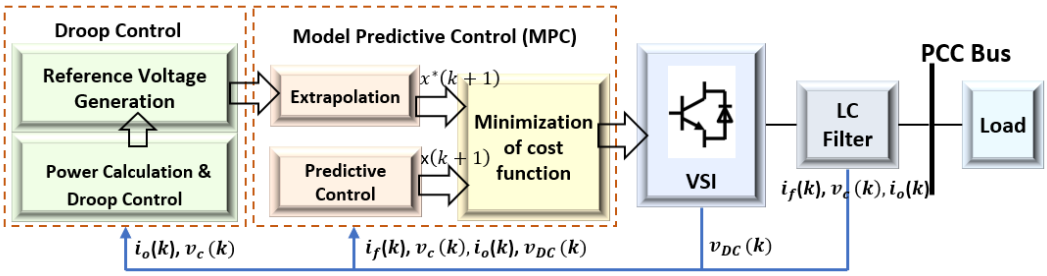

Fig. 2.6 MPC based droop control algorithm proposed in [86]

2.4.2 Secondary Control Level

The secondary control removes the frequency and voltage deviations caused by the primary droop control, which includes power flow control of the interconnection lines. Secondary control aims to improve the power quality, adjust the power generation of distributed energy resources (DERs) according to technical requirements and permit smooth connection/ disconnection of the MG from the main system.

A. Centralised Control/Conventional Secondary Control

Centralised control with communication networks is a common solution at the secondary control level in most of the present research works discussed in [32, 88]. As mentioned previously, centralised, and decentralised control are methods of secondary control for adjusting the output of each different DG. Microgrid Central Controller (MGCC) plays the main role in managing the power between the different DGs and interfaces with the main grid (Fig. 2.7). The MGCC detects all the values from the main grid and DGs and provides a reference value to send to the primary and inner control loops. Fig. 2.7 illustrates the processing of the secondary control level in the central method. When disconnected from the main grid, the MG central controller (MGCC) plays an essential role in islanded and autonomous operations.

In centralised control, the frequency and voltage amplitude of DG is measured and compared with the reference value (comparison is for grid-connected mode only). The measurement error will then be sent to primary control to restore the frequency and voltage. The error measurement is done by the following:

$$\Delta f = G_{pf}\left(P_{mg}^{ref} - P_{mg}\right) + G_{if}\int\left(P_{mg}^{ref} - P_{mg}\right)dt\} \tag{2.8}$$

$$\Delta v = G_{pv}\left(Q_{mg}^{ref} - Q_{mg}\right) + G_{iv}\int\left(Q_{mg}^{ref} - Q_{mg}\right)dt\} \tag{2.9}$$

The detailed specifications of the above equations can be found in [89]

The significant disadvantage of this method is the dependence of the control on MGCC, which means that the system faces a problem when there is any malfunction in the central control. Moreover, a

communications link between all DGs and MGCC is required for centralized mode, making the method more unreliable. As a result, distributed control methods with minimum communication setup have the utmost importance [35]. Other disadvantages are reduced flexibility/expandability and a necessity for a lot of computational resources. Therefore, centralized control hierarchy is usually more suitable for localised and small size MGs where the information to be gathered is limited and centralized optimization can be realized with low communication and computation costs.

B. Distributed Secondary Control

On the other hand, in order to achieve more flexible operation and avoid a single point of failure (SPOF), distributed control systems have been brought to stage. A general structure is shown in Fig. 2.7. Instead of information concentration in a central controller, a distributed information sharing algorithm is needed for all the local controllers to obtain essential global information. Recent progress in alternative communication technologies [68] (WiFi, Zigbee, etc.) and information exchange algorithms [69]– [73] (Peer-To-Peer, Gossip, Consensus, etc.) enable the possibility of distributed control and management in practical applications. In that sense, functions provided by the conventional centralized control mechanism, such as frequency and voltage restoration, DER coordination, and energy management, can also be realized in a distributed way, while the level of decentralization can range from centralized to fully distributed.

C. Consensus-based Distributed Secondary Control

As mentioned earlier, the general purpose of consensus algorithms is to allow a set of agents to arrive at an agreement on a quantity of interest by exchanging information through a communication network, while these agents are only required to communicate with direct neighbouring agents [66, 76, 79, 85, 90]. Several current works based on the distributed control structure, as shown in Fig. 2.7, at the secondary level are stated here. MAS-based control has recently attracted much more attention at the secondary control level. MAS-based two-layer reactive power sharing and control technique is proposed in [91] for a droop-controlled MG, in which the lowermost layer is the electrical distribution MG, while the uppermost layer is a MAS communication network composed of agents.

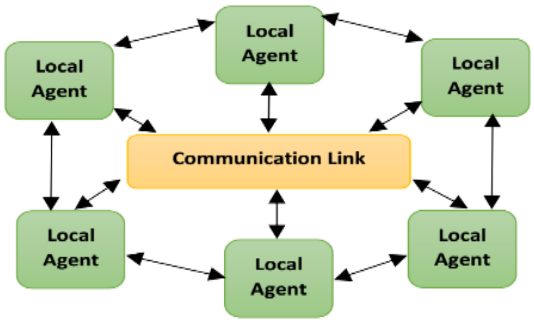

Fig. 2.7 Schematic of general distributed architecture for MAS control.

Consensus-based DSC for reactive power sharing is offered in [91] with control laws derived for a given communication network. And then in regard to the control laws, agents control the reactive power outputs of

controllable DGs to which they connect, to accomplish the proportional power-sharing. Initially, the ratios of outputs of controllable DGs to their respective power ratings are properly defined. Assuming the i^{th} DG is controllable, the active and reactive power ratios can be evaluated. Fig. 2.8 depicts the block diagram of the proposed distributed control for reactive power-sharing.

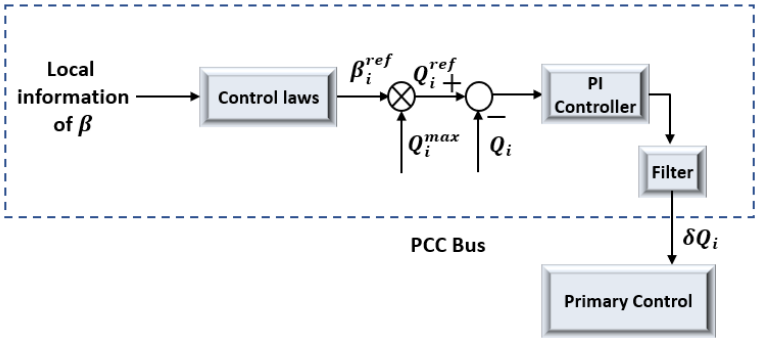

Fig. 2.8 Block diagram of the proposed distributed control for reactive power sharing [91]

$$\alpha_i = P_i/P_i^{max} \tag{2.10}$$

$$\beta_i = Q_i/Q_i^{max} \tag{2.11}$$

where α_i and β_i denote active and reactive power ratios, P_i and β_i are active and reactive power outputs of controllable DG_i, P_i^{max}, Q_i^{max} are active and reactive power ratings of DG_i, respectively. Agents can gather the information on reactive power outputs of controllable DGs to which they are connected. Hence, getting the information, the reactive power ratios can be determined via agents as in (2.11), and then agents exchange the information of reactive power ratios with their neighbours on the communication network. Afterward, regarding the control laws and attained information, the average reactive power ratios of neighbouring controllable DGs can be determined, i.e., the reference reactive power ratios, as shown in Fig. 2.8.

MAS-based synergetic control is proposed in [92]. The consensus-based secondary control is first proposed and established in [93], where reactive power-sharing and convergence rate problem remains for further research. The research studied in [94] offers a consensus-based control for a lossy network, but then again, voltage convergence appears to turn into a matter. Some other studies [82, 95-97] also address the consensus control at the secondary level to restore the voltage and frequency in a distributed way.

A distributed averaging proportional-integral controller for the secondary control is proposed in [98], considering the contradictory aims of voltage control and reactive power-sharing.

Frequency regulation and active power-sharing:

$$\omega_i = \omega_{ref} - m_{pi}P_i + \Omega_i \tag{2.12}$$

$$k_i \frac{d\Omega_i}{dt} = -(\omega_i - \omega_{ref}) - \sum_{j\in N_i} a_{ij}(\Omega_i - \Omega_j) \tag{2.13}$$

where Ω_i is the secondary control variable, and k_i is a positive gain. The first equation is the standard droop controller with the additional secondary control input Ω_i.

Voltage regulation and reactive power sharing:

$$E_i = E_{ref} - n_i Q_i + e_i \tag{2.14}$$

$$\kappa_i \frac{de_i}{dt} = -\beta_i(E_i - E_{ref}) - \sum_{j \in N_i} b_{ij} \left(\frac{Q_i}{Q_{imax}} - \frac{Q_j}{Q_{jmax}} \right) \tag{2.15}$$

where e_i is secondary control variable, Q_{imax} is the i^{th} DG's reactive power rating, and β_i, κ_i are positive gains. Then $n \times n$ matrix B with elements $b_{ij} > 0$ is the adjacency matrix of a communication network between the DGs. The secondary controller achieves a tunable compromise between voltage regulation and reactive power-sharing.

The application of distributed finite-time control for distributed secondary control and power-sharing is studied in [99, 100]. Some other techniques like MPC [101-103], feedback linearization [93], secondary control based on fuzzy logic [104], and Global Positioning System (GPS) based control [105] are also proposed for restoring voltage and frequency. In this method, each DG at the primary control level is synchronized with a common synchronous frame through GPS timing technology.

The study proposed in [106] shows a cooperative secondary voltage and frequency control strategy to reduce the number of controller updates by using an event-triggered approach [106]. The proposed approach is applied to the secondary control that will offset primary control deviations in islanded MGs with limited computation resources. The controller updating mechanism considered here is event-triggered which judges whether a certain measurement error has reached the event-triggered condition (ETC) associated with the norm of a function with a standard state. Two secondary control options to form an ETC are considered, including a centralized strategy in which an auxiliary controller would collect all agents' states, and a distributed control strategy which only requires the neighbouring agents information. The corresponding stability and convergence analyses are presented and simulation results for an islanded MG test system consisting of four distributed generators (DGs) are provided. The simulation results validate the effectiveness of the proposed control strategies and show that the proposed strategies based on an event-triggered approach can dramatically reduce controller updates.

The even triggering mechanism can be divided into two types according to whether each agent updates the control input at the same time, that is, centralised triggering and distributed triggering, as shown in Fig. 2.9 and Fig. 2.10, respectively. The occurrence of an event is defined by the event-triggered time generator which judges whether a certain measurement error has reached the ETC associated with the norm of a function with standard states. Voltage control is taken as an example to describe the event-triggered scheme; the stated process can easily be extended to frequency control.

Centralised Approach:

The control input u_i for voltage control is described as:

$$u_i = k_v\left[\sum_{j\in N_i} a_{ij}\left(v_{dj} - v_{di}\right) + g_i\left(v_{ref} - v_{di}\right)\right] \tag{2.16}$$

where $k_v \in R$ is the control gain for voltage control and g_i is the weight of the edge by which DG i is connected to the reference node v_{ref}. It is assumed that at least one node i receives information from the reference node v_{ref}.

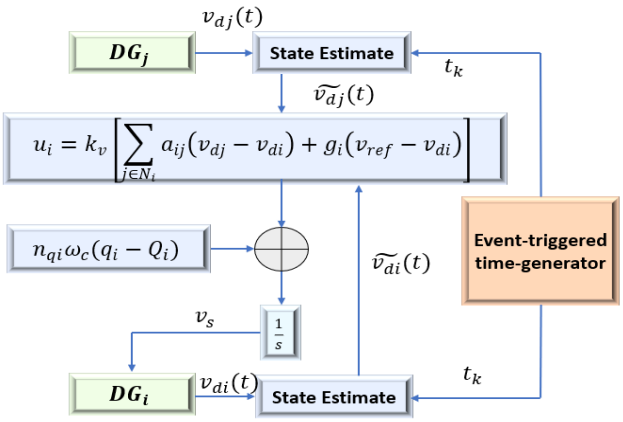

Fig. 2.9 Centralized event-triggered time generator [106]

Distributed Approach:

Unlike the centralised approach, each agent in the distributed approach will have a different event-triggered time. The distributed control input u_i for agent i is

$$u_i = k_v\left[\sum_{j\in N_i} a_{ij}\left(v_{dj}(t_k{}^{r\,j}) - v_{di}(t_k{}^{i})\right) + g_i\left(v_{ref} - v_{di}(t_k{}^{i})\right)\right] \tag{2.17}$$

For each $t \in [t_k{}^{i}, t_{k+1}{}^{i}]$, $t_k{}^{r\,j}$ is the last event time of agent j.

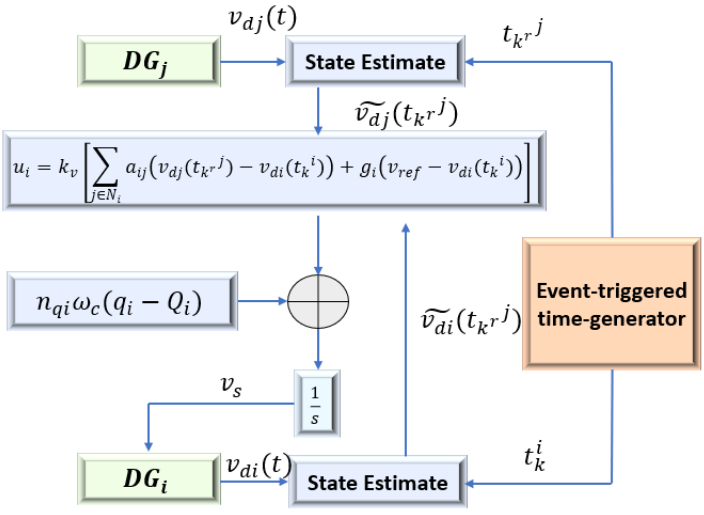

Fig. 2.10 Distributed event-triggered time generator [106]

2.4.3 Tertiary Control Level

The purpose of the level control is to manage power flow by regulating amplitude voltage and frequency when the MG is in grid-connected mode. By measuring the P/Q ratio through the PCC, the grid's active and reactive power can be compared against the desired reference. A simple structure of the tertiary control is shown in Fig. 2.11. The frequency and voltage reference defined in the below equations are used in secondary control [89].

$$\Delta f = G_{pp}\left(P_{grid}^{ref} - P_{grid}\right) + G_{ip}\int (P_{grid}^{ref} - P_{grid})dt \tag{2.18}$$

$$\Delta v = G_{pq}\left(Q_{grid}^{ref} - Q_{grid}\right) + G_{iq}\int (Q_{grid}^{ref} - Q_{grid})dt \tag{2.19}$$

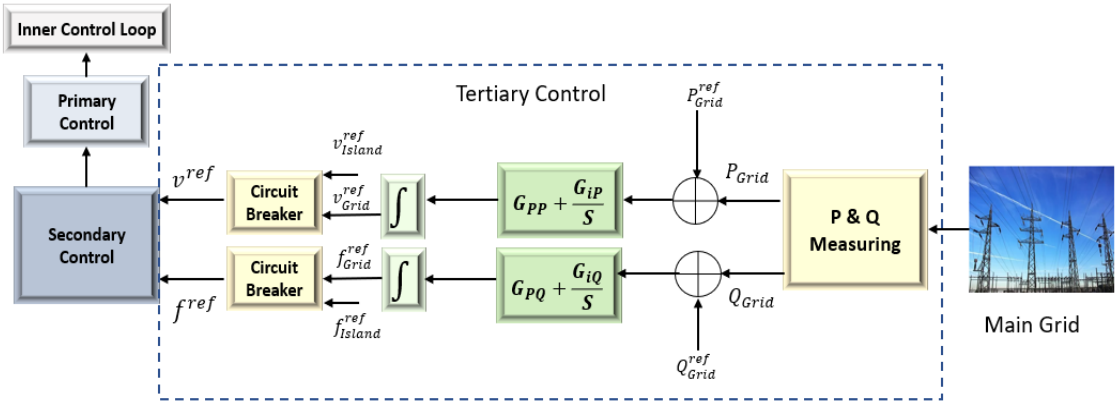

Fig. 2.11 Tertiary control level structure [89]

The details of these equations can be found in [89]. Tertiary control level is the last (and the slowest) control level that reflects the cost-effective matters of the MG and accomplishes the power flow between the MG and the main grid. In the latest studies, the goal of tertiary control is to familiarise intelligence of the entire network. In consequence, tertiary control will undertake to maximise the MG operation on the basis of merits of interests, mostly efficiency and economics. Information from both the MG side and external grid is crucial to implementing the optimisation functions. Information and communication technology (ICT) is a significant mechanism for that reason. Optimization algorithms can be utilised to develop the gathered information and take appropriate actions. In conventional power systems, the tertiary-level control resolves economic dispatch in a centralised approach [107]. In comparison, the cost-effective matter is minimized asymptotically by properly scaled droop controllers in an entirely distributed way, online, and without requiring a model as presented in [108]. At the tertiary control level, MAS-based control techniques can be implemented for MG power management. The smart agents can adjust the given performance index (minimizing task, maintenance, and fuel prices, or minimizing the environmental influences). Some of the control strategies mentioned above are briefly summarized with advantages and disadvantages in Table 2.1.

Table 2.1 Comparison of Different Distributed Control Schemes at the Primary and Secondary Control Level

Control level	Methodology	Advantages	Disadvantages
Primary control level	• Conventional Droop Control [38, 49, 51, 52] • Q-V dot droop [109, 110]	• Simple control structures to implement • Stability is maintained	• Applicable for highly inductive transmission lines • Inaccurate reactive power-sharing • Poor performance for non-linear load
	• VPD/FQB based Droop[111]	• Good performance in highly resistive line • Simple structure to implement	• Dependent on system parameter variation • Poor performance for non-linear load
	• Multi-variable Based [61] • Universal Droop [62] • Pining Droop	• Maintaining good voltage and frequency regulation with accurate power-sharing with different output impedances	• Implementation difficulty in large systems
	• Adaptive Voltage Droop[112]	• Good voltage regulation and power-sharing even with heavy loads	• System parameters should be identified in advance
	• Voltage-current droop[16]	• Applicable for high-resistance network of MG • Accurate power balancing	• Complex structure for practical implementation
	• Virtual Output Impedance with Droop Control[27,31,32]	• Improves the performance of power-sharing	• System stability is a great concern
	• Virtual Flux Drooping [54]	• Good frequency regulation	• Slow dynamic performance • Not suitable for large system
	• Angle Droop [113]	• Good frequency regulation	• Poor power-sharing
	• Hybrid/Signal Injection based droop [114]	• Suitable for linear and non-linear load • Independent of system parameter variation	• Complex system structure to implement • Poor voltage regulation due to harmonic issues
	• Non-linear load sharing based droop [60]	• Precisely share the current harmonics and cancels the voltage harmonics	• Poor voltage regulation • Dependent on system parameters
	• Predictive control-based algorithm [86] • Predictive power control [40]	• Suitable for use in non-linear systems, less switching frequency • Proper current control with comparatively lower THD and harmonics	• Requires complex computing • Complex control structure • Dependent on system parameter variations
	• GPS-based primary control [105]	• Take advantage of GPS timing technology and remove the transformation errors resulting from Park / inverse Park Transformations • Independent of system parameters.	• Need to incorporate the GPS timing into grid-connected control applications
	• Consensus-Control [35,36] • Consensus-based p-f droop Control	• Increase flexibility, support plug-and-play, use low bandwidth communication networks	• Voltage convergence is a major concern • Need to choose cluster parameters correctly to establish stability condition
	• Consensus-based distributed voltage control [33,35,36,] • Consensus-based distributed frequency control [43, 95, 96, 115, 116]	• Enhanced redundancy and good for plug-and-play functionality, increased flexibility • Use low bandwidth communication	• Convergence rate is a great concern • System stability is affected by the system parameters

Secondary control level	• MAS Control [33-35]	• Capable of handling uncertain disturbances and decentralised data updating, causing a faster decision-making method and action • Increase flexibility and computational efficiency	• The coordination and synchronization process requires the exchange of information among agents based on some restricted communication protocols
	• Distributed finite-time control [99]	• Robust system with respect to parametric uncertainties, unmodeled dynamics, and disturbances that increases system reliability	• Cannot ensure robust stability • Cannot restore frequency/voltage in a finite time separately
	Methodology	Advantages	Disadvantages
	• Distributed Average Proportional Integral based on Consensus [39]	• Offer a flexible plug-and-play architecture with frequency and voltage regulation along with precise active and reactive power-sharing	• Synchronization problem of voltage and frequency restoration
	• Model Predictive Control [42-44]	• Can maintain stable operation as well as timeously deal with the uncertainties such as time-varying communication topologies, parameter perturbations, and load disturbances	• Complex structure, reactive power-sharing and restraining circulating currents deserve further investigation.
	• Feedback Linearization [93]	• More reliable • Feedback linearization converts the secondary voltage and frequency controls to a first-order tracking synchronization problem	• Frequency restoration depends on system parameters.
	• Fuzzy Logic based secondary control [45]	• Independent of parameter variations • Suitable for non-linear system	• Slow control process
	• GPS based secondary control [105]	• Large time constant at the secondary level enables working with a low bandwidth communication network • Independent of system parameter variation	• Require integrating the GPS timing into grid-connected control applications

2.5 DISTRIBUTED CONTROL OF ENERGY STORAGE UNITS

2.5.1 Structure of Energy Storage Systems in MGs

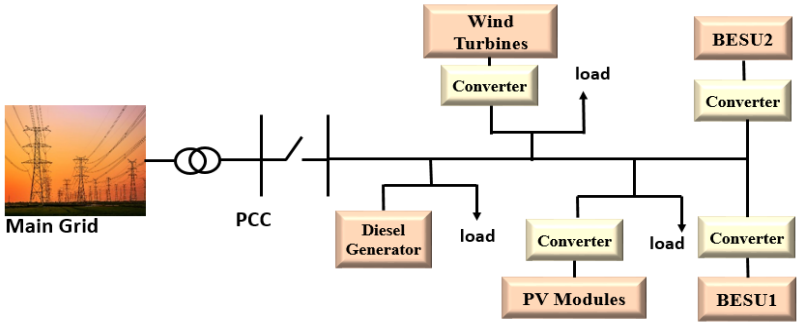

Fig. 2.12 A simple MG structure with battery energy storage units (BESUs)

Fig. 2.12 presents the typical architecture of an MG. The MG is linked via *PCC* to the main grid. In this chapter, DESU is considered as BESU. Two Battery Energy Storage Units (BESUs) and three DGs are in this MG. One of the DGs can generate electricity and heat at the same time. In general, an MG is operated two modes of operation, namely islanded mode and grid-connected mode. A transmission switch is located at the *PCC* because of mode transfer. MG requires to fix the unbalances between the loads and the renewable generations and gives ancillary assistance to the main power grid in grid-connected mode [19], i.e., the main grid can trade power with the MG and assist the MG stability. Within the islanded mode, the supply must locally match the demand. In both modes, the coordination of numerous BESUs is essential for the MG operation. In general, BESUs stabilise the loads and the renewable generations by means of charging or discharging their power [19].

BESUs usually work together with DG units, including photovoltaic (PV) panels, wind turbines, etc. For PV panels, the BESUs work either in charging or discharging mode according to the output power of PV panels. Balancing the power between renewable energy sources (RESs) and local loads is the key function of the BESU throughout the day. At night-time, the BESU is a grid-forming unit due to the deficiency of solar energy. As such, only BESUs are desired to offer stability and reliability support to the islanded MG. The output power of the DG units and BESU should be coordinated to supply the load in regard to the DG capacity and ESS state-of-charge (SoC) to prevent operation failure of MGs.

2.5.2 Different Types of Energy Storage System (ESS)

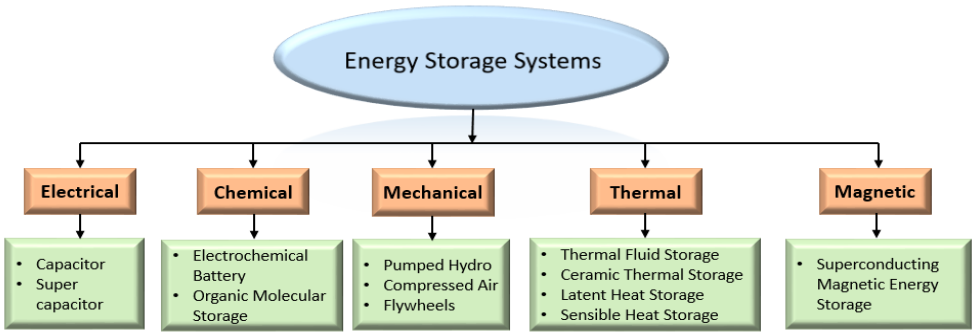

Fig. 2.13 Classification of ESSs

Despite developments in technology, electricity cannot be put in storage in the electrical form on a large scale. It can be kept in gravitational, adiabatic, mechanical, chemical, thermal, magnetic or other forms [117]. The energy storage system (ESS) can be categorised with its power and energy density, lifespan, ramp rate, etc. So far, none of the ESSs can properly fulfil the power system constraints.

Fig. 2.13 categorises diverse ESSs established on their primary energy supply. As seen, the ESSs are allocated into 5 groups, electrical, mechanical, thermal, electrochemical and magnetic. Currently, the most familiar ESS worldwide is the battery energy storage system (BESS) [118-120]. It is an electrochemical ESS producing or absorbing electrical power through a chemical response. Every battery is built of various stacks. To gain higher power and energy density, various BESSs should be coupled in parallel and series. There exist various kinds of BESS, for instance, lead-acid, nickel, sodium-sulphur, lithium-ion, metal-air batteries, etc.

[121]. As well as the BESS, some of the hydrogen-based production units; in particular, fuel cell (FC) can be sorted as the chemical ESSs. In this instance, the presence of the hydrogen reservoir offers the possibility of electricity generation when it is necessary. The pumped-hydro storage power plants are believed to be an ESS with huge energy density employed in the power system for years [117, 119, 121, 122]. This system reserves water in two reservoirs; high and low height reservoirs. When electrical energy is requisite, the water moves to the lower-height reservoir during the demand of electrical energy, and the potential energy is transformed to first kinetic and later to electrical energy.

2.5.3 Control methods of ESS/BESU in MGs

In recent years, BESUs have been usually employed in MGs to improve power quality and network reliability. Further, they can function as energy buffers to manage renewable generation because of the uncertain behaviour of renewable energy sources (i.e., PV and wind farms) as well. There are many studies on the operation and control strategies of ESSs in MGs. Similar to the control of DGs, ESS/BESU control also uses a hierarchical control framework which has three control stages in different time domains, termed as primary, secondary and tertiary control.

A. Primary control level

Primary control is the first control level which is started immediately after a variation in MG parameters such as frequency, voltage or load variations and tries to retain the frequency and voltage in stable ranges. The operation time of this level is about several milliseconds. The primary control layer is the fastest level in the hierarchical control system [123].

The main objectives of the primary control for energy storage units are:

- Frequency and voltage control
- Active and reactive power-sharing
- SoC balancing

At the primary control stage, one usual applied strategy is decentralised droop control that is relied just on the regional information of BESUs, excluding the necessity of any interaction [117, 124, 125]. Highlighted the fact that the standard f- P and V- Q droop control is not appropriate for BESUs as it does not reflect SoC levels of BESUs at all. Therefore, SoC-based droop control is considered in [124] to correct the reference frequency/voltage of MGs. It is normally stated that the droop control presents frequency/voltage fluctuations from their standard values, so degrading the correctness of power-sharing and frequency/voltage control. The main limitation is the BESU with a lower initial SoC is depleted sooner than that with a higher initial SoC and thus cannot contribute to the power-sharing any longer. Besides, operating the BESUs at a low SoC reduces their lifetime and efficiency [71]. The SoC of a BESU is also affected by the remaining end period, temperature of the atmosphere, operational competencies for the charging and discharging of the BESU [78].

The traditional power-sharing strategies predominantly aim for the identical power-sharing ratio according to their rated capacities among BESU units as presented in [124, 126]. This situation may reduce the

overall utilisation efficiency of the available BESUs because the BESU element with the highest SoC should produce the most power to the common loads, and a BESU unit needs to be turned off when its SoC is lower the threshold during the peak load period to ensure a balanced SoC utilisation.

B. Secondary control level

As a result of transients in power produced by RESs and difference on the demand side, there exist several unexpected circumstances that can happen throughout MG operation. An SC is implemented for frequency and voltage restoration of the MG in response to usual operating requirements after every change. In the SC stage, all the compulsory information is gathered from the DGs, BESUs, and loads, and the updated reference values are directed to the primary control stage. The block diagram of this control layer is presented in Fig. 2.7. The key intention of the SC is to adjust the properties of the droop control to bring back the frequency and voltage to their reference values [127]. The secondary control has some added accountabilities for the storage system. The BESU operation may fail if only the BESU is involved in stabilizing the MG. As shown in Fig. 2.7, the output power set-point of each MG should be measured as well as dispatched using the secondary control function. First, based on the IEC/ISO 62264 standards, the accountability of the SC in the storage system is observing the system fluctuation. Next, SC compensates the power differences which results from the primary control of the storage system. As stated in Section 2.5.3-A, it is the local controls that are eventually accountable for supervising the output power locally in each element, whereas the SC compares the measured output power of the storage system with the reference value to find the deviation. The total demanded power for charge and discharge is acquired with this inaccuracy (Fig. 2.14).

Authors in [124] recommended SoC balancing technique. Before presenting the SoC balancing technique, the expression of traditional *P–f* droop control is introduced first. The conventional *P–f* droop control expression [128] discussed earlier is as follows:

$$\omega_i = \omega_{ref} - m_{pi} P_i$$

The SoC of DESU can be defined as follows:

$$S = S_0 - \frac{1}{C} \int i_{dc} dt \tag{2.20}$$

In (2.20), S_0 is the initial SoC value, C is the capacity of the DESU, i_{dc} is the output DC current of the battery. Let P_{dc} and v_{dc} denote the DC output power and voltage of the DESU and *P* denote the active power of VSI. Assuming the power loss of the interfacing VSI is negligible, we have $P \approx P_{dc} = v_{dc} i_{dc}$, where the DESU is operating with unity efficiency (i.e., η = 1). With the above assumption, Eq. (2.20) can be re-written as:

$$S = S_0 - \frac{1}{C} \int \frac{P}{v_{dc}} dt \tag{2.21}$$

Therefore, the control of the output active power of DESUs can be used for the SoC-balancing strategy. In a DESU parallel-connected system where the capacities of DESUs are not same, as stated by (2.21), the SoC balancing of DESUs will be changed by S_0, *P*, and *C*. If the active powers *P* of two DESUs are sharing and S_0

are the same, the SoC balancing cannot be achieved due to the C. With the intention of achieving SoC balancing of DESUs with different capacities, a droop-based SoC balancing technique is offered as follows [124]:

$$\omega_i = \omega_{ref} - \frac{m_{pi}}{C} P_i (1 - k_S S_i) \tag{2.22}$$

where m_{pi} and k_S are the droop coefficients. Fig. 2.14 shows the block diagram of the proposed SoC balancing scheme.

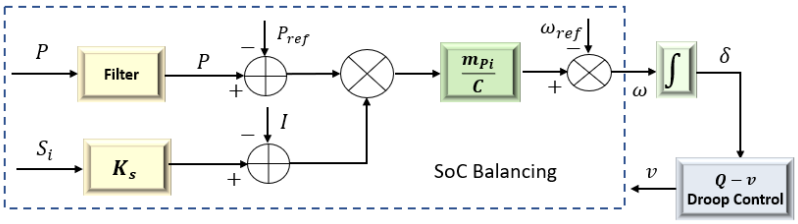

Fig. 2.14 Block diagram representation of SoC balancing [124]

Contrasting to the primary control stage−in which a decentralised control loop is employed, and a controller is situated alongside every DG and DESU−SC can be applied as either centralised, decentralised or distributed control techniques which are designated in the next subsection. The centre of attention of this doctoral thesis is on the DSC. One drawback of implementing an MGCC in the SC is that it may fail, which can disturb the reliability of the MG. To clarify this, a DSC can assist as a replacement to upgrade the reliability of the MG. In the decentralised approach, the primary and SCs are combined and are linked to a local controller. The grouping of the control system framework is the same as the case of controlling the BESUs and follows the same standard as the DG control. The DSC strategies, which can overcome some disadvantages of centralised control strategies, are suitable for the BESUs coordination control in the smart grid. In summary, the primary objective of DSC for energy storage units are as below:

- Frequency and voltage restoration
- Active and reactive power-sharing
- SoC balancing

Numerous studies have been performed in recent times on the BESSs coordination control. A brief overview on different exiting methods of decentralised/distributed SC is described below:

Droop-based Methods

The conventional droop control method can be employed in battery energy storage systems (BESS) of an MG utilising centralised and decentralised control strategy. This control technique is analogous to the control of synchronous generators where frequency and voltage drop in proportion to the generated active and reactive power, respectively [124]. In [129], a droop-based control strategy with voltage restoration is proposed. The control of an islanded MG, including ESSs with different capacities, is studied in [124]. A multifunctional droop control strategy for ESS units is proposed in [130]. In these works, the ESS characteristics, such as their energy and power density, have not been considered.

BESS can be used to deliver controllable MG storage. Each DESU comprises a battery and a four-quadrant inverter permitting control of the real and reactive power it injects or absorbs from the MG. To preserve network stability, the DESU must be controlled to balance the mismatch between power generation and demand in the MG. This can be achieved with the droop control method, which also delivers power-sharing between the DESUs[131].

$$\omega_i=\omega_{ref}\text{-}m_{pi}(P_i - P^*) \tag{2.23}$$

$$v_i=v_{ref}\text{-}n_{qi}(Q_i - Q^*) \tag{2.24}$$

where P^* and Q^* are the real and reactive power references. To utilise the power capacities of DESUs to maintain the voltage frequency and magnitude, the droop coefficients should be set as below so that we will get the equations (2.25).

$$m_{pi} = \frac{\omega_{max}-\omega_{min}}{2P_{max}},\ n_{qi} = \frac{v_{max}-v_{min}}{2Q_{max}} \tag{2.25}$$

The real droop control equation in (2.23) is modified so that

$$\omega_i=\omega^*\text{-}\frac{m_{pi}}{\alpha}(P_i - P^*) \tag{2.26}$$

where $\alpha = \max\left(\frac{E-E_{min}}{E-E_{min}}, 0.01\right)$

In these equations, E is the current DESU energy and E_{max} and E_{min} are the battery energy limits. The value of α is limited to 0.01 to prevent $\frac{m_{pi}}{\alpha}$ from going to infinity. When the DESU device is full, α=1 and the full real power capacity of the inverter is utilised. Based on the equations mentioned above, a new control strategy is developed in this paper [63]. A BESS is a master such as a slack bus in traditional power systems, and the other BESSs help it for MG control. The master BESS *P–f* droop equation is as follows:

$$f = f_{ref} - m_{pi}P_i + (k_p + \frac{k_i}{s})(S_{ref} - S_i) \tag{2.27}$$

where f_{ref} is the desired frequency and S_{ref} is the intended SoC for master DESU. The difference between the S_{ref} and S_i (estimated value) passes through the proportional-integral (PI) controller. Authors in [71, 132] proposed a droop-control-based method of BESU SoC balancing for an MG during the islanded operation. The frequency and voltage are considered with SoC balancing, but the dynamics of the system, like plug-and-play capability, fault occurrences, etc., are not discussed. In [122, 132, 133], various distributed SoC balancing control approaches are proposed to deliver safety redundancy in preserving BESS units from over-charging or over-discharging, based on vector control methods. Vector control, which originates from the control of electric machine drive systems, is widely adopted for controlling the three-phase inverters to convert DC power to AC power by the *abc* to *d-q* transformation. However, an extra synchronization unit, e.g., the phase-locked-loop (PLL), is required for the *abc* to *d-q* transformation. The PLL dynamics may cause stability problems for inverters, particularly in weak grids, and the response of PLL will also affect the control performance [134]. In the above-mentioned control methods, the voltage and frequency recovery cannot be done by applying the droop-

based SoC balancing techniques. Hence, researchers search for reaching the SoC balancing amongst multi-ESSs at the secondary stage by distributed control approaches [71, 78, 124, 127]. Some distributed control methods are discussed below.

Consensus Control/ Multi-Agent Based System

Distributed multi-agent control approaches have been proposed for both the secondary and tertiary control stages of MGs along with distributed BESUs. At the secondary level, each BESU works as an autonomous agent, sharing data among neighbouring BESUs (e.g., SoC level, output power) to manage load sharing and reach cooperative goals. With the intention of achieving global coordination among DGs or BESUs, consensus-based distributed controls are extensively suggested. As stated in [135], a leaderless consensus mechanism is presented by means of neighbour interaction to offer new references of the control level. In [136], a leader-follower consensus algorithm for distributed BESUs in distribution networks is introduced. A finite-time consensus approach in support of secondary voltage and frequency restoration of DG units is recommended in islanded AC MGs [137]. Consensus control methods of BESUs in MGs are investigated in [71, 117, 137-139]. For instance, an optimal distributed consensus controller for BESUs is offered in [71]. Nevertheless, it is essential to calculate the smallest positive eigenvalue of the communication graph during the controller design; this indicates the control approaches are not distributed. A distributed cooperative control method for SoC balancing among the battery modules of BESUs is analysed in [122], which synchronises the SoC levels of all BESUs in an MG employing its neighbour's data. The authors in [117] propose a dynamic energy level balancing method among distributed storage elements as a strategy for frequency regulation and reliability in droop-controlled MGs. This is accomplished with a distributed multi-agent cooperative control system which amends the output power of droop-controlled storage devices so that they achieve a balanced energy level. A control input saturation constraint is established, guaranteeing that the cooperative control mechanism will not burden the MG storage elements.

A multiagent-based distributed control algorithm has been proposed to achieve SoC balancing of DESUs in an ac microgrid [140]. The authors proposed the following equations for SoC balancing:

$$\omega_i = \omega^* + K_s(S_i - S_{mean}) \tag{2.28}$$

$$= \omega^* + \frac{K_S}{N}\sum_{k\neq i}(S_i - S_k)$$

The consensus approach used here is based on the dynamic average consensus algorithm [141], which is the discrete-time algorithm of [18]. The information discovery process for agent i is represented as follows:

$$S_{mean\_i}\,[k+1] = S_i\,[k] + \sigma \sum_{j\in N_i} \delta_{ij}\,[k+1], \qquad (i \neq j)$$

$$\delta_{ij}\,[k+1] = \delta_{ij}\,[k] + S_{mean\_j}\,[k] - S_{mean\_i}\,[k], \quad (i \neq j)$$

S_i is the measured SoC of DES unit i, and σ is a scaling factor, which is designed according to the trade-off between convergence speed and stability [141].

All the stated references simply reflect BESUs as homogeneous components and overlook the consequence of the heterogeneous property of batteries. A multi-agent consensus control for heterogeneous BESUs using a hierarchical control framework is developed in [138], but the suggested asymptotic controller can only assure global asymptotic stability of the BESUs, denoting that consensus can be achieved only over an infinite settling duration. A novel distributed finite-time control technique for heterogeneous BESUs in droop-controlled MGs is recommended in [139]. The proposed consensus-based technique is applied to reach energy level balancing, active/reactive power-sharing, and voltage/frequency synchronization of energy storage elements by employing inter-BESU information-sharing, where the heterogeneous property of batteries and hierarchical control framework are taken together into attention. Distributed multi-agent SoC balancing along with robustness to communication delays is offered in [132]. Nevertheless, less research has been conducted considering the SoC balancing in DSC of BESUs for AC MGs, which is truly a significant matter to be investigated.

Authors in [79] present a novel distributed finite-time control system for heterogeneous DESUs in droop-controlled MGs. Dissimilar to the current centralised control techniques, the proposed control strategy is completely distributed so that every DESU just needs its own information and the information from its neighbours via a sparse communication network. The proposed consensus-based technique is employed to accomplish energy level balancing, active/reactive power-sharing, and voltage/frequency synchronisation of energy storage devices by using inter-DESU communications, where both the heterogeneous nature of batteries and the hierarchical control structure are considered. In the proposed method, the dynamics of droop controllers and the heterogeneous nature of each battery of the DESU model can be formulated as follows:

$$\dot{E}_i=\frac{-K_i^E}{3600}P_i+u_i^E, \tag{2.29}$$

$$\dot{P}_i=u_i^P, \tag{2.30}$$

$$V_i = V_i^{nom} - K_i^Q Q_i, \tag{2.31}$$

$$\omega_i = \omega_i^{nom} - K_i^P P_i \tag{2.32}$$

where coefficient K_i^E represents the heterogeneous nature of each battery in the droop-controlled microgrid, and u_i^E and u_i^P are the control inputs of energy level and active power of the i^{th} BESS, respectively. Denote $\widetilde{P}_i = K_i^P P_i$ and $\widetilde{Q}_i = K_i^Q Q_i$, $\forall\, i \in \{1, \dots\dots, N\}$. The active/reactive power sharing accuracy of BESSs can be guaranteed by the consensus of $\widetilde{P}_i$ and $\widetilde{Q}_i$. The following distributed finite-time protocols are developed in [79] for active and reactive power-sharing.

$$u_i^E = c_E \sum_{j=1}^{N} a_{ij}\, sgn\,(E_j - E_i)\left|E_j - E_i\right|^{\alpha} \tag{2.33}$$

$$u_i^P = \frac{c_P}{K_i^P} \sum_{j=1}^{N} a_{ij}\, sgn\left(\widetilde{P}_j - \widetilde{P}_i\right)\left|\widetilde{P}_j - \widetilde{P}_i\right|^{\alpha} \tag{2.34}$$

$$u_i^Q = \frac{c_Q}{K_i^Q} \sum_{j=1}^{N} a_{ij}\, sgn\,(\widetilde{Q_j} - \widetilde{Q_i})\left|\widetilde{Q_j} - \widetilde{Q_i}\right|^{\alpha} \tag{2.35}$$

where c_E, c_P and c_Q are positive control gains, and $0<\alpha<1$. Similarly, the distributed finite-time voltage and frequency protocols are designed as follows:

$$u_i^v = c_v \sum_{j=1}^{N} a_{ij}\, sgn\,(v_j - v_i)\left|v_j - v_i\right|^{\alpha} + g_i\, sgn\,(v_{ref} - v_i)\left|v_{ref} - v_i\right|^{\alpha} \tag{2.36}$$

$$u_i^{\omega} = c_{\omega} \sum_{j=1}^{N} a_{ij}\, sgn\,(\omega_j - \omega_i)\left|\omega_j - \omega_i\right|^{\alpha} + g_i\, sgn\,(\omega_{ref} - \omega_i)\left|\omega_{ref} - \omega_i\right|^{\alpha} \tag{2.37}$$

where c_v and c_{ω} are positive control gains. Fig. 2.14 represents the block diagram of the proposed control in [79].

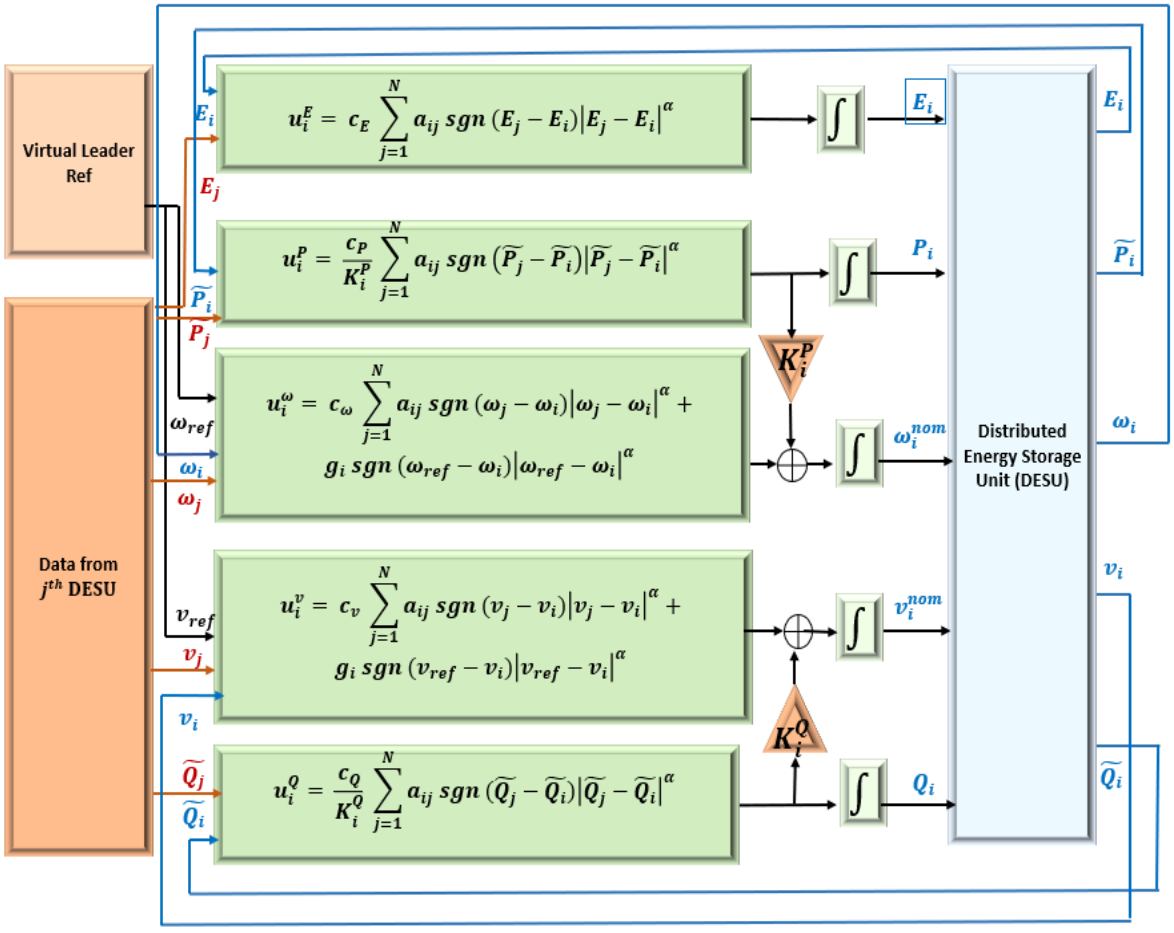

Fig. 2.15 The diagram of distributed finite-time control scheme of DESUs [79]

Other Distributed Methods

Depending on the distributed control framework, several control techniques have been applied to coordinate numerous DGs. The active power-sharing and frequency synchronization problem for an islanded AC

MG is investigated in [81] based on primary frequency droop control and DSC, respectively. Then, the work is extended in [72] to develop a common and entirely distributed network for secondary frequency and voltage control in islanded MGs. A distributed averaging proportional-integral controller is recommended to achieve a compromise between voltage regulation and reactive power-sharing. Another distributed secondary voltage control scheme is presented in [93], where the voltage regulation issue is converted to a synchronization limitation by using the feedback linearization technique. A distributed control method using low-bandwidth communication is offered to guarantee proportional load sharing and increase voltage quality in a DC MG [142]. In [127], with the aim of maintaining the frequency and voltage stability, a distributed networked algorithm is employed to model the SC in a droop-controlled MG. The above-mentioned approaches are applied to coordinate the DGs rather than the BESUs.

In power systems, the ability of MPC can be applied to reduce operational costs and BESUs degradation as well as simultaneously progressing renewable energy consumption. In [143], a distributed MPC technique is offered to synchronise the BESUs for voltage control. Likewise, the distributed MPC technique is applied as well to handle the optimization issue of BESUs to maintain supply-demand balance and preserve voltage and frequency stability [120]. Conversely, the distributed method in [144] does not consider the SoC balance of BESUs, which may consequence in the overcharging and over-discharging actions of BESUs. On the other hand, the objective in [119] is to smooth the wind power based on an MPC strategy with operational constraints by selecting accurate battery energy storage sizing. The control structure is twofold: the outer loop determines the expected set-point power in the next hour, and the inner loop ensures the actual output power to follow the set-point power by charging/discharging the BESU. The progresses in energy planning, succeeded with MPC, are emphasised over compatibility with a heuristic-based technique, like Fuzzy inference.

Lastly, the effort in [118] practices MPC to develop demand response abilities in an MG to progress the PV power usage. The latest findings associated with the application of MPC in power systems have concentrated on employing them on large-scale electricity networks, applying online distributed optimisation methods to minimise operational costs [145]. The prior efforts are emphasised primarily on adopting MPC for grid-connected networks through the goal of economic optimisation (operating cost or energy arbitrage). Conversely, the ability of the MPC can handle outside of this. Islanded MGs exhibit a fascinating and applicable application for MPC-based energy management, allowing the raising possibility of similar operation in future grids. The management of islanded MG is more difficult because of the shortage of an unlimited energy reservoir in the form of main grid, to mitigate imbalance power that cannot be supplied by the ESS and load. This needs power reduction capability and dispatchable generators to guarantee reliable operation. Islanded MGs also necessitate a hybrid BESU of high energy and power density to handle the islanded operation. In this background, MPC can be operated in islanded MGs beyond the field of economic optimisation [146, 147].

C. Tertiary control level

Generally, the main objective of this level is the economic or market problems [118, 145, 148]. At the tertiary stage, distributed multi-agent implementations of the Dynamic Optimal Power Flow (DOPF) agree cooperative autonomous agents with limited network information to settle on a set of optimal MG energy flows

by iteratively resolving restricted size sub-problems in parallel and sharing their outcomes with their neighbours [149]. An alternative to a cooperative tertiary-level control for DOPF is an economic tertiary-level strategy [150]. Under a competitive strategy, autonomous agents endeavour to maximise their local utility established on price details.

2.6 SUMMARY

Many research works have been accomplished on the design of autonomous MG control systems over the last decade. In the latest research trends, the concept of MG control has been shifting to distributed control to lessen the computational and communication requirement due to the high penetration of DGs. The main contribution of this chapter is to provide a brief review of the existing distributed control techniques mentioned in the literature so far for autonomous AC MGs with DGs and ESUs and categorizes them with a comparison based on their design approach and viewpoint.

Chapter 3: Distributed Secondary Control for Frequency Restoration and Active Power Sharing

3.1 INTRODUCTION

Secondary Control (SC) structures in a distributed way have been initiated for the control of MGs mainly to reduce the system's cost and complexity while contributing more to the dynamic performance of the system. Typically, distributed control methods are based on multi-agent systems or consensus protocols [43, 151]. Distributed control based on a consensus algorithm exhibits a good performance utilising a sparse communication system. However, the dynamic behaviour of MG with DSC is responsible for introducing the unwanted characteristics related to the system damping, response time, and stability region. Transfer function [152] based approach, state-space modelling and small-signal analysis with initial condition and estimating the eigenvalues in the time domain, and the impedance-based method in the frequency domain [153] are the most common techniques for the stability analysis in detail. The main advantages of impedance analysis and the eigenvalue analysis methods are reducing the computation time while controller dynamics and the grid impedance are considered. The latter two methods are therefore more appropriate for the stability analysis with power electronics interfaced power systems. In this chapter, a detailed stability analysis with state-space modelling based on the eigenvalue-analysis approach is conducted to see the effect of the proposed Distributed Secondary Frequency Control (DSFC) on the overall system stability.

Furthermore, another key concern needs to be further researched which is based on cost minimisation. The MG control system should be designed to get the economic benefit and stability of the MG while regulating the active power balance. Most of the prior works only considered the case that the power outputs (both active and reactive) from inverters can proportionally share the total load in accordance with their power ratings [154]. An optimal amount of output power, a combination of all generators, is a suitable solution for lowering the operational cost and, at the same time ,retaining system generation demand steadiness constraints. There are some active power control systems for cost minimisation which have been proposed in the last few decades. In [42], an equal increment cost theory based droop control approach is suggested to reduce the overall generation budget. However, the optimal control parameters are not considered. The work in [155] offered an active power sharing control arrangement both in a distributed and optimal way based on the equal incremental cost condition where the distributed approach is utilised for minimising the total generation costs of the system, while the detailed stability analysis is not taken into consideration. The key contributions of this chapter are:

- Restoring the system frequency at the nominal value ω_{ref} within a finite time.
- Minimising the operation cost by applying the optimal active power sharing using the equal-cost increment values of distributed generation (DG) units, i.e., $\eta_1(P_1) = \eta_2(P_2) = \cdots = \eta_N(P_N)$ where $\eta_i(P_i)$ denotes the cost incremental value function of i^{th} DG unit.
- The stability analysis represents the effect of DSFC parameters on system stability.
- Utilising the particle swarm optimisation (PSO) technique, the proposed DSFC shows better convergence and stability performance through the optimal control parameters.

3.2 DISTRIBUTED SECONDARY CONTROL

This section familiarises the conception of distributed control in the controller design for MG based on the proposed secondary frequency restoration scheme. The SC selects the accurate primary control reference for frequency synchronisation. In relation to the distributed control theory, the SC objectives are proposed, and then a DSFC law is designed for the MG to restore the deviated frequencies to the reference values. In the distributed control environment [43], a consensus problem is considered as one of the most vital and difficult problems. From a general point of view, the MG acts as a multi-agent system where every DG works as an agent in the consensus control. Agents can exchange the required data/information with their neighbours through a simple and less expensive communication network to achieve the consensus. In this section, some basics of graph theory and consensus-based DSFC are discussed.

3.2.1 Preliminaries

A. Graph Theory

A directed graph (digraph) $G = (N_G, E_G)$ with a set of N nodes, $N_G = \{1,2,3,4 \dots \dots N\}$, a set of edges $E_G \subset N_G \times N_G$ and an adjacency matrix $A_G = \left(a_{ij} \geq 0\right) \in R^{N \times N}$ (where $a_{ij} = 1$ if there is a path from the i^{th} node to the j^{th} node and otherwise $a_{ij} = 0$) is considered here. An agent is represented by each node, and each edge (i, j) (pointing from j to i) indicates that the information flows from j to i related with a_{ij}. The neighbors of node i are represented as $N_i = \{j \in N_G : (i, j) \in E_G\}$. According to this, an agent/node i only has access to the data from its neighbours in N_i. If every agent (node) can be represented as a single-state system defined by $\dot{x}_\iota = u_i$ where u_i is the input as a function of the i^{th} agent's neighbouring state $x_j, j \in N_i$, the common form of consensus protocol is as below:

$$\dot{x_\iota} = u_i = -\sum_{j \in N_i} a_{ij}\left(x_i - x_j\right) \tag{3.1}$$

B. Droop Based DG unit

Generally, in an MG system, every inverter interfaced DG comprises a primary constant dc power source, a voltage source inverter (VSI), an LCL filter (combining the LC filter with coupling inductor) and an output connector, as shown in Fig. 3.1. A test MG model of three DG units is considered here which are connected in parallel. Every DG is associated with the load and linked with neighbouring DG through feeder lines. The power

controller (Fig. 3.1) permits DG units to share the active and reactive power requirement according to their maximum ratings based on the droop gain, i.e.,

$$\omega_i = \omega_{ref} - m_{pi} P_i \tag{3.2}$$

$$v_i = v_{ref} - n_{qi} Q_i \tag{3.3}$$

where, P_i and Q_i are the measured active and reactive power at the output of i^{th} DG units, respectively; m_{pi} and n_{qi} are the droop coefficient for frequency and voltage control of i^{th} DG units, respectively; ω_{ref} and v_{ref} are the reference angular frequency and reference voltage, respectively.

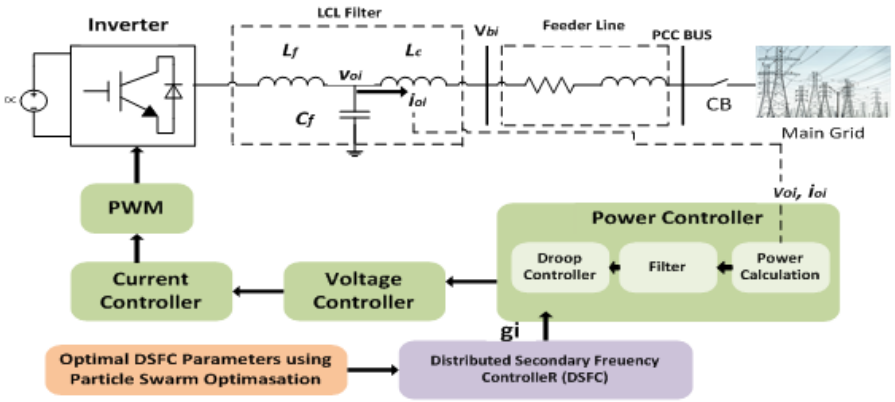

Fig. 3.1 Simplified structure of an inverter-based DG (primary and DSFC)

3.3 PROPOSED CONTROL FOR FREQUENCY RESTORATION AND OPTIMAL ACTIVE POWER-SHARING

Distributed optimal control algorithm is untaken in this section as a resolution of the economic dispatch (ED) problem which suggests a technique to minimise the operation costs of the system. In general, if there are n DGs, an ED problem is well-defined as follows:

$$\text{Min } F = \sum_{i=1}^{n} F_{Ci}(P_i) \tag{3.4}$$

s.t. $\sum_{i=1}^{n} P_i = P_{load}$; $P_i^{min} \le P_i \le P_i^{max}$; $\sum_{i=1}^{n} P_i^{min} < P_{load} < \sum_{i=1}^{n} P_i^{max}$

where P_{load} is the entire load demand; P_i^{min} and P_i^{max} are the minimum and maximum output of i^{th} DG, respectively. For traditional diesel generators, the cost function $F_{Ci}(P_i)$ is expressed as a convex quadratic function of the outputs of active power as

$$F_{Ci}(P_i) = q_i P_i^2 + r_i P_i + s_i \tag{3.5}$$

where $q_i \ge 0$, $r_i > 0$ and $s_i > 0$, and they are all the cost parameters of DG_i.

The cost parameters used in the generation cost function $F_{Ci}(P_i)$ (\$/kW) of each DG unit are given in [156]. References [42, 155, 156] suggest a droop-based control to offer the optimal active power-sharing for DG

units which is based on the equal increment cost principle (ECP) to minimise the total generation costs ($F_{Ci}(P_i)$) of the MG, as specified by

$$\omega_i = \omega_{ref} - e\eta_i(P_i) \tag{3.6}$$

$$\eta_i(P_i) = \frac{d(GC_i(P_i))}{dP_i} = 2q_iP_i + r_i \tag{3.7}$$

In (3.6), e is a positive scalar. The frequency ω_i of all DG units must be same at the steady-state condition. Therefore, $\eta_i(P_i)$'s are also same for all the DG units, which fulfils the ECP of the ED. In this chapter, to get the optimal active power, Eq. (3.6) instead of (3.2) for the active power-sharing is used.

The SC is accomplished by selecting the frequency magnitude ω_i to the reference ω_{ref} synchronously with all the agents performing as a group. Hence, the consensus-based DSFC signal for the i^{th} DG can be written as follows:

$$g_i = -C_\omega \int \left[\sum_{j\in N_i} a_{ij}\left(\omega_i - \omega_j\right) + b_i(\omega_i - \omega_{ref})\right] - C_p \sum_{j\in N_i} a_{ij}\left(e\eta_i(P_i) - e\eta_j(P_j)\right) \tag{3.8}$$

where g_i is the SC signal both for frequency restoration and optimal active power sharing. It should be noted that, in (3.8), b_i=1 if the i^{th} DG is directly connected with the controller at the point of common coupling and otherwise $b_i = 0$. Adding the control signals in (3.6), we get the final inverter frequency shown below:

$$\omega_i = \omega_{ref} - e\eta_i(P_i) + g_i \tag{3.9}$$

3.4 SMALL-SIGNAL STATE-SPACE MODEL FOR STABILITY ANALYSIS

The entire test MG model is considered for state-space modelling where the inverter, network and load are modelled as three main sub-groups as in [154].

3.4.1 Modelling of Single Inverter

The rotational frequency of an inverter is determined by its local controller, and every inverter has its own reference frame. In this chapter, dynamics are considered for modelling an inverter that comprises the power controller, output filter (combining LC filter and coupling inductor) and voltage and current controller (Fig. 3.1). Small-signal modelling of inverters connected in parallel is done while the network and load dynamics are in consideration as well. Here, state equations of the lines and loads are represented on the common reference frame. All the inverters, lines and loads are transformed to this common reference frame via the park transformation [154]. Here, the axis set (*D*-*Q*) is the common reference frame rotating at a frequency w_{com}, whereas the axis $(d-q)_i$ is the reference frame of the i^{th} inverter rotating at ω_i.

$$\left[f_{DQi}\right] = [T_i]\left[f_{dqi}\right] \tag{3.10}$$

$$[T_i] = \begin{bmatrix} cos(\delta_i) & -sin(\delta_i) \\ sin(\delta_i) & cos(\delta_i) \end{bmatrix} \tag{3.11}$$

where δ_i is the angle between the common reference frame and the reference frame of i^{th} inverter. The detailed equations of modelling of all these sub-groups can be found in [154], considering the primary droop control. In the following sections, only 3-phase voltages and currents are considered as vector quantities in *D-Q* reference frame, and other parameters are considered as scalar quantities.

3.4.2 Modelling of Single Inverter considering DSFC

According to [154], the resulting small-signal linearised state-space model of an individual inverter unit in the common reference frame considering the primary control (droop control) only can be written as below (the detailed specifications can be found in [154]):

$$[\dot{\Delta x_i}] = [A_i][\Delta x_i] + [B_i][\Delta v_{bDQi}] + [C_i][\Delta \omega_{com}] \tag{3.12}$$

$$\begin{bmatrix} \Delta\omega_i \\ \Delta i_{0DQi} \end{bmatrix} = \begin{bmatrix} D_{\omega i} \\ D_{ci} \end{bmatrix} [\Delta x_i] \tag{3.13}$$

where, $\Delta x_i = [\Delta\delta_i, \Delta P_i, \Delta Q_i, \Delta\emptyset_{dqi}, \Delta\gamma_{dqi}, \Delta i_{ldqi}, \Delta v_{0dqi}, \Delta i_{0dqi}]^T$; $\emptyset_{dqi}$ and γ_{dqi} are the state variables related to voltage and current controller, respectively; i_{ldqi} represents the state variables of filter current; v_{0dqi} and i_{0dqi} represent the state variables of inverter output voltage and current, respectively.

In accordance with this, the proposed DSFC can be added with primary control and forms the following small-signal linearised state-space equation for an inverter considering control in the common reference frame:

$$[\dot{\Delta x_i}] = [A_i][\Delta x_i] + [B_i][\Delta v_{bDQi}] + [C_{iw}][\Delta w_{com}] + \sum_{j\in N_i}[F_{ij}][\Delta x_j] \tag{3.14}$$

$$\begin{bmatrix} \Delta\omega_i \\ \Delta i_{0DQi} \end{bmatrix} = \begin{bmatrix} D_{\omega i} \\ D_{ci} \end{bmatrix} [\Delta x_i] \tag{3.15}$$

In (3.14), the state variables of each DG unit are considered as:

$$\Delta x_i = [\Delta\delta_i, \Delta P_i, \Delta Q_i, \Delta g_i, \Delta\emptyset_{dqi}, \Delta\gamma_{dqi}, \Delta i_{ldqi}, \Delta v_{0dqi}, \Delta i_{0dqi}, \Delta\mu_i]^T.$$

In (3.14) & (3.15), $[A_i], [B_i], [C_{iw}], [F_{ij}], [D_{\omega i}]$ and $[D_{ci}]$ are the parameter matrices. $[F_{ij}]$ indicates the correlation between DG_i and DG_j. $[\Delta v_{bDQi}]$ denotes the deviation of bus voltages.$[\Delta i_{0DQi}]$ shows the deviations of inverter output currents. The equation for new states of the secondary controller can be written as

$$\Delta g_i = -C_w \int \left[\sum_{j\in N_i} a_{ij}(\Delta\omega_i - \Delta\omega_j) + b_i\Delta\omega_i\right] - C_p\left[\sum_{j\in N_i} a_{ij} e(2q_i\Delta P_i - 2q_j\Delta P_j)\right]) \tag{3.16}$$

3.4.3 Combined State-Space Model of all the Inverters

In this chapter, three DGs connected in parallel are considered for the proposed model. Now, by combining (3.12)-(3.16) for three inverters, the resulting small-signal model of all the inverter units is obtained, as shown below:

$$[\dot{\Delta x}] = [A][\Delta x] + [B][\Delta v_{bDQ}] \tag{3.17}$$

$$\begin{bmatrix} \Delta\omega \\ \Delta i_{0DQ} \end{bmatrix} = \begin{bmatrix} D_{\omega} \\ D_{c} \end{bmatrix} [\Delta x] \tag{3.18}$$

To get the combined model for the system, the sub-model of all the individual DG inverters along with the network and individual load models need to be combined in the common reference frame.

3.4.4 Network Modelling

Small-signal linearised state-space model of the network sub-module, including two RL-type lines, can be given in the common reference frame [154] as shown below:

$$\left[\Delta \dot{\imath}_{lcDQ}\right] = [A_{nc}]\left[\Delta i_{lcDQ}\right] + [B_{nc}]\left[\Delta v_{bDQ}\right] + [C_{nc}][\Delta \omega_{com}] \tag{3.19}$$

where $[\Delta i_{lcDQ}]$ denotes the deviations of line current in the network.

$$A_{nc} = diag(A_{nc1}, A_{nc2});\ \ B_{nc} = \begin{bmatrix} B_{nc1} & -B_{nc1} & 0 \\ 0 & B_{nc2} & -B_{nc2} \end{bmatrix},$$

$$B_{nci} = diag\left({L_{lci}}^{-1}, {L_{lci}}^{-1}\right); C_{nc=}[C_{nc1}, C_{nc2}]^T;\ C_{nci} = [I_{lcQi}, -I_{lcDi}]^T;$$

3.4.5 Load Modelling

A small-signal linearised state-space model of the RL type load sub-module can be written [154] as in (3.20). $\Delta i_{loadcDQ}$ denotes the deviations of load current.

$$\left[\Delta \dot{\imath}_{loadcDQ}\right] = [A_{lo}]\left[\Delta i_{loadcDQ}\right] + [B_{loadc}]\left[\Delta v_{bDQ}\right] + [C_{loadc}][\Delta \omega_{com}] \tag{3.20}$$

$$A_{loadc} = diag(A_{loadc1}, A_{loadc2});$$

$$B_{loadc} = diag(B_{loadc1}, B_{loadc2});$$

$$C_{loadc} = [C_{loadc1}, C_{loadc2}]^T, B_{loadci} = diag({L_{loadci}}^{-1}, {L_{loadci}}^{-1}), C_{loadci} = [I_{loadcQi}, -I_{loadcDi}]^T$$

3.4.6 Combined Modelling of MG

Denote the deviation of i_{oi}, of all the DG units as $[\Delta i_{oDQ}]$. Then the bus voltage, Δv_{bDQ} is represented by

$$\left[\Delta v_{bDQ}\right] = R_N\left(M_I\left[\Delta i_{oDQ}\right] + M_N\left[\Delta i_{lcDQ}\right] + M_L\left[\Delta i_{loadcDQ}\right]\right) \tag{3.21}$$

The detailed specifications of (3.21) can be found in [154]. The complete MG state-space model and the resulting system matrix are achieved by utilising the individual sub-group models given by (3.17) - (3.21) as in (3.22). The assessment of complete system dynamics and stability performance considering the eigen-analysis of the system matrix is given in the following sections.

$$\begin{bmatrix} \Delta \dot{x} \\ \Delta \dot{\imath}_{lci} \\ \Delta \dot{\imath}_{loadc} \end{bmatrix} = A_{MG} \begin{bmatrix} \Delta x \\ \Delta i_{lci} \\ \Delta i_{loadc} \end{bmatrix} \tag{3.22}$$

3.5 STABILITY ANALYSIS

A test MG of three inverter-based DG units, including the local loads as in Fig. 3.2, is considered here for analysis through several case studies. The MG presented here is a 311 V and 50 Hz system, operated in islanded

mode, and is simulated in MATLAB. The initial conditions around an operating point are found from the time-domain simulation of the test MG model. DG1 and DG3 are connected to Load1 and Load2, respectively, through the coupling inductance *Lc* (0.1 mH) as in Fig. 3.2. The load is chosen as a 3-phase series RL load, and each feeder is designed as a series RL branch in every phase. Tables 3.1 provides the specifications of the system.

Table 3.1 Inverters Parameters Used in the Test MG

Description	Parameter	Value	Unit
Parameters for MG Modelling			
DC Bus Voltage	V_{dc}	700	V
Nominal Voltage	v_{ref}	311	V
Nominal Frequency	f_{ref}	50	Hz
Filter Resistance	R_f	0.1	Ω
Filter Inductance	L_f	1.35	mH
Filter Capacitance	C_f	50	μF
Coupling Inductor Resistance	R_c	0.03	Ω
Coupling Inductor Inductance	L_C	0.1	mH
Parameters for Voltage Control			
Proportional Voltage Gain	K_{Pv}	0.05	
Integral Voltage Gain	K_{Iv}	390	
Feed Forward Gain	F	0.75	
Parameters for Current Control			
Proportional Current Gain	K_{Pc}	10.2	
Integral Current Gain	K_{Ic}	16e3	

A directed graph as in Fig. 3.2 (blue dashed line) is considered for the communication among DG units. For the frequency restoration problem, DG2 output is taken as the reference one. Fig. 3.2 also indicates that (i) all the DGs like can be considered as root nodes, and (ii) DG2 is the leader node which provides the reference value and the pinning gain b_2=1. The results can be divided into two parts. One is eigenvalue analysis, and another is time-domain simulation; the results from both are analysed with and without optimisation implementation.

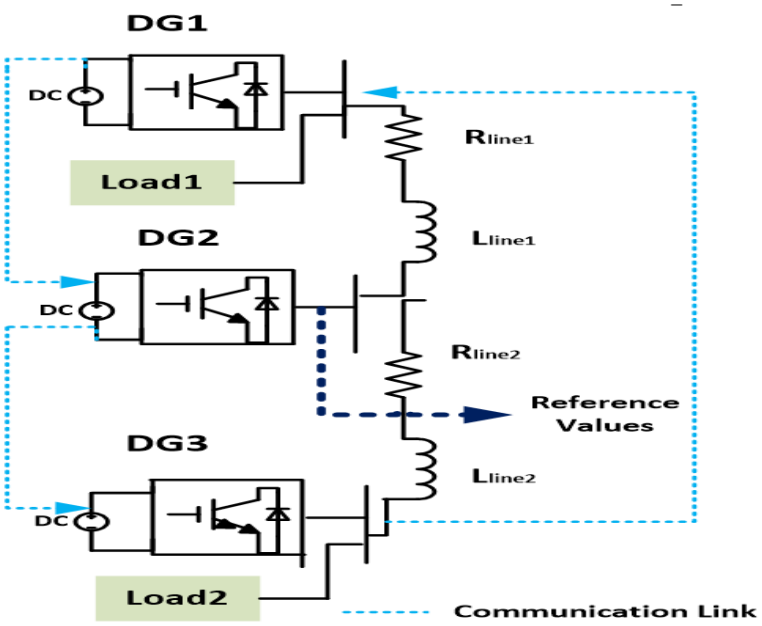

Fig. 3.2 MG test model for simulation and the communication diagraph

3.5.1 Eigenvalue Analysis

This subsection presents the dynamic system behaviour and small-signal stability analysis along with the proposed DSFC. The eigenvalues of the system matrix A_{MG} can be used to assess the system stability around the equilibrium. According to the established small-signal model in the previous section, the resulting eigenvalues considering DSFC are shown in Fig. 3.3 for stable operation. The main emphasis for stability analysis is on the low-frequency modes as the eigenvalues of high and intermediate frequency modes have weak influence on the system stability [154]. The leading less damped modes are shown in Fig. 3.3 (a), indicating that the DSFC significantly participates in creating the shape of the eigenvalues on the complex plane which introduces a new pair of oscillatory modes making less damping responses as compared with the primary responses [157]. Therefore, the SC needs to be designed accurately to get a stable system operation.

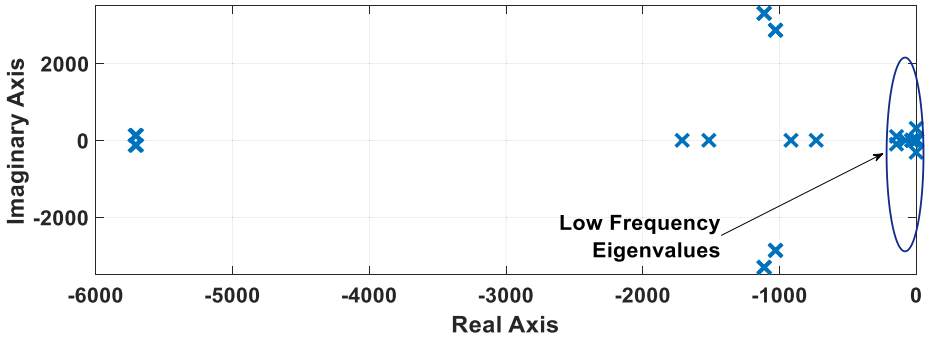

Fig. 3.3 Eigenvalues of system matrix considering DSFC for stable operation

3.5.2 Eigenvalue Sensitivity to Secondary Control Parameters on System Stability

In this chapter, the sensitivity analysis is done considering the SC parameters $\boldsymbol{C_\omega}$, and $\boldsymbol{C_p}$. The effects of the SC parameters on the system stability are shown in Fig. 3.4. Figs. 3.4 (a-b) show the traces of the system's low-frequency modes (modes 1-6) as functions of $\boldsymbol{C_\omega}$ and $\boldsymbol{C_p}$. Fig. 3.4 (a) and Fig. 3.4 (b) present variations in the damping of the oscillatory modes when $\boldsymbol{C_\omega}$ and $\boldsymbol{C_p}$ both vary from 0 to 100 and 0 to 1000, respectively. These variations occur in modes 1-6. Fig. 3.4 (a) and Fig. 3.4 (b) show that, (i) for a given value of $\boldsymbol{C_p}$, the stability is increased when $\boldsymbol{C_\omega}$ increases, and (ii) for a particular value of $\boldsymbol{C_\omega}$, the oscillation increases when $\boldsymbol{C_p}$ increases. DSFC parameters can be chosen based on the above analysis which gives a general idea about designing DSFC parameters as well.

3.6 PSO-BASED OPTIMAL ACTIVE POWER SHARING

The stability analysis given in Section 3.4 shows that DSFC parameters can greatly affect the system stability. Therefore, the optimal values of DSFC parameters are needed. The main goal of the optimisation problem chosen here is to enhance the system stability by choosing the accurate position of eigenvalues. Eigenvalues on the left side of the imaginary axis make the system stable, and stability increases when the distance from the imaginary axis increases. Denote the eigenvalues as $\lambda_i = Re_i + jImg_i$, where Re_i and Img_i are the real and imaginary parts of the eigenvalue, respectively. So, the objective function is *Min J=maximum* of (Re_i) such that C_ω, C_p are within the limit (Table 3.3). According to the general principle of PSO, each particle is a real-valued vector with a dimension equal to the number of parameters to be optimized. Each particle is one solution to the defined optimisation problem, and the size of the population named as P particles will be there. Firstly, a random solution is considered which is the position in the search space within the parameter limit. The position of each particle is updated based on its inertia, personal best and group best as below:

$$V_i^{k+1} = w.V_i^k + C_1.r_1\left[X_{pbest}^k - X_i^k\right] + C_2.r_2[X_{gbest}^k - X_i^k]$$

$$X_i^{k+1} = X_i^k + V_i^{k+1} \tag{3.23}$$

where, X_i^k and V_i^k are the position and velocity of i^{th} particle in k^{th} iteration, respectively; w is the coefficient of inertia; C_1 and C_2 are the coefficients of acceleration; X_{pbest}^k and X_{gbest}^k are the local and global best positions of i^{th} particle in k^{th} iteration.

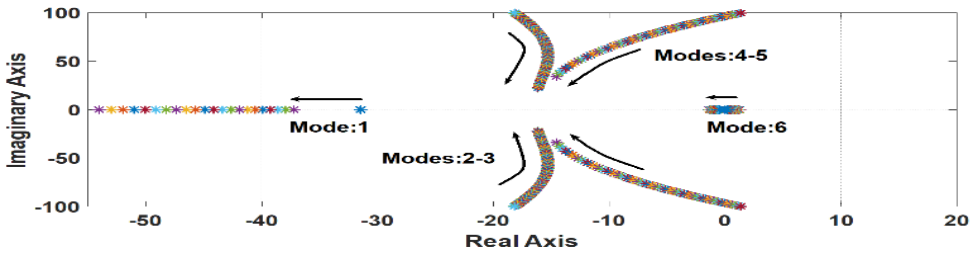

(a) C_ω increases from 0 to 100

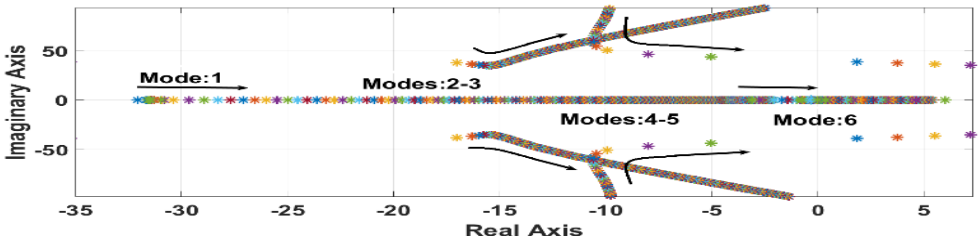

(b) C_p increases from 0 to 1000

Fig. 3.4 Traces of low frequency modes (a) & (b) Modes 1-6

The optimum value is obtained by performing this updating method for velocity and position at the end of a few iterations. The parameters chosen for the optimisation problem discussed earlier are given in Table 3.2

Table 3.2 Parameters Used for PSO

Parameter	Values
Maximum Iteration	100
Swarm Size	70
Coefficient of Inertia	1
Damping Ratio of Inertia Coefficient	0.99
Coefficient of Local Acceleration	2
Coefficient of Global Acceleration	2
Unknown Variables	$[C_\omega, C_p]$
Lower Limit of Unknown Variables	[0, 100]
Upper Limit Unknown Variables	[0,1000]

By utilising the optimisation discussed above for the DSFC parameters$[C_\omega, C_p]$, the optimal values are obtained as [50.459, 620.39] and the J=-30.06. The convergence curve of the objective function is shown in Fig. 3.5. The differences of dominant eigenvalues before and after optimisation are given in Fig. 3.6 (a) and Fig. 3.6 (b). In Fig. 3.6 (a), the real part of the extreme right eigenvalue is at -5.001, and it is moved to -30.06 after the optimization as in Fig. 3.6 (b). Therefore, stability can be enhanced by selecting the optimal values of control parameters C_ω, C_p for the proposed DSFC. The optimal values for the DSFC are summarised in Table 3.3

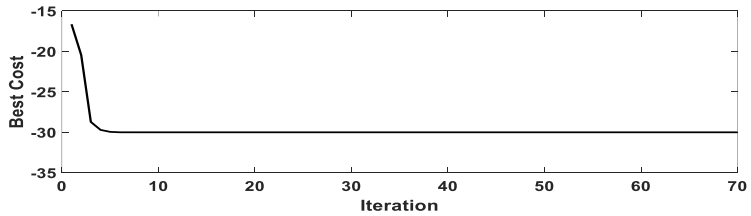

Fig. 3.5 Convergence curve of the objective function

Table 3.3 Secondary Controller Parameters

Controller Parameters		Values	
		Before Optimisation	After Optimisation
Frequency Gain	C_ω	50	50.459
Active Power Gain	C_P	200	620.39

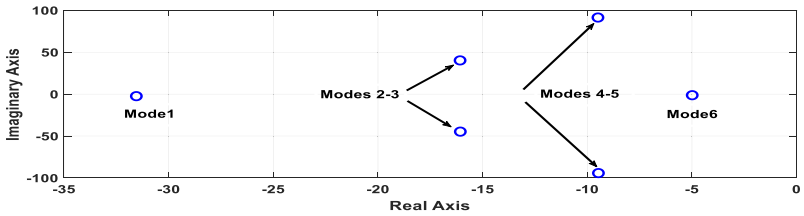

(a)

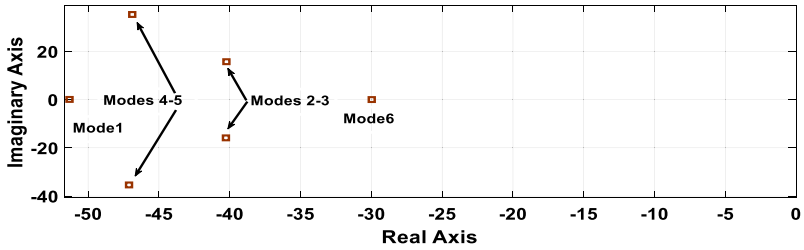

(b)

Fig. 3.6 Dominant eigenvalues (a) before and (b) after optimisation in S plane

3.7 SIMULATION AND RESULTS

The performance of the proposed DSFC is validated by the time-domain simulation with two case studies performed in the Matlab/Simpower system platform.

3.7.1 Case 1 (DSFC without PSO optimisation)

The performance of primary control (3.5) is shown in Figs. 3.7 (a) and (b). Fig. 3.7 (a) indicates due to the primary control, the frequencies of 3 DGs deviate to 49.88 Hz. Thus, the primary control exhibits a clear deviation of frequencies from the nominal value, 50 Hz, which must be restored to their rated values by applying the SC. Fig. 3.8 (a) shows that the proposed DSFC can give a fast response for restoring the deviated frequencies to 50 Hz. Moreover, Fig. 3.7 (b) indicates that the active power-sharing is based on their capacities with the ratio P_1:P_2:P_3 =2:$\frac{3}{2}$:1 for the primary control only. Fig. 3.8 (c) shows the incremental costs, $\eta_i(P_i)$, converge to the same value \$4.56/kW. That is, the proposed DSFC imposes the reference optimal active power sharing according to the cost function to be P_1 = 24kW, P_2=29 kW and P_3=21 kW as in Fig. 3.8(b).

3.7.2 Case 2 (DSFC with PSO optimal values after reaching nominal values)

To show the effectiveness of DSFC after PSO optimisation, the outcomes from the simulation are given in Fig. 3.9. The results indicate that optimal control parameters can reduce the overshoot of frequencies and active power outputs compared with Fig. 3.8 while maintaining the same optimal active power-sharing. Moreover, the corresponding convergence is increased (less than 1s) in Fig. 3.9 (a) compared with Fig. 3.8 (a) (approximately1.5s), which indicates the corresponding settling time is decreased. Fig. 3.9 (b-c) indicates the smooth performance of the proposed controller, and the PSO optimisation is able to successfully reduce the overshoot.

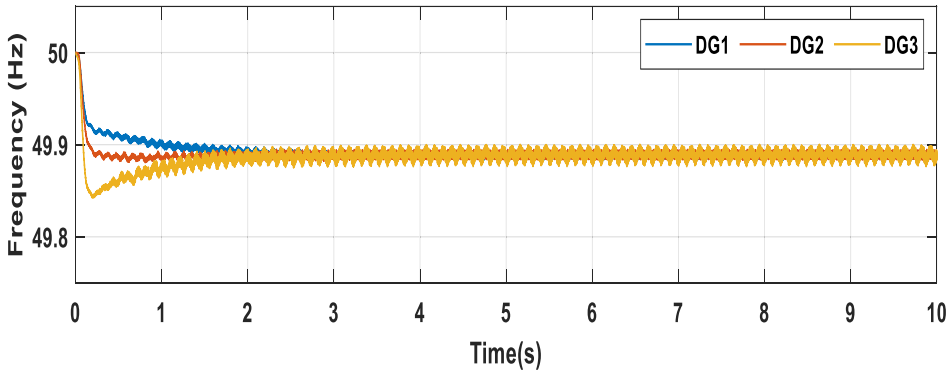

(a)

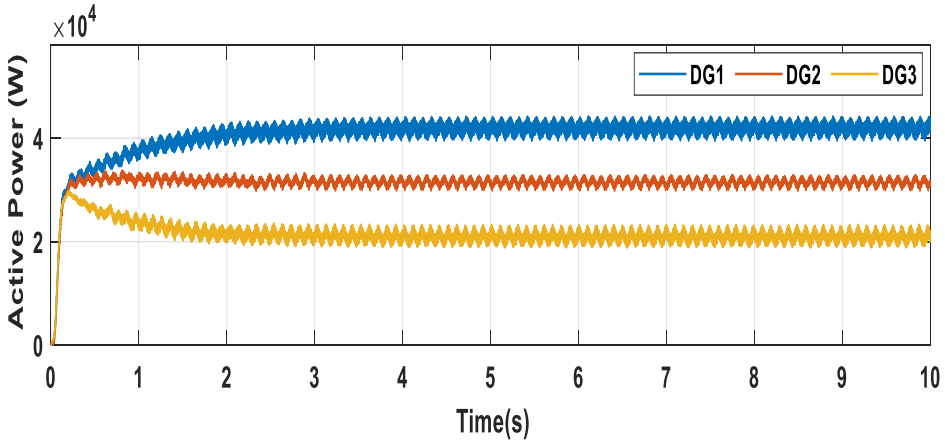

(b)

Fig. 3.7 Output of DGs under only primary control (Droop control) (a) Frequencies (b) Active powers

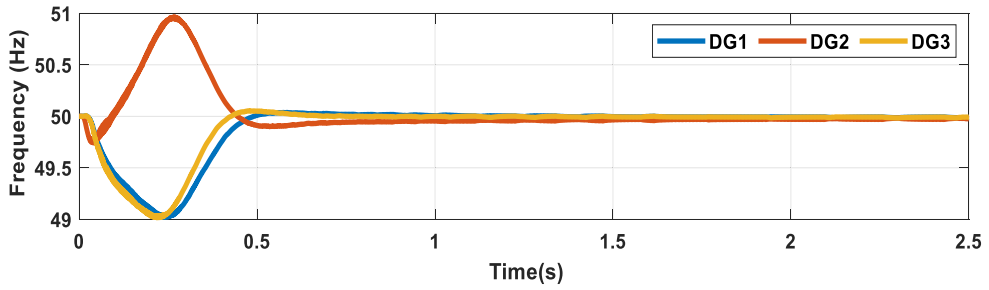

(a)

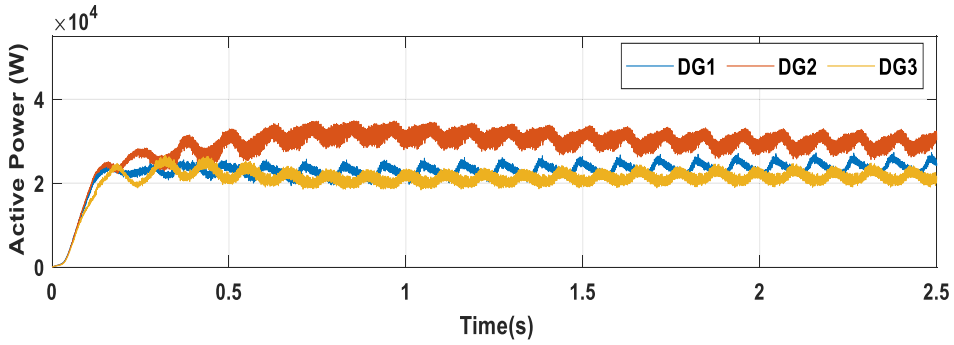

(b)

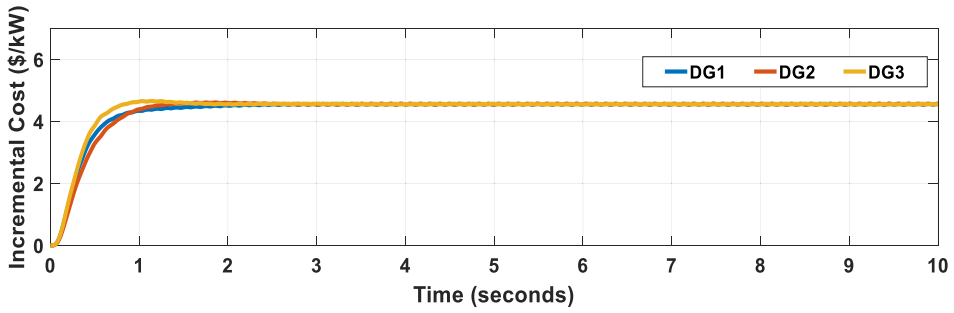

(c)

Fig. 3.8 Output of DGs with DSFC before PSO optimization (a) Frequencies (b) Optimal values for active powers for 10s (c) Optimal values for active powers for 2.5s

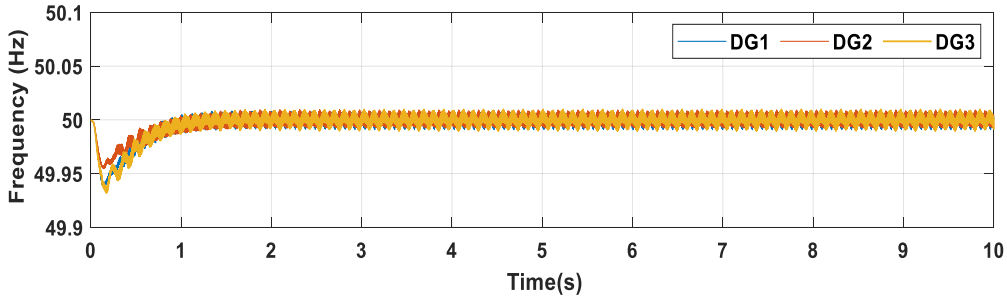

(a)

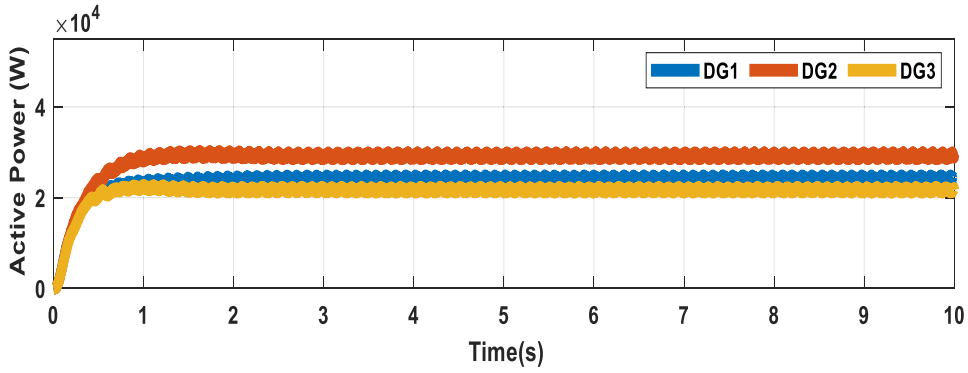

(b)

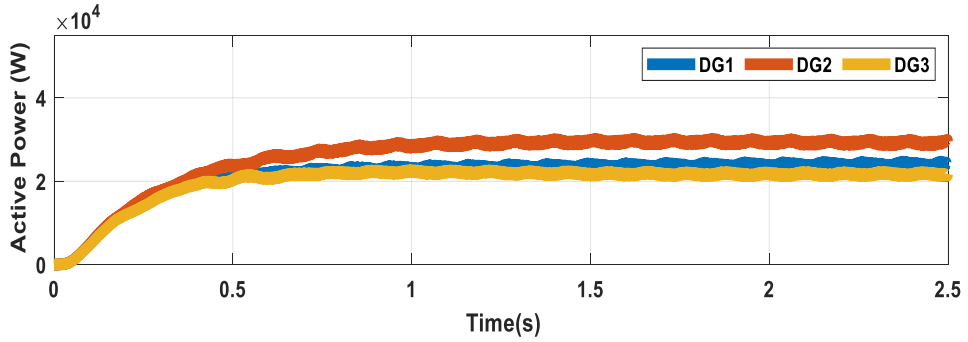

(c)

Fig. 3.9 Output of DGs with DSFC after PSO optimization (a) Frequencies (b) Optimal values for active powers for 10s (c) Optimal values for active powers for 2.5s

3.8 SUMMARY

This chapter presents a DSFC based on the cost function optimization along with a detailed stability analysis. The stability analysis based on eigenvalue analysis reveals that the system stability may be reduced by the DSFC which adds oscillatory modes. An appropriate optimisation method is needed to get the system to operate in a more stable condition. In this chapter, the PSO algorithm is utilised for designing the optimal control parameters for DSFC. The proposed DSFC can restore the system frequencies to their nominal values. The resulting system can converge to the optimal reference values for active power-sharing which are given by the cost function. The outcomes from the eigenvalue study and time-domain simulation ensure that the system stability of the test MG model is improved after applying the proposed optimal control parameter design method. As there are inadequate approaches for solving the problems of frequency recovery with optimal active power-sharing in a distributed way, this research presents a DSFC with optimal active power-sharing along with stability analysis and optimisation for DSFC parameters. These analyses can be used for designing the DSFC for frequency recovery and active power control in a distributed and optimal way.

Chapter 4: Distributed Secondary Control for Voltage Restoration and Reactive Power Sharing

4.1 INTRODUCTION

Distributed secondary control (DSC) frameworks have been introduced in order to control of MGs to make the system less complicated, gain frequency synchronisation and voltage regulation, preserve precise active and reactive power-sharing, and mitigate harmonics and unbalances. These distributed control methodologies are specially established on multi-agent systems or consensus protocols [43, 92, 158]. Consensus-based distributed techniques have obtained popularity in recent times, as they ensure excellent performance utilising a sparse communication network. On the other hand, the dynamic behaviour of MG with the DSC may be unwanted in the context of the system damping, reaction time, stability margin, and things like that. Further, the DSC may create additional less-damped modes to the system directing to oscillatory performance, that is, the distributed control may disturb the system damping behaviour. Therefore, they require to be well-tuned. To develop a control strategy for MGs and investigate its small-signal stability, first, an adequate state-space model is required. There are few papers that focus on inverter-based MG modelling. In [154], a modelling approach which only includes VSIs, and the effect of primary control is shown. Previous dynamic analysis of standalone MGs is carried out with some simplifying assumptions in the modelling of the system [153, 159]; therefore, the analysis of voltage control is not accurate in these models. Although several works carried out small-signal stability studies for the DSC [160], according to our familiarity, a mechanism assessment of the unwanted dynamic performance and the likely oscillations produced by the DSC has not been stated enough earlier. Furthermore, for real-world low voltage (LV) MGs, the effect of the line resistance (R) is not insignificant and must be considered in the system.

Most of the existing approaches to the stability study of such a system are based on the transfer function [153], state-space modelling and small-signal analysis based on the linearization around an operating point and calculating the eigenvalues [160, 161], and the impedance-based method [162]. The transfer function-based stability analysis does not include the impact of the grid impedances. Alternatively, the impedance-based and the eigenvalue-based analyses need less computation and include the impact of controller dynamics and the grid impedance; therefore, these two methods are more suitable for the stability analysis of power electronics-based power systems. The state-space modelling and the eigenvalue-based approach is a global stability analysis method that determines the system stability regardless of the source location of instability. Although many methods have been investigated to improve stability of the primary control [161], to the best of our knowledge, very few works are carried out considering the distributed SC in the state space modelling for detailed small-signal stability study. Inspired by the limitations mentioned above, this chapter emphasises on integrated modelling, analysing and stabilizing of MGs with the distributed SC. The primary contributions of this chapter are:

- An integrated small-signal dynamic representation of the proposed distributed secondary voltage controller, allowing the line resistance in the model.
- The proposed voltage controller can keep precise reactive power-sharing after voltage restoration.
- A thorough evaluation of the effect of distributed controllers on the MG dominant oscillatory modes constructed on that small-signal dynamic model.
- A precise verification for the understanding of the preferred control targets of the offered distributed controllers built on time-domain simulation.

4.2 PROPOSED CONTROL FOR VOLTAGE RESTORATION AND REACTIVE POWER-SHARING

In this chapter, a basic MG comprising three DG units is considered, and it can also be applicable for more DG units in parallel connection. Every DG unit is associated with the corresponding load as well as interlinked with neighbouring DG units via feeder lines. Coordination of the primary controllers can be reached by taking the droop control into account as in Fig. 4.1.

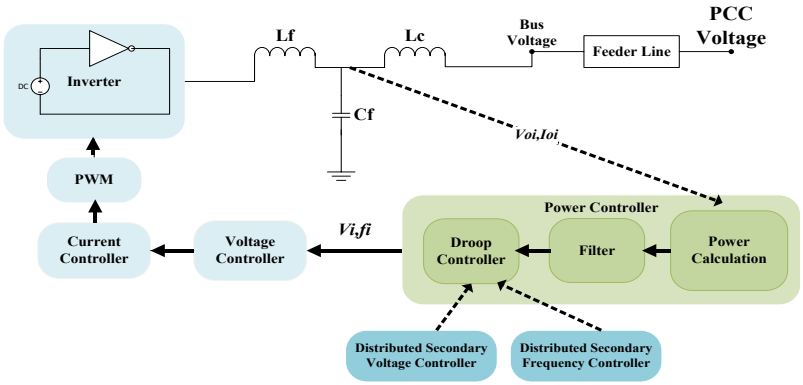

Fig. 4.1 Block diagram for a DG unit with droop controller

The following equation represents the droop controller of the i^{th} DG for voltage regulation:

$$v_i = v_{ref} - n_q Q_i \tag{4.1}$$

where Q_i is the reactive power of the i^{th} DG units, n_q is the voltage droop gain, and v_{ref} is the nominal voltage. Thus, the SC is achieved by choosing the proper control input u_i to adjust the individual voltage magnitude v_i to the reference v_{ref} synchronously with all the agents acting as a group. Therefore, the consensus-based DSC signal for the i^{th} DG can be written as

$$h_i = -C_{vi} \int \left[\sum_{j \in N_i} \left(v_{diffi} - v_{diffj} \right) + g_i \left(v_{diffi} - v_{diff} \right) \right] \tag{4.2}$$

$$\tau_i = -C_{Qi} \int \left[\sum_{j \in N_i} a_{ij} \left(\frac{Q_i}{Q_{imax}} - \frac{Q_j}{Q_{jmax}} \right) \right] \tag{4.3}$$

where h_i is the SC signal for voltage restoration, and τ_i is the SC signal for reactive power-sharing. Here, v_{diff} calculated at the point of common coupling (*PCC*) as in Fig. 4.5 and v_{diffi} are given through the following equations

$$v_{diff} = k_p\left(v_{ref} - v_{PCC}\right) + k_I \int \left(v_{ref} - v_{PCC}\right)dt \tag{4.4}$$

$$v_{diffi} = k_p\left(v_{ref} - v_{odi}\right) + k_I \int \left(v_{ref} - v_{odi}\right)dt \tag{4.5}$$

Note that, in (4.2), g_i=1 if the i^{th} DG has direct communication with the controller at *PCC* and otherwise $g_i = 0$. Combining the SC signal in (4.2) and (4.3) with the primary control signal in (4.1), the resulting inverter voltage reference can be shown below,

$$v_{refi}=v_i + h_i + \tau_i \tag{4.6}$$

4.3 SMALL-SIGNAL STATE-SPACE MODEL OF AUTONOMOUS AC MG

The modelling procedure proposed in this chapter sub-divides the entire system into three primary sub-modules: inverter, network and load [154]. Please refer to Section 3.4.1 to see the detailed modelling of the individual inverter.

4.3.1 State-Space Model of Individual Inverter with Distributed Secondary Voltage Control (DSVC)

According to [154], the complete small-signal linearised state-space model of an individual inverter unit in the common reference frame considering the primary control (droop control) only can be written as below:

$$\left[\Delta \dot{x_{invi}}\right] = [A_{invi}][\Delta x_{invi}] + [B_{invi}]\left[\Delta v_{bDQi}\right] + [B_{iwcom}][\Delta \omega_{com}] \tag{4.7}$$

$$\begin{bmatrix} \Delta\omega_i \\ \Delta i_{0DQi} \end{bmatrix} = \begin{bmatrix} C_{INV\omega i} \\ C_{INVci} \end{bmatrix} [\Delta x_{invi}] \tag{4.8}$$

where $\Delta x_{invi} = \left[\Delta\delta_i, \Delta P_i, \Delta Q_i, \Delta \emptyset_{dqi}, \Delta\gamma_{dqi}, \Delta i_{ldqi}, \Delta v_{0dq}, \Delta i_{0dq}\right]^T$. Similarly, the small-signal linearised state-space model of the individual inverter unit in the common reference frame considering the proposed DSC can be written as below:

$$\left[\Delta \dot{x_{invi}}\right] = [A_{invi}][\Delta x_{invi}] + [B_{invi}]\left[\Delta v_{bDQi}\right] + [B_{iwcom}][\Delta w_{com}] + \sum_{j\in N_i}\left[F_{invij}\right]\left[\Delta x_{invj}\right] + [H_{invi}]\left[\Delta v_{PCCref}\right] \tag{4.9}$$

$$\begin{bmatrix} \Delta\omega_i \\ \Delta i_{0DQi} \end{bmatrix} = \begin{bmatrix} C_{INV\omega i} \\ C_{INVci} \end{bmatrix} [\Delta x_{invi}] \tag{4.10}$$

In (4.9), the parameter matrices F_{invij} exhibits the relationship between DG_i and the neighbour DG_j delivered by DSC. In (4.9) & (4.10), the state variables of each DG unit are considered as

$$\Delta x_{invi} = [\Delta\delta_i \quad \Delta P_i \quad \Delta Q_i \quad \Delta h_i \quad \Delta\tau_i \quad \Delta\emptyset_{dqi} \quad \Delta\gamma_{dqi} \quad \Delta i_{ldqi} \quad \Delta v_{0dq} \quad \Delta i_{0dq}\ \Delta\sigma_i\ ]^T$$

Here, the equation for new states of the secondary controller can be written as

$$\Delta h_i = C_{vi} \int \left[\sum_{j\in N_i} a_{ij}\left(\Delta v_{diffj} - \Delta v_{diffi}\right) + g_i\left(\Delta v_{diff} - \Delta v_{diffi}\right)\right] \tag{4.11}$$

$$\Delta\tau_i = C_{Qi} \int \left[\sum_{j\in N_i} a_{ij}\left(\frac{Q_j}{Q_{jmax}} - \frac{Q_j}{Q_{jmax}}\right)\right] \tag{4.12}$$

Letting $\in = \int (v_{ref} - v_{PCC})\, dt, \dot{\in} = v_{ref} - v_{PCC}$, we have

$$\Delta\dot{\in} = -\Delta v_{PCC} \tag{4.13}$$

Similarly, let $\sigma_i = \int (v_{ref} - v_{odi})\, dt$, $\dot{\sigma_i} = v_{ref} - v_{odi}$ to get

$$\Delta\dot{\sigma_i} = -\Delta v_{odi} \tag{4.14}$$

4.3.2 Combined State-Space Model of all the Inverters

In this chapter, three DGs are considered in the proposed model. Now, by combining (4.9)-(4.14) for 3 inverters, the combined small-signal model of all the inverter units is obtained, as shown below:

$$[\Delta\dot{x_{inv}}] = [A_{inv}][\Delta x_{inv}] + [B_{inv}][\Delta v_{bDQ}] + [B_{wcom}][\Delta w_{com}] + [H_{inv}][\Delta v_{PCCref}] \tag{4.15}$$

$$\begin{bmatrix} \Delta\omega \\ \Delta i_{0DQ} \end{bmatrix} = \begin{bmatrix} C_{INV\omega} \\ C_{INVc} \end{bmatrix} [\Delta x_{inv}] \tag{4.16}$$

The modelling procedure in this work is to build a sub-model of all the individual DG inverters and combine them with the network and individual load models.

4.3.3 Network Sub-module Model

Small-signal linearised state-space model of the network sub-module comprising of two RL type lines can be given in the common reference frame [154] as shown below,

$$[\Delta\dot{\imath_{lineDQ}}] = [A_{net}][\Delta i_{lineDQ}] + [B_{1net}][\Delta v_{bDQ}] + [B_{2net}][\Delta w] \tag{4.17}$$

Here, $\Delta w = \Delta w_{com}$; $A_{net} = \begin{bmatrix} A_{net1} & 0 \\ 0 & A_{net2} \end{bmatrix}$; $B_{1net} = \begin{bmatrix} B_{1net1} & -B_{1net1} & 0 \\ 0 & B_{1net2} & -B_{1net2} \end{bmatrix}$

$$B_{1neti} = \begin{bmatrix} \frac{1}{L_{linei}} & 0 \\ 0 & \frac{1}{L_{linei}} \end{bmatrix};\ B_{2net} = \begin{bmatrix} B_{2net1} \\ B_{2net2} \end{bmatrix};\ B_{2neti} = \begin{bmatrix} I_{lineQi} \\ -I_{lineDi} \end{bmatrix};$$

4.3.4 Load Sub-module Model

Small-signal linearised state-space model of the RL type load sub-module can be written [154] as in (4.18)

$$[\Delta\dot{\imath_{loadDQ}}] = [A_{load}][\Delta i_{loadDQ}] + [B_{1load}][\Delta v_{bDQ}] + [B_{2load}][\Delta w] \tag{4.18}$$

where, $A_{load} = \begin{bmatrix} A_{load1} & 0 \\ 0 & A_{load2} \end{bmatrix}$; $B_{1load} = \begin{bmatrix} B_{1load1} & 0 \\ 0 & B_{1load2} \end{bmatrix}$; $B_{2load} = \begin{bmatrix} B_{2load1} \\ B_{2load2} \end{bmatrix}$;

$$B_{1loadi} = \begin{bmatrix} \frac{1}{L_{loadi}} & 0 \\ 0 & \frac{1}{L_{loadi}} \end{bmatrix};\qquad B_{2loadi} = \begin{bmatrix} I_{loadQi} \\ -I_{loadDi} \end{bmatrix}$$

4.3.5 Network Sub-module Model

The line resistance (R) cannot be ignored in the model of LV MGs. Denote the deviation of i_{oi}, of all the DG units as Δi_{oDQ}. Then the bus voltage, Δv_{bDQ} is represented by

$$[\Delta v_{bDQ}] = R_N\left(M_{inv}[\Delta i_{oDQ}] + M_{NET}[\Delta i_{lineDQ}] + M_{Load}[\Delta i_{loadDQ}]\right) \tag{4.19}$$

Similarly, V_{pcc} is the deviation of the *PCC* voltage and can be expressed in terms of i_{0dq}, i_{linedq} and i_{loaddq} as in (4.19). The finalised MG small-signal state-space representation and the system matrix can be achieved by considering the individual sub-system models specified in (4.15) - (4.19) and the final representation in (4.20). The system dynamics and stability can then be assessed founded on the eigen-structure of the system matrix as given in the following parts.

$$\begin{bmatrix} \Delta\dot{X}_{inv} \\ \Delta\dot{\imath}_{line} \\ \Delta\dot{\imath}_{load} \\ \Delta\dot{\in} \end{bmatrix} = A_{MG} \begin{bmatrix} \Delta X_{inv} \\ \Delta i_{line} \\ \Delta i_{load} \\ \Delta\in \end{bmatrix} \tag{4.20}$$

4.4 SIMULATION AND RESULT

4.4.1 Test System

A test MG model of three inverter-based DG units, including the local loads, is presented in Fig. 4.2. The MG considered here is a 311 V and 50 Hz system and is simulated in MATLAB. The steady-state operating point settings are acquired from a MATLAB/Simulink time-step simulation of the system. DG unit 1 and DG unit 3 are coupled to load1 and load3 correspondingly through the coupling inductance *Lc* (0.1 mH) as in Fig. 4.2. The MG functions in the autonomous mode, each three-phase load is symbolised as a series RL branch, and each feeder line is modelled by a lumped, series RL branch in every phase. Tables 4.1, 4.2 and 4.3 provide the system and the DG primary and SC parameters, correspondingly.

It is assumed that DG units interact with neighbours through the directed graph as in Fig. 4.2. For the voltage restoration issues, the voltage reference is the DG2 unit outputs. Fig. 4.2 also points out that (i) all DGs like *DG*1 ~*DG*3 are root nodes, and (ii) *DG*2 is assumed as the root node for receiving the reference value with the pinning gain of g_2=1. The results are divided into two parts. One is eigenvalue analysis, and the other is time-domain simulation. The steps of the simulations can be depicted in Fig. 4.3.

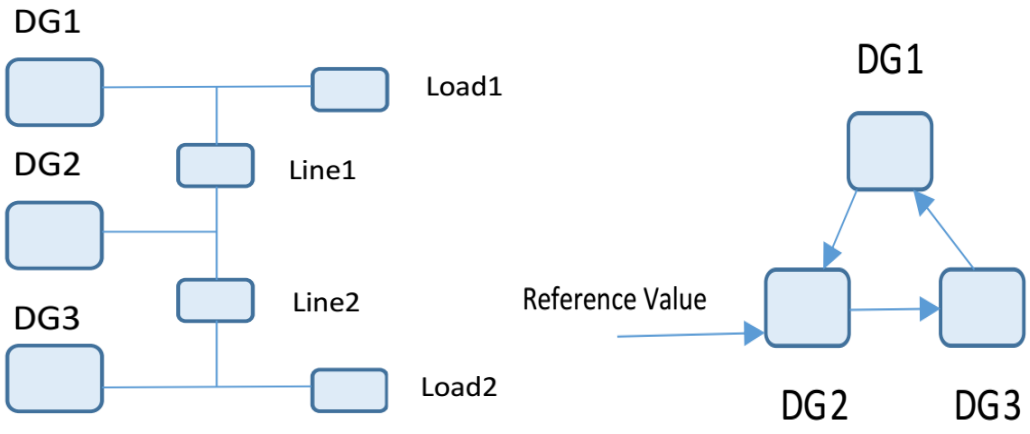

Fig. 4.2 Simulation diagram of the MG test model and the communication diagraph

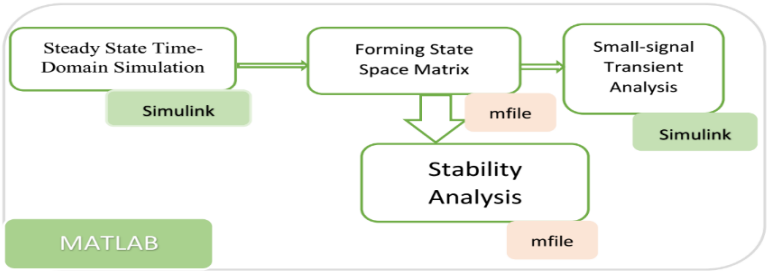

Fig. 4.3 Steps of the stability analysis process in MATLAB

Table 4.1 Parameters for the Inverters Used in the MG Test Model System

Description	Parameter	Value	Unit
MG Model Parameters			
DC Voltage Value	V_{dc}	700	V
Reference Voltage	v_{ref}	311	V
Reference Frequency	f_{ref}	50	Hz
Resistance of Filter Inductor	R_f	0.1	Ω
Inductance of Filter Inductor	L_f	1.35	mH
Capacitance of Filter Inductor	C_f	50	μF
Resistance of Coupling Inductor	R_c	0.03	Ω
Inductance of Coupling Inductor	L_C	0.1	mH
Voltage Controller Parameters			
Proportional Gain	K_{pv}	0.05	
Integral Gain	K_{iv}	390	
Feed Forward Gain	F	0.75	
Current Controller Parameters			
Proportional Gain	K_{pc}	10.2	
Integral Gain	K_{ic}	16e3	

Table 4.2 Line and Load Data Used in the Test System

Line Data			Load Data		
No.	R (Ω)	L (μH)	No.	R (Ω)	L (mH)
Line 1	0.23	318	Load1	40	15
Line 2	0.30	312	Load2	50	22

Table 4.3 Secondary Controller Parameters

Controller Parameters		Values
Proportional Gain	K_P	0.001
Integral Gain	K_I	50
Voltage Gain	C_V	100
Reactive Power Gain	C_Q	28

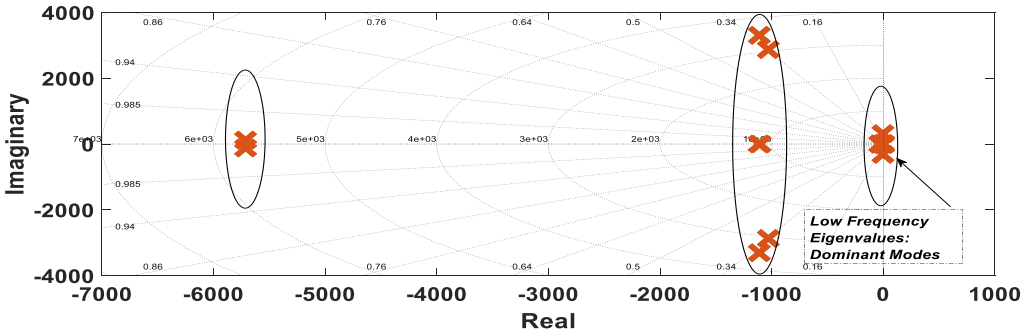

Fig. 4.4 Eigenvalues of system matrix considering DSVC for stable operation

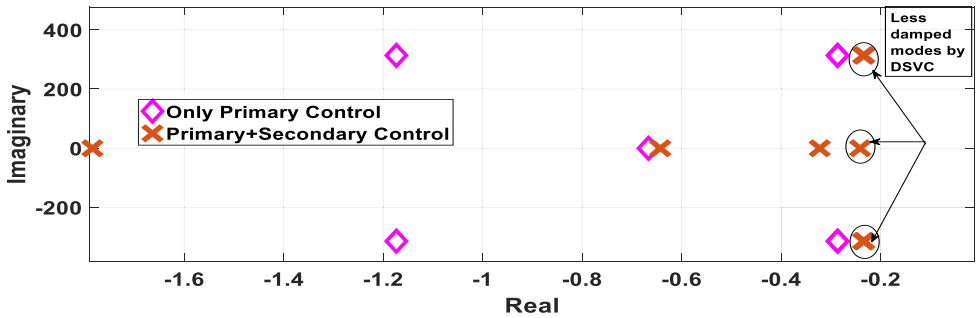

Fig. 4.5 Dominant modes for both primary and considering DSVC for stable operation

Table 4.4 Secondary Controller Most Dominant Modes with and without Secondary Control

Eigenvalues Comparison								
Modes	primary control+secondary control					primary control		
	1,2	3,4	5,6	7,8	9	1,2	3,4	5,6
Real	-52	-48	-32	-1	-0.5	-59	-49	-39
Imaginar	±89.3	±40	±79.7	±2.2	0	±98.2	±45	±32.6

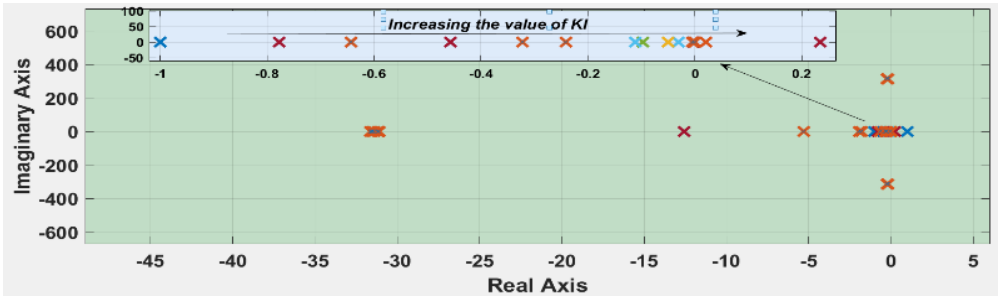

(a) K_I increases from 0 to 60

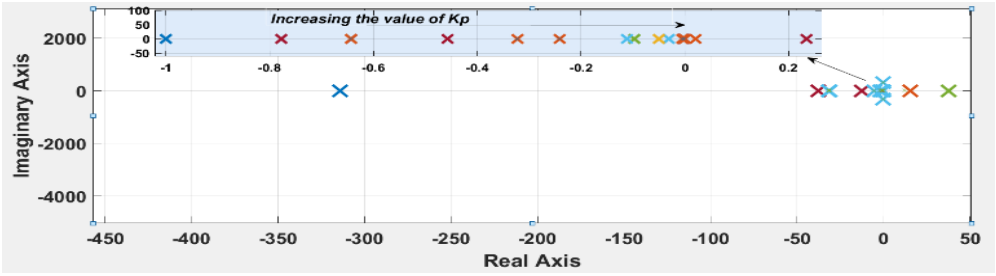

(b) K_P increases from $1e^{-4}$ to $1e^{-1}$

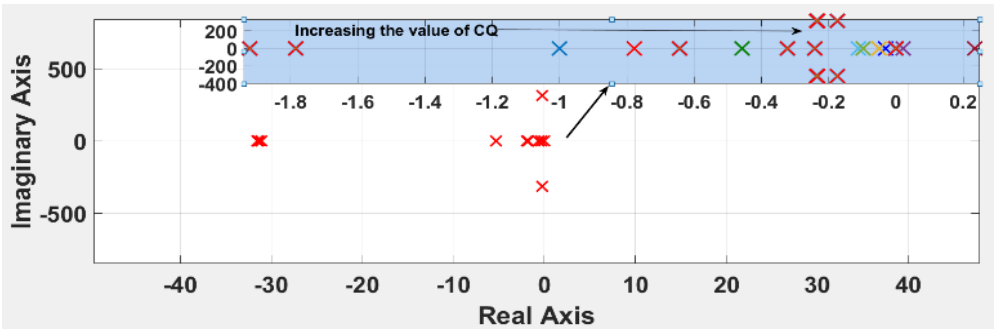

(c) C_Q increases from 10 to 100

Fig. 4.6 Traces of low-frequency modes

4.4.2 Eigenvalue Analysis

The following subsection will represent the dynamics of the MG system and outcomes of the stability analysis for the test MG under the proposed DSVC. The MATLAB function eig(·) is employed to calculate the eigenvalues of the system matrix A_{MG}. According to the established small-signal model in the previous section, the resulting eigenvalues considering DSVC are shown in Fig. 4.4 for stable operation. As the eigenvalues of high and intermediate frequency modes have less contribution to the system damping performance [154], in this chapter will concentrate on the study of the low-frequency modes. The dominant oscillatory modes are shown in Fig. 4.5. Fig. 4.6 shows the eigenvalues (for both without and with DSVC), which indicates that the SC (i) considerably amends the pattern of the eigenvalues on the complex plane and (ii) creates an additional pair of less-damped modes yielding more oscillatory system reactions in contrast with the primary responses. Hence, the system damping behaviour is greatly disturbed by the SC.

Participation Factors: Participation factor is the multiplication of the equivalent element in the right and left eigenvectors of the state matrix to determine the connection between the state variables and the modes. Participation factors suggest that in the case of the primary droop control, the low-frequency modes are mostly influenced by means of the states of the active power droop controller (1), i.e., $\Delta\delta_i$ and ΔP_i [154]. The

participation factor relating the k^{th} state variable to the i^{th} eigenvalue, in a system with n eigenvalues, is defined as where λ_i is

$$p_{ki} = \frac{\lambda_i}{a_{kk}} = \frac{|v_{ki}||\omega_{ki}|}{\sum_{k=1}^{n}|v_{ki}||\omega_{ki}|} \tag{4.21}$$

i^{th} eigenvalue, a_{kk} is the k^{th} diagonal element of the system matrix, and ω_{ki} and v_{ki} are the k^{th} elements of the left and right eigenvectors associated with λ_i [154]. Table 4.4 compares the most dominant oscillatory modes of the MG with and without considering the SC. It is indicated that the SC creates three additional less-damped eigenvalues, i.e., modes 7, 8 and 9.

4.4.3 Eigenvalue Sensitivity to Secondary Control Parameters on System Stability

Traces of low-frequency modes as functions of $\boldsymbol{K_I}$, $\boldsymbol{K_P}$, $\boldsymbol{C_V}$ and $\boldsymbol{C_Q}$ of the whole network is shown in Fig. 4.6. Fig. 4.6(a) and Fig. 4.6(b) show transformations in the damping of the "least damped" mode when K_I and K_P both differ from 0 to 60 and $1e^{-4}$ to $1e^{-1}$, respectively. These variations mainly affect mode 9. Fig. 4.6(c) shows that C_Q also has opposite effects on damping. C_V has much less effect on stability, and that's why it is not shown here. The above analysis gives an overall idea and guidelines for the SC parameters design.

4.4.4 Time-Domain Simulation

To validate the responses of the offered secondary controller, a set of time-domain simulation verifications in the Matlab/Simpower system platform are also performed.

Case 1: Performance of DSVC to reach the nominal values: The performance of primary droop control is shown in Figs. 4.12 (a) and (c). Fig. 4.11 (a) indicates due to the droop function in the primary control, the voltage amplitudes of 3 DGs fall down to different values (DG1=278V, DG2=269V, DG3=267V). The voltages deviate from their reference values of $311V$; hence, they need to be restored to their reference values in the SC layer. When our proposed DSC is applied, voltages can be quickly restored to their reference values, which is shown in Fig. 4.7 (b). Moreover, Fig. 4.7 (c) specifies that under the primary control, the reactive power-sharing is not perfect, while the proposed DSVC executes precise reactive power-sharing with the ratios of Q_1 to Q_3 being 4:2:1 as in Fig. 4.7 (d).

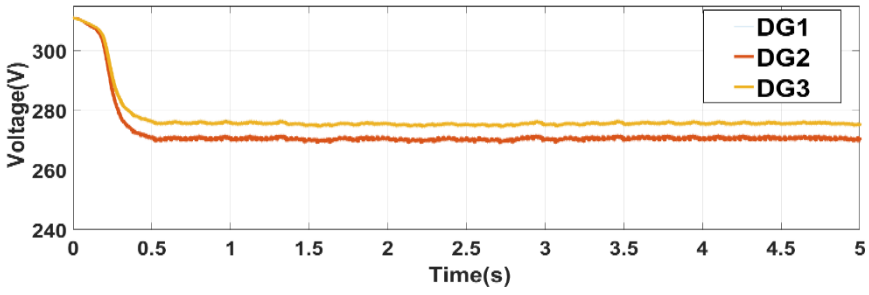

(a)

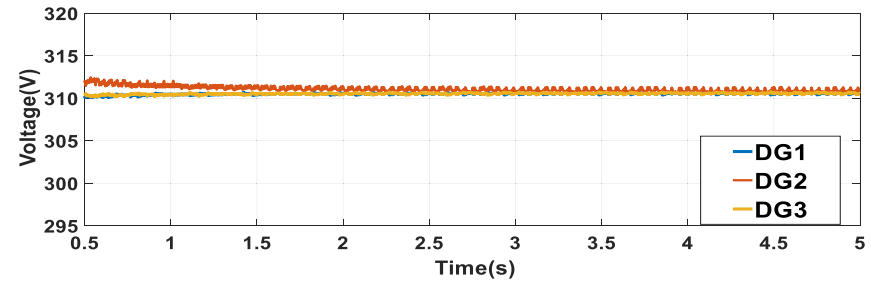

(b)

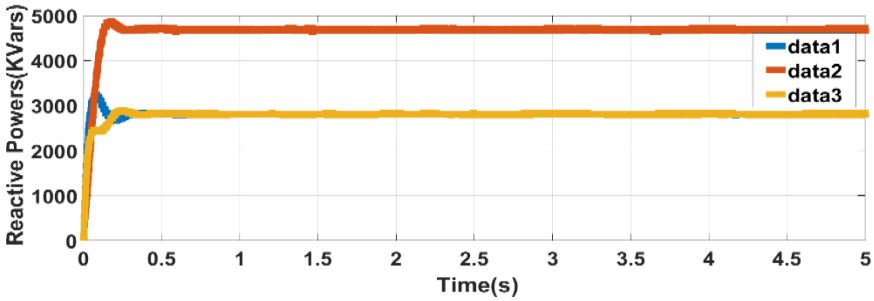

(c)

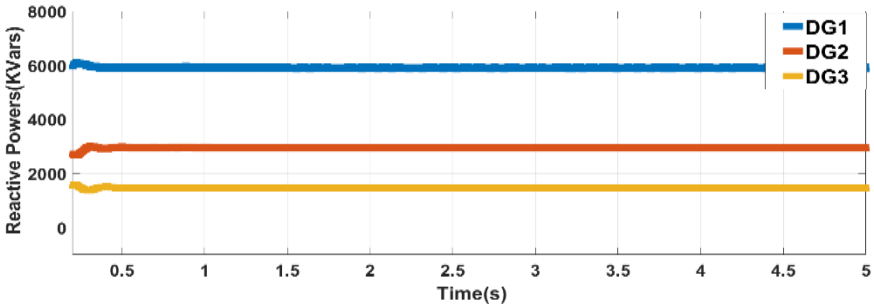

(d)

Fig. 4.7 Outputs of three DGs for Case 1, voltage outputs (a) without and (b) with DSVC and reactive power sharing (c) without and (d) with DSVC

Case 2: Performance of DSVC with step load change after reaching nominal values: To show the performance of DSVC with the load change, the simulation can be grouped into 2 stages: Stage1 (2 - 4s): Constant load *Loadc* (*R=20Ω* and *L=10mH*) is added to DG3; Stage2 (4 - 5s): *Loadc* is removed from DG3. The outcomes present that the designed distributed secondary controller can remove the voltage error initiated by the primary control. The steady-state voltages of the three DGs remain at *311V* with no difficulty when the constant load *Load2* is connected to or disconnected from DG3, although there are transient fluctuations, as seen in Fig. 4.8 (a). The simulation results also show that the DGs can also maintain a good reactive power sharing accuracy in Fig.4.9 (b), when the additional load is connected to or disconnected from the system.

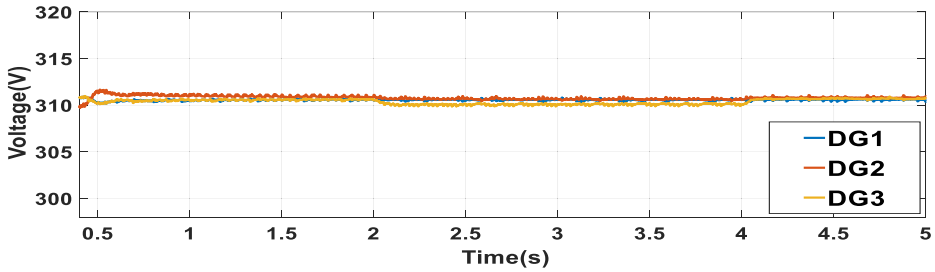

(a)

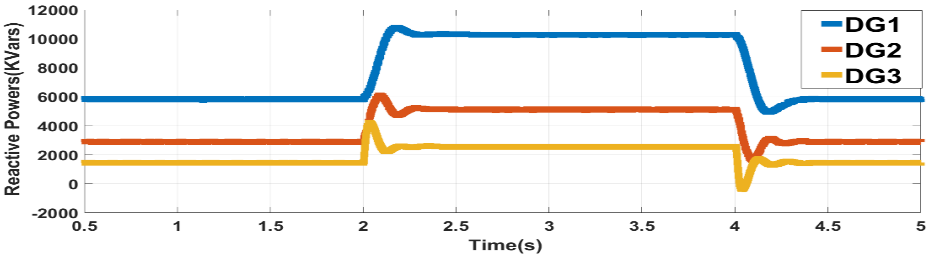

(b)

Fig. 4.8 Outputs of three DGs for Case 2, (a) voltage outputs (b) reactive power sharing with DSVC

4.5 COMPARISON OF THE PROPOSED CONTROL WITH THE ONE IN [17]:

4.5.1 Brief Description of the Model in [17]

In [17], a basic MG comprising of 4 DG units is considered. Each DG unit is linked to the respective load and interconnected with neighbouring DG units through transmission lines. Coordination of the primary controllers can be achieved by considering same the droop control mentioned above for voltage regulation and reactive power-sharing. The following equation represents the droop controller of the i^{th} DG:

$$f_i = f_{ref} - n_f P_i \tag{4.22}$$

$$v_i = v_{ref} - n_v Q_i \tag{4.23}$$

where P_i is the real power and Q_i is the reactive power of the i^{th} DG units, n_f is the frequency droop gain, n_v is the voltage droop gain, v_{ref} is the nominal voltage, and f_{ref} is the nominal frequency. Thus, the SC is achieved by choosing the proper control input u_i to adjust the individual frequency f_i and voltage magnitude v_i to the respective references f_{ref} and v_{ref} synchronously, with all the agents acting as a group. Therefore, the consensus-based SC for the i^{th} DG for voltage restoration can be written as

$$\dot{\Delta v_i} = \left[\sum_{j\in N_i}(\Delta v_j - \Delta v_i) + g_i(\Delta v - \Delta v_i)\right] \tag{4.24}$$

where Δv_i is the secondary controller output and Δv is the control signal calculated at the point of common coupling (*PCC*) through the following equation

$$\Delta v = k_p\left(v_{ref} - v_{PCC}\right) + k_I \int\left(v_{ref} - v_{PCC}\right)dt \tag{4.25}$$

Here, $g_i = 1$ if the i^{th} DG has direct communication with the controller at *PCC* and otherwise $g_i = 0$. Combining the SC signal in (4.24) with the primary control signal in (4.23), the inverter voltage reference is shown below,

$$v_{refi} = v_i + \Delta v_i \tag{4.26}$$

4.5.2 Simulation and Results

In [43], the simulation model consists of four DG units with the individual loads and transmission lines (Fig. 4.9) and is simulated in MATLAB using SimPower Systems toolbox. The parameters for the MG model and control system are listed in Table 4.5, Table 4.6 and Table 4.7. We assume that DG units communicate with neighbours through the directed graph (Fig. 4.9). For both the frequency and voltage restoration problems, we consider the voltage and frequency references to be the DG2 unit output. The whole simulation can be divided into 3 cases (Case 1, Case 2 and Case 3) in order to compare the effectiveness of the proposed secondary controller in [43].

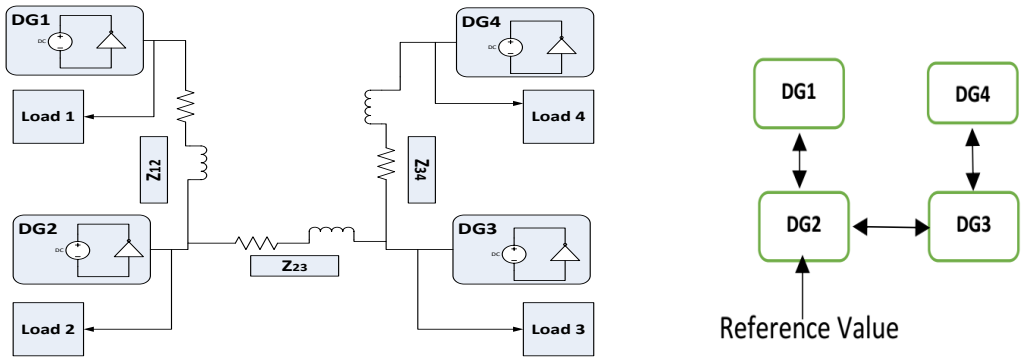

Fig. 4.9 Simulation diagram of the MG test model and the communication diagram

The three cases are:

Case 1: Only primary control is activated.

Case 2: In this case, conventional secondary control is applied with the primary control.

Case 3: In this case, the proposed secondary control is activated from the beginning in combination with primary control.

For all the cases, five scenarios are analyzed in the simulation according to the power flow and the loading condition at each DG as follows:

1) At t=2s, Load #3 is connected.

2) At t=4s, Load #2 is increased by including an additional load, Load#5.

3) At t=6s, Load #5 is disconnected from DG2.

4) At t=8s, DG# 4 is disconnected.

5) At t=10s, DG#4 is again connected.

Table 4.5 Parameters for the Inverters Used in the MG Test Model System

Description	Parameter	Value	Unit
MG Model Parameters			
DC Voltage Value	V_{dc}	700	V
Reference Voltage	v_{ref}	311	V
Reference Frequency	f_{ref}	50	Hz
Resistance of Filter Inductor	R_f	0.1	Ω
Inductance of Filter Inductor	L_f	1.35	mH
Capacitance of Filter Inductor	C_f	50	μF
Resistance of Coupling Inductor	R_c	0.03	Ω
Inductance of Coupling Inductor	L_C	0.35	mH
Voltage Controller Parameters			
Proportional Gain	K_{pv}	0.05	
Integral Gain	K_{iv}	390	
Feed Forward Gain	F	0.75	
Current Controller Parameters			
Proportional Gain	K_{pc}	10.2	
Integral Gain	K_{ic}	16e3	

Table 4.6 Load and Line Data Used in the MG Test Model System

Line Data	Line Resistance (Ω)	Line Inductance (μH)
Line 1, Z_{12}	0.23	318
Line 2, Z_{23}	0.23	318
Line 3, Z_{34}	0.30	312
Load Data	**Load Resistance, R(Ω)**	**Load Inductance, L (mH)**
Load# 1	50	35
Load # 2	50	35
Load # 3	35	35
Load # 4	35	35
Load # 5	25	25

Table 4.7 Parameters of the Power Controller Used in the MG Test Model System

DG unit	Active Power rating (KW)	Reactive Power Rating (KVar)	Frequency Droop Gain,n_f	Voltage Droop Gain,n_v
DG1	60	30	3.33e-5	1.67e-5
DG2	60	30	3.33e-5	1.67e-4
DG3	30	15	6.67e-5	3.33e-4
DG4	30	15	6.67e-5	3.33e-4

The simulation results for Case 1, Case 2 and Case 3 are shown in Fig. 4.10, Fig. 4.11 and Fig. 4.12, respectively. As seen from Fig. 4.10, due to the droop function in the primary control, the voltage amplitudes of 4 DGs fall down to different values (DG1=298V, DG2=296V, DG3=280V and DG4=282V) while the frequency can synchronize to a common value (49.76Hz). From the simulation results, both voltage and frequency deviate from their reference values; hence, they need to be restored to their reference values in the SC layer.

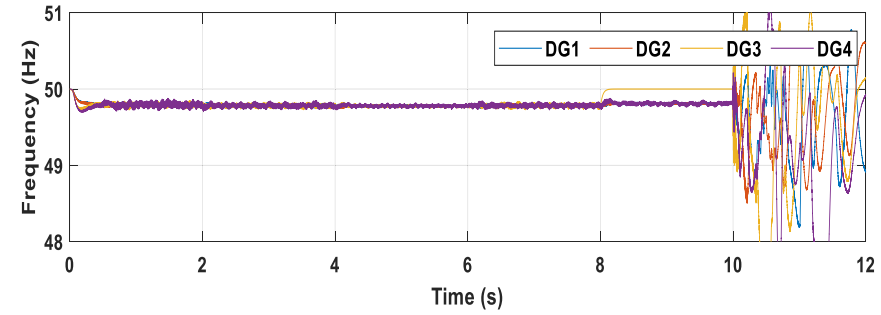

(a)

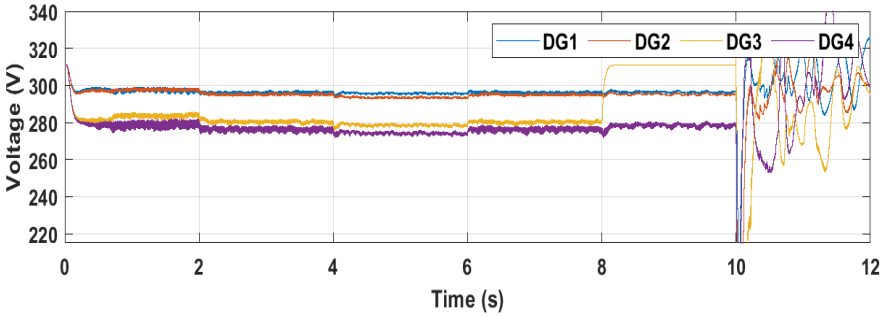

(b)

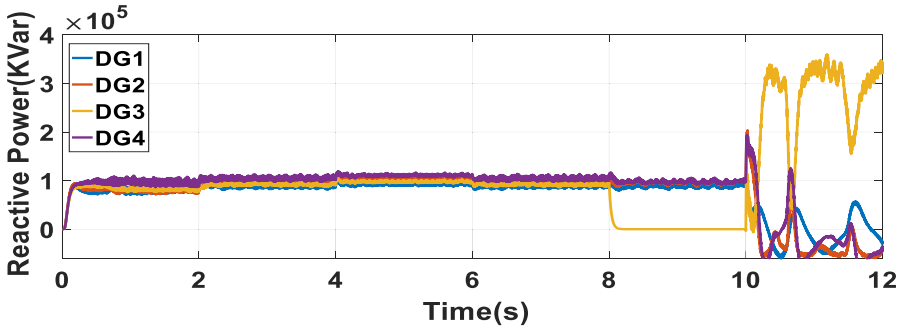

(c)

Fig. 4.10 Outputs of 4 DGs for Case 1, (a) frequency (b) voltage and (c) reactive power

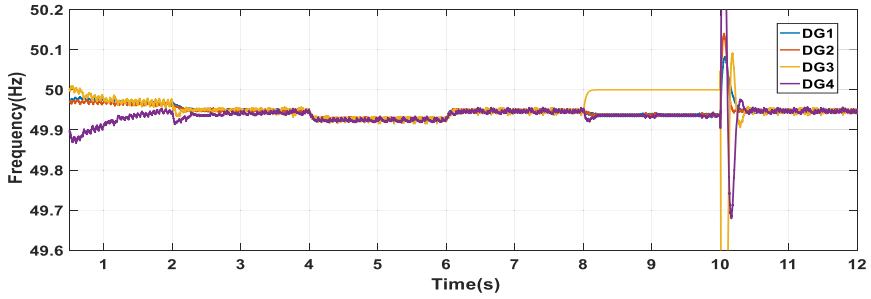

(a)

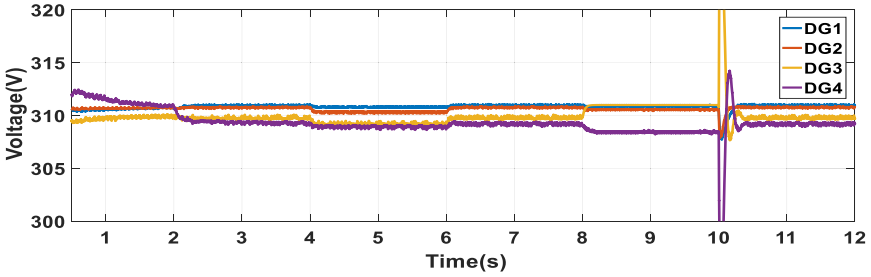

(b)

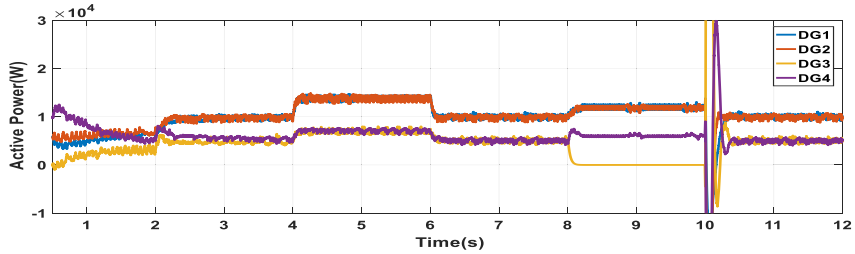

(c)

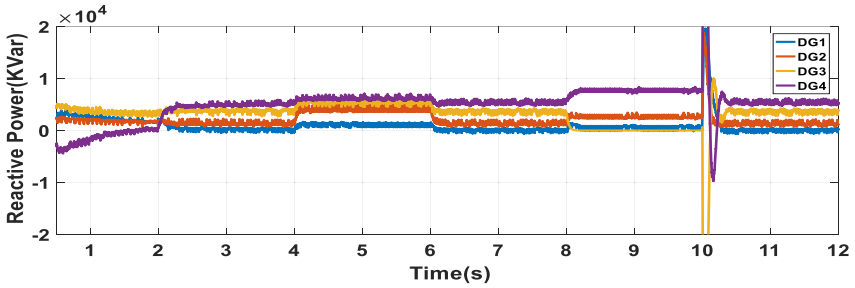

(d)

Fig. 4.11 Outputs of 4 DGs for Case 2, (a) frequency (b) voltage and (c) active power and (d) reactive power

When the conventional central control technique is applied in the secondary layer (Case 2), the voltage and frequency can be restored to their reference values, but their responses are slower than that of our proposed distributed control; see Fig. 4.12. When our proposed DSC is applied (Case 3), both voltage and frequency can be quickly restored to their reference values, respectively ($v_{ref} \approx 311V$, $f_{ref} \approx 50\text{Hz}$), which is shown in Fig. 4.12. The steady-state frequencies of the four DGs remain at the reference value (≈50Hz) no matter whether any load is connected to DG2 and DG4 or any load is disconnected from DG2. Moreover, in Case 3, the performance of plug-and-play (scenarios 4&5) capability shows better results compared with the performance in Case 2 and Case 1. This result shows that the designed distributed secondary controller can eliminate the voltage and frequency deviation caused by the primary control.

The real power outputs of the four DGs are also tested (Fig. 4.11 and Fig. 4.12). Before the SC is activated (for Case 1), the real power-sharing is well achieved by the primary control, i.e., $P_1 : P_2 : P_3 : P_4 = 1/n_{f1} : 1/n_{f2} : 1/n_{f3} : 1/n_{f4} = 2 : 2 : 1 : 1$. When the SC is started (for Case 2), real powers are still well shared according to the designed droop grains regardless of load increasing or decreasing. Reactive power-sharing is also good enough for the proposed DSC, while it is difficult for primary droop control techniques (Fig. 4.11 and Fig. 4.12).

As mentioned in the introduction, there are limited approaches to solving voltage and frequency restoration problems in a distributed way. However, we just made the comparison between the conventional method in both primary and secondary levels (Case 1 and Case 2) and our proposed method. Another thing is that the settling time for our proposed method is 0.5s compared to some similar studies where the settling times are 1.5s - 2.5s [163]. Thus, it is clear from the simulation results that our proposed method also ensures fast convergence.

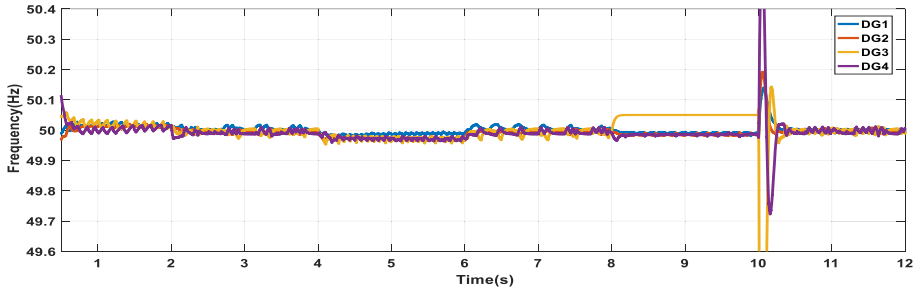

(a)

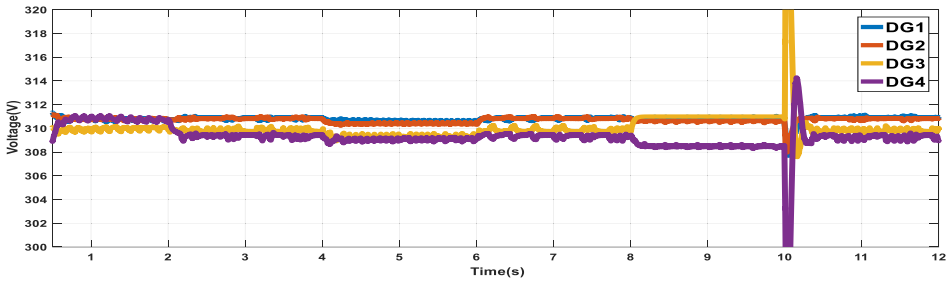

(b)

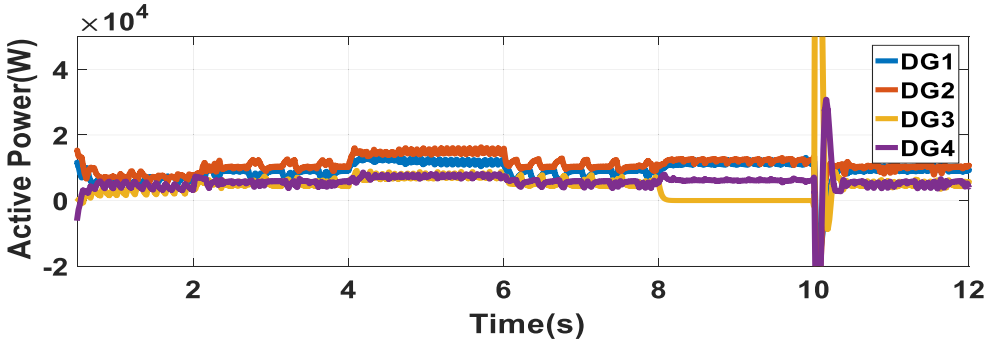

(c)

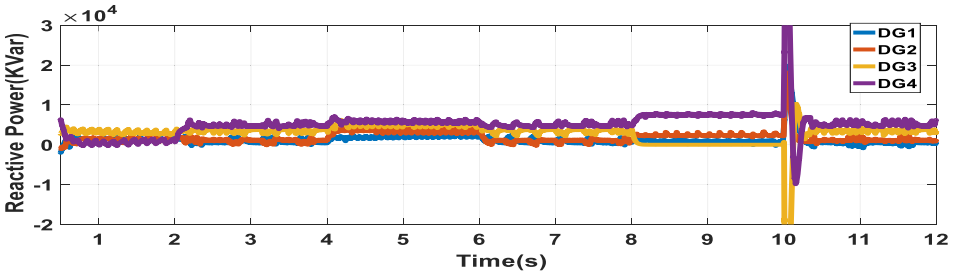

(d)

Fig. 4.12 Outputs of 4 DGs for Case 3, (a) frequency (b) voltages (c) active power and (d) reactive power

4.5.3 Comparison

While the previous sections show the behaviour of the two control methods (where their performances are compared relating to voltage restoration and reactive power-sharing), this section intends to give a more detailed view of the comparison. As such, the obtained results are summarized in Table 4.7.

For both control strategies, they can recover the voltage to the nominal values where the convergence time is pretty similar for both cases. The proposed control method in this chapter exhibits more damping characteristics than in [17] (Fig. 4.8 and Fig. 4.12). Also, the reactive power sharing accuracy is better for the control in chapter 4. In addition to that, when load disturbance occurs, the performance of [17] is not accurate enough, or the reactive power sharing among VSI is no longer satisfactory. The proposed control strategy ensures that all VSI operate as near as possible for reactive power sharing in accordance with their capacities. Although the main concerns of both methods are voltage restoration and accurate reactive power-sharing, the following comparisons can be made after taking the simulation results into account, summarised in Table 4.8.

Table 4.8 Comparison of the Performance of Two Methods

Selection criteria	The proposed method	The method in [17]
Convergence time	0.5s	0.5s
Stability	Show more stable operation for a longer period even with load disturbances	Less stable with load disturbances, plug and play capability
Reactive power sharing	Power sharing accuracy lessens with load disturbances	Can share accurate reactive power sharing even with load changes
Power quality	Better	Average

4.6 SUMMARY

There are limited approaches to solving voltage restoration problems in a distributed way. This chapter introduces a distributed secondary control method for voltage restoration, grounded on the idea of the consensus control, for islanded LV MGs to complement the primary control objective and concurrently (i) recover the system's nominal voltage, (ii) deliver precise reactive power-sharing among DG units. An integrated small-signal dynamic model of the MG has been built, taking the effect of the resistive line network into account for

proposed control methods. It is clear from the small-signal stability study that (i) the distributed secondary controller can create additional less damped modes to the system, where the contribution of the distributed secondary controllers of all the DG units is significant, (ii) the system's dynamic response is not good enough without carefully tuned control parameters, with changed load conditions and diverse sparse communication network topologies. The performance of the presented concepts/approaches has been assessed and confirmed from eigen-analysis and digital time-domain simulation of an MG test model. Based on the simulation results for the presented small-signal dynamic model, the distributed optimal controller is considered a possibly suitable solution for effectively enhancing the system stability which is done in the next chapter. The proposed control approach is also compared with the closely related control method proposed in [17]. A brief comparison between the two methods is given. According to the comparison, it can be concluded that the presented approach in this chapter is more effective in fulfilling the goal of DSC for voltage control and reactive power-sharing.

Chapter 5: Fuzzy-Based Distributed Cooperative Secondary Control with Stability Analysis for MGs

5.1 INTRODUCTION

A microgrid (MG) (containing of small-scale developing generators, loads, batteries and a regulatory element) is defined as a regulated small-scale power network, which can be functioned in an islanded and/or grid-connected operation mode assisting the requirement of complementary power and/or preserve a usual service [1]. Like the traditional power system, MG systems also follow the hierarchical control strategy for standardization of the MG operation and overall function. Generally, this hierarchical control system comprises three layers, namely, primary, secondary and tertiary control layers. The traditional droop control technique considered as the most used control at the primary control level because of its decentralised nature, which lessens the communication requirements [2]. However, the primary droop control shows some other shortcomings, including its frequency/voltage deviations according to load characteristics, inaccurate reactive power-sharing, and poor performance with nonlinear loads [3,4]. The SC level is thus introduced as a complement of primary control [2,5]. Limitations of centralised (single-point of failure) and decentralised (poor dynamic and steady-state response) control strategies have led to distributed control structures [3,6]. Recently, multi-agent structures or consensus algorithms [7,8] have received increased attention for their simple control structure utilizing sparse communication systems, improved reliability and acceptable dynamic/steady-state performance [6,8–10]. Nevertheless, the dynamic response of the MG considering distributed secondary control (DSC) could be unexpected regarding the system oscillation, reaction time, stability margins [10] and steady-state behaviour. Despite several advantages of distributed control, the limitations mentioned above are taken as key challenges for an islanded MG with DSC. The MG control system design should address these drawbacks in a proper way to manage the stability and resilience of the whole network. In this light, the following issues should be considered in the design process.

There are many methods studied for the development of the stability of the primary control [11–13]. Small-signal stability is now a significant issue in the reliable operation of an MG due to low-inertia and intermittent renewables [14]. Small-signal modelling is considered for the stability analysis for MGs with the decentralised droop control techniques at the primary level in most research works [11]. Authors in [15] succeeded in precise power-sharing considering a consensus-based droop constant controller. Small-signal stability analysis considering DSC is studied in some recent works [7,8,10,13,16,17]. Additionally, the impact assessment of DSC parameters based on the dynamic model, the requirement of fine tuning of DSC parameters for stability enhancement, and the corresponding suitable solution (i.e., fuzzy-based controller) for that are not considered. Authors in [8] study the above issue of DSC for stability analysis but the detailed mechanism of

choosing the DSC parameters for stability enhancement is not discussed. A detailed mechanism study for undesired dynamic behaviour and the probable oscillations introduced by DSC is reported in [10]. However, the use of an optimal controller for stability enhancement of the DSC leads to the system being more complex for control system design. Besides, in most works, the power lines are considered to be purely inductive, which makes the models and proposed solutions inaccurate and impractical for a networked MG [18]. References [19–21] assume purely inductive grids are used for dynamic studies of distributed secondary frequency controller (DSFC) [20] and the distributed secondary voltage controller (DSVC) [19, 21]. Virtual impedance is mostly implemented into the droop control for converting the feeder impedance inductive, which will decouple the active and reactive power regulation [22–27]. Some researchers have suggested applying the virtual impedance as a means of employing precise reactive power in MGs [24, 27]. Another approach in [24, 28] proposed an adaptive virtual impedance for eliminating the impedance incompatibility in the feeders. Still the stability study is unresolved, and the DG units are considered by means of equal rating.

Apart from this, the conventional voltage-reactive power droop control results in inaccuracy in reactive power-sharing with small feeder line impedances [18, 29]. An improved droop control was suggested in [30], where incorrect reactive power-sharing is yet noticed under clearly non-uniform line impedances. In addition, current SC approaches are categorized as centralised [31], decentralised [32–34] and distributed control [6,8,9,21,35]. This is somewhat motivated by the cooperative control concept for multi-agent structures [6,8,9,32,33], letting all distributed energy resources (DERs) connect through their neighbours across local communication systems. Maximum distributed reactive power control (DRPC) techniques apply the voltage sensitivity analysis-based scheme [33,36] as per the literature for calculating the exact amount of reactive power, which each DER requires to maintain the system voltage within allowable boundaries. Nevertheless, the sensitivity technique necessitates linearization of the power flow equations around the usual operating point, which can cause the wrong re-estimation of the necessary reactive power, specifically for MG networks with low X/R ratio and high penetration of DERs. Therefore, the overall system losses are increased, which introduces a probable inconvenience on the primary distribution network, including extreme requirement of reactive power.

However, another work, introduced in [37], applies predefined equal local voltage regulator functions designed for every DER in the network. This kind of method greatly suffers from one requirement, which necessitates a thorough procedure for finding optimal parameters by tuning and describing these functions. The voltage regulation may be useless or can affect an excessive quantity of reactive power flow in the scheme without accurate tuning [36]. To resolve this issue, suitable and efficient tuning is a prerequisite that is significant to accomplish the system stability and have reliable operation against load change and large disturbances. Computational intelligence algorithms such as fuzzy logic (FL) [4,38,39], genetic algorithm (GA) [40,41] and particle swarm optimization (PSO) [13,42] have been commonly used. However, GA has some limitations, e.g., premature convergence. On the other hand, PSO is a population-based search technique deriving from models of insect swarm. In the existing works [43], intelligent techniques such as FL, PSO and GA are used to obtain optimal controller parameters. Authors proposed in [41] a non-linear and non-convex optimization problem, which contains eigenvalues constraints. Therefore, PSO is implemented to resolve the issue for attaining the optimal distributed control parameters. When associated with more stochastic algorithms, it has been realized that PSO necessitates less computational effort. Even though PSO has presented its potential in many aspects for

resolving diverse optimization problems, it still needs significant execution time to get solutions for large-scale engineering problems [41].

Alternatively, the fuzzy logic controllers (FLCs) algorithms can tune the system constraints and outputs based on the information feed automatically to the system, which enhances the system's simplicity and flexibility. FLC can handle problems with imprecise and incomplete data, and FLCs are cheaper to build. To reduce the complexity and enhance the controller flexibility, this chapter proposed the FLC tuner for DSC. The authors in [44] introduce a DSC framework of islanded MGs. An intelligent FL-based scheme is suggested for proper tuning of the consensus parameters, but only voltage regulation and reactive power sharing are taken into account [44]. Authors in [45] considered both voltage and frequency regulation of an islanded MG relied on a FLC structure. Dynamics of the scheme, i.e., plug-and-play capability and fault occurrence, are not included. Authors in [4] proposed a novel scheme to control the reactive power nominal value of distributed generation (DG) components consistent with their involvement in reactive power sharing in islanded MG. According to the recommended method, FL is implemented to design the X/R ratio of the connecting power lines into the consensus signals for proper participation of DG units for precise active and reactive power sharing irrespective of the nature of feeder impedance. Although the proposed control can share the power accurately, the control level was studied for the primary control level only. In addition, the point of common coupling (*PCC*) bus voltage, reliant on the DSVC, essentially is being re-established to confirm the nonstop action of sensitive loads. Authors in [46] offer critical bus voltage reestablishment; though, it does not concurrently preserve precise reactive power-sharing among DG units. The conventional droop control technique exhibits some other limitations such as steady-state frequency deviation from the rated value, poor dynamic behaviour and high sensitivity to measurement noises [5,18,29]. Thus, conventional droop control cannot assure the high accuracy of frequency control and power-sharing. As a result, a secondary regulation system has been introduced to guarantee a steady frequency profile in the MG [5]. In the existing literature for frequency control and active power-sharing, SC systems of MGs are generally classified into three groups: centralised [47], decentralised [32,48,49] and distributed [8,9,21,35,36,50,51]. The central controller for frequency restoration also faces the possibility of a single point of failure and could have trustworthiness and scalability concerns [2,8,25,31,49]. Recently, numerous DSC strategies have been stated in the literature. Most methods are based on consensus practice [4,8,9,50–53], where the agents achieve consensus by means of exchanging information over a sparse communication system. The control method described in [51] reports simply frequency restoration through a distributed averaging proportional-integral controller but requires a centralised communication configuration regardless of its decentralised execution. In [54], a DSFC scheme using linear input and output feedback was offered. The communication among neighbouring DG units is straightforward, but power-sharing is less focused. The authors in [21,49,52] proposed a DSC for frequency control and accurate active power-sharing in islanded MGs where the voltage regulation is not considered. The distributed control methodologies referred to in [46,55] deal with both voltage and frequency restoration, but a comprehensive model of the MG system is a prerequisite. Authors in [56] addressed the issue of frequency restoration and active power-sharing, but methods of choosing DSC parameters make the system more complex. On the other hand, the selection of controller gains relies on the algebraic connectivity of the communication system.

However, centralised or DSC requires assistance from communication networks. Communication delay is an unavoidable and intrinsic matter for the period of the signal transmission procedure. A large communication

delay can worsen the system's dynamic behaviour, reduces the system stability margin and even causes an unstable structure [57]. Hence, it is essential to examine the effect of communication delay on system stability, also examine the relating delay compensation technique to get a stable system [16,35]. Furthermore, inevitable noise disruptions from communication channels and the external surroundings (i.e., produced by environmental reasons, for example, rain, etc.) could disturb MG's dynamic behaviour [58]. Thus, to study the DSC problem for AC autonomous MG considering communication delay, communication link failure and noise is required. This has not been significantly or accurately reflected in a single control approach in prior research [8,21,33,35,45]. Extensive time-domain simulations considering different case studies like communication restriction, fault occurrence and plug-and-play capability considered at the same time are not taken into account in the previous research works to verify the robustness of the DSC (see all the references mentioned in this chapter).

According to the literature review, it can be realized that DSC is more effective than the centralised one [3]. Due to the limited research undertaken so far, as mentioned in the literature review, a proper DSC is still needed that considers all the drawbacks in a single control strategy. To this end, motivated by the existing limitations, this chapter proposes a new DSC, which has contributions from the following viewpoints:

- A novel DSC is proposed for lossy MGs to restore frequency and voltage simultaneously while accurate active and reactive power-sharing are preserved.
- Unlike the existing consensus methods, the proposed method utilizes a proportional-integral (PI) controller at the output voltage of the inverter. Thus, voltage mismatches are reduced to a great extent.
- The small-signal stability analysis under the proposed DSC for the networked MG model is carried out in detail. Note that eigenvalue analysis for parallel-connected DGs in the MG was previously studied in many studies, but very few studies have addressed the small-signal stability analysis for a networked MG model considering DSC.
- In most of the previous related works, other tuning methods/optimal controllers are used for finding DSC parameters. Utilizing the intelligent FL parameter-tuner in accordance with small-signal stability analysis for the networked MG model has been presented as a new solution. The FLC not only enhances the performance of the proposed DSC but also lessens the complexity of the DSC design.

The rest of this chapter is oriented as follows. Section 5.2 represents the specifics of the suggested DSC design. Section 5.3 shows the small-signal dynamic model of MG. Section 5.4 shows the small-signal stability analysis, and Section 5.5 discusses the time-domain simulation results. Conclusions along with future works are presented in Section 5.6.

5.2 THE PROPOSED DISTRIBUTED SECONDARY CONTROLLER

An autonomous MG consists of DG units, the power network, and local loads as depicted in Fig. 5.1. In the test MG model, there are several nodes where some are associated with DG units and loads, and some are associated with only loads. The grid-forming voltage source inverters (VSIs) are essential in the islanded

operation mode to form voltage and frequency within the MG. The control system of a droop-controlled VSI, including inner voltage and current loops, is illustrated in Fig. 5.1.

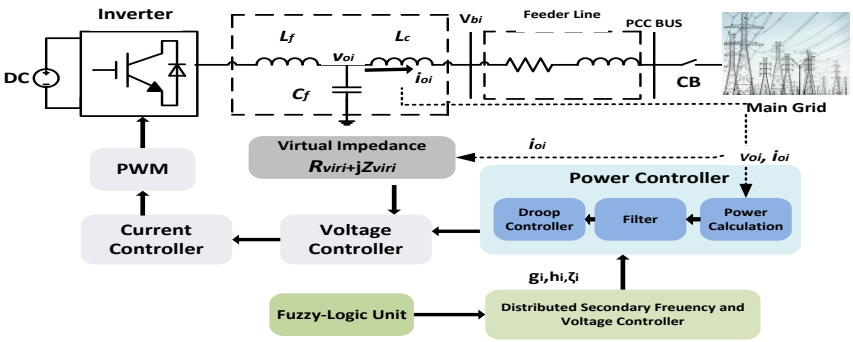

Fig. 5.1. Simplified block diagram for the distributed generation (DG) unit with primary and secondary controllers

5.2.1 Traditional Droop Controller

The following equations represent the traditional droop controller of the i^{th} DG for frequency control and voltage control to accomplish active and reactive power sharing, correspondingly:

$$f_{refi} = f_n - k_{fi}P_i \tag{5.1}$$

$$\begin{cases} v_{drefi} = v_n - k_{vi}Q_i - R_{viri}i_{odi} + \omega_n L_{viri}i_{oqi} \\ v_{qrefi} = -R_{viri}i_{oqi} - \omega_n L_{viri}i_{odi} \end{cases} \tag{5.2}$$

where P_i and Q_i are the active and reactive powers of the i^{th} DG units, respectively, k_{fi} and k_{vi} are the frequency and voltage droop gains, respectively, f_n and v_n are the nominal frequency and voltage, respectively, v_{drefi} and v_{qrefi} are the reference values for the direct-quadratic (d-q) components of voltage magnitude in the synchronous reference frame, ω_n denotes the nominal angular frequency, R_{vir} and L_{vir} are embedded to model the virtual resistance and virtual inductance, respectively, v_{odi} *and* v_{oqi} are the *d-q* components of the inverters output voltage and i_{odi} and i_{oqi} are the *d–q* components of the inverters output current. Based on Equations (5.1) and (5.2), the frequency and voltage excursions would be established in the autonomous MG due to load variations.

5.2.2 Consensus-Based Distributed Secondary Control

The fundamentals of the consensus algorithm and graph theory are described in Literature Review (Chapter 2) and thus not included here. In this research, a DSC system was applied locally by selecting the suitable control inputs g_i and h_i to adjust the frequency f_{refi} and voltage magnitude v_{refi} so that the frequency and voltage magnitude at MG nodes converge to the reference values f_n and v_n, respectively, while active and reactive power-sharing are established. In the proposed DSC, as explained later, g_i is related to frequency restoration and active power-sharing, h_i and τ_i are correlated to voltage restoration and reactive power-sharing, respectively. Therefore, the proposed DSC signals, which give the reference values for the i^{th} DG (synchronously including all the agents acting as a cluster) can be derived by the following equations.

Frequency restoration and active power-sharing: DSFC is used to re-establish the frequency and active power-sharing like this:

$$f_{refi} = f_n - k_{fi}P_i + g_i \tag{5.3}$$

$$g_i = -D_{fi}\int\left[\sum_{j\in N_i} a_{ij}\left(f_{refi}\text{-}f_{refj}\right)+b_i\left(f_{refi}\text{-}f_n\right)\right] - D_{Pi}\int\left[\sum_{j\in N_i} a_{ij}\left(k_{fi}P_i - k_{fj}P_j\right)\right] \tag{5.4}$$

Here D_{fi} and D_{Pi} are all positive control gains, and b_i is the communication link indicator explained later. N_i represents neighbouring nodes of node *i,* and an adjacency matrix is defined as $A_G = \left[a_{ij} \geq 0\right] \in R^{N\times N}$ where $a_{ij} = 1$ if the ith node is coupled to the j^{th} node and $a_{ij} = 0$ otherwise.

Voltage restoration and reactive power-sharing: DSVC, which includes both the voltage controller and reactive power-sharing controller, is chosen for the voltage regulation and reactive power-sharing, respectively, and can be designated by the following equations:

$$v_{refi} = v_n - k_{vi}Q_i + \omega_n L_{viri} + h_i + \tau_i \tag{5.5}$$

$$h_i = -D_{vi}\int\left[\sum_{j\in N_i} a_{ij}\left(v_{diffi} - v_{diffj}\right)+b_i\left(v_{diffi} - v_{diffpcc}\right)\right] \tag{5.6}$$

$$\tau_i = -D_{Qi}\int\left[\sum_{j\in N_i} a_{ij}\left(\frac{Q_i}{Q_{imax}} - \frac{Q_j}{Q_{jmax}}\right)\right] \tag{5.7}$$

where D_{vi} and D_{Qi} are all positive control gains and Q_{imax} is the maximum reactive power of ith DG unit. v_{diffi} and $v_{diffpcc}$ are designed through a PI controller such that both can restore to their reference values (v_n), where $v_{diffpcc}$ is calculated at the point of common coupling (*PCC*). v_{diffi} and $v_{diffpcc}$ can be expressed by the following equations:

$$v_{diffi} = K_P\left(v_{ref} - v_{oi}\right) + K_I\int\left(v_{ref} - v_{oi}\right)dt \tag{5.8}$$

$$v_{diffpcc} = K_P\left(v_{ref} - v_{pcc}\right) + K_I\int\left(v_{ref} - v_{pcc}\right)dt \tag{5.9}$$

Here, K_P and K_I are the proportional and integral control coefficients for the secondary controller. $v_{oi} = \sqrt{(v_{odi})^2 + (v_{oqi})^2}$ is the output voltage of ith inverter as shown in Fig. 5.1. $v_{pcc} = \sqrt{(v_{pccD})^2 + (v_{pccQ})^2}$ is the voltage at *PCC*. The subscripts *d* and *q* (D and Q) indicate the direct and quadrant component in the local (common) reference frame. In Equations (5.4) and (5.6), b_i = 1 indicates the direct communication of the i^{th} DG with the controller at *PCC* and otherwise $b_i = 0$.

5.3 SMALL-SIGNAL MODELLING

The small-signal state-space model for networked MG is obtained considering the small-signal modelling of VSIs, the power network and load dynamics. A systematic approach to obtaining the state-space equations of the network and loads is shown and combined with the inverters' state-space equations. The reference frame of a given DG unit, preferably the biggest one (which has the smallest droop gain and thus less frequency variation to follow the slack bus concept in bulk power systems), is taken as a common reference frame. All other inverters were converted to this common reference frame utilizing the corresponding transformation, which is already described in Section 3.4.1.

5.3.1 Individual Inverter Modelling

Now, to derive the state-space model, first define $\sigma_i = \int (v_{ref} - v_{oi})\, dt$ in (5.8) and get the following:

$$\Delta\dot{\sigma}_i = -\Delta v_{oi} \tag{5.10}$$

$$\Delta v_{oi} = n_{di}\Delta v_{odi} + n_{qi}\Delta v_{oqi} \tag{5.11}$$

where, $n_{di} = \frac{v_{odi}}{\sqrt{(v_{odi})^2+(v_{oqi})^2}}, n_{qi} = \frac{v_{oqi}}{\sqrt{(v_{odi})^2+(v_{oqi})^2}}$

Considering virtual impedances, the linearised inverter output voltage equations become

$$\begin{cases} \Delta v_{0di} = -k_{vi}\Delta Q_i + \Delta h_i + \Delta\tau_i - R_{viri}\Delta i_{0di} + X_{viri}\Delta i_{0qi} \\ \Delta v_{0qi} = -R_{viri}\Delta i_{0qi} - X_{viri}\Delta i_{0di} \end{cases} \tag{5.12}$$

In reference to our proposed control strategy, the modelling of an individual inverter unit after linearization in the common reference frame considering only the primary control (droop control) can be written as follows:

$$[\dot{\overline{\Delta X}}_{inv\imath}] = [\bar{A}_{invi}]\,[\overline{\Delta X}_{invi}] + [\bar{B}_{invi}]\,[\Delta i_{0DQi}] + [\bar{C}_{invi}]\,[\Delta\omega_{com}] \tag{5.13}$$

where $\overline{\Delta X}_{invi} = [\Delta\delta_i, \Delta P_i, \Delta Q_i]^T$, and $\Delta i_{0DQi} = [\Delta i_{0Di}, \Delta i_{0Qi}]^T$ represents the deviation of the inverter output current in the DQ frame.

Consequently, the state-space model of an individual DG with DSC is obtained after linearization (around an operating point) and a combination of Equations (5.1)– (5.13) as follows:

$$\begin{cases} [\dot{\Delta X}_{inv\imath}] = [A_{1invi}][\Delta X_{invi}] + [A_{2invi}][\Delta i_{0DQi}] + [A_{3invi}][\Delta\omega_{com}] + [\sum_{j\epsilon N_i} A_{4invij}][\Delta X_{invj}] + [A_{5invi}][\Delta v_{diffpcc} \\ \begin{bmatrix}\Delta\omega_{refi} \\ \Delta v_{0DQi}\end{bmatrix} = \begin{bmatrix}C_{inv\omega i} \\ M_{invi}\end{bmatrix}[\Delta X_{invi}] + \begin{bmatrix}0 \\ N_{invi}\end{bmatrix}[\Delta i_{0DQi}] \end{cases} \tag{5.14}$$

where $\Delta X_{invi} = [\Delta\delta_i, \Delta P_i, \Delta Q_i, \Delta g_i, \Delta h_i, \Delta\tau_i, \Delta\sigma_i]^T$.

In Equation (5.14), A_{1invi}, A_{2invi}, A_{3invi}, A_{4invij}, A_{5invi}, $C_{inv\omega i}$, M_{invi} and N_{invi} are all the parameter matrices of the i^{th} DG and given in Appendix A. A_{4invij} represents the correlations between DG_i and the neighbor DG_j provided by the DSC. $\Delta\omega_{refi}$ and $\Delta\omega_{com}$ are the frequency deviations of the individual and common reference frame. $\Delta v_{0DQi} = [\Delta v_{0Di}, \Delta v_{0Qi}]^T$ represents the deviations of inverter output voltage in the DQ frame.

5.3.2 Combined Model of All the Inverters

In this chapter, four DGs were considered in the proposed MG model (Fig. 5.2). Thus, by merging (5.14) for four inverters, the combined model of all inverters in the linearised form can be written as:

$$\begin{cases} [\dot{\Delta X}_{inv}] = [A_{1inv}][\Delta X_{inv}] + [A_{2inv}][\Delta i_{0DQ}] + [A_{3inv}][\Delta\omega_{com}] + [A_{5inv}][\Delta V_{diffpcc}] \\ [\Delta v_{0DQ}] = [M_{inv}][\Delta X_{inv}] + [N_{inv}][\Delta i_{0DQ}] \end{cases} \tag{5.15}$$

where

$$\Delta X_{inv} = [\Delta X_{inv1}\ \Delta X_{inv2}\ \Delta X_{inv3}\ \Delta X_{inv4}]^T,$$

$$\Delta i_{0DQ} = [\Delta i_{0DQ1} \quad \Delta i_{0DQ2} \quad \Delta i_{0DQ3} \quad \Delta i_{0DQ4}]^T, \ [\Delta\omega_{refi}]=[\Delta\omega_{com}]$$

$$\Delta v_{0DQ} = [\Delta v_{0DQ1} \quad \Delta v_{0DQ2} \quad \Delta v_{0DQ3} \quad \Delta v_{0DQ4}]^T,$$

$$A_{1inv} = \begin{bmatrix} A_{1inv1} & A_{4inv1} + A_{3inv2}.C_{invω2} & 0 & A_{4inv2} \\ A_{4inv3} & A_{4inv2} + A_{3inv2}.C_{invω2} & A_{4inv4} & 0 \\ 0 & A_{4inv5} + A_{3inv2}.C_{invω2} & A_{1inv3} & A_{4inv6} \\ A_{4inv7} & A_{3inv2}.C_{invω2} & A_{4inv8} & A_{1inv4} \end{bmatrix},$$

$$A_{2inv} = diag(A_{2inv1}, A_{2inv2}, A_{3inv3}, A_{4inv4}),$$

$$A_{3inv} = [0\ 0\ A_{3inv2}\ 0], A_{5inv} = [0\ 0\ A_{5inv2}\ 0],$$

$$C_{invω} = [0 \quad C_{invωi} \quad 0 \quad 0],$$

$$M_{inv} = diag(M_{inv1}, M_{inv2}, M_{inv3}, M_{inv4}),$$

$$N_{inv} = diag(N_{inv1}, N_{inv2}, N_{inv3}, N_{inv4})$$

In this modelling technique, all the individual DG inverters are modelled separately and then combined, which will finally be integrated with the network and load models.

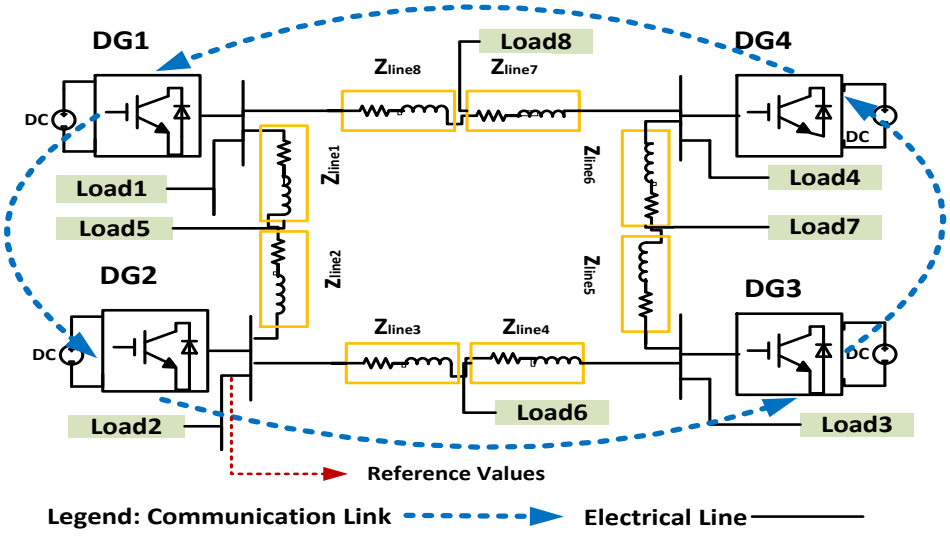

Fig. 5.2. Single line diagram of the MG test model with the communication link

5.3.3 Network and Load Model

The network and load models were obtained by linearizing the node voltage equations considering Fig. 5.2. There were no incoming currents in the network or load nodes. From the linearised node voltage equations, we have the following:

$$Y_1\Delta v_{0DQ} + Y_2\Delta v_{netloadDQ} = \Delta i_{0DQ} \tag{5.16}$$

$$Y_3\Delta v_{0DQ} + Y_4\Delta v_{netloadDQ} = 0 \tag{5.17}$$

where Δi_{0DQ} represents Δi_{0DQi} of all the DG units, Δv_{0DQ} represents Δv_{oDQi} of all the inverters and the voltage deviations of all the network and load nodes are represented by $\Delta v_{netloadDQ}$. Y_1, Y_2, Y_3 and Y_4 are the submatrices of the nodal admittance matrix Y, i.e., $Y = \begin{bmatrix} Y_1 & Y_2 \\ Y_3 & Y_4 \end{bmatrix}$. By eliminating $\Delta v_{netloadDQ}$, we have

$$\Delta v_{0DQ} = \left(Y_1 - Y_2 {Y_4}^{-1} Y_3\right)^{-1} \Delta i_{0DQ} \tag{5.18}$$

Substituting Equation (5.19) into Equation (5.18), we can write

$$\Delta i_{0DQ} = ((Y_1 - Y_2 Y_4^{-1} Y_3)^{-1} - N_{inv})^{-1} \; M_{inv} \; \Delta X_{inv} \tag{5.19}$$

Δv_{diff} is defined in terms of Δi_{0DQ} as follows:

$$\Delta v_{diffDQ} = IMP_{pcc} \Delta i_{0DQ} \tag{5.20}$$

where IMP_{pcc} is the impedance matrix and can be calculated from the nodal admittance matrix Y of node voltage equations.

5.3.4 Complete Small-Signal Model

Similarly, to define v_{pcc} considering (5.9) and letting $\in = \int \left(v_{ref} - v_{pcc}\right) dt$, we have

$$\dot{\Delta \in} = -\Delta v_{pcc} \tag{5.21}$$

$$\Delta v_{diffpcc} = -K_P \Delta v_{pcc} + K_I \Delta \in \tag{5.22}$$

Here, $\Delta v_{pcc} = m_D \Delta v_{pccD} + m_Q \Delta v_{pccQ}$ where, $m_D = \frac{v_{pccD}}{\sqrt{(v_{pccD})^2 + (v_{pccQ})^2}}, m_Q = \frac{v_{pccQ}}{\sqrt{(v_{pccD})^2 + (v_{pccQ})^2}}$

The complete MG dynamic model in the linearised form can be formulated by combining Equations (5.15) – (5.22) as follows.

$$\begin{bmatrix} \dot{\Delta X_{inv}} \\ \dot{\Delta \in} \end{bmatrix} = A_{system} \begin{bmatrix} X_{inv} \\ \Delta \in \end{bmatrix} \tag{5.23}$$

The detailed stability analysis includes the mechanism of the unwanted dynamic behaviour, along with the oscillations, which can be accomplished utilizing the eigen-arrangement of the system's state matrix, A_{system} as given in the next section.

5.4 STABILITY ANALYSIS

A single line drawing of the experimental MG model, including four inverter-based DG units, local loads and feeder lines, is shown in Fig. 5.2. The MG considered here was a 311 V and 50 Hz system and was simulated in MATLAB. The MG functioned in the autonomous mode. Here, every load was considered as a 3-phase series RL load, and every feeder line was a 3-phase series RL branch. Fig. 5.2 also shows the sparse communication link (blue dashed lines) of the MG system, and its related adjacency matrix was A_G = [aij], where the DG2 outputs were considered as the nominal values and the pinning gain b_2 in Equations (5.3) and (5.5) was set as b_2 = 1.

5.4.1 Eigenvalue Analysis

System dynamic behaviour and the outcomes from the stability analysis for the test MG under the suggested DSC were discussed in this section. In line with the stated linearised model in the prior section, the subsequent eigenvalues for the system with DSC were presented in Fig. 5.3 for stable operation. As the eigenvalues of high and intermediate frequency modes had insignificant influences on system stability [14], this chapter mainly put an emphasis on the analysis of the low-frequency modes. There were nine less damped modes, among which four were introduced by the proposed DSC, i.e., modes 6–9. It was assumed that the communications among the DG units are followed by the directed graph as in Fig. 5.2 (blue dashed line).

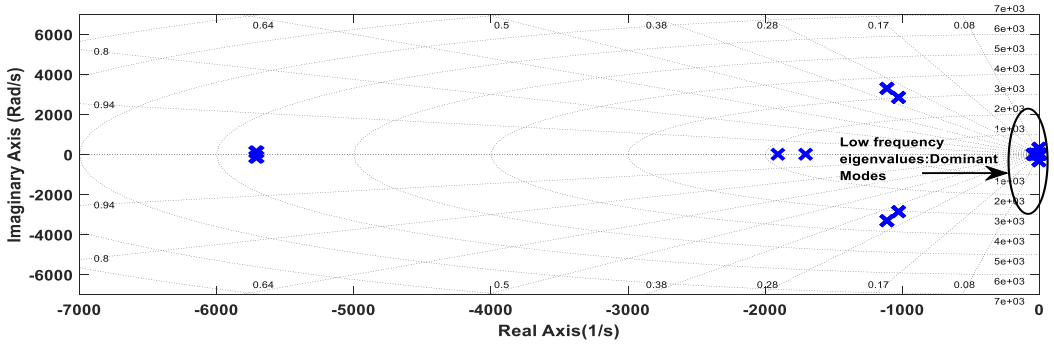

Fig. 5.3. Eigenvalues of system matrix with distributed secondary control (DSC) for stable operation

Participation Factor: The participation factor was employed to obtain the connection between the state variables and the modes and is the multiplication of the corresponding quantity in the right and left eigenvectors of the state matrix [14]. For the primary droop control, the low-frequency modes are primarily affected by the states of the active power droop controller (5.1), i.e., $\Delta\delta_i$ and ΔP_i recommended by participation factors in [154]. Fig. 5.4 shows the relation of the participation factors of the system state variables associated with the modes 6–9 considering the proposed DSC in action. Participation factors related to modes 1–5 were mainly for the primary droop control, and this was the same as the case when only primary droop control was functional to the system, which was not the main concern in this chapter. Thus, only the effects of the proposed DSC in the modal analysis were discussed, and those of modes 1–5 were not shown. A brief description of the outcomes (Fig. 5.4) is given as follows.

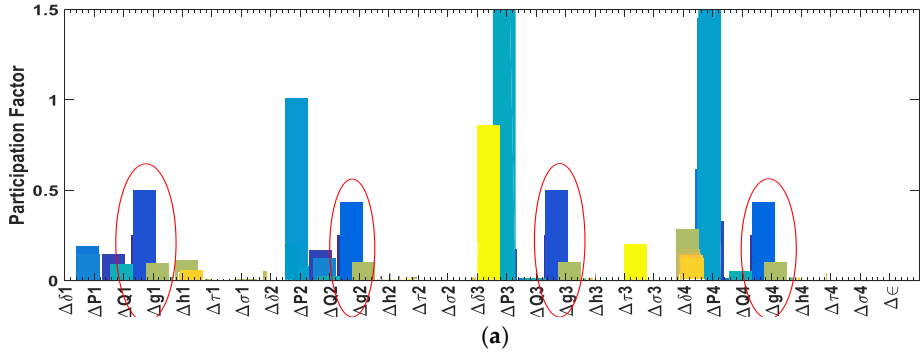

(a)

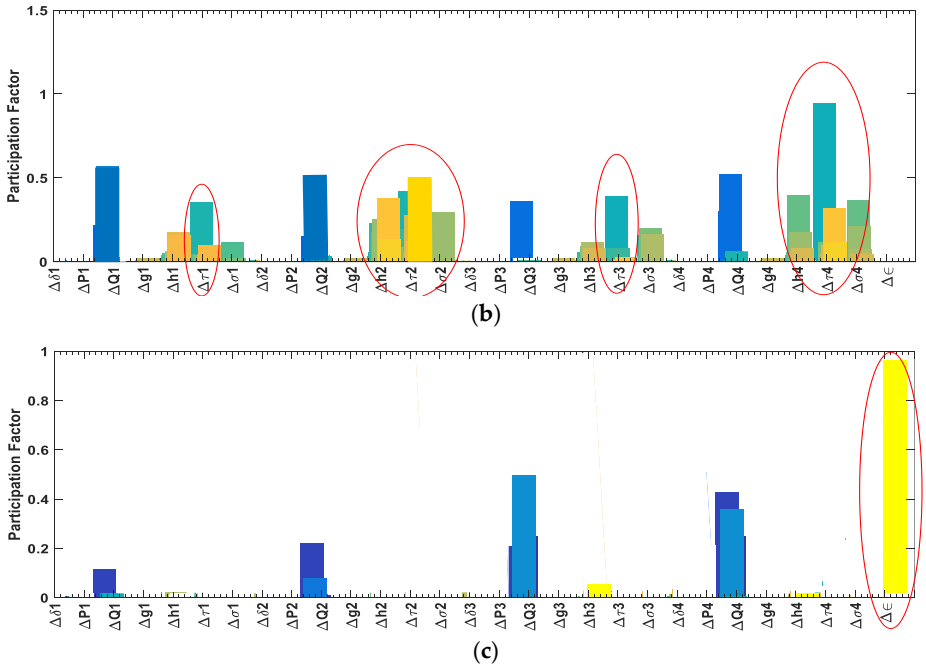

Fig. 5.4. Participation factors of modes 6–9 (a) Mode 6; (b) Modes 7 and 8 and (c) Mode 9

Fig. 5.4(a) indicates that $\Delta\delta_i$, ΔP_i and Δg_i of every DG unit actively participated in the oscillation caused by mode 6, revealing the direct participation of these states of all the DG units in the stability. As Δg_i is the state variable for the DSC as in (5.3) it is remarkably affected by the secondary controller gains D_{fi} and D_{Pi} and thus affects the stability of the system.

Fig. 5.4(b) illustrates that the states ΔQ_i, Δh_i and $\Delta\tau_i$ of the proposed DSC for voltage control and reactive power-sharing considerably contributed to creating modes 7 and 8 and were strongly affected by the controller gain D_{Qi}. DSC gain D_{vi} had less of an effect on stability.

Fig. 5.4(c) revealed that mode 9 was caused by the states ΔQ_i and $\Delta\in$. The states $\Delta\in$ and ΔQ_i were strongly associated with DSC proportional control gain (K_P), integral control gain (K_I) and virtual reactance (X_{viri}), respectively.

The detailed effects of the controller parameters K_P, K_I, D_{fi}, D_{vi}, D_{Pi}, D_{Qi} and virtual impedance values Z_{viri} on the less damped modes were analysed in detail in the following section.

5.4.2 Relationship between System Stability and DSC Parameters

The sensitivity of the system stability to the distributed control parameters was analysed with the help of stability margin. The traces of low-frequency modes of the system as functions of K_I, K_P, D_{fi}, D_{Pi}, D_{Qi} and Z_{viri} (which includes R_{viri} and X_{viri}) were taken into account to determine the effect on stability. Fig. 5 presents the traces of less damped modes as the function of X_{viri}, K_I, K_P, D_{Qi}, D_{fi} and D_{Pi}. The traces of low-frequency modes as functions of R_{viri} were like X_{viri}, and those of K_P were similar to K_I, which are not shown here. Note that the variation of D_{vi} had comparatively less effect on system stability, and thus it is not shown here. Fig. 5a shows the changes in the damping of mode 9 when K_I varied from 5 to 40. These variations mainly affected the least damped mode 9.

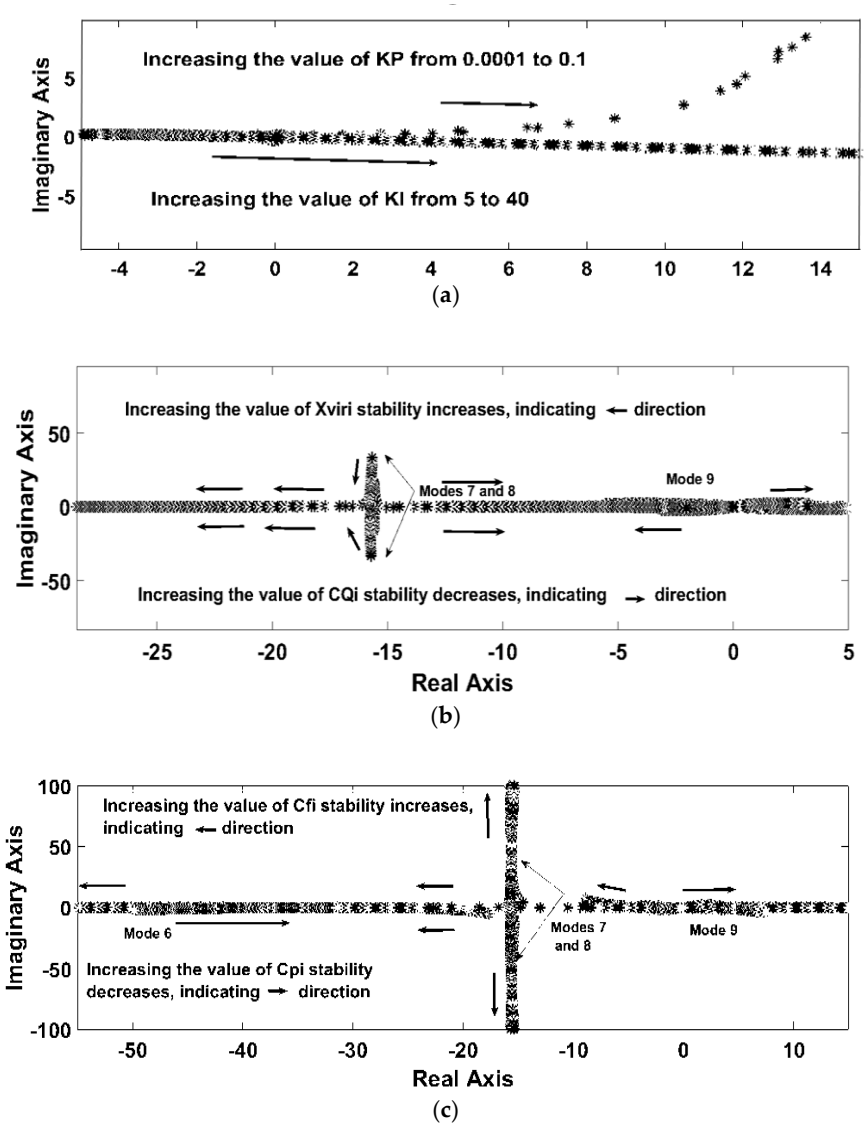

Fig. 5.5. Traces of dominant modes 6–9. (a) Traces of dominant mode 9 when K_P varies from 0.0001 to 0.1 and K_I varies from 5 to 40; (b) traces of dominant modes 7 and 8 when X_{viri} varies from 0.01 to 0.5 Ω and D_{Qi} varies from 10 to 40 and (c) traces of dominant mode 6 when D_{fi} varies from 100 to 400 and D_{Pi} varies from 100 to 400

Fig. 5.5(b) shows variation in the damping of the modes 7 and 8 when X_{viri} varied from 0.01 to 0.1 Ω, and D_{Qi} varied from 10 to 40, respectively. From this, increasing the value of X_{viri} and D_{Qi} had the opposite effects on system stability. Fig. 5.5c shows that D_{fi} and D_{Pi} also had reverse effects on the oscillation. Table 5.1 gives a summary of the above analysis. On the other hand, finding suitable values for DSC parameters was difficult by traditional approaches, e.g., trial and error scheme and from the traces of low-frequency modes for stability improvement. Accordingly, intelligent fuzzy logic was used for proper tuning of controller parameters for stability improvement in terms of fast response, appropriate damping and satisfactory stability margin.

Table 5.1 System Dynamics and Stability Analysis Result.

Less damped modes	Major participants (states)	Major participants (Controller parameters)	Effects on damping/stability	
			Stability	Controller parameters
Modes 1–6	$\Delta\delta_i,\ \Delta P_i, \Delta g_i$	D_{fi}	↑	D_{fi} ↑
		D_{Pi}	↓	D_{Pi} ↑
Modes 7 and 8	$\Delta Q_i, \Delta\tau_i$	D_{Qi}	↓	D_{Qi} ↑
		X_{viri}	↑	X_{viri} ↑
Mode 9	$\Delta\in$	K_I	↓	K_I ↑
		K_P	↓	K_P ↑

5.4.3 Tuning the DSC Parameters Based on Fuzzy-Logic

This chapter presents a fuzzy logic-based tuner for regulating the DSC parameters and virtual impedance used in the consensus-based DSC framework. Membership function, fuzzy logic operators and if-then rules are the usual elements of a fuzzy inference system. These elements were used to manipulate the mapping from the input values to the output values, and it involved three sub-processes: fuzzification, aggregation and defuzzification. Here, the Mamdani fuzzy inference scheme was applied. The goal was to determine the DSC parameters K_I, K_P, D_{fi}, D_{Pi}, D_{Qi} and virtual impedance values R_{viri} and X_{viri} related to the fuzzy logic system as in Fig. 5.6. A set of fuzzy rules containing 16 rules was taken for tuning the controller parameters. The triangular membership function (MF) was employed for arranging the fuzzy rules, which is the most popular one. The input rules were collected by using the AND operator. The training arrangement is presented as follows.

Fuzzifier: The inputs, outputs and their ranges were identified in this step. The membership functions for inputs and outputs were organized as: not stable (NOTS), very low stability (VLS), low stability (LS) and normal stability (NS). Fig. 5.7 displays the MFs for input and output constraints of every input and output. In this chapter, frequency stability margin and voltage stability margin were considered as inputs, while DSC parameters and virtual impedance were considered as outputs.

Aggregation: The knowledge base for the fuzzy logic system is a group of fuzzy if-then rules as expressed in the following formula, e.g., rule 10 from Table 5.2 describes the following:

$$R^{10}: If\ f_{ref}\ is\ ¥_{f_{ref}(LS)}\ and\ v_{ref}\ is\ ¥_{v_{ref}(VLS)}, then\ D_{pi}\ is\ ¥_{D_{pi}(LS),}$$

$$D_{vi}\ is\ ¥_{D_{vi}(LS)}, D_{Qi}\ is\ ¥_{D_{Qi}(LS),}\ R_{viri}\ is\ ¥_{R_{viri}(LS),}\ and\ X_{viri}\ is\ ¥_{X_{vir}(LS)}\ .$$

According to this rule, if the degree of MFs (¥) for frequency stability region is LS and for voltage stability region is VLS, the outcomes for all outputs are LS. The rules are summarized in Table A1 (Appendix A).

Defuzzifier: The fuzzy outputs were transformed to non-fuzzy values in this step. Thus, the centre average defuzzification principle based on triangular was applied to measure the crisp outputs, i.e., DSC parameters.

Based on the above rules, the estimated values for DSC parameters and virtual impedance were determined and given in Table 5.3. In this study, we assumed that the DSC is activated from the beginning with the droop control (primary control). The importance of parameters X_{viri} and D_{Qi} was designated in accordance with voltage and reactive power. The value of X_{viri} was less than *0.22 Ω*, which indicates that, for values bigger

than *0.22 Ω*, the system might be unstable. Similarly, the suitable values of K_I, K_P, D_{fi}, D_{Pi}, D_{Qi} and R_{viri} were found to utilize the fuzzy logic tuner. These values were also verified by the time-domain simulation results. The following sections give detailed explanations with the simulation results. Fig. 5.8 shows the 3-dimensional representations of outputs D_{fi} and X_{viri} with inputs. The eigenvalue spectrum of dominant modes is presented in Fig. 5.9, which confirms the usefulness of the fuzzy logic tuner for system stability improvement.

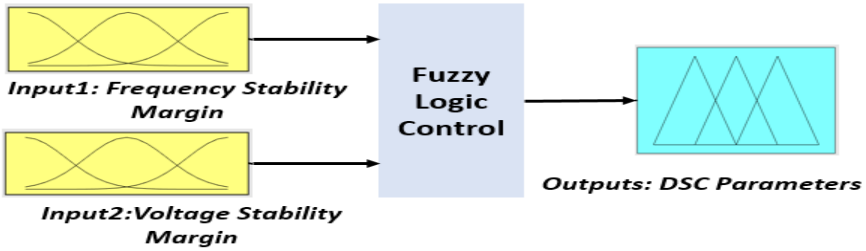

Fig 5.6. Input–output relations of the proposed fuzzy logic tuner

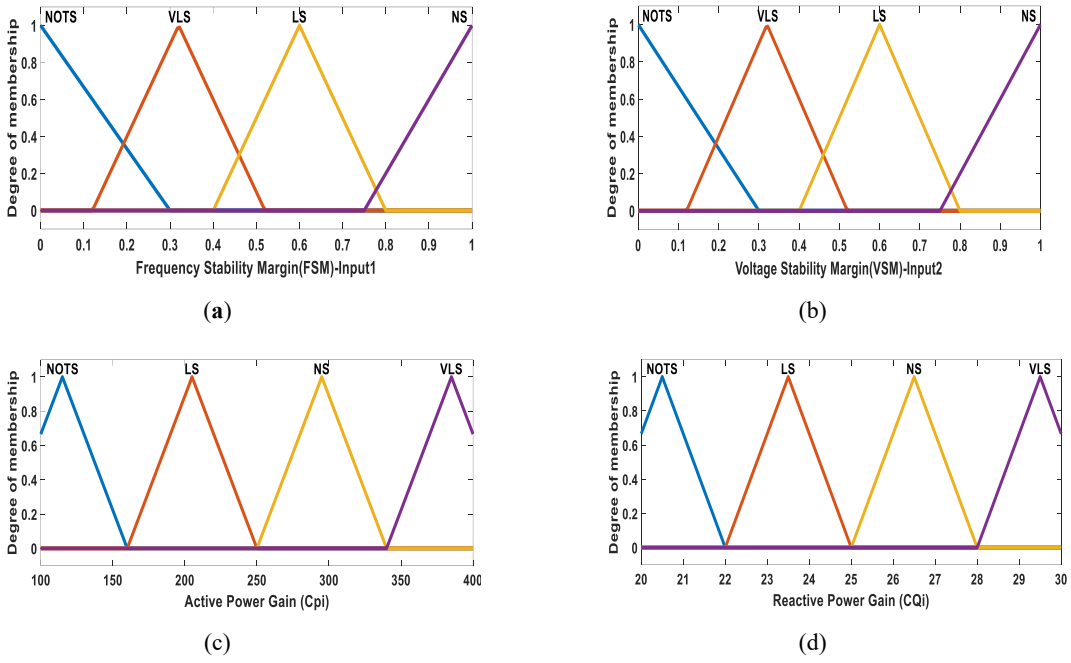

(**a**) (b)

(c) (d)

Fig 5.7. Membership functions for (a) input1, frequency stability region; (b) input2, voltage stability region; (c) output1, active power gain, D_{Pi} and (d) output2, reactive power gain, D_{Qi}

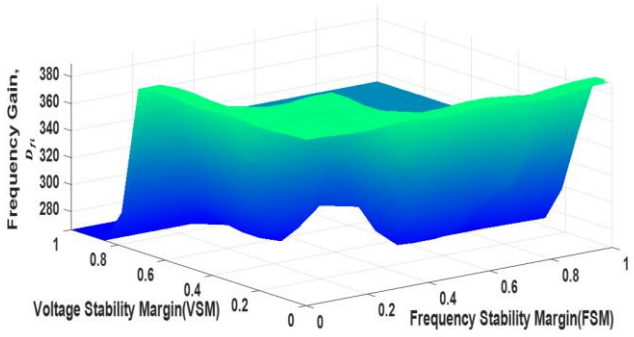

(a)

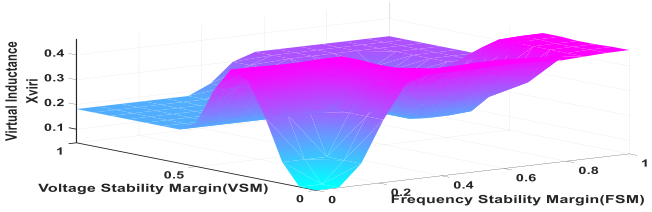

(b)

Fig. 5.8. Output surface for stability. (a) D_{fi} and (b) X_{vir}

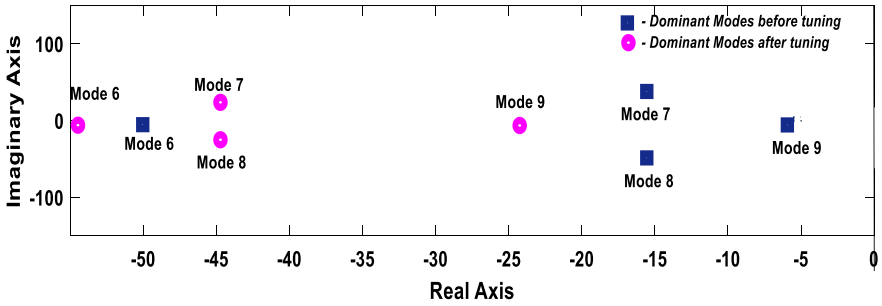

Fig. 5.9. Comparison of dominant modes with before and after tuning of DSC for stable operation

Table 5.2 Distributed Secondary Control (DSC) Parameters with and without the Fuzzy Logic Controller

Controller parameters	Values		Controller parameters	Values	
	Before tuning	After tuning		Before tuning	After tuning
K_P	0.01	0.001	D_V	100	100
K_I	18	25	D_Q	40	26.7
D_f	200	333	R_{vir}	0.08	0.133
D_P	400	295	X_{vir}	0.2	0.329

5.5 TIME-DOMAIN SIMULATION RESULTS

An MG test model as in Fig. 5.2 was considered to validate the effectiveness of the offered DSC scheme. Matlab/Simscape software was used for the simulation of the test MG model. The MG, load and line parameters used in the simulations are given in Tables A2–A4 (Appendix A). All the DSC gains were considered to be the same for all the DGs.

5.5.1 Case Studies

First, the simulation results could be categorized into the following two groups:

Group 1: Results with proposed DSC with initial parameters (without tuning).

Group2: Results with proposed DSC with the tuned parameters by the fuzzy logic tuner.

In group 1, the performance of the proposed DSC with not-tuned parameter values is shown in Fig. 5.10. The simulation results of the frequency and voltage restoration are shown in Fig. 5.10. From the results, the initial DSC parameters produced transient oscillations, which was also verified by the eigenvalue analysis. For

group 1, the convergence time for frequencies were 1.1 s and for voltages was 1.2–1.5 s. As we want to verify several case studies (case 1–case 7) to show the robustness of our proposed DSC, we considered the tuned parameters for those case studies due to space limitations. However, to get better performance, the fuzzy-logic tuner was used for tuning the DSC parameters and virtual impedance values. The simulations from group 2 are conducted with the following six case studies.

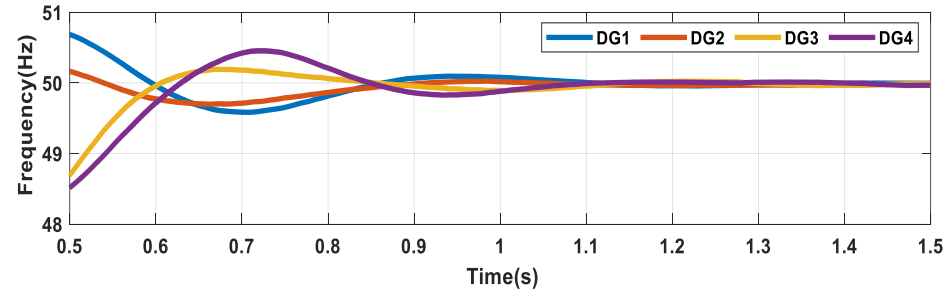

(a)

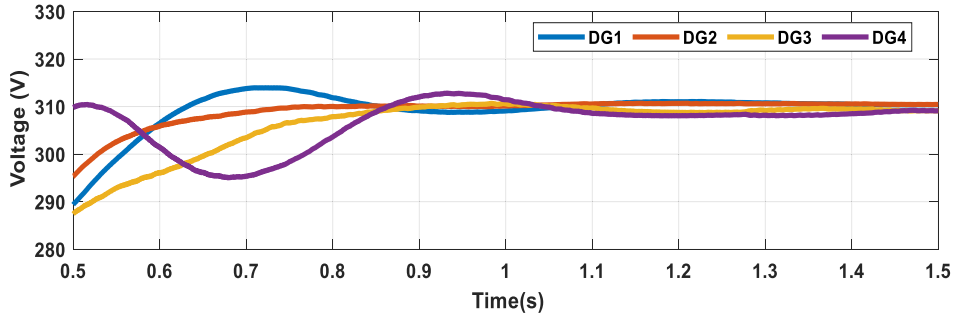

(b)

Fig. 5.10. Outputs of 4 DGs: (a) frequency and (b) voltage restoration for group 1

Case 1: Voltage and Frequency Restoration

The simulation outcomes of case 1 are given in Fig. 5.11

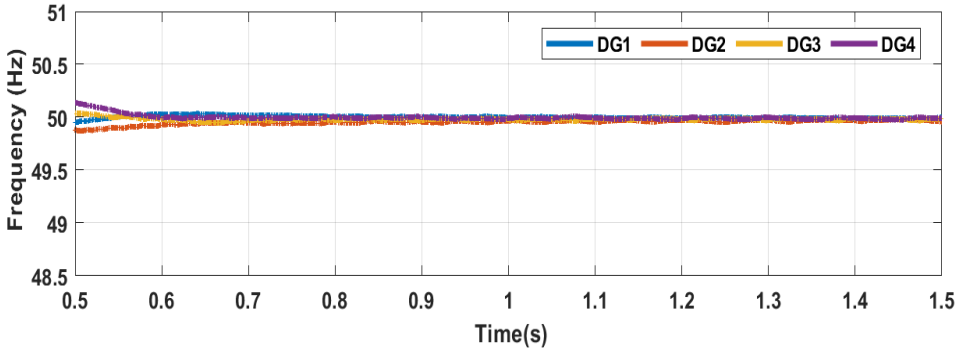

(a)

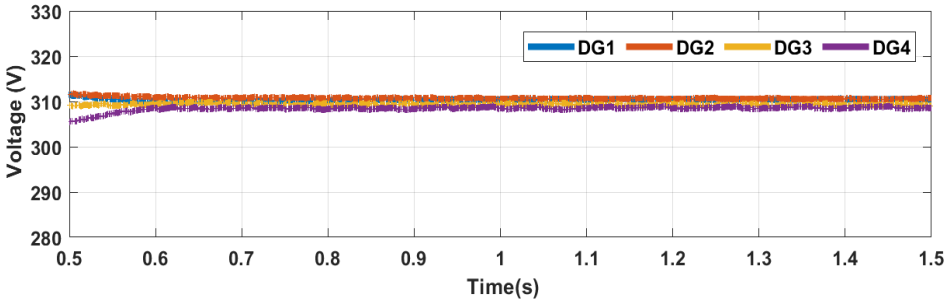

(b)

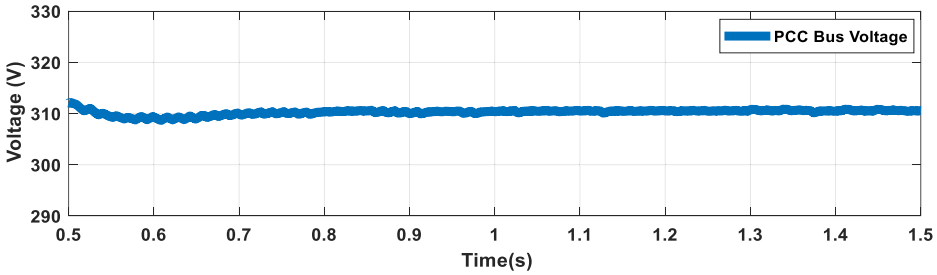

(c)

Fig 5.11. Outputs of 4 DGs: (a) frequency restoration; (b) voltage restoration and (c) point of common coupling (PCC) bus voltage restoration as in case 1

When our proposed DSC was employed, the restoration process of both voltage and frequency to their reference values, respectively ($v_{ref} = 311\ V, f_{ref} = 50$ Hz) was very fast with less oscillation as compared with Fig. 5.10. Thus, the fuzzy tuner could improve (convergence time improved for frequencies from 1.1 to 0.6 s and for voltages from 1.2–1.5 s to 0.7–0.8 s) the performance of DSC.

Case 2: Load Changing after Reaching the Steady State

In this case, several scenarios were analysed in the simulations according to the power flow and loading condition at each DG after reaching the steady state (Fig. 5.12) as follows.

According to our proposed DSC, power-sharing was in proportion to the capacities of DGs (ratio of capacities is DG_1:DG_2:DG_3:DG_4 = 2:2:1:1) as shown in Fig. 5.12. At t = 3 s, Load #3 was disconnected from DG_3, and at t = 5 s, Load #3 was again connected to DG_3. At t = 6 s, Load #2 was increased by including an additional load equivalent to Load #5 and at t = 8 s, the additional load was removed from Load #2.

The simulation results from Fig. 5.12 for load change show that the proposed DSC could accurately share active and reactive powers according to their capacities under load disturbances.

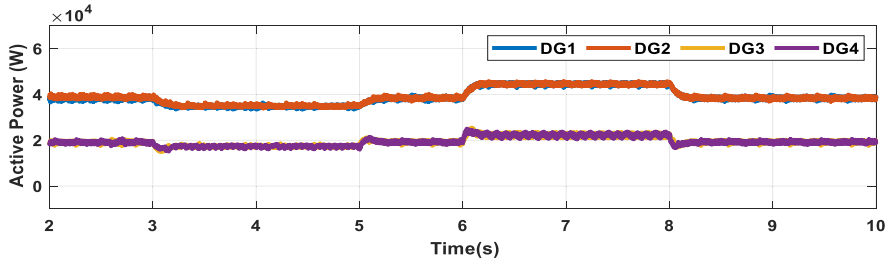

(a)

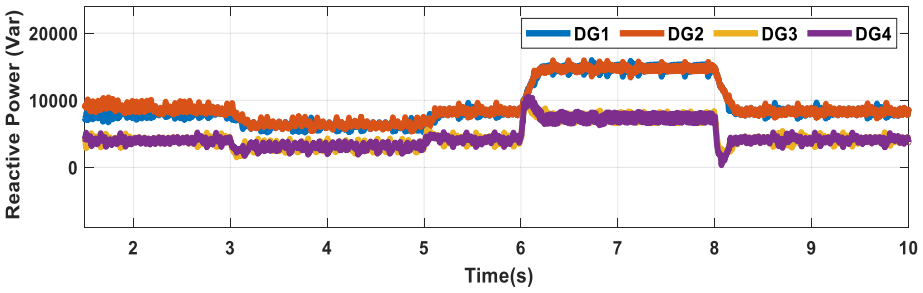

(b)

Fig. 5.12. Output power of 4 DGs for random load change: (a) active power and (b) reactive power as in case 2

Case 3: Occurrence of Communication Delay

In this case study, communication delay on the proposed DSC scheme was conducted with four scenarios, i.e., fixed communication delay of 0.1 s, 0.5 s, 1 s and 2 s in the MG. The proposed DSC was commenced from the beginning. For easiness, simply the voltage responses for the DG units were given for the four scenarios as shown in Fig. 5.13. It can be realized from Fig. 13(a)-(b) that the controller performed properly with small time delays of 0.1 s and 0.5 s. Fig. 13(c)-(d) shows that, with the increase of the time delay to 1–2 s, the voltage was restored with minor deviations, but with increased convergence times. Thus, it could be concluded that the proposed DSC can still help the system with restoration under the communication latency.

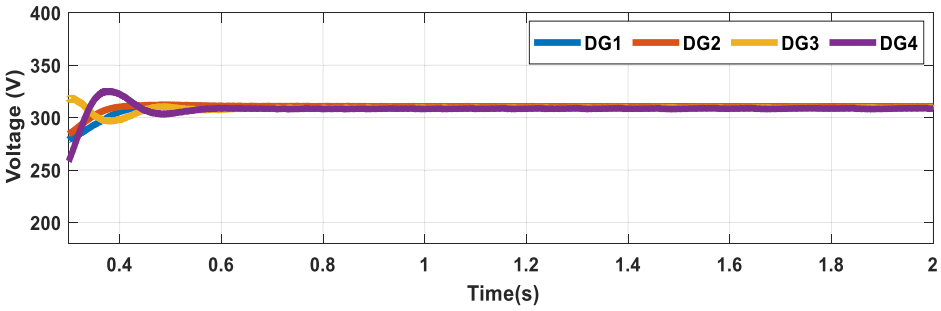

(a)

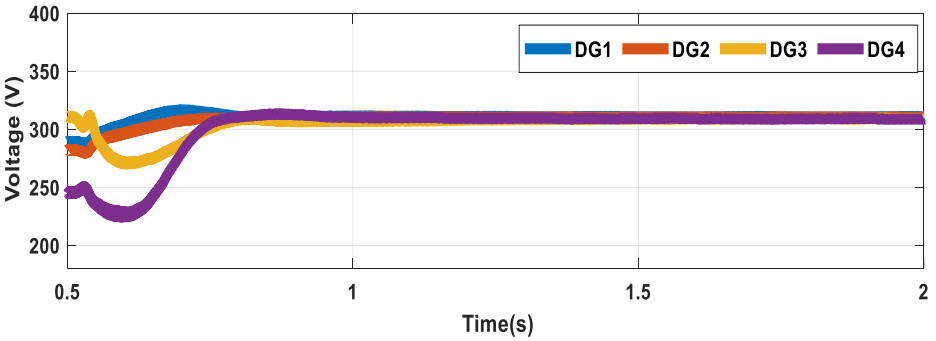

(b)

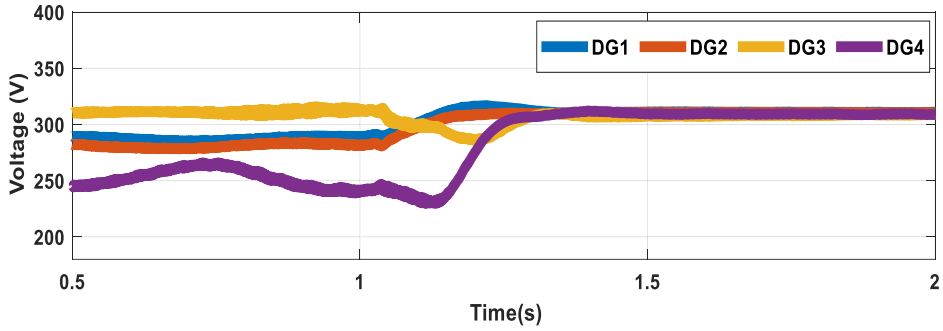

(c)

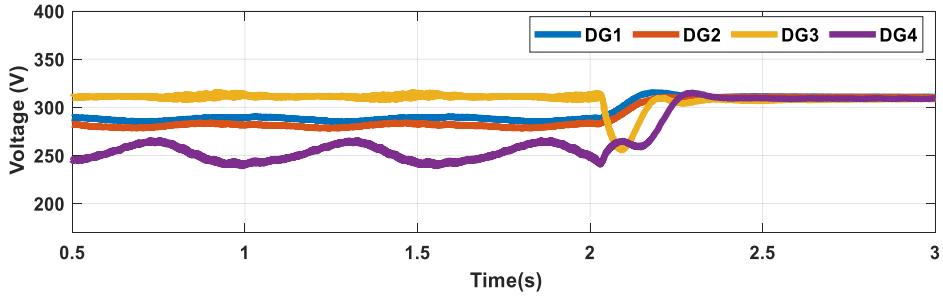

(d)

Fig. 5.13 Output results of 4 DGs for voltage restoration with time delays (a) 0.1 s; (b) 0.5 s; (c) 1 s and (d) 2 s as in case 3

Case 4: Loss of the Communication Link

Communication link failure is a common incident in real-world applications. The MG system still needs to be stable in such conditions. In this case study, the simulation is done with the following scenarios.

Stage 1: There is no loss of communication link when $t \leq 2.6$ s, and the MG system rapidly reaches the steady state.

Stage 2: The MG system experiences a loss of communication link from DG4 to DG1 when $t > 2.6$ s.

The simulation results are given in Fig. 5.14, showing that the proposed DSC technique could deal well with the conditions of communication link failure, though there was transient oscillation that occurred for the loss of the communication link.

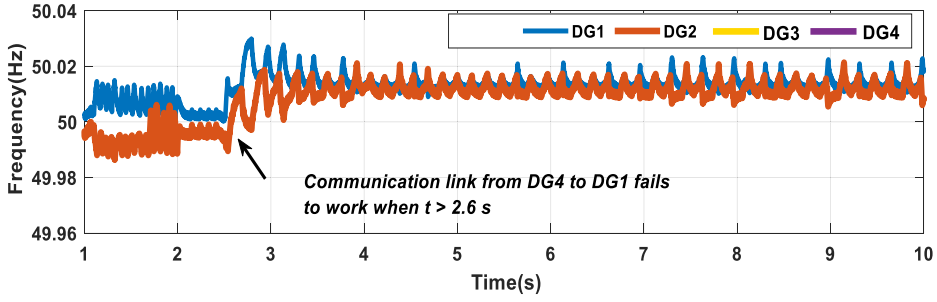

(a)

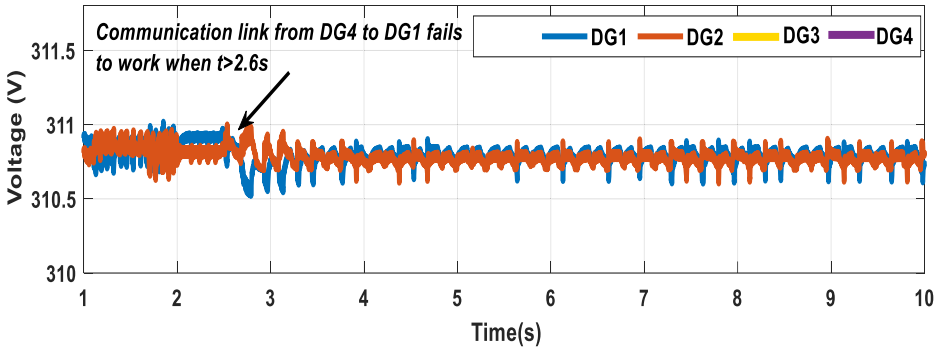

(b)

Fig. 5.14. Output results of 4 DGs for (a) frequency and (b) voltage restoration with communication link failure when t > 2.6 s in case 4

Case 5: Effects on Different Communication Topologies

The effects of diverse communication topologies (line, ring and mesh) as shown in Fig. 5.15 on the proposed model were analysed in this case. Convergence time with different topologies is summarized in Table 5.3. Table 5.3 reveals that the system's dynamic behaviour changed with different communication topologies. A low amount of communication links (line) increased the convergence time, while a high number of communication links (mesh) raised the complexity of the communication network and also the system implementation cost. It can be said that mesh topology is most suitable to restore the voltage and frequency (converge within 0.56s) whereas line topology is less suitable (converge within 0.63s), though communication links increase the implementation cost.

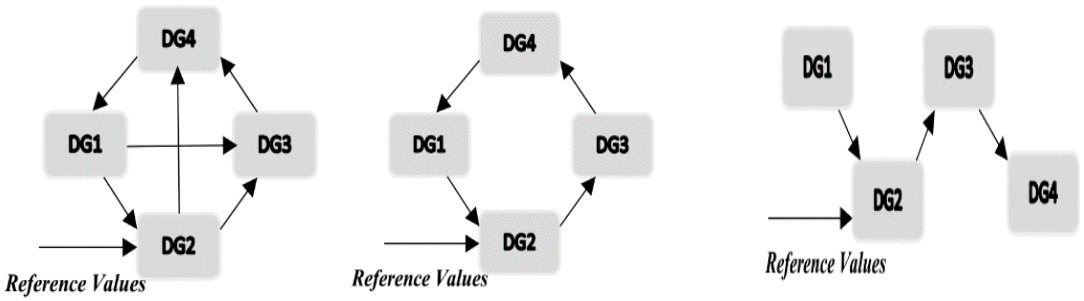

(a) (b) (c)

Fig. 5.15. Various communication topologies for the test MG system: (a) mesh (b) ring and (c) line for case 5

Table 5.3 Convergence Time for Various Communication Topologies

Communication topology	Mesh	Ring	Line
Convergence Time (s)	0.56 s	0.59 s	0.63 s

Case 6: Plug-and-Play Capability

Once synchronizing and reaching steady-state condition by the DSC, the plug-and-play capability of the controllers was assessed in this case study by disconnecting DG_3 at t = 10 s and connecting it at t = 14 s. The following observations were made from the simulation results, (i) disconnection of a DG unit indicates the failure of all the communication links associated with that DG unit, (ii) the lost communication links are restored after the DG unit is reconnected and (iii) a synchronisation procedure was required to coordinate DG3 with the remaining MG before reconnection. Fig. 5.16 shows the performance of DSC with plug-and-play operation. According to Fig. 5.16, it could be concluded that reconnection (at t = 14s) of DG produced more oscillation than the disconnection/sudden loss (t = 10 s) of any DG unit.

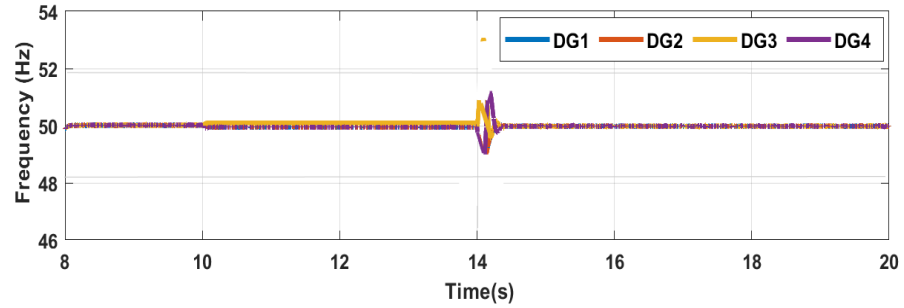

(a)

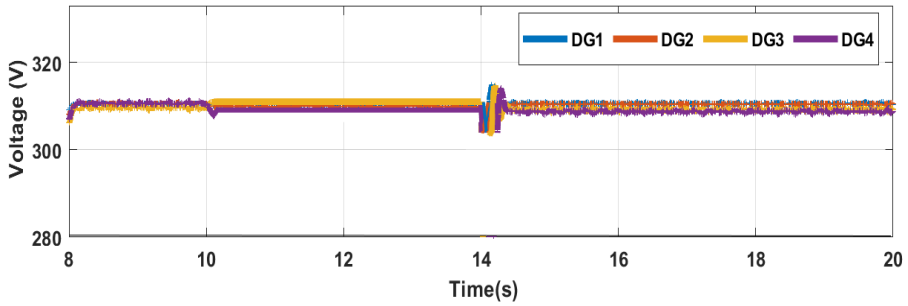

(b)

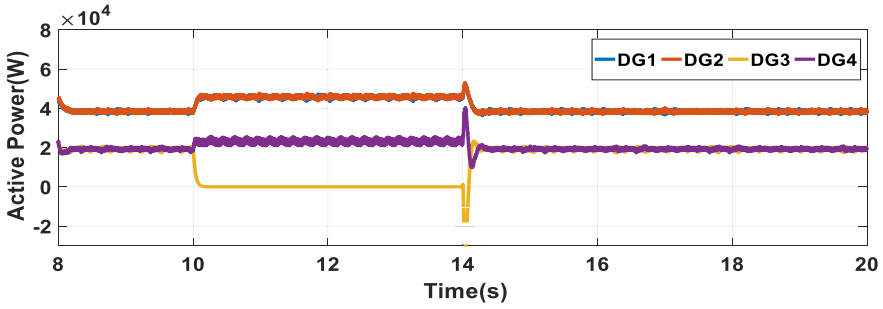

(c)

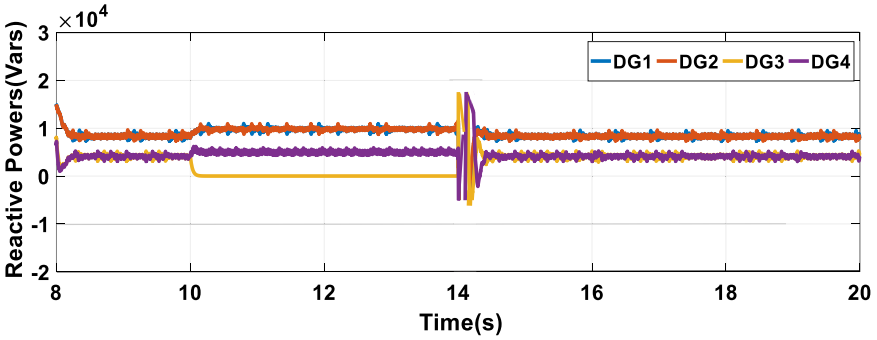

(d)

Fig. 5.16. Output results of 4 DGs: (a) frequencies (b) voltages and (c) active power and

(d) reactive power for case 6

Case 7: MG with Fault Conditions

To examine the dynamic response of the MG model with the proposed DSC, performances of voltage and frequency and power-sharing are observed under the maximum fault condition. After reaching the steady-state condition, a three-phase to ground fault occurred at bus 1 at $t = 3$ s, and the fault was cleared at $t = 4$ s. Fig. 5.17 shows the controller performance under that fault condition, and it can be seen that the voltage and frequency controllers had the ability to preserve the system stability after the fault clearance. Moreover, accurate power-sharing was achieved within a very short time after the fault clearance. It can be said that the proposed DSC was robust in maintaining the system stability under the sudden fault condition.

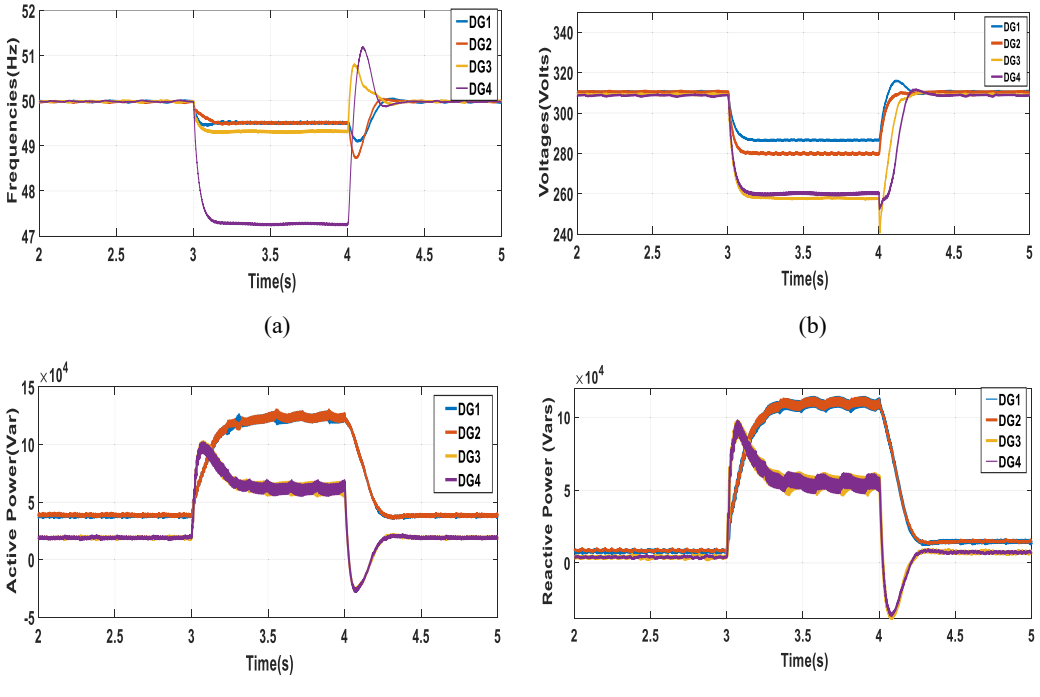

(a) (b)

(c) (d)

Fig 5.17. Output results of 4 DGs: (a) frequencies, (b) voltages and (c) active power and (d) reactive power for case 7

5.5.2 Convergence Time

As stated in the literature review, inadequate studies were stated that consider both the voltage and frequency restoration issues in a distributed way. In comparison with the most relevant works, as in [59], Table 5.3 reveals that the proposed control approach required less time to drive the frequencies to the steady-state values, which were 0.56 s, compared to 1.9 s in [59]. Additionally, the proposed control strategy performed well even though changes occurred in load, communication topology and loss of DG and even in fault conditions, which means by the proposed DSC the dynamics of the underlying system could quickly converge to the reference values under different disturbing conditions.

5.6 SUMMARY

A noble cooperative DSC for islanded AC MG has been established, taking the lossy-line network into account, which similarly preserves the precise active and reactive power-sharing while keeping *PCC* bus voltage at its reference value at the same time. State-space modelling and small-signal stability analysis for the networked MG have shown that new less-damped modes are the consequences of the DSC. An intelligent fuzzy-based parameter-tuner is applied to improve system stability. One of the major advantages of using a fuzzy-logic tuner is its low computational complexity in comparison to other existing methods. Theoretical analysis and time-domain simulation case scenarios of a test MG system have been explained to show the robust performance of the suggested DSC scheme. Under the proposed control method, the networked MG model can reach a steady state after different disturbances (even after fault conditions) without significant transients in the system frequency, voltage and active and reactive power-sharing. The proposed DSC shows a fast response to achieve consensus and indicates better robust characteristics in terms of controller establishment, structure design and the variation of loads compared with most related existing work on DSC, which is also discussed in the simulation section.

However, as communication is a major part of the SC level, cyber security is of primary importance to the assurance of safe tasks of cyber-physical systems, which has obtained growing attention in the control community. To prevent our presented scheme in Fig. 5.2 from malicious activities like “Replay Attack” or “False Data Injection” [60, 61], we will consider it as a future work of this chapter.

Chapter 6: Distributed Secondary Control of Energy Storage Units with SoC balancing in AC MG

6.1 INTRODUCTION

MGs (MGs) are becoming one of the most significant research topics as the electricity network is transitioning from conventional generation and distribution networks to multi-directional, more dynamic action with distributed energy resources (DERs) [34]. MG offers a suitable solution for power system stability problems introduced by the high penetration of the DERs. They are also being used in the improvement of power system reliability and resilience, managing the addition of DERs like wind and solar photovoltaic (PV) generation to support the sustainable energy solution as well as supporting rural areas by supplying electricity where centralised electrical networks are unable to serve.

Due to the intermittent nature of DERs and less inertia of power electronic converters, distributed energy storage units (DESUs) are a crucial part of MG for balancing the electricity generation and consumption, especially in the islanded mode of operation through charging and discharging power. Likewise, more than one group of DESUs are demanded to enhance grid reliability. However, the control system design of autonomous MG with DESUs is one of the critical technologies which must be done accurately as the lack of controllability negatively disturbs the MG performance and efficiency. Recently, control strategies of MG with DESUs have been studied by a lot of researchers which also assist as stabilising energy buffers [121]. The DESUs have become a very important factor in the process of system stability and optimal operation. The complexity of the control structure is even more for the islanded mode in order to confirm the stable and reliable performance of MG. To this end, this chapter provides the guidelines for designing DSC laws with SoC balancing and active/reactive power-sharing among DESUs, to present the convergence property of the proposed control laws. In general, the main responsibilities of DESU control can be summarised as: i) preserve the balance condition between generation and load demand, ii) regulate the system frequency and voltage, iii) balance the state of charge (SoC) of DESUs, especially when DESUs have different initial SoC, iv) give the protection of DESUs from power surplus as well as rapid discharging or overcharging v) balance the active and reactive power of DESUs.

The operational functionality of standard MG systems with DESUs follows the hierarchical control structure comprising three control levels, explicitly, primary, secondary and tertiary control. Power-sharing among the DESUs, proportional to their energy capacities, can be reached with the conventional primary droop control technique. However, there are some drawbacks when using traditional droop control to assist power-sharing among DESUs. The main limitation is the DESU with lower initial SoC is depleted faster than that with higher initial SoC, and thus it cannot contribute to power-sharing any longer. Besides, DESUs at a low SoC

reduce their lifetime and efficiency. SoC of a DESU is also affected by the remaining end period, ambient temperature, and operational competences for the charging and discharging of the DESU.

On the other hand, the deviance of the MG voltage and frequency is inversely proportional to the SoC level of the DESU. A droop control of DESU is offered in [130] for active utilisation of the existing stored energy and capacity of the DESU; it accomplishes the SoC balancing by applying the SoC-based P-f droop control scheme locally in order to extend the service lifespan of DESUs, but the constraints of dissimilar capacities in power-sharing still exit. Another SoC-based droop control for SoC balancing is presented in [124] to exclude the effect of capacity on SoC balancing and preserve a satisfactory power quality, but the dynamic characteristics (plug-n-play) of DESU are not considered. Authors in [164] emphasize on discharging rates of DESUs for SoC balancing by proposing a coordinated SC method based on an independent current-sharing control approach for islanded AC MGs, but the SoC balancing is preserved at the cost of necessitating a centralised communication structure, and the control system will be inactive when the centralised communication stops working. Apart from this, the centralised structure limits the scalability, network extension, and redundancy of the MG. Stability of the MG with centralised control is extremely affected by the communication restrictions and breakdown of the control centre. Moreover, the centralised SoC balancing techniques [164] cannot support the MGs with high penetration of DESUs, due to the restraints in scalability and communication costs. A control system is considered distributed if it is composed of autonomous agents connected through a communication network, each autonomously pursuing their individual control objective using just local information and information from their neighbours. Distributed approaches can avoid single-point failure, high communication system costs as well as high computation load. Therefore, applications of distributed methods are various, and the distributed control method is a potential way to increase system reliability and scalability [20, 165].

There are several control techniques proposed in the literature for DESU control. In [143], a distributed model predictive control (MPC) arrangement is offered to synchronise the DESUs for voltage control. Likewise, the distributed MPC technique is used for the optimisation of DESUs to manage supply-demand balance and maintain voltage and frequency stability. Conversely, the distributed method in [143] ignores the SoC balancing of ESUs, which may lead to the over-charging and over-discharging actions of ESUs. Distributed multi-agent control considers systems controlled by autonomous agents sharing information through a sparse communication network [43, 157] for attaining the global coordination among DGs. A dynamic consensus algorithm (DCA)-based coordinated distributed secondary control (DSC) with a current sharing control approach is suggested in [34, 166] for balancing the discharge rate of DESUs in an islanded AC MG. A distributed multi-agent cooperative control scheme for dynamic energy level balancing among DESUs as a technique to advance frequency regulation and reliability in droop-controlled MGs is recommended in [71]. Authors in [167] introduced a coordinated control scheme to control the charge/discharge of DESUs utilising an arrangement of the local droop-based control strategy and a DSC; it guarantees that the feeder voltages persist within the acceptable limit as well as balancing the SoC of DESUs, but the heterogeneous behaviour is not considered. Distributed finite-time consensus control considering heterogeneous behaviour of batteries is proposed in [138, 139], but the sudden loss/out of work of energy storage units and their effects on balancing SoC are not included. It is evident from the above reviews that less research has been considered for the regulation of voltage and frequency along with SoC balancing of DESUs, which becomes a vital issue to be further researched. Authors in [137] propose a distributed cooperative control method based on a second-order multi-agent system to govern the

charging/discharging behaviour of multiple ESUs. But they only consider the consensus of SoC and active power-sharing. Moreover, the operation of islanded mode is not mentioned there. SoC balancing is confirmed by the proposed method, while the concern of reactive power-sharing is not considered.

In this chapter, a novel DSC scheme is proposed to recover the MG frequency and voltage as well as getting the accurate power-sharing with SoC-balancing through a distributed control architecture, using local communications with neighbour DESUs of an islanded MG considering the limitations mentioned above. Thus, the cyber resilience of the MG is enhanced by the proposed controller. The reference values are fixed by the virtual leaders which are virtually located at the tertiary control level. This methodology looks like a pinning control method. The power variation is shared among the DESUs through a leader-follower consensus. The presence of at least one virtual leader is compulsory, while the establishment of an intermittent sparse communication network consisting of a spanning tree is sufficient for the stable operation of the MG [168]. The relation between the SoC and active power of each DESU is defined to be a second-order dynamic. Then, a virtual leader is built to produce reference values for SoC and active power for all the DESUs. As such, the coordination of multi-DESU system is turned into designing a control algorithm for a second-order multi-agent system. Built on the first order and second-order multi-agent model, a distributed coordination method is implemented to design controllers for all the DESUs. The constructed controllers can enable all the DESUs achieve consensus on frequency, voltage magnitude, and SoC as well as the active and reactive power proportional to their capacities. In addition, the designed cooperative controller has better robustness and scalability. The main contributions of this chapter are highlighted below.

- Consensus-based DSC is proposed for DESUs in an AC islanded MG system to recover the frequency and voltage to the reference values within a finite time.
- The proposed control is responsible for SoC balancing in the case of batteries with different initial SoC and sharing the active and reactive power.
- In comparison with the existing DESUs, the proposed control is robust against load disturbances, different communication topologies and plug-n-play capabilities.
- The proposed DSC is verified with real-time PV data, which ensures the effectiveness of the proposed DSC.
- The convergence speed of SoC balancing and frequency/voltage restoration depends on the DSC parameters, and finite-time tracking can be guaranteed.

The rest of the chapter is organised as follows. MG configuration which includes the preliminaries of MG is presented in Section 6.2. Section 6.3 describes the proposed DSC for DESUs which includes consensus designs and their proofs. Section 6.4 discusses the time-domain simulation results of the proposed DSEUs with several case studies. Lastly, conclusions are shown in Section 6.5 with the future work.

6.2 PRELIMINARIES

6.2.1 Simple Structure of DESUs

A simple arrangement of AC MG architecture with three DESUs and one PV array which can be considered as a multi-agent system (MAS) is shown in Fig. 6.1. The communication network has also been established which will be detailed later. Mostly in an MG structure, each inverter-DER system includes a primary DC power source, a voltage source inverter (VSI), an LCL filter (combining the LC filter with coupling inductor) and an output filter named as coupling inductor, as displayed in Fig. 6.2. Hierarchical control is used for the DESUs. Vector control is implemented to transform the rotating *abc* frame to the *dq* frame and compute the active and reactive power from the converter of the DERs. The control framework has three main control loops, primary control, SC and tertiary control. In this chapter, the primary and SC strategies are explained in the following sections, while tertiary control is out of the scope of this research.

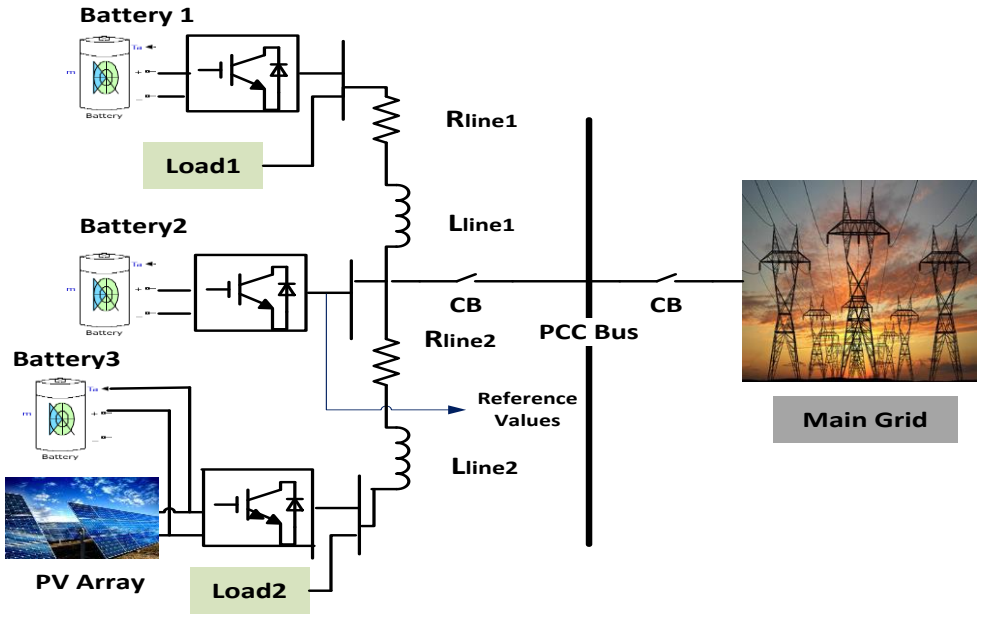

Fig. 6.1. Simple configuration of test MG model

6.2.2 Primary Control of DESUs

DESU can be employed to deliver controllable MG storage. Each DESU includes a battery and a four-quadrant inverter permitting control of the real and reactive power it export to or import from the MG. To preserve network stability, the DESU must be controlled to balance the difference between power generation and demand in the MG. The droop method at the primary control level is applied for sharing the active and reactive power mismatch, similar to the parallel operation of traditional synchronous generators. The power controller (Fig. 6.2) allows DESUs to share the active and reactive power requirements permitting their maximum ratings based on the droop gain. In the power calculation block, the measured active and reactive power can be obtained as

$$\dot{P}_i = -\omega_{ci} P_i + \frac{3}{2}\left(\omega_{ci} v_{odi} i_{odi} + v_{oqi} i_{oqi}\right) \tag{6.1}$$

$$\dot{Q}_i = -\omega_{ci} Q_i + \frac{3}{2}\left(\omega_{ci} v_{odi} i_{oqi} - v_{oqi} i_{odi}\right) \tag{6.2}$$

where v_{odi}&v_{oqi} and i_{odi}&i_{oqi} are the direct and quadrature elements of v_{oi} and i_{oi} in Fig. 6.1, respectively, ω_{ci} is the cutoff frequency of the low-pass filters employed in power measurement, P_i and Q_i are the calculated active and reactive power at the output of i^{th} DESU, correspondingly. The dynamic droop characteristic of frequency and voltage for i^{th} DESU can be represented below:

$$\omega_i = \omega_{nom} - m_{pi} P_i \tag{6.3}$$

$$v_i = v_{nom} - n_{qi} Q_i \tag{6.4}$$

where, ω_i and v_i are the angular frequency and voltage of the ith DESU, m_{pi} and n_{qi} are the droop coefficient for frequency and voltage control of i^{th} DESU, correspondingly; ω_{nom} and v_{nom} are the nominal angular frequency and nominal voltage, respectively. Graph theory for communication networks is discussed in Chapter 3 and hence not included in this chapter.

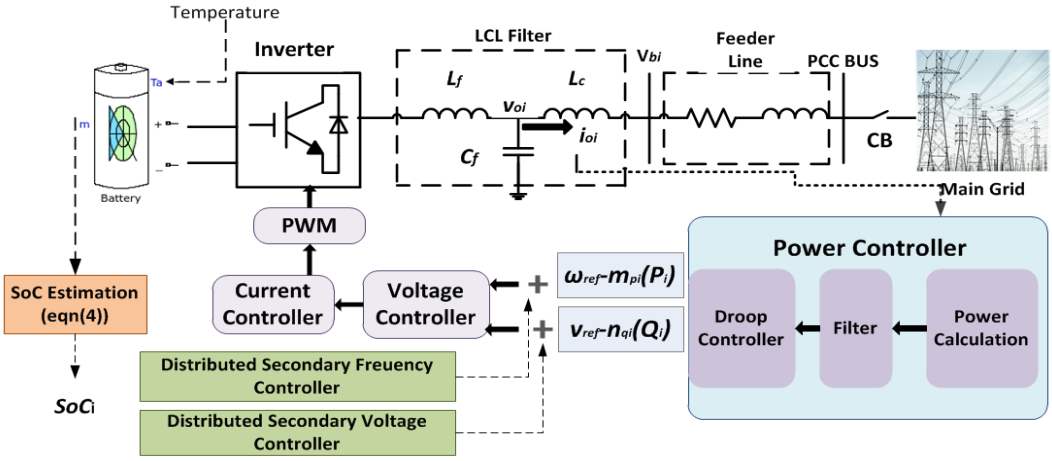

Fig. 6.2. Block diagram of inverter interfacing individual energy storage unit

6.2.3 SoC Estimation of DESUs

In this chapter, SoC estimation of the DESUs is done by using the basic coulomb counting method [124], represented as

$$S = S_0 - \frac{1}{C}\int i_{dc} dt \tag{6.5}$$

In (6.5), S_0 is the initial SoC value, C is the capacity of the DESU, i_{dc} is the output DC current of the battery. Let P_{dc} and v_{dc} denote the DC output power and voltage of the DESU and P denote the active power of VSI. Assuming the power loss of the interfacing VSI is negligible, we have $P \approx P_{dc} = v_{dc} i_{dc}$, where the DESU is operating with unity efficiency (i.e., $\eta = 1$). With the above assumption, Eq. (6.5) can be re-written as:

$$S = S_0 - \frac{1}{C}\int \frac{P}{v_{dc}} dt \tag{6.6}$$

Therefore, the control of the output active power of DESUs can be used for the SoC-balancing strategy. However, the power output is primarily affected by the droop coefficient in traditional droop control methods which cannot balance the SoC with different S_0. Therefore, SoC-based DSC is needed to overcome the

limitations of primary droop control for DESUs. In the proposed technique, the droop constant of the DESU with higher SoC is virtually reduced in the control loop, which simultaneously rises the output active power of the DESUs and vice versa, and thus the proposed DSC gradually balances the SoC of DESUs. In addition, energy storage devices are expensive, and thus their operation needs further attention, especially on the SoC level of the battery unit. Therefore, SoC balancing among the multiple DESUs in the MG utilises the role of all DESUs to achieve the maximum power capacities.

6.3 DSC FOR SOC BALANCING AND POWER-SHARING OF DESUS

According to the primary control introduced in the prior section, the main contribution of SC can be achieved by varying the frequency and voltage set points. The goal of frequency and voltage restorations is to control the frequency and voltage of individual DESU back to their reference nominal values ω_{nom} and v_{nom}, respectively, maintain the steady-state stability of the MG at a balanced operating point, balance the power demand initially with respect to S_0 and then balance the SoC of the DESUs. Each DESU in the MG will be charged or discharged slowly according to its SoC level during the operation. The suggested DSC of DESUs is described in detail in the following subsections.

6.3.1 Control Objectives of DESU System

The objectives of DSC of energy storage networks in this chapter are to accomplish: i) frequency restoration; ii) voltage restoration; iii) SoC balancing; iv) active and reactive power sharing of DESUs. Established on the primary control described in the past section, the functionalities of SC can be gained by modifying the frequency and voltage set points. In this section, a novel distributed cooperative tracking approach is presented to regulate the DESUs voltage magnitude v_i and frequency ω_i to the nominal voltage reference, v_{nom} and nominal frequency reference ω_{nom}, respectively. It is assumed that each DESU only demands its individual information and the information from its neighbouring DESUs over an undirected communication network, and at least one DESU can detect the reference which is the virtual leader.

The objectives of frequency and voltage restorations are to control the frequency and voltage of each DESU back to reference values ω_{ref} and v_{ref}. This control can be easily gained by applying the adjacent ESSs information. In the following sub-section, we study distributed coordinated tracking for first-order kinematics.

In this chapter, we consider that the voltage magnitude and frequency are controlled by controlling nominal reference points v_{nomi} and ω_{nomi}, respectively. New control inputs can be constructed to synchronize voltage magnitude and frequency of DESUs by adjusting v_{nomi} and ω_{nomi}. Hence, the new battery energy storage dynamics can be stated in the following equations:

$$\dot{S}_\iota = -\frac{P_i}{C_i v_{dc}} \tag{6.7}$$

$$\text{Let, } P_\iota^{\dot{c}on} = u_i^P,\ Q_i^{\dot{c}on} = u_i^Q \tag{6.8}$$

$$\dot{P'}_\iota = P_i^{con} - P_i \text{ and } \dot{Q'}_\iota = Q_i^{con} - Q_i$$

$$\left.\begin{matrix}\omega_i=\omega_{nomi}-m_{pi}P_i\\ v_i=v_{nomi}-n_{qi}Q_i\end{matrix}\right\} \tag{6.9}$$

$$\left.\begin{matrix}\dot{\omega}_{nomi}=u_i^{\omega}+m_{pi}u_i^{P}+k_P^{\omega P}\left(P_i^{con}-P_i\right)+k_I^{\omega P}P'_i\\ \dot{v}_{nomi}=u_i^{V}+n_{qi}u_i^{Q}+k_P^{vQ}\left(Q_i^{con}-Q_i\right)+k_I^{vQ}Q'_i\end{matrix}\right\} \tag{6.10}$$

where S_i is the SoC value of ith DESUs, $\omega_i \in \mathbb{R}, v_i \in \mathbb{R}$, and $u_i^{\omega} \in \mathbb{R}, u_i^{V} \in \mathbb{R}$ are the control inputs associated with i^{th} DESU; u_i^{P} is the control input for both active power-sharing and SoC balancing whereas u_i^{Q} is the control input of reactive power-sharing; $k_P^{\omega P}$ ($k_I^{\omega P}$) and k_P^{vP} (k_P^{vQ}) are PI control coefficients for active (reactive) power tracking which are tuned online using Fussy logic, detailed in section 6.3.4. Due to the fast response of PI tracking compared to the consensus control, the following is assumed:

$$P_i = P_i^{con}, Q_i = Q_i^{con}$$

Therefore, the distributed control for frequency and voltage restorations can be transformed as follows:

$$\dot{S}_i = -\frac{P_i}{C_i v_{dc}} = k_i P_i, \qquad \dot{P}_i = u_i^{P} \tag{6.11a}$$

$$\dot{Q}_i = u_i^{Q} \tag{6.11b}$$

$$\dot{\omega}_i = u_i^{\omega} \tag{6.11c}$$

$$\dot{v}_i = u_i^{V} \tag{6.11d}$$

where $k_i = -\frac{1}{C_i v_{dc}}$. Define $\overline{P_i}=m_{pi}P_i$, $\bar{Q}_i=n_{qi}Q_i$, and $\bar{S}_i = \frac{m_{pi}}{k_i}S_i = k_S S_i$ where $k_S = \frac{m_{pi}}{k_i}$ is a constant. Note that the active/reactive power-sharing among each DESU is provided by primary control in accordance with:

$$\overline{P_i} = \overline{P_j}, \qquad \bar{Q}_i = \bar{Q}_j, \qquad \forall i, j \in N_G \tag{6.12}$$

That means for frequency and voltage magnitude restoration as well as SoC balancing, the following convergence conditions must be satisfied at the steady state:

$$\omega_i = \omega_j = \cdots = \omega_N, v_i = v_j = \cdots = v_N, \; S_1 = S_2 = \cdots = S_N \tag{6.13}$$

The conditions in (6.12) & (6.13) can be satisfied through realising the consensus of all DESUs described by the first-order dynamic model for frequency and voltage restoration as well as reactive power sharing and second-order dynamic model for SoC balancing and active power-sharing.

6.3.2 Design of Virtual Leader (VL)

To solve the frequency and voltage restoration problem, reference values ω_{ref} and v_{ref} are chosen as virtual leaders (VLs) for tracking the frequency and voltage at their reference values, respectively, i.e., $\omega_0 = \omega_{ref}$ and $v_0 = v_{ref}$. For the DESUs in the MG to track the accurate active and reactive power-sharing, a virtual leader is considered for both cases which are related to active and reactive power demands as follows:

$$\text{VL for active power sharing: } P_0 m_0 = P_d m_p = \overline{P_0} \tag{6.14}$$

$$\text{VL for reactive power sharing: } Q_0 n_0 = Q_d n_q = \overline{Q_0} \tag{6.15}$$

where P_d and Q_d are the total active and reactive power demand, respectively, and can be formulated as follows:

$$P_0 = P_d = \sum_{i=1}^{N} P_i, \quad Q_0 = Q_d = \sum_{i=1}^{N} Q_i \quad \text{and} \tag{6.16}$$

$$m_0 = m_p = \left(\sum_{i=1}^{N} \frac{1}{m_{pi}}\right)^{-1}, n_0 = n_q = \left(\sum_{i=1}^{N} \frac{1}{n_{qi}}\right)^{-1} \tag{6.17}$$

The VL for SoC balancing is selected as the same SoC of the leader node. In this chapter, we select DESU 2 as the leader node and DESU1 and DESU3 are the follower nodes.

6.3.3 Proposed DSC for DESU System

To achieve the control objectives of DESUs, a virtual leader-based DSC can be designed for the distributed energy storage system. In this section, a novel distributed finite-time cooperative tracking strategy is presented to synchronize the DESU voltage magnitude v_i and frequency ω_i to the nominal voltage reference v_{ref} and frequency reference ω_{ref}, correspondingly. Inspired by [168], we propose the following distributed consensus tracking algorithm utilizing the first-order dynamic model (6.18), (6.19) and (6.21) and the second-order dynamic model (6.20) as follows:

$$u_i^{\omega} = \left(-\alpha_{\omega} \sum_{j=0}^{N} a_{ij}[(\omega_i - \omega_j)] - \beta_{\omega} sgn \sum_{j=0}^{N} a_{ij}[(\omega_i - \omega_j)] \right) \tag{6.18}$$

$$u_i^{V} = \left(-\alpha_{V} \sum_{j=0}^{N} a_{ij}[(v_i - v_j)] - \beta_{V} sgn \sum_{j=0}^{N} a_{ij}[(v_i - v_j)] \right) \tag{6.19}$$

$$u_i^{P} = \frac{1}{m_{pi}} \left(- \sum_{j=0}^{N} a_{ij} \left[\alpha_S (\bar{S}_i - \bar{S}_j) + \alpha_P (\bar{P}_i - \bar{P}_j) \right] - \beta_P \, sgn \sum_{j=0}^{N} a_{ij} \left[\gamma_S (\bar{S}_i - \bar{S}_j) + \gamma_P (\bar{P}_i - \bar{P}_j) \right] \right) \tag{6.20}$$

$$u_i^{Q} = \frac{1}{n_{qi}} \left(-\alpha_Q \sum_{j=0}^{N} a_{ij}[(\bar{Q}_i - \bar{Q}_j)] - \beta_Q sgn \sum_{j=0}^{N} a_{ij}[(\bar{Q}_i - \bar{Q}_j)] \right) \tag{6.21}$$

In the above equations, $a_{ij}, i, j = 1, \ldots\ldots, N$ is the $(i,j)^{th}$ entry of the adjacency matrix A, $a_{i0}, i = 1, \ldots, N$ is a positive constant if the virtual leader's position is accessible to follower i and $a_{i0} = 0$ otherwise, $\alpha_{\omega}, \alpha_V, \alpha_S, \alpha_P, \alpha_Q, \beta_{\omega}, \beta_V, \beta_P, \beta_Q$ and γ_S, γ_P are all positive constants, and sgn (.) is the signum function. Before moving on, we need to consider the consensus proof of (6.18) - (6.21) utilizing the Theorem 6.1 and Theorem 6.2 as follows:

It can be seen that (6.18), (6.19) and (6.21) as well as their associated system model in (6.11c), (6.11d) and (6.11b), respectively, have a similar form, so only the consensus verification for one of them (reactive power) is examined here and the consensus proof for frequency and voltage can be obtained likewise. The following theorem, Theorem 6.1 describes the reactive power sharing associated with (6.18), and its proof follows that in [169].

Theorem 6.1: *Assume that* $\left|\dot{\bar{Q}}_0\right| \leq \gamma_{\ell}$, *where* γ_{ℓ} *is a positive constant. Assume that the fixed undirected graph* $\mathcal{G}$ *is coupled and at least one* a_{i0} *is nonzero (and hence positive). Employing (6.21) in (6.11b), if* $\beta_Q > \gamma_{\ell}$, *then* $\bar{Q}_i(t) \longrightarrow \bar{Q}_0(t)$ *in finite time. In particular,* $\bar{Q}_i(t) = \bar{Q}_0(t)$ *for any* $t \geq \bar{t}$, *where*

$$\bar{t} = \frac{\sqrt{\tilde{\bar{Q}}^T(0)\, M\, \tilde{\bar{Q}}\ (0)}\sqrt{\lambda_{max}(M)}}{(\beta_Q - \gamma_{\ell})\lambda_{min}(M)} \tag{6.22}$$

and $\tilde{\bar{Q}}$ *is the column stack vector of* $\tilde{\bar{Q}}_i$, $i = 1, \ldots, n$ *with* $\tilde{\bar{Q}}_i = \bar{Q}_i - \bar{Q}_0, M = \mathcal{L} + diag(a_{10}, \ldots., a_{n0})$ *with* $\mathcal{L}$ *being the Laplacian matrix, and* $\lambda_{min}(.)$ *and* $\lambda_{max}(.)$ *represent, correspondingly, the smallest and the largest eigenvalue of a symmetric matrix.*

Proof: As $\tilde{\bar{Q}}_i = \bar{Q}_i - \bar{Q}_0$, using (6.15), the closed-loop system of (6.11b) can be rewritten as:

$$\dot{\tilde{\bar{Q}}}_\iota = -\alpha_Q \sum_{i=0}^{n} a_{ij}(\bar{Q}_i - \bar{Q}_0) - \beta_Q sgn\left[\sum_{j=0}^{n} a_{ij}(\bar{Q}_i - \bar{Q}_0)\right] \tag{6.23}$$

Eq. (6.23) can be expressed in matrix form as:

$$\dot{\tilde{\bar{Q}}} = -\alpha_Q M\tilde{Q} - \beta_Q sgn(M\tilde{Q}) - 1\dot{\bar{Q}}_0$$

where $\tilde{\bar{Q}}$ and M are well-defined in (6.22), and sgn (.) is defined component-wise. Since the fixed undirected graph $\mathcal{G}$ is linked and at least one a_{i0} is nonzero (and hence positive), M is symmetric positive definite. Reflect the Lyapunov function candidate as: $V = \left(\frac{1}{2}\right)\tilde{\bar{Q}}^T M\tilde{\bar{Q}}$. The derivative of V is

$$\begin{aligned} \dot{V} &= \tilde{\bar{Q}}^T M[-\alpha_Q M\tilde{\bar{Q}} - \beta_Q sgn(M\tilde{\bar{Q}}) - 1\dot{\bar{Q}}_0] \\ &\leq -\alpha_Q \tilde{\bar{Q}}^T M^2 \tilde{\bar{Q}} - \beta_Q \left\|M\tilde{\bar{Q}}\right\|_1 + |\dot{\bar{Q}}_0| \left\|M\tilde{\bar{Q}}\right\|_1 \\ &\leq -\alpha_Q \tilde{\bar{Q}}^T M^2 \tilde{\bar{Q}} - (\beta_Q - \gamma_\ell)\left\|M\tilde{\bar{Q}}\right\|_1 \end{aligned} \tag{6.24}$$

where we use the Holder's inequality to get the first inequality and use $\left|\dot{\bar{Q}}_0\right| \leq \gamma_\ell$ to get the second inequality. Note that M^2 is symmetric positive definite, α_Q is nonnegative, and $\beta_Q > \gamma_\ell$. Hence, it follows that $\dot{V}$ is negative definite. It then follows from *Theorem 1* in [168] that $\left\|\tilde{\bar{Q}}\right\| \to 0$ as $t \to \infty$.

We next show that V will reduce to zero in finite time (i.e., $\tilde{\bar{Q}}_i(t) \to 0$ in finite time). Note that $V \leq \left(\frac{1}{2}\right)\lambda_{max}(M)\left\|\tilde{\bar{Q}}\right\|_2^2$. It then follows from (6.24) that

$$\begin{aligned} \dot{V} &\leq -(\beta_Q - \gamma_\ell)\left\|M\tilde{\bar{Q}}\right\|_2 = -(\beta_Q - \gamma_\ell)\sqrt{\tilde{\bar{Q}}^T M^2 \tilde{\bar{Q}}} \\ &\leq -(\beta_Q - \gamma_\ell)\sqrt{\lambda_{min}^2(M)\left\|\tilde{\bar{Q}}\right\|_2} \\ &= -(\beta_Q - \gamma_\ell)\lambda_{min}(M)\left\|\tilde{\bar{Q}}\right\|_2 \\ &\leq -\left(\beta_Q - \gamma_\ell\right)\frac{\sqrt{2}\lambda_{min}(M)}{\sqrt{\lambda_{max}(M)}}\sqrt{V} \end{aligned}$$

After some calculation, we can obtain that

$$2\sqrt{V(t)} \leq 2\sqrt{V(0)} - \left(\beta_Q - \gamma_\ell\right)\frac{\sqrt{2}\lambda_{min}(M)}{\sqrt{\lambda_{max}(M)}}t.$$

Therefore, we have $V(t) = 0$ when $t \geq \bar{t}$, where $\bar{t}$ is given by (6.22). This completes the proof. In this way, the finite-time consensus can be achieved for reactive power sharing in (6.21). For the consensus proof of active power and SoC balancing in (6.20), we have the following Theorem 6.2 before which Lemma 6.1 is needed.

Lemma 6.1. Assume that the undirected graph $\mathcal{G}$ is connected and at least one a_{i0} is nonzero. Let

$$E=\begin{bmatrix} (1/2)\alpha_s\gamma_p M^2 & (1/2)\gamma_s M \\ (1/2)\gamma_s M & (1/2)\gamma_p M \end{bmatrix}, \qquad F=\begin{bmatrix} \alpha_s\gamma_s M^2 & (\alpha_P\gamma_s/2)M^2 \\ (\alpha_P\gamma_s/2)M^2 & \alpha_P\gamma_p M^2-\gamma_s M \end{bmatrix}$$

where α_P, α_s and γ_s, γ_p are all positive constants. If γ_s satisfies

$$0<\gamma_s<\min\left\{\sqrt{\alpha_s{\gamma_p}^2\lambda_{min}(M)},\quad 4\alpha_s\alpha_P\gamma_p\lambda_{min}(M)\Big/[4\alpha_s+{\alpha_P}^2\lambda_{min}(M)]\right\} \tag{6.25}$$

Then both E and F are positive definite.

Proof: Note that *M* is symmetric positive definite from the proof of Theorem 6.1. Then *E>0* is equivalent to (by Schur complement):

$$(1/2)\gamma_p M-(1/2)\gamma_s M(1/2\,\alpha_s\gamma_p M^2)^{-1}(1/2)\gamma_s M>0$$

That is, $\gamma_p M-{\gamma_s}^2{\alpha_s}^{-1}{\gamma_p}^{-1}I>0$. Therefore, *E*>0 if $0<\gamma_s<\sqrt{\alpha_s{\gamma_p}^2\lambda_{min}(M)}$. By performing a similar derivation, we can derive that *F*>0 if

$$0<\gamma_s<\frac{4\alpha_s\alpha_P\gamma_p\lambda_{min}(M)}{4\alpha_s+{\alpha_P}^2\lambda_{min}(M)}$$

The lemma is proved with the above arguments.

Theorem 6.2: Assume that $\left|\dot{\bar{P}}_0\right|\le\psi$, *where* ψ *is a positive constant. Assume that the fixed undirected graph* $\mathcal{G}$ *is connected and at least one* a_{i0} *is nonzero (and hence positive).*

Assuming that the undirected graph $\mathcal{G}$ *is associated and at least one* a_{i0} *is nonzero. Using (6.20) for (6.11a), if* $\beta_P\ge\psi$ *and* γ_p *satisfied (6.25), then* $S_i(t)\to S_0(t)$ *and* $\bar{P}_i(t)\to\bar{P}_0(t)$ *globally exponentially as t*$\to\infty$. *It follows that*

$$\left\|\left[\tilde{\bar{S}}^T(t)\quad\tilde{\bar{P}}^T(t)\right]^T\right\|_2\le\tau_1 e^{-\tau_2 t}, \tag{6.26}$$

where $\tilde{\bar{S}}$ *and* $\tilde{\bar{P}}$ *are the column stack vectors of* $\tilde{\bar{S}}_i=\bar{S}_i-\bar{S_0}$ *and* $\tilde{\bar{P}}_i=\bar{P}_i-\bar{P}_0$ *for i=1, 2,…,n, respectively; and* τ_1 *and* τ_2 *can be calculated as:*

$$\tau_1=\sqrt{\frac{\left[\tilde{\bar{S}}^T(0)\quad\tilde{\bar{P}}^T(0)\right]E\left[\tilde{\bar{S}}^T(0)\quad\tilde{\bar{P}}^T(0)\right]^T}{\lambda_{min}(E)}}$$

$\tau_2=\frac{\lambda_{min}(F)}{2\lambda_{max}(E)}$ *where E and F are defined in Lemma 6.1.*

Proof: As mentioned before, $\tilde{\bar{S}}_i=\bar{S}_i-\bar{S_0}$ and $\tilde{\bar{P}}_i=\bar{P}_i-\bar{P}_0$. Then the close-loop system of (6.20) using (6.11a) becomes:

$$\dot{\tilde{\bar{S}}}_i=\tilde{\bar{P}}_i$$

$$\dot{\tilde{\bar{P}}}_i=\Big(-\sum_{j=0}^{N}a_{ij}\left[\alpha_S(\tilde{\bar{S}}_i-\tilde{\bar{S}}_j)+\alpha_P(\tilde{\bar{P}}_i-\tilde{\bar{P}}_j)\right]-\beta_P\,sgn\sum_{j=0}^{N}a_{ij}\left[\left[\gamma_S(\tilde{\bar{S}}_i-\tilde{\bar{S}}_j)+\gamma_P(\tilde{\bar{P}}_i-\tilde{\bar{P}}_j)\right]\right]\Big)-\dot{\bar{P}}_0 \tag{6.27}$$

Eq. (6.27) can be expressed in a matrix form as

$$\dot{\tilde{S}} = \tilde{\tilde{P}}$$

$$\dot{\tilde{P}}_i = -\alpha_S M\tilde{S} - \alpha_P M\tilde{P} - \beta_P\, sgn\left[M\left(\gamma_S\tilde{S} + \gamma_P\tilde{P}\right)\right] - \mathbf{1}\dot{\bar{P}}_0$$

Now, the Lyapunov function candidate is chosen as:

$$V = [\tilde{S}^T \quad \tilde{P}^T]\ \ E\ \ \begin{bmatrix}\tilde{P}\\ \tilde{\tilde{S}}\end{bmatrix}$$

$$= \tfrac{1}{2}\alpha_s\gamma_P\tilde{S}^T M^2\tilde{S} + \tfrac{1}{2}\gamma_P\tilde{P}^T M\tilde{P} + \gamma_S\tilde{S}^T M\tilde{P} \tag{6.28}$$

From Lemma 6.1, F is symmetric positive definite if γ_S satisfies (6.25). The derivative of V is

$$\dot{V} = \alpha_s\gamma_P\tilde{\tilde{S}}^T M^2\tilde{P} + \gamma_s\tilde{P}^T M\tilde{\tilde{P}} + \gamma_S\tilde{\tilde{S}}^T M\dot{\tilde{P}} + \gamma_P\tilde{P}^T M\dot{\tilde{P}}$$

$$= -[\tilde{S}^T \quad \tilde{P}^T]\ F\ \begin{bmatrix}\tilde{\tilde{S}}\\ \tilde{P}\end{bmatrix}$$

$$-\ (\gamma_S\tilde{\tilde{S}}^T + \gamma_P\tilde{P}^T)M\left\{\beta_P\, sgn\left[M\left(\gamma_S\tilde{\tilde{S}} + \gamma_P\tilde{P}\right)\right] + \mathbf{1}\dot{\bar{P}}_0\right\}$$

$$\leq -[\tilde{\tilde{S}}^T \quad \tilde{P}^T]\ F\ \begin{bmatrix}\tilde{\tilde{S}}\\ \tilde{P}\end{bmatrix} - (\beta_P - \psi)\left\|M\left(\gamma_S\tilde{\tilde{S}} + \gamma_P\tilde{P}\right)\right\|_1 \tag{6.29}$$

where the last inequality allows that $\left|\dot{\bar{P}}_0\right| \leq \psi$. Also, $\beta_P \geq \psi$. It follows that $\dot{V}$ is negative definite. Consequently, it follows from Theorem 2 in [170] that $\tilde{\tilde{S}} \to 0_n$ and $\tilde{\tilde{P}} \to 0_n$ as $t \to \infty$, where 0_n is the $n \times 1$ zero vector. Consistently, it follows that $\bar{S}_i(t) \to \bar{S}_0(t)$, and therefore, $S_i(t) \to S_0(t)$, and $\bar{P}_i(t) \to \bar{P}_0(t)$ as $t \to \infty$. Distributed Consensus tracking is reached at least globally exponentially.

Note that $V \leq \lambda_{max}(E)\|[\tilde{\tilde{S}}^T \quad \tilde{P}^T]^T\|_2^2$. Following from (6.29), it can be written that

$$\dot{V} \leq -[\tilde{\tilde{S}}^T \quad \tilde{P}^T]\ F\ \begin{bmatrix}\tilde{\tilde{S}}\\ \tilde{P}\end{bmatrix}$$

$$\leq -\lambda_{min}(F)\|[\tilde{\tilde{S}}^T \quad \tilde{P}^T]^T\|_2^2 \leq -\frac{\lambda_{min}(F)}{\lambda_{max}(E)}V.$$

Hence, we can establish that $V(t) \leq V(0)\, e^{-\frac{\lambda_{min}(F)}{\lambda_{max}(E)}t}$.

Also $V \geq \lambda_{min}(F)\|[\tilde{\tilde{S}}^T \quad \tilde{P}^T]^T\|_2^2$. At last, some manipulation has been done to get (6.26).

Similarly, the consensus proof for (6.18) -(6.21) can be completed following the steps mentioned above.

6.3.4 Design of Fuzzy-based PI Controller for Power Tracking

In the above subsection, we assume that $P_i^{con} = P_i$ and the same for reactive power control. But in simulation, these two are not exactly equal from the very beginning. In this chapter, we propose a PI control to reduce the error ($P_i^{con} - P_i$). To get the best result from the PI control, we use fuzzy logic-based PI control. The conventional PI controllers have been most widely used as a tracker in the control system design, because of the simple architecture, easy design and low cost. Despite these benefits, the conventional PI controllers result in poor performance when the controlled system is extremely nonlinear. Therefore, retaining the advantages of the PI controller, in this chapter, a fuzzy-tuned PI controller is presented for power (active and reactive) tracking,

used in (6.10). Fig. 6.3 shows the input-output of the proposed fuzzy logic tuner for the active power. The PI controller outputs can be expressed as follows:

$$\text{For Active Power, } U_{PI}^{P} = k_P^{\omega P}(P_i^{con} - P_i) + k_I^{\omega P}\int (P_i^{con} - P_i)\, dt \text{ and}$$

$$\text{For Reactive Power, } U_{PI}^{Q} = k_P^{vQ}(Q_i^{con} - Q_i) + k_I^{vQ}\int (Q_i^{con} - Q_i)\, dt$$

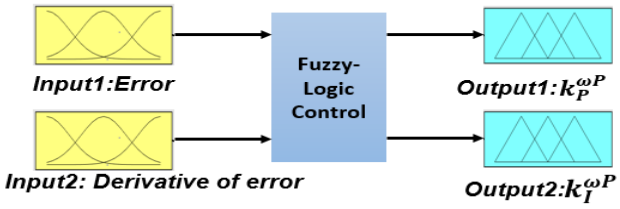

Fig. 6.3 Input-Output relation of the proposed fuzzy logic tuner

In this chapter, the configuration of PI controller is the same for both active and reactive power, and that's why only the fuzzy-PI control design for active power is shown here. Note that the PI controller tracks the error between P_i^{con} and P_i. The inputs to the fuzzy logic system are the error $(P_i^{con} - P_i)$ and the derivative of the error $\frac{d}{dt}(P_i^{con} - P_i)$, and two outputs are $k_P^{\omega P}$ and $k_I^{\omega P}$. The control structure of the fuzzy tuning of PI controller is presented in Fig. 6.4. In Fig. 6.4, $k_P^{\omega P}(P_i^{con} - P_i) + k_I^{\omega P} P'_i$ is the output obtained from the fuzzy-PI controller which is the input to the SC along with u_i^{ω} and u_i^{P}.

As presented in Fig. 6.4, the fuzzy controller has the fuzzy and PI block. The fuzzy block comprises three blocks. The *fuzzification* block transforms the crisp input to the linguistic variable, which is a knowledge-based process. The *inference* block is a rule-based task produced by experts' knowledge. The *deffuzzification* block transforms the linguistic variable back to a crisp value.

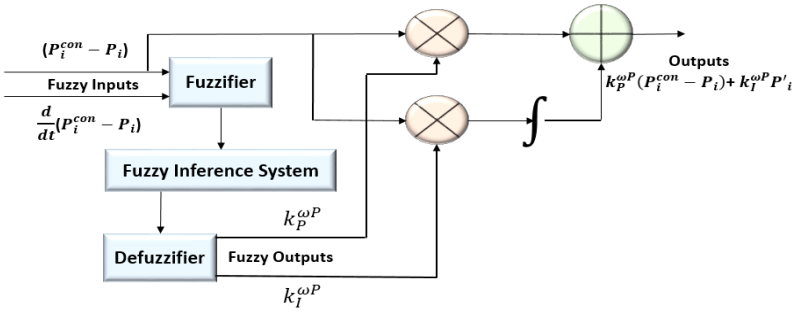

Fig. 6.4 Block diagram of fuzzy-logic control system for active power

The membership functions used here for both inputs are Gaussian membership functions which are shown in Fig. 6.5. The input membership functions are represented by fuzzy sets, i.e., Negative (N), Zero (Z) and Positive (P), and the output membership functions are symbolized as Small (S), Medium (M) and Big (B). More details of fuzzy-logic design are found in [20]. The rules for describing the output variables $k_P^{\omega P}$ and $k_I^{\omega P}$ for active power-sharing are shown in Table 6.1. The overall control structure is presented in Fig. 6.6.

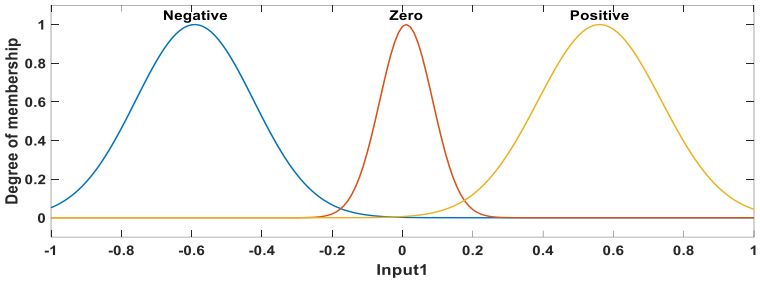

(a)

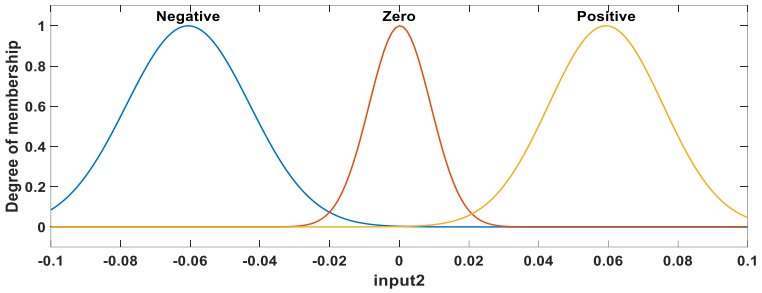

(b)

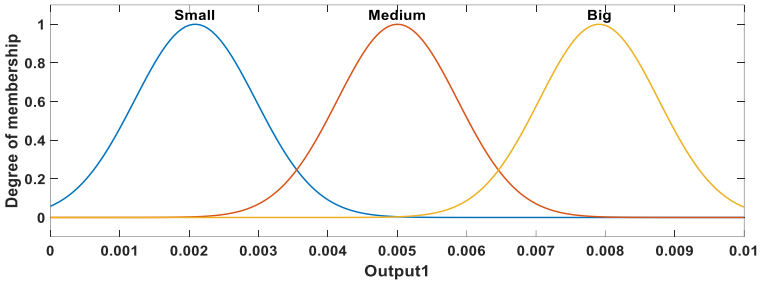

(c)

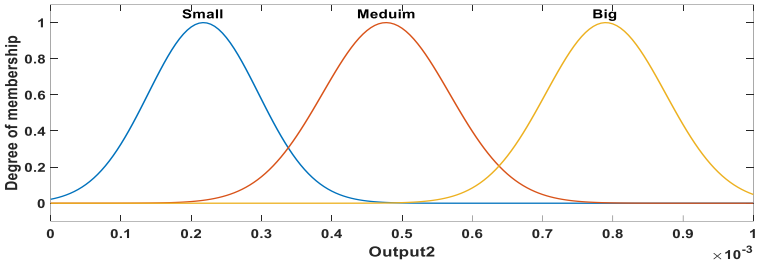

(d)

Fig. 6.5 Membership functions for (a) input1, error (b) input2, derivative of error (c) output1 and (d) output2

Table 6.1 Fuzzy Rule Set for Inputs and Outputs

Rule	*error*	$\frac{d}{dt}(error)$	$k_P^{\omega P}$	$k_I^{\omega P}$
1.	N	N	S	S
2.	N	Z	M	M

3.	N	P	B	B
4.	N	N	S	S
5.	Z	Z	M	M
6.	Z	P	B	B
7.	P	N	S	S
8.	P	Z	M	M
9.	P	P	B	B

6.4 TIME-DOMAIN SIMULATIONS

Case studies are done applying the simple DESS dynamics shown in (6.18) - (6.21). The test MG model for case studies which has 3 DESUs and one PV array is shown in Fig. 6.1. The recommended multi-agent controller is supplemented to the DESSs. MATLAB/Simulink platform is employed for dynamic simulations. Seven case studies are presented to verify the responses of the proposed controllers in different circumstances. The simulations have been performed considering that the MG is disconnected from the high voltage substation, which means that MG must run in islanded mode. The AEMO power quality obligations are used as working standards for the control arrangements, which include a frequency range of 49.5Hz to 50.5Hz [171] and a voltage magnitude range of -6% to +10% [71]. The DESU parameters, line and load data are listed in Table 6.2. In this chapter, it is supposed that all the DESUs of lithium-ion batteries have the equal rated capacity, rated power and charging/discharging characteristics. The maximum charging/discharging power of each ESU is set to be P_{max} = 50 kW. The initial SoCs of DESUs 1-3 are chosen as different from each other intentionally [90%, 80% & 70%], while the capacities are the same (different capacities are used in case 5). The controller parameters in (6.18) -(6.21) for each DESU are shown in Table 6.2.

In our simulation, we consider the whole simulation in two parts. In the first part, we consider the proposed control with DESUs without any DG/RES. In this part, DESUs are fully responsible for supplying the load. To consider the charging/discharging condition, the PV array is considered as RES here in the second part with DESUs. The output power of PV array is intermittent and depends on weather conditions, and it always operates in the maximum power output mode, while DESUs are utilised to mitigate the active power fluctuation of MG. It is needed that during discharging mode, the DESU with higher SoC will deliver more power than the others and vice versa for the charging mode of operation. The proposed DSC is active from the beginning. Several scenarios are considered through different case studies.

Table 6.2 Specifications of Test MG

Description	Parameter	Value	Unit
DC Bus Voltage	V_{dc}	700	V
Reference Voltage	v_{ref}	311	V
Reference Frequency	f_{ref}	50	Hz
Capacities of DESUs	$C_1 = C_2 = C_3$	200	Ah

Active Power Droop Gain	$m_{p1} = m_{p2} = m_{p3}$	$4e^{-5}$	rad/W
Reactive Power Droop Gain	$n_{q1} = n_{q2} = n_{q3}$	$2.9e^{-5}$	V/Var
Impedance of Line1	R_{line1}, L_{line1}	0.23, 318	Ω, μH
Impedance of Line2	R_{line2}, L_{line2}	0.12, 312	Ω, μH
Impedance of Load1	R_{load1}, L_{load1}	18, 10	Ω, mH
Impedance of Load2	R_{load2}, L_{load2}	22, 12	Ω, mH

Table 6.3 Secondary Controller Parameters

Controller Parameters	Values	Controller Parameters	Values
α_ω	*2.6*	β_ω,	*10.4*
α_V	*4*	β_V	*16*
α_S	1^{e-4}	β_P,	*20*
α_P	5^{e-3}	β_Q	2^{e-2}
α_Q	5^{e-3}		

6.4.1 Part 1: Proposed DSC Control for DESUs without any DG/RES

Case 1: Frequency and voltage restoration with SoC balancing by the proposed DSC

The performance of primary droop control (6.1) and (6.2) is shown in Fig. 6.6 which indicates due to the primary control, the frequencies deviate to 49.38 Hz, and voltages of 3 DESUs deviate to different values from the reference value (311V). Fig. 6.6(c) shows that the active power-sharing is based on their capacities, and Fig. 6.6(d) shows that the *SoCs* of DESUs are unbalanced when DESUs use the conventional *P-f* droop control. Reactive power should be shared among the DESUs according to their capacities, but the reactive power sharing mismatches occur due to the limitations of the primary droop control, which is presented in Fig. 6.6(e). Figs. 6.7(a) and 6.7(b) show that the proposed DSC can provide a fast response to restoring the deviated frequencies and voltages to their nominal values. Moreover, Fig. 6.7(c) and Fig. 6.7(e) show that the active and reactive powers converge to the same value after the SoCs are balanced at t=65s, respectively, and Fig. 6.7(d) indicates that the *SoCs* of all DESUs trend to be balanced.

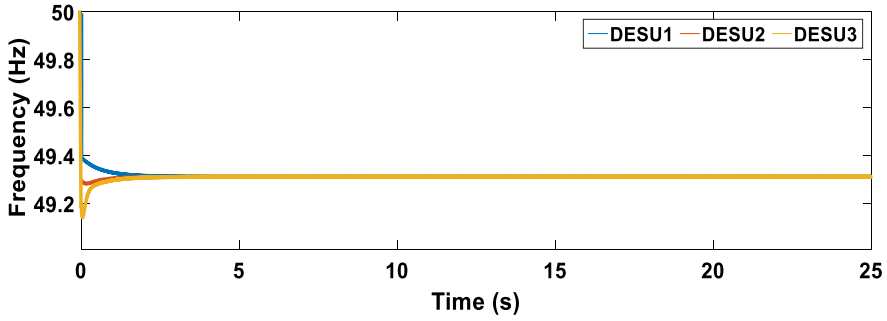

(a)

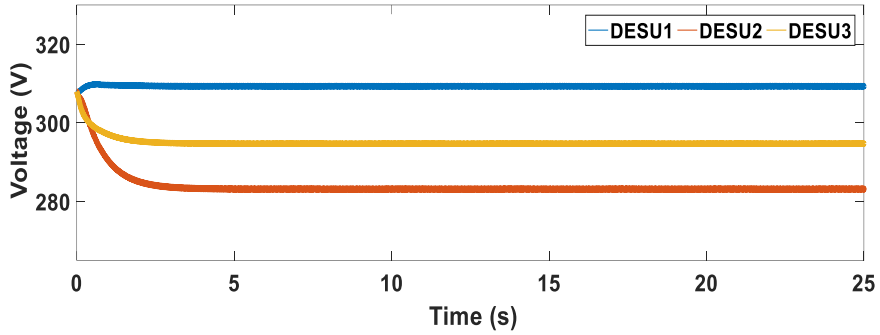

(b)

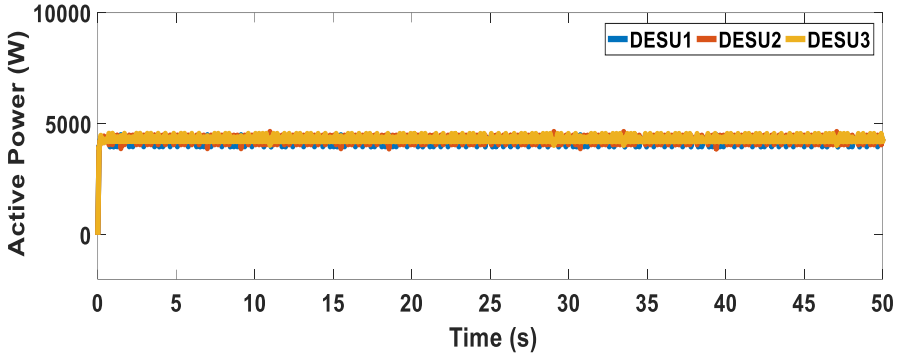

(c)

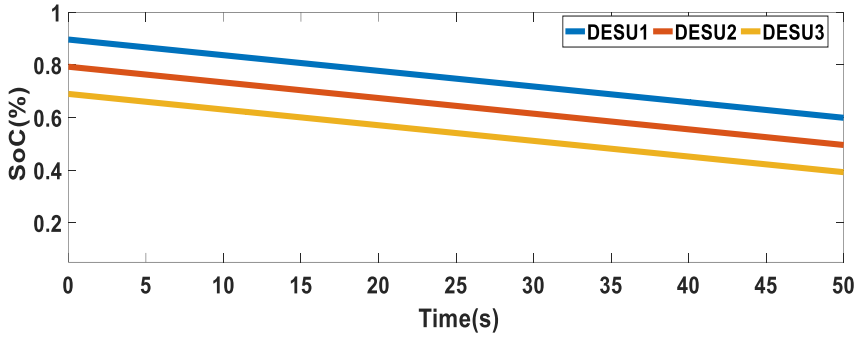

(d)

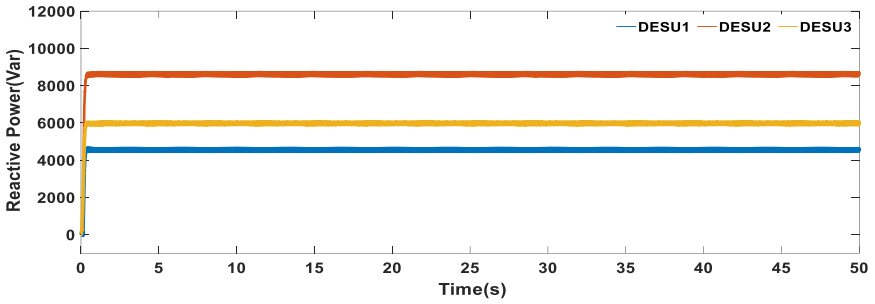

(e)

Fig. 6.6. Output of DESUs under only primary control (Droop control) (a) Frequency (b) Voltage (c) Active power and (d) SoC (e) Reactive power

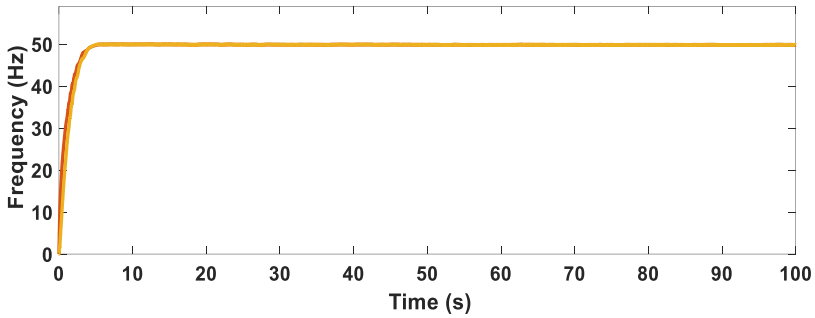
Frequency (Hz)
Time (s)

(a)

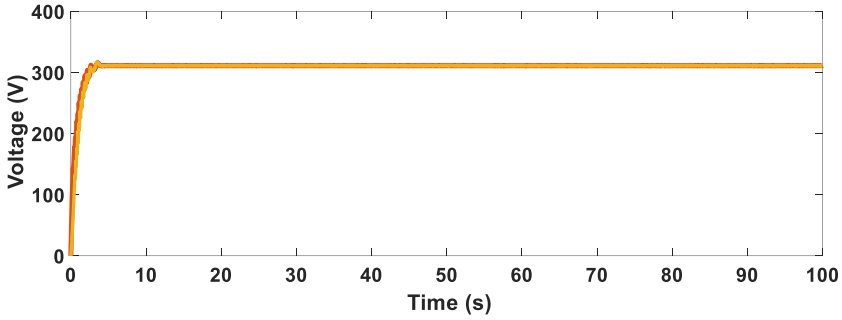
Voltage (V)
Time (s)

(b)

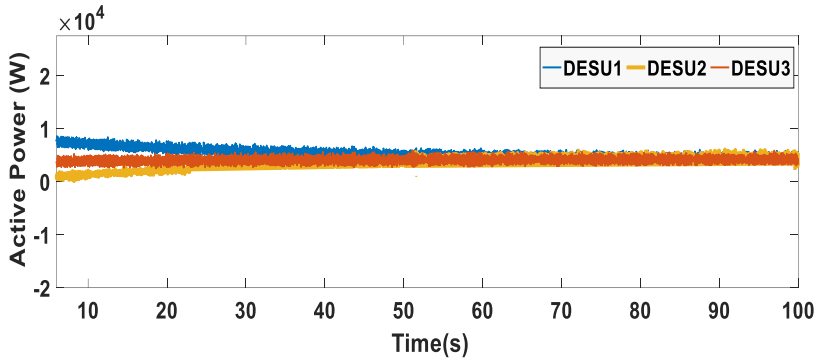
×10^4
DESU1
DESU2
DESU3
Active Power (W)
Time(s)

(c)

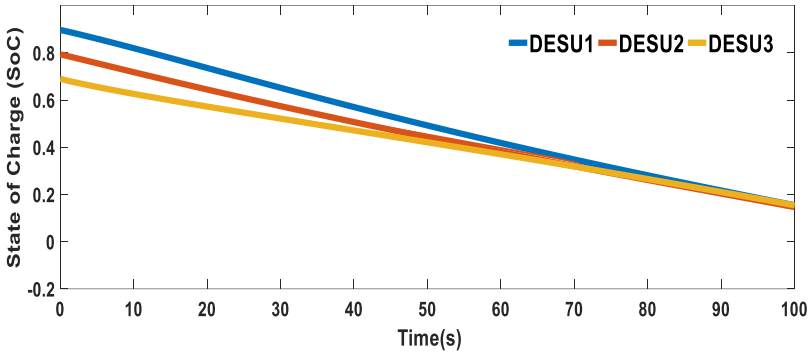
DESU1
DESU2
DESU3
State of Charge (SoC)
Time(s)

(d)

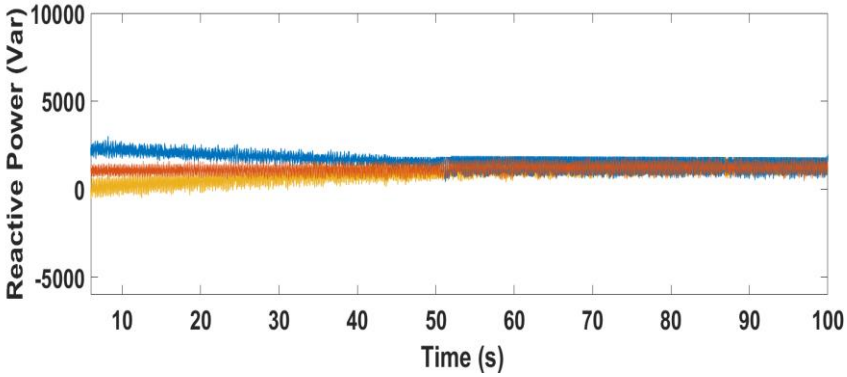

(e)

Fig. 6.7 Output of DESUs after applying proposed DSC in DESUs (a) Frequency (b) Voltage (c) Active power and (d) SoC (e) Reactive power

Case 2: Power Sharing with Step Load Changes

The suggested DSC is tested with step load changes, as shown in Fig. 6.8. Initially, load 1 and load 2 are connected to the system. After reaching the steady state, load 3 is added at t=60s and is disconnected at t=70s. Simulation results are shown in Fig. 6.8, indicating that the offered control technique can accomplish power-sharing (active and reactive) and SoC control at step load changes.

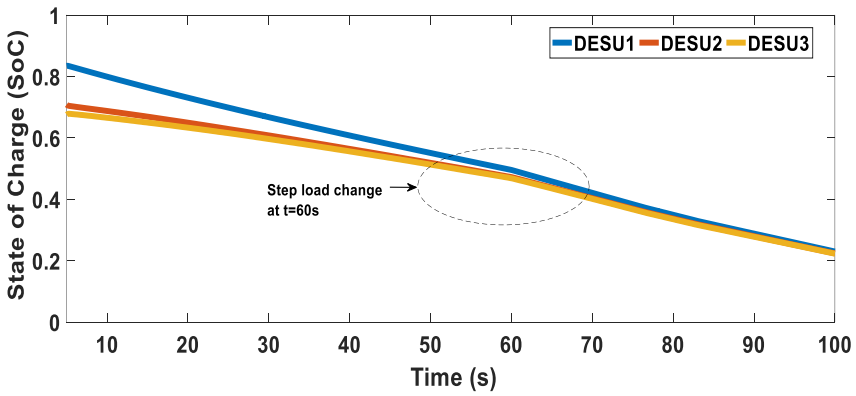

(a)

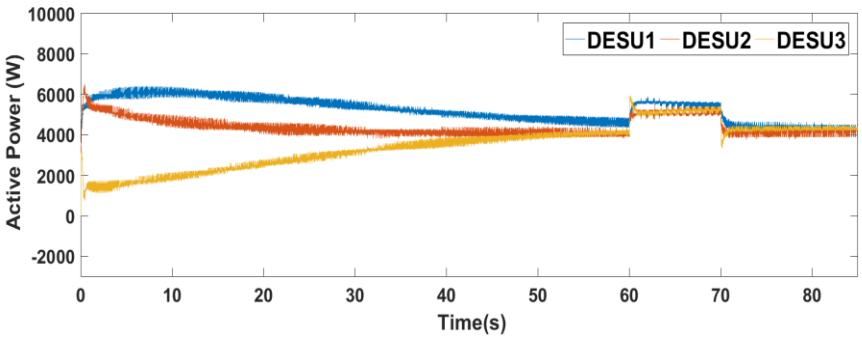

(b)

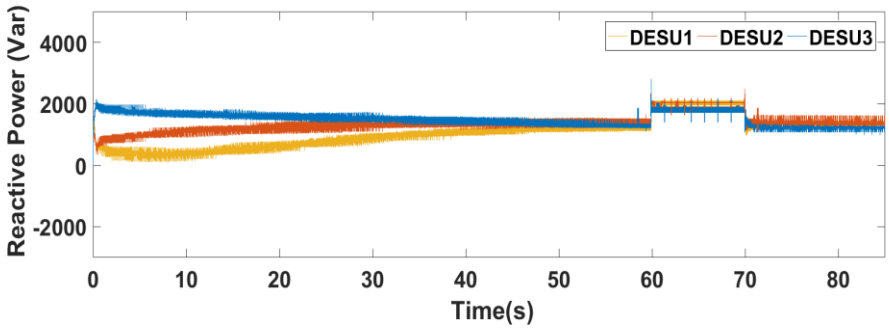

(c)

Fig. 6.8 Output of DESUs after applying proposed DSC in DESUs with step load change (a) SoC (b) Active power and (c) Reactive power

Case 3: Plug-n-play operation of the proposed DSSC.

Plug-n-play ability of the suggested distributed control method is presented in Fig. 6.9. It is assumed that the initial SoCs are identical (90%) in this case. To verify the plug-n-play capability, DESU3 is disconnected at t = 10s and connected again at t=20s. The frequencies and voltages are controlled after fast transients. From 10s to 20s, the load is shared between the existing DESUs (battery1 and battery2) and the SoCs are decreased at a faster rate. When the battery3 is again connected at t=20s, the active and reactive power are also shared as $t \leq$ 10s.

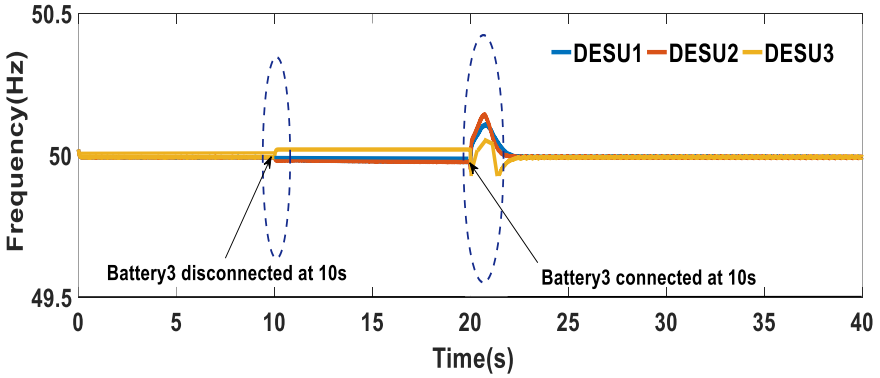

(a)

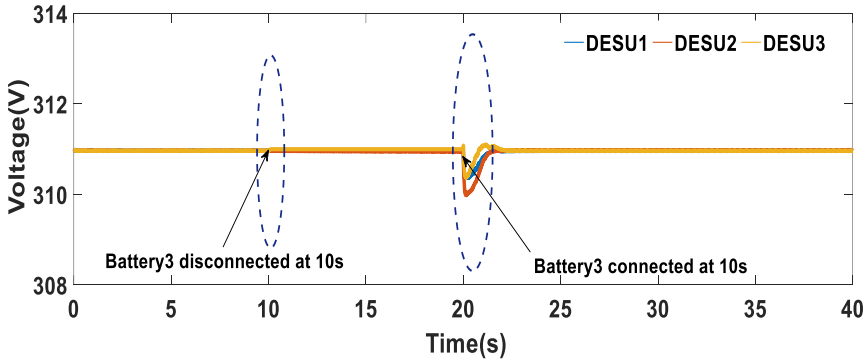

(b)

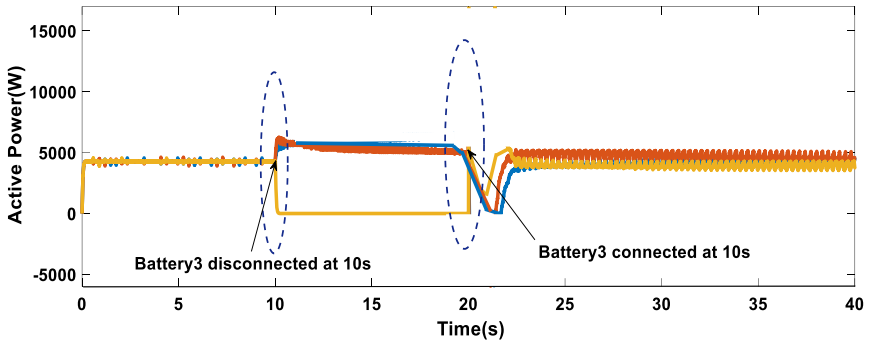

(c)

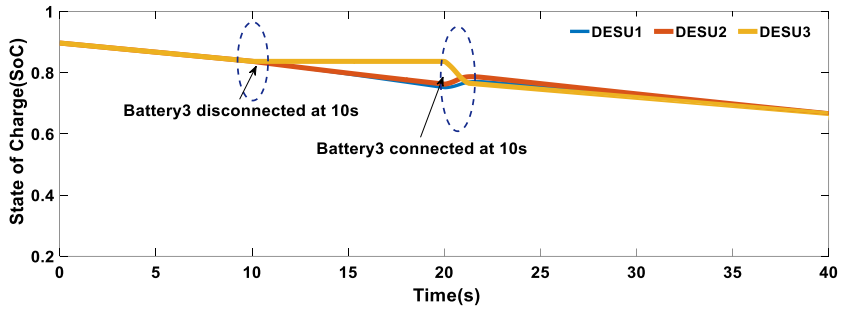

(d)

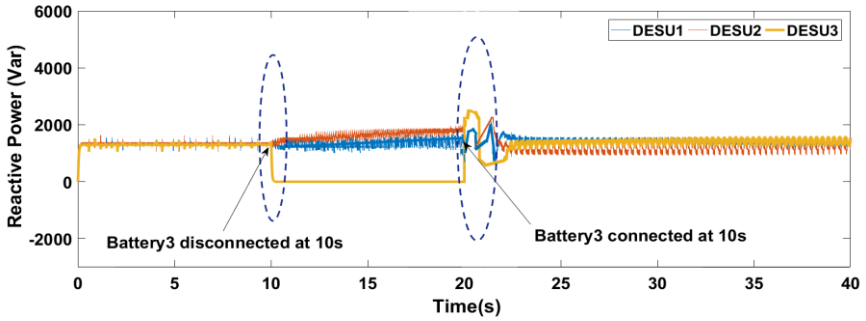

(e)

Fig. 6.9 Output of DESUs after applying proposed DSC in DESUs with plug-n-play (a) Frequency (b) Voltage (c) Active power and (d) SoC and (e) Reactive power

Case 4: Effect of Measurement Noise

The effect of measurement noise on the performance of the control system is displayed in Fig. 6.10. Here, we assume that the output active power, reactive power, voltage, and frequency measurements of every DESUs are disturbed by distinct band-limited white noises with the power of 10, 2 and 0.1, respectively. From the simulation results as in Fig. 6.7, it is clear that the proposed DSC is still operative in the existence of measurement noise, restores the voltage and frequency to the reference values, and maintains the stability at steady state.

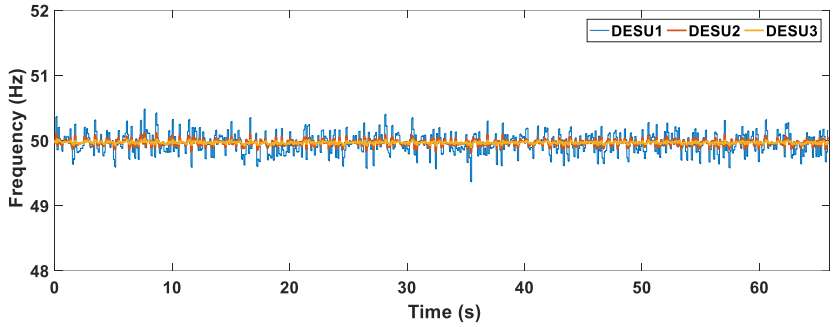

(a)

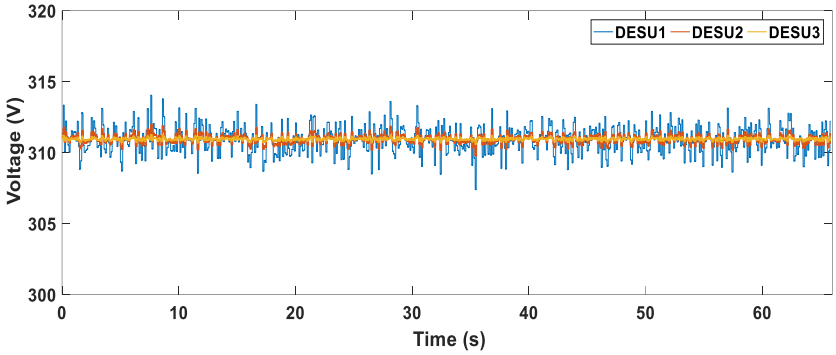

(b)

Fig. 6.10 Output of DESUs after applying proposed DSC in DESUs with measurement noise (a) Frequency and (b) Voltage

Case 5: With Different Communication Topologies

Response of the proposed DSC is examined by applying two sample communication network topologies as shown in Figs. 6.11(a) and 6.11(b). In this case, we assume the graphs of SoC and active power for comparing the performance with different communication topologies. Figs. 6.11(c)-6.11(d) shows the outcomes of the proposed DSC with communication topology in Fig. 611(b), whereas the outcomes with communication topology in Fig. 6.11(a) are shown in Figs. 6.7(c)-6.7(d). Stability of the MG is maintained for diverse configurations of communication by using the proposed technique. Compared with Figs. 6.8(c)-6.8(d), the SoC and steady-state power dispatch in Fig. 6.11(c)-6.11(d) through applying the communication configuration in Fig. 6.11(b) is similar to the outcomes employing the configuration of Fig. 6.11(a). The output active power of all the DESUs is same, since their SoCs are balanced.

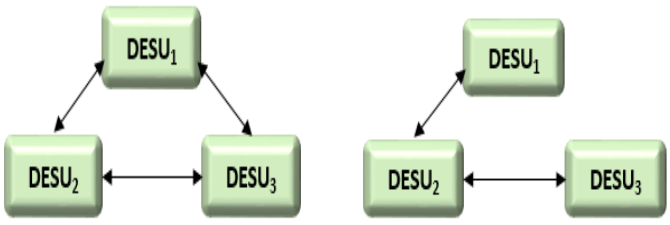

(a) (b)

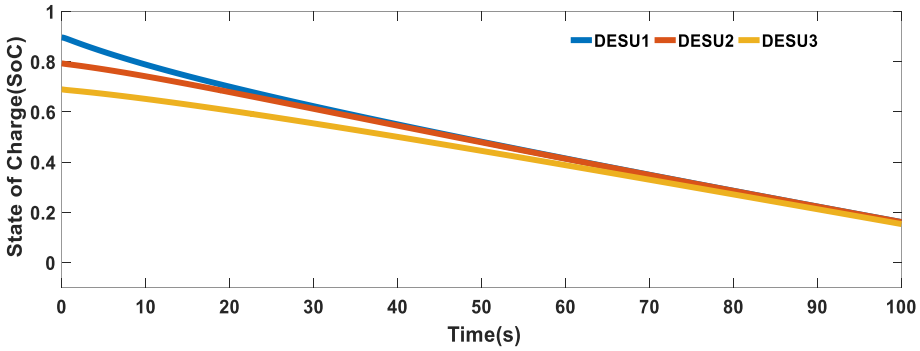

(c)

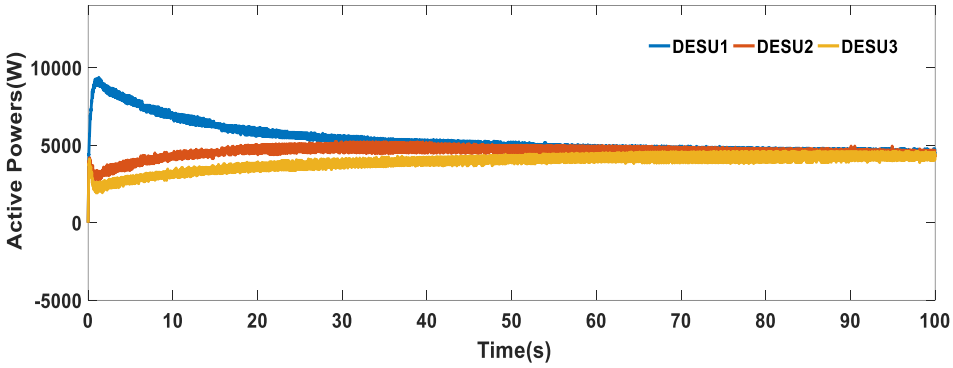

(d)

Fig. 6.11 Output of DESUs after applying proposed DSC in DESUs with different communication topologies (a) Communication topology 1 (b) Communication topology 2 (c) SoC for (b) and (d) Active power for (b)

Case 5: SoC balancing of DESUs with different capacities

The performance of the proposed control scheme for DESUs with different capacities is shown in Fig. 6.12. Fig. 6.12(a) shows the SoC balancing. Fig. 6.12(b) and 6.12(c) illustrates that the DESUs share the active and reactive power, respectively, in accordance with their capacities (ratios are $DESU_1$:$DESU_2$:$DESU_3$=2:2:1) after SoC balancing at t=50s. Thus, the heterogeneous nature of the storage units is verified for the proposed control.

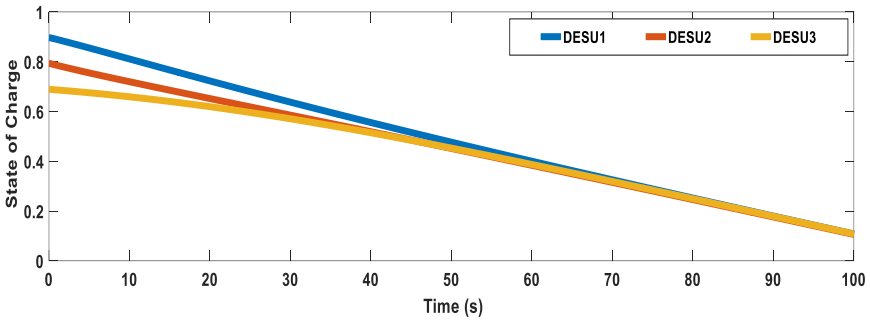

(a)

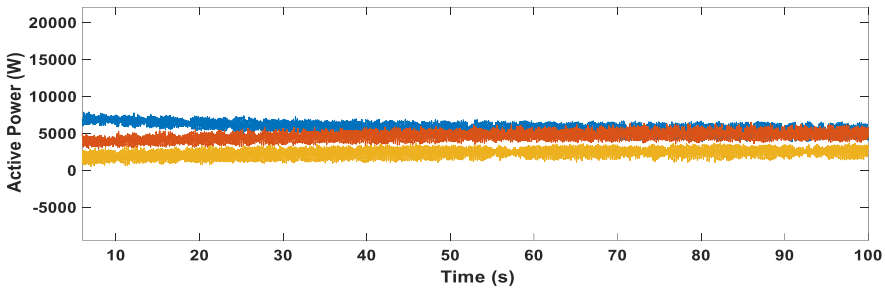

(b)

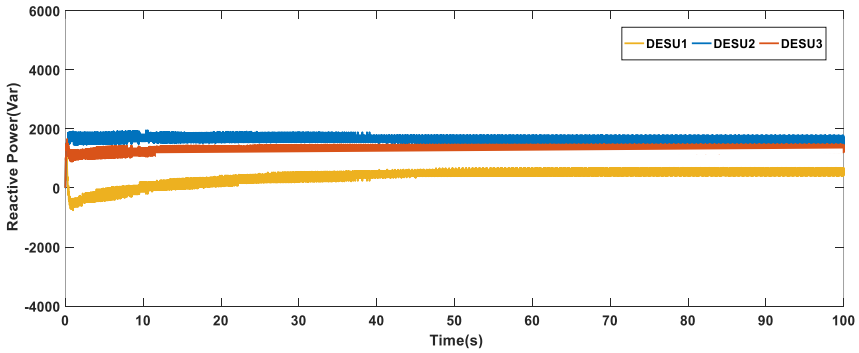

(c)

Fig. 6.12 Output of DESUs after applying proposed DSC in DESUs with different capacities of storage units (a) SoC (b) Active power and (c) Reactive power

Case 6: Effects on Controller Gain

The parameters of the recommended controllers have an absolute contribution to the dynamic reaction of the energy storage systems. This case is aimed to analyse the sensitivity of consensus input gains on the system performance. According to the proposed DSC in (6.18) -(6.21), the convergence time can be set by tuning the consensus gains α_ω, α_v, α_S and α_Q. In this case, the effect of consensus gain is examined, where α_ω in frequency recovery control is measured, and a similar study is applicable to the other three consensus gains. At first, different values of α_ω are applied for the proposed DSC into the test MG model. It can be seen from the simulation results in Fig. 14 that the convergence speed of the system will rise by choosing a higher consensus gain ($\alpha_\omega = 1.3$ in Fig. 6.13(a) and $\alpha_\omega = 5.2$ in 6.13(b)). On the other hand, these consensus gains cannot be arbitrarily large as large gains introduce overshoots (Fig. 6.13(c)) while increasing the convergence speed. Besides, the large gain is not suitable due to the physical constraints of the control inputs to DESSs. The effects on other controller parameters have a similar performance, that is, the convergence speed increases with the increase of the controller gain; therefore, they are not shown here.

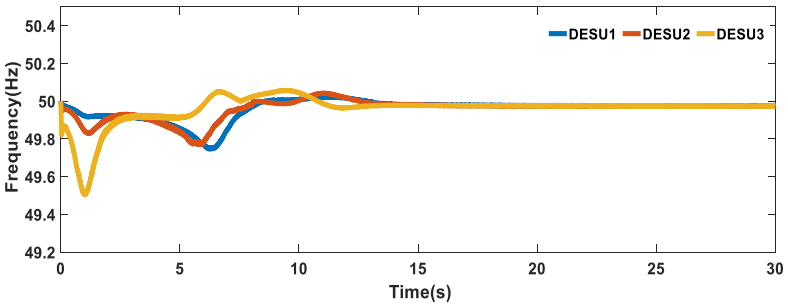

(a)

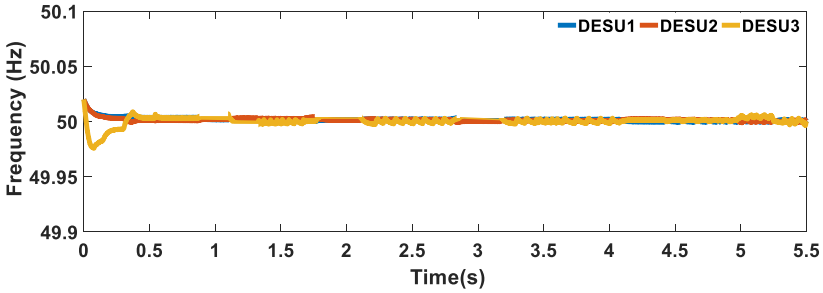

(b)

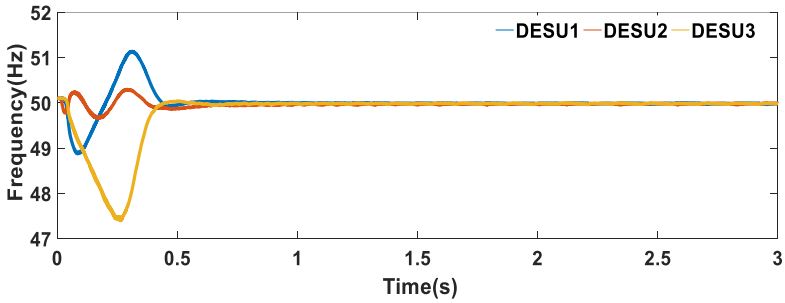

(c)

Fig. 6.13. Output of DESUs after applying different values of α_ω in DSC (a) $\alpha_\omega = 1.3$ (b) $\alpha_\omega = 5.2$ (c) $\alpha_\omega = 10.5$

6.4.2 Part 2: Proposed DSC Control for DESUs with DG

Case 7: SoC Balancing with PV Array

In part 2, the response of the suggested DSC of DESUs in islanded MG is examined with a PV array (as DG). PV array is connected with battery3 as shown in Fig. 6.1. Maximum power point tracking (MPPT) mechanism is applied as in Fig.6.14 (e), considering the perturbation and observation method commonly used in MPPT algorithms. It is a two-level arrangement where a DC-DC boost converter is applied for MPPT control. The control system also allows a battery back-up during emergencies while keeping the voltage and frequency of the MG or while attempting to supply the critical loads. A battery is associated in parallel to the PV to export or import active power via a bidirectional DC-DC converter. During the power absorption of the battery, the converter operates in the buck mode and during power injection of the battery, it operates in the boost mode. However, the detailed design of control for the operational mode of the buck-boost converter is out of scope for

this chapter. In this chapter, we consider that the converter is working in boost mode and PV is delivering very low power as in Fig. 6.14 (b). The PV data are acquired from EPRI website. PV power is kept intentionally very low (~1000W) compared to load demand (~ 13000W) to see the discharging performance of the DESUs. DESUs 1-3 are governed by the proposed DSC control from the beginning. The initial SoCs are not identical (SoC1=90%, SoC2=80 % & SoC3=70%). The simulation results of system frequency and voltages are almost similar to Fig. 6.7(a) & 6.7(b) and thus not included here. SoCs, PV power, real and reactive power outputs of DESSs are shown in Figs. 6.14(a)-6.14(d). From Fig. 6.14(a), it can be shown that the proposed control can effectively balance the SoC, and due to the presence of PV power, the discharging rate is a little bit slower than the case without PV power. Other results in Fig. 6.14 (b)-6.14(d) further demonstrate the effectiveness of the presented method.

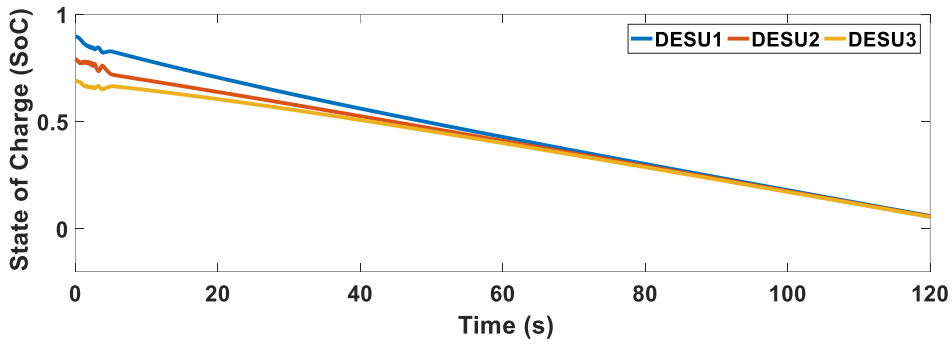

(a)

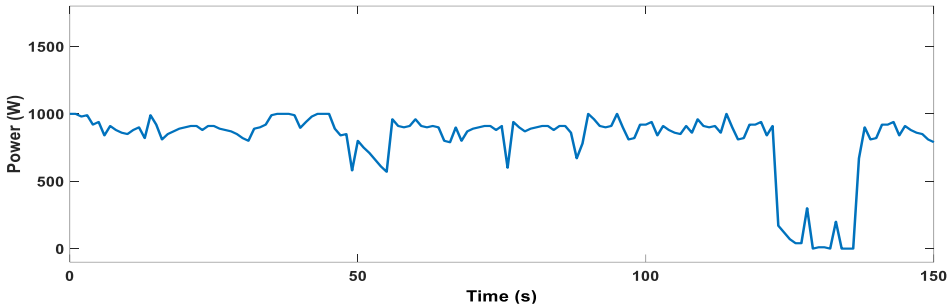

(b)

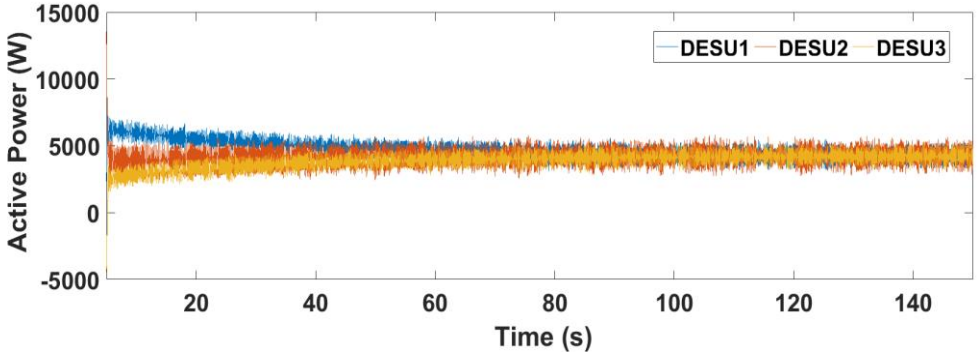

(c)

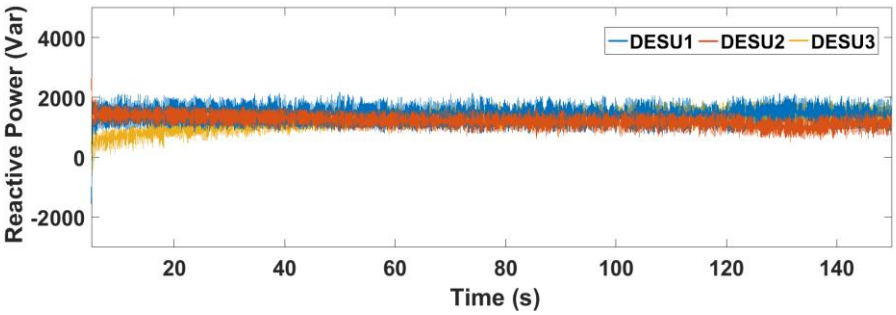

(d)

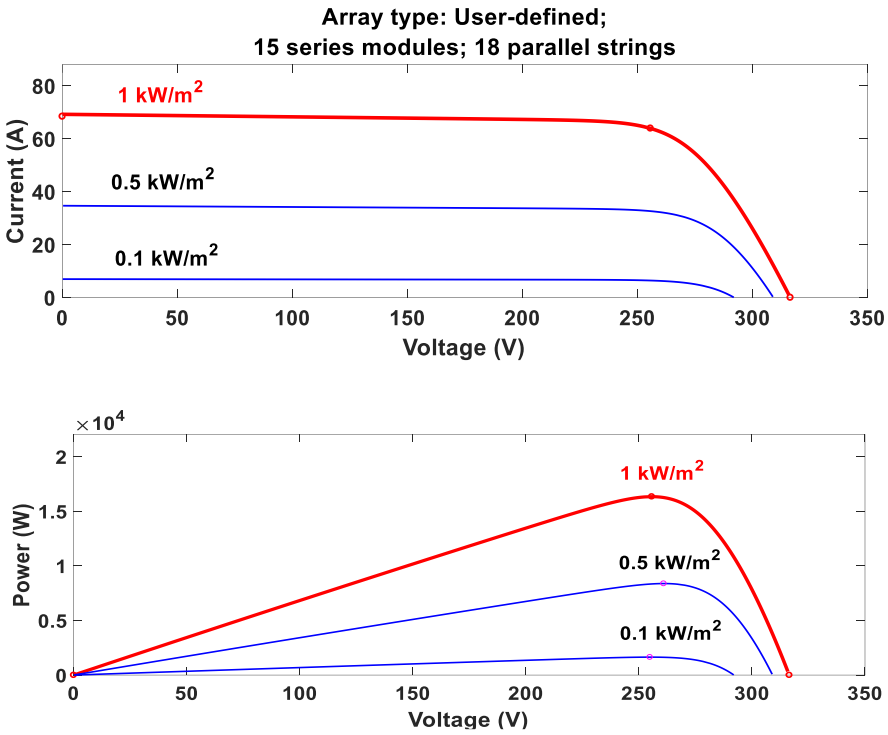

(e)

Fig. 6.14 Output of DESUs with real-data from PV (a) SoC (b) PV power (c) Active power and (d) Reactive power and (e) V-I and V-P graph based on MPPT for PV

6.5 SUMMARY

In this chapter, a novel DSC is established to mitigate the frequency and voltage deviations and balance the SoC for the DESUs in the islanded MG. Moreover, active power mismatch caused by droop-based primary control is also resolved by the proposed DSC, while SoCs of the DESUs are also balanced at the same time. The performance of the proposed DSC of DESUs is verified by several case studies considering the dynamic behaviour of MG like step-load change, plug-n-play capability, performance with random noise, and the proposed control of DESUs with real-time data from the PV array is also tested. The offered DSC exhibits smooth transient response and precise steady-state condition in restoring the voltage and frequency of the MG, sharing

the power mismatch, and balancing the SoCs of the DESUs. The detailed stability analysis considering the DSC and the effects of controller gains on the stability as well as accurate control for DESUs for switching of charging/discharging mode based on SoC levels is considered promising work for the future.

Chapter 7: Conclusions and Future Works

7.1 CONCLUSIONS

In this thesis, an overall study on distributed control of MGs in many aspects, together with MG modelling, control and selection of optimal control parameters, has been presented. MG system comprises of numerous important subsystems, similar as renewable generation, engine systems, electrical generators, storage systems and loads. Every subsystem can be a highly complicated system. Besides, it is also a system that includes electrical, mechanical, chemical, controls, economics and other aspects. The control of such a system is critical and applying a hierarchical control system is compulsory to accomplish optimum performance. MG control studies are mainly focused on the hierarchical control framework comprising three control levels, namely, primary, secondary and tertiary control level. The goal of this research is to deliver technical contributions towards MG growth in terms of control technologies, mainly for making the MG solution feasible. The eventual goal of this research is to make the best use of the advantages of MG by addressing its technical challenges at the SC level and propose the possible solutions to further enable its capabilities from a control perspective.

7.2 SUMMARY OF CONTRIBUTIONS

In this chapter, we would like to summarise our contributions in the sense of

- Providing a brief overview of the current research trend in MG control and finding research gaps in this area
- Presenting systematic methodology for mathematical modelling of MG network
- Performing the detailed stability analysis for the MG network which covers different MG configurations as well as linear and non-linear system models
- Proposing novel DSC strategies for MG networks considering different control strategies in a single control model which includes frequency and voltage
- Control with precise active and reactive power-sharing
- Considering different control strategies for DESUs which include frequency and voltage control with precise active and reactive power sharing along with SoC balancing
- Representing the impact of DSC parameters on stability and proposing the intelligent control methods for finding optimum control parameters for stability enhancement

A review of the notable technical contributions to MGs control in this research is as follows:

7.2.1 Literature review on current research trend on distributed control for MGs

The major contribution provided on this topic is related to the literature review. In the last two decades, electricity networks have increasingly moved towards decarbonisation, digitalisation, and decentralisation. As a result, the concept of MG control has been shifting towards distributed control to lessen the computational and

communication requirement in the latest research trends. Current research trends on MG control and a brief overview of the existing distributed control techniques mentioned in the literature so far for autonomous AC MGs with DGs and ESUs can be found in Chapter 2. The mentioned control strategies are categorized with a comparison based on their design approach and viewpoints. This chapter provides a clear idea on the future direction of the control technologies in MG networks.

7.2.2 Cost-effective DSC for frequency restoration of MG systems

SC structures in a distributed way have been initiated for the control of MGs mainly to reduce the system's cost and complexity while contributing more to the dynamic performance of the system. Typically, distributed control methods are based on multi-agent systems or consensus protocols. The SC selects the accurate primary control reference for frequency synchronisation. In relation to the distributed control theory, the SC objectives are proposed, and then a DSFC law is designed for the MG to restore the deviated frequencies to the reference value. In the distributed control environment [43], a consensus problem is considered as one of the most vital and difficult problems. From a general point of view, the MG acts as a multi-agent system where every DG works as an agent in the consensus control. Agents are able to exchange the required data/information with their neighbours through a simple and less expensive communication network to achieve the consensus. On the other hand, the MG control system should be designed to get the economic benefit and stability of the MG while regulating the active power balance. Most of the prior works only considered the case that the power outputs (both active and reactive) from inverters can proportionally share the total load in accordance with their power ratings. Chapter 3 shows the DSC for frequency restoration with minimising the operation cost by applying the optimal active power sharing using the equal-cost increment values of distributed generation (DG) units. Utilising the PSO technique, the proposed DSFC shows better convergence and stability performance through the optimal control parameters.

7.2.3 DSC for voltage restoration with accurate reactive power-sharing

Consensus-based distributed techniques have achieved popularity in recent years, as they achieve good performance utilising a sparse communication network. However, the dynamic performance of MG with the DSC cannot be suitable in regards to system damping, response time, stability margin, etc. Therefore, DSC parameters need to be well-tuned. The systematic way of mathematical model development can be found in Chapter 4. A unified small-signal dynamic model of the proposed DSVC is thus presented in Chapter 4, also taking the line resistance into account in the model. The major contribution of this chapter is that the proposed voltage controller can keep accurate reactive power sharing after voltage restoration which leads to a possible solution to the existing control problem of accurate reactive power sharing for the resistive distribution network. Another contribution is the comprehensive impact assessment of the distributed controllers on the dominant oscillatory modes of MG constructed on the small-signal dynamic model.

7.2.4 Novel DSC strategies for MG networks with DGs

In Chapter 5, a novel DSC is proposed for lossy MGs to restore frequency and voltage simultaneously, while accurate active and reactive power sharing are preserved. The major contribution of this chapter is to propose different control strategies in a single control strategy. Unlike the existing consensus methods, the proposed method utilizes a PI controller at the output voltage of the inverter. Thus, voltage mismatches are

reduced to a great extent, which can lead to the future direction of solving the voltage mismatch between the inverter reference voltage and actual output voltage. Another contribution of this chapter is to conduct the small-signal stability analysis under the proposed DSC for the networked MG model in detail. Note that eigenvalue analysis for parallel-connected DGs in the MG was previously studied in many studies; however, very few studies have addressed the small-signal stability analysis for a networked MG model considering DSC. Therefore, this research shows the path for designing DSC for the networked MG model for future research. In most of the previous related works, other tuning methods/optimal controllers were used for finding DSC parameters. Utilizing the intelligent FL parameter-tuner in accordance with small-signal stability analysis for the networked MG model has been presented as a new solution. The FLC not only enhances the performance of the proposed DSC, but also contributes to the complexity reduction of the DSC design.

7.2.5 Novel DSC strategies for MG networks with DESUs

Control of DESUs is shown in Chapter 6. Consensus-based DSC is proposed for DESUs in an AC islanded MG system to recover the frequency and voltage to the nominal values within a finite time. The proposed control is responsible for SoC balancing in the case of batteries with different initial SoC as well as sharing the active and reactive power with hierarchical control architecture utilising simplified dynamic representation. In comparison with the existing DESUs, the proposed control is robust against load disturbances, different communication topologies and plug-n-play capabilities. The proposed DSC is verified with real-time PV data, which ensures the effectiveness of the proposed DSC. The convergence speed of SoC balancing and frequency/voltage restoration depends on the DSC parameters, and finite-time tracking can be guaranteed. The major contribution of this chapter is to consider the frequency and voltage restoration within finite time for DESUs while considering SoC balancing and accurate power-sharing for DESUs. This research can lead to the DSC design for DESUs in a more efficient and effective way.

7.3 RECOMMENDATION FOR FUTURE WORKS

In summary, current research trends in MG control have been discussed in detail. The thesis did a thorough literature review to find the research gap in the area. As DSC for autonomous MGs is the most suitable technology for the high implementation of DERs, more and more research needs to be accomplished in this area. Appropriate control system design for DSC is the most crucial part for the successful implementation of DERs. Although decentralised droop control at the primary control level is well established for MG control, distributed control at the secondary control level is still under research. As the DSC is the new technology to implement in real-time operation system and implementation of new technology relates to high expense, more investigation is required to further improve it in the research. This research covers some areas to proceed further, but there are some areas which are out of the scope of this research and can be further investigated as per research interest. This research provides a DSC framework for autonomous MGs which include DGs and DESUs, and proposes different MG models with proper mathematical representation for detailed stability analysis. The following recommendations are suggested for future research.

i. From a realistic point of view, sensitive loads in an MG need to operate at the reference voltage and frequency. Consequently, it is desirable to speed up the synchronisation process and ensure the consensus in a finite time. In the future, the consensus in a finite time can be investigated.

ii. Communication delay can be included in the mathematical model, which is another good area to continue this research to make the system robust.

iii. Furthermore, consensus-based distributed control methods have robust performance and stability, higher accuracy, adaptability and disturbance rejection properties. This thesis proposed several control methods for DSC for different MG configurations both for frequency and voltage restoration as well as simultaneous accurate active and reactive power-sharing. To get the best control performance, different optimisation techniques for choosing the DSC parameters like PSO, FLC are applied, and the results are verified in the time-domain simulation in Matlab/Simpower system platform. In the future, more optimisation-based methods can be applied to the proposed models, and a good comparison can be presented.

iv. The cooperative control strategies have been proposed for DESUs considering SOC balancing with accurate power-sharing. The established models can be applied to power system studies as well as control system studies. As proper tuning of DSC parameters plays a vital role in the performance of DSC, choosing the intelligent control methods is also an important task in designing DSC. A comparative analysis for choosing the DSC parameters for DESUs will be performed in future works.

v. The analysis of the relationship among the cost, the design and the operation of MGs is one of the most important areas in the future research of MGs.

Bibliography

[1] M. F. Zia, M. Benbouzid, E. Elbouchikhi, S. M. Muyeen, K. Techato, and J. M. Guerrero, "Microgrid Transactive Energy: Review, Architectures, Distributed Ledger Technologies, and Market Analysis," *IEEE Access,* vol. 8, pp. 19410-19432, 2020, doi: 10.1109/ACCESS.2020.2968402.

[2] *Renewable Capacity Highlights 2020*, International Renewable Energy Agency (IRENA), Australia, 2020.[Online]. Available: http://irena.org.

[3] Q. Fu, A. Nasiri, A. Solanki, A. Bani-Ahmed, L. Weber, and V. Bhavaraju, "Microgrids: Architectures, Controls, Protection, and Demonstration," (in English), *Electric Power Components and Systems,* vol. 43, no. 12, p. 1453, 2015

[4] X. S. Zhou, L. Y. Yin, and Y. J. Ma, "An Overview of Micro-Grid," (in English), *Applied Mechanics and Materials,* vol. 552, pp. 99-102, Jun 2014

[5] J. M. Guerrero, J. C. Vasquez, J. Matas, L. G. de Vicuna, and M. Castilla, "Hierarchical Control of Droop-Controlled AC and DC Microgrids—A General Approach Toward Standardization," *IEEE Transactions on Industrial Electronics,* vol. 58, no. 1, pp. 158-172, 2011, doi: 10.1109/tie.2010.2066534.

[6] A. Kumar and M. L. Azad, "CHALLENGES IN RECENT MICROGRID SYSTEMS: A REVIEW," (in English), *International Journal of Advances in Engineering & Technology,* vol. 8, no. 2, pp. 203-210, Apr 2015

[7] D. Petreus, R. Etz, T. Patarau, and C. Orian, "MICROGRID CONCEPT BASED ON DISTRIBUTED RENEWABLE GENERATORS FOR A GREENHOUSE," (in English), *Acta Technica Napocensis,* vol. 56, no. 2, pp. 31-36, 2015

[8] T. Caldognetto, P. Tenti, and D. I. Brandao, "Fully-dispatchable microgrid: Architecture, implementation and experimental validation," in *2017 IEEE 26th International Symposium on Industrial Electronics (ISIE)*, 19-21 June 2017 2017, pp. 93-98, doi: 10.1109/ISIE.2017.8001229.

[9] D. Kumar, F. Zare, and A. Ghosh, "DC Microgrid Technology: System Architectures, AC Grid Interfaces, Grounding Schemes, Power Quality, Communication Networks, Applications, and Standardizations Aspects," *IEEE Access,* vol. 5, pp. 12230-12256, 2017, doi: 10.1109/ACCESS.2017.2705914.

[10] M. S. Ortmann *et al.*, "Architecture, components and operation of an experimental hybrid ac/dc smart microgrid," in *2017 IEEE 8th International Symposium on Power Electronics for Distributed Generation Systems (PEDG)*, 17-20 April 2017 2017, pp. 1-8, doi: 10.1109/PEDG.2017.7972564.

[11] A. Hirsch, Y. Parag, J. J. R. Guerrero, and s. E. reviews, "Microgrids: A review of technologies, key drivers, and outstanding issues," vol. 90, pp. 402-411, 2018.

[12] A. Mehrizi-Sani and R. Iravani, "Potential-Function Based Control of a Microgrid in Islanded and Grid-Connected Modes," *IEEE Transactions on Power Systems,* vol. 25, no. 4, pp. 1883-1891, 2010, doi: 10.1109/TPWRS.2010.2045773.

[13] R. Majumder, B. Chaudhuri, A. Ghosh, R. Majumder, G. Ledwich, and F. Zare, "Improvement of Stability and Load Sharing in an Autonomous Microgrid Using Supplementary Droop Control Loop," *IEEE Transactions on Power Systems,* vol. 25, no. 2, pp. 796-808, 2010, doi: 10.1109/TPWRS.2009.2032049.

[14] T. L. Vandoorn, B. Renders, L. Degroote, B. Meersman, and L. Vandevelde, "Active Load Control in Islanded Microgrids Based on the Grid Voltage," *IEEE Transactions on Smart Grid,* vol. 2, no. 1, pp. 139-151, 2011, doi: 10.1109/TSG.2010.2090911.

[15] M. Ahmed, L. Meegahapola, A. Vahidnia, and M. Datta, "Stability and Control Aspects of Microgrid Architectures–A Comprehensive Review," *IEEE Access,* vol. 8, pp. 144730-144766, 2020, doi: 10.1109/ACCESS.2020.3014977.

[16] R. An, Z. Liu, J. Liu, and B. Liu, "A Comprehensive Solution to Decentralized Coordinative Control of Distributed Generations in Islanded Microgrid Based on Dual-Frequency-Droop," *IEEE Transactions on Power Electronics,* vol. 37, no. 3, pp. 3583-3598, 2022, doi: 10.1109/TPEL.2021.3115522.

[17] H. V. S. Dhawan and A. Tamrakar, "Standalone Microgrid: A Sustainable Option for Energy Handling," in *2022 International Conference for Advancement in Technology (ICONAT)*, 21-22 Jan. 2022 2022, pp. 1-4, doi: 10.1109/ICONAT53423.2022.9725965.

[18] S. Baudoin, I. Vechiu, and H. Camblong, "A review of voltage and frequency control strategies for islanded microgrid," in *2012 16th International Conference on System Theory, Control and Computing (ICSTCC)*, 12-14 Oct. 2012 2012, pp. 1-5.

[19] J. M. Guerrero, J. C. Vasquez, J. Matas, L. G. d. Vicuna, and M. Castilla, "Hierarchical Control of Droop-Controlled AC and DC Microgrids—A General Approach Toward Standardization," *IEEE Transactions on Industrial Electronics,* vol. 58, no. 1, pp. 158-172, 2011, doi: 10.1109/TIE.2010.2066534.

[20] M. Begum, L. Li, and J. Zhu, "Distributed control techniques for autonomous AC Microgrid-A brief review," in *2017 IEEE Region 10 Humanitarian Technology Conference (R10-HTC)*, 21-23 Dec. 2017 2017, pp. 357-362, doi: 10.1109/R10-HTC.2017.8288974.

[21] A. Bidram and A. Davoudi, "Hierarchical Structure of Microgrids Control System," *IEEE Transactions on Smart Grid,* vol. 3, no. 4, pp. 1963-1976, 2012, doi: 10.1109/tsg.2012.2197425.

[22] J. Hu, Y. Shan, K. W. Cheng, and S. Islam, "Overview of Power Converter Control in Microgrids Challenges, Advances, and Future Trends," *IEEE Transactions on Power Electronics,* pp. 1-1, 2022, doi: 10.1109/TPEL.2022.3159828.

[23] M. Adibi and J. V. d. Woude, "Secondary Frequency Control of Microgrids: An Online Reinforcement Learning Approach," *IEEE Transactions on Automatic Control,* pp. 1-1, 2022, doi: 10.1109/TAC.2022.3162550.

[24] S. Choudhury, "Review of energy storage system technologies integration to microgrid: Types, control strategies, issues, and future prospects," *Journal of Energy Storage,* vol. 48, p. 103966, 2022.

[25] M. H. Saeed, W. Fangzong, B. A. Kalwar, and S. Iqbal, "A Review on Microgrids' Challenges & Perspectives," *IEEE Access,* vol. 9, pp. 166502-166517, 2021, doi: 10.1109/ACCESS.2021.3135083.

[26] N. Salehi, H. Martínez-García, G. Velasco-Quesada, and J. M. Guerrero, "A Comprehensive Review of Control Strategies and Optimization Methods for Individual and Community Microgrids," *IEEE Access,* vol. 10, pp. 15935-15955, 2022, doi: 10.1109/ACCESS.2022.3142810.

[27] S. Marzal, R. Salas, R. González-Medina, G. Garcerá, E. J. R. Figueres, and S. E. Reviews, "Current challenges and future trends in the field of communication architectures for microgrids," vol. 82, pp. 3610-3622, 2018.

[28] F. Martin-Martínez, A. Sánchez-Miralles, M. J. R. Rivier, and s. e. reviews, "A literature review of Microgrids: A functional layer based classification," vol. 62, pp. 1133-1153, 2016.

[29] A. Aluko, R. Musumpuka, and D. Dorrell, "Cyberattack-Resilient Secondary Frequency Control Scheme for Stand-Alone Microgrids," *IEEE Transactions on Industrial Electronics,* pp. 1-1, 2022, doi: 10.1109/TIE.2022.3159965.
[30] B. Nadai Nascimento *et al.*, "Centralised secondary control for islanded microgrids," *IET Renewable Power Generation,* vol. 14, no. 9, pp. 1502-1511, 2020, doi: 10.1049/iet-rpg.2019.0731.
[31] L. Yan, M. Sheikholeslami, W. Gong, M. Shahidehpour, and Z. Li, "Architecture, Control, and Implementation of Networked Microgrids for Future Distribution Systems," *Journal of Modern Power Systems and Clean Energy,* vol. 10, no. 2, pp. 286-299, 2022, doi: 10.35833/MPCE.2021.000669.
[32] K. T. Tan, X. Y. Peng, P. L. So, Y. C. Chu, and M. Z. Q. Chen, "Centralized Control for Parallel Operation of Distributed Generation Inverters in Microgrids," *IEEE Transactions on Smart Grid,* vol. 3, no. 4, pp. 1977-1987, 2012, doi: 10.1109/TSG.2012.2205952.
[33] P. N. Vovos, A. E. Kiprakis, A. R. Wallace, and G. P. Harrison, "Centralized and Distributed Voltage Control: Impact on Distributed Generation Penetration," *IEEE Transactions on Power Systems,* vol. 22, no. 1, pp. 476-483, 2007.
[34] A. Hirsch, Y. Parag, and J. Guerrero, "Microgrids: A review of technologies, key drivers, and outstanding issues," *Renewable and Sustainable Energy Reviews,* vol. 90, pp. 402-411, 2018/07/01/ 2018, doi: https://doi.org/10.1016/j.rser.2018.03.040.
[35] M. Yazdanian and A. Mehrizi-Sani, "Distributed Control Techniques in Microgrids," *IEEE Transactions on Smart Grid,* vol. 5, no. 6, pp. 2901-2909, 2014, doi: 10.1109/TSG.2014.2337838.
[36] E. Espina, J. Llanos, C. Burgos-Mellado, R. Cárdenas-Dobson, M. Martínez-Gómez, and D. Sáez, "Distributed Control Strategies for Microgrids: An Overview," *IEEE Access,* vol. 8, pp. 193412-193448, 2020, doi: 10.1109/ACCESS.2020.3032378.
[37] J. M. Guerrero, J. Matas, L. G. d. Vicuna, M. Castilla, and J. Miret, "Decentralized Control for Parallel Operation of Distributed Generation Inverters Using Resistive Output Impedance," *IEEE Transactions on Industrial Electronics,* vol. 54, no. 2, pp. 994-1004, 2007, doi: 10.1109/TIE.2007.892621.
[38] M. S. Golsorkhi and D. D. C. Lu, "A Control Method for Inverter-Based Islanded Microgrids Based on V-I Droop Characteristics," *IEEE Transactions on Power Delivery,* vol. 30, no. 3, pp. 1196-1204, 2015, doi: 10.1109/TPWRD.2014.2357471.
[39] C. Ahumada, R. Cárdenas, D. Sáez, and J. M. Guerrero, "Secondary Control Strategies for Frequency Restoration in Islanded Microgrids With Consideration of Communication Delays," *IEEE Transactions on Smart Grid,* vol. 7, no. 3, pp. 1430-1441, 2016, doi: 10.1109/TSG.2015.2461190.
[40] B. Ning, Q. L. Han, and L. Ding, "Distributed Finite-Time Secondary Frequency and Voltage Control for Islanded Microgrids With Communication Delays and Switching Topologies," *IEEE Transactions on Cybernetics,* pp. 1-12, 2020, doi: 10.1109/TCYB.2020.3003690.
[41] J. W. Simpson-Porco, "On Stability of Distributed-Averaging Proportional-Integral Frequency Control in Power Systems," *IEEE Control Systems Letters,* vol. 5, no. 2, pp. 677-682, 2021, doi: 10.1109/LCSYS.2020.3004024.
[42] X. Wu, C. Shen, and R. Iravani, "A Distributed, Cooperative Frequency and Voltage Control for Microgrids," *IEEE Transactions on Smart Grid,* vol. 9, no. 4, pp. 2764-2776, 2018, doi: 10.1109/tsg.2016.2619486.
[43] M. Begum, M. Abuhilaleh, L. Li, and J. Zhu, "Distributed secondary voltage regulation for autonomous microgrid," in *2017 20th International Conference on Electrical Machines and Systems (ICEMS)*, 2017: IEEE, pp. 1-6.
[44] Y. Khayat *et al.*, "Decentralized Optimal Frequency Control in Autonomous Microgrids," *IEEE Transactions on Power Systems,* vol. 34, no. 3, pp. 2345-2353, 2019.
[45] Y. C. C. Wong, C. S. Lim, A. Cruden, M. D. Rotaru, and P. K. Ray, "A Consensus-Based Adaptive Virtual Output Impedance Control Scheme for Reactive Power Sharing in Radial Microgrids," *IEEE Transactions on Industry Applications,* vol. 57, no. 1, pp. 784-794, 2021, doi: 10.1109/TIA.2020.3031884.
[46] Q. Li, F. Chen, M. Chen, J. M. Guerrero, and D. Abbott, "Agent-Based Decentralized Control Method for Islanded Microgrids," *IEEE Transactions on Smart Grid,* vol. 7, no. 2, pp. 637-649, 2016.
[47] S. Hou, Z. Fan, L. Fang, and J. Chen, "Accurate Reactive Power Sharing for Microgrid Using Distributed Adaptive Virtual Impedance," in *2020 IEEE 29th International Symposium on Industrial Electronics (ISIE)*, 17-19 June 2020 2020, pp. 624-629, doi: 10.1109/ISIE45063.2020.9152493.
[48] M. J. H. Moghaddam, M. Bigdeli, and M. R. Miveh, "A Review of the Primary-Control Techniques for the Islanded Microgrids/Pregled primarnih krmilnih tehnik za otocne mikromreze," (in English), *Elektrotehniski Vestnik,* vol. 82, no. 4, pp. 169-175, 2015
[49] U. B. Tayab, M. A. B. Roslan, L. J. Hwai, and M. Kashif, "A review of droop control techniques for microgrid," *Renewable and Sustainable Energy Reviews,* vol. 76, pp. 717-727, 2017.
[50] T. L. Vandoorn, J. D. M. De Kooning, B. Meersman, and L. Vandevelde, "Review of primary control strategies for islanded microgrids with power-electronic interfaces," *Renewable and Sustainable Energy Reviews,* vol. 19, pp. 613-628, 2013/03/01/ 2013, doi: https://doi.org/10.1016/j.rser.2012.11.062.
[51] H. Han, X. Hou, J. Yang, J. Wu, M. Su, and J. M. Guerrero, "Review of Power Sharing Control Strategies for Islanding Operation of AC Microgrids," *IEEE Transactions on Smart Grid,* vol. 7, no. 1, pp. 200-215, 2016, doi: 10.1109/tsg.2015.2434849.
[52] C. Natesan, S. Ajithan, S. Mani, and P. Kandhasamy, "Applicability of Droop Regulation Technique in Microgrid - A Survey," *Engineering Journal,* vol. 18, no. 3, pp. 23-36, 2014, doi: 10.4186/ej.2014.18.3.23.
[53] N. F. Avila and C. C. Chu, "Distributed Pinning Droop Control in Isolated AC Microgrids," *IEEE Transactions on Industry Applications,* vol. 53, no. 4, pp. 3237-3249, 2017, doi: 10.1109/TIA.2017.2691298.
[54] J. Hu, J. Zhu, D. G. Dorrell, and J. M. Guerrero, "Virtual Flux Droop Method—A New Control Strategy of Inverters in Microgrids," *IEEE Transactions on Power Electronics,* vol. 29, no. 9, pp. 4704-4711, 2014, doi: 10.1109/tpel.2013.2286159.
[55] L. Mingxuan *et al.*, "A power decoupling control strategy for droop controlled inverters and virtual synchronous generators," in *2016 IEEE 8th International Power Electronics and Motion Control Conference (IPEMC-ECCE Asia)*, 22-26 May 2016 2016, pp. 1713-1719, doi: 10.1109/IPEMC.2016.7512552.
[56] R. Moslemi, J. Mohammadpour, and A. Mesbahi, "A modified droop control for reactive power sharing in large microgrids with meshed topology," in *2016 American Control Conference (ACC)*, 6-8 July 2016 2016, pp. 6779-6784, doi: 10.1109/ACC.2016.7526739.
[57] Z. Shuai, D. He, J. Wang, Z. J. Shen, J. Fang, and C. Tu, "Robust droop control of DC distribution networks," *IET Renewable Power Generation,* vol. 10, no. 6, pp. 807-814, 2016, doi: 10.1049/iet-rpg.2015.0455.
[58] Z. Shuai, S. Mo, J. Wang, Z. J. Shen, W. Tian, and Y. Feng, "Droop control method for load share and voltage regulation in high-voltage microgrids," *Journal of Modern Power Systems and Clean Energy,* vol. 4, no. 1, pp. 76-86, 2016, doi: 10.1007/s40565-015-0176-1.
[59] J. Su, "An Integrated Control Strategy Adopting Droop Control with Virtual Inductance in Microgrid," *Engineering,* vol. 05, no. 01, pp. 44-49, 2013, doi: 10.4236/eng.2013.51B008.

[60] A. Tah and D. Das, "An Enhanced Droop Control Method for Accurate Load Sharing and Voltage Improvement of Isolated and Interconnected DC Microgrids," *IEEE Transactions on Sustainable Energy,* vol. 7, no. 3, pp. 1194-1204, 2016, doi: 10.1109/tste.2016.2535264.
[61] Q.-C. Zhong, "Robust Droop Controller for Accurate Proportional Load Sharing Among Inverters Operated in Parallel," *IEEE Transactions on Industrial Electronics,* vol. 60, no. 4, pp. 1281-1290, 2013, doi: 10.1109/tie.2011.2146221.
[62] Q.-C. Zhong and Y. Zeng, "Universal Droop Control of Inverters With Different Types of Output Impedance," *IEEE Access,* vol. 4, pp. 702-712, 2016, doi: 10.1109/access.2016.2526616.
[63] A. A. K. Arani, G. B. Gharehpetian, and M. Abedi, "Decentralised primary and secondary control strategies for islanded microgrids considering energy storage systems characteristics," *IET Generation, Transmission & Distribution,* vol. 13, no. 14, pp. 2986-2992, 2019.
[64] X. Jin, H. Wang, W. Zhou, and M. Zhang, "Distributed Cooperative Secondary Control With Vitual Impedance for Islanded Microgrid," in *2021 International Conference on Advanced Electrical Equipment and Reliable Operation (AEERO)*, 15-17 Oct. 2021 2021, pp. 1-6, doi: 10.1109/AEERO52475.2021.9708117.
[65] M. A. Joordens and M. Jamshidi, "Consensus control for a system of underwater swarm robots," *IEEE Systems Journal,* vol. 4, no. 1, pp. 65-73, 2010.
[66] Y. Li and C. Tan, "A survey of the consensus for multi-agent systems," *Systems Science & Control Engineering,* vol. 7, no. 1, pp. 468-482, 2019.
[67] M. Park, S. Lee, J. Son, O. Kwon, and E. Cha, "Leader—following consensus control for networked multi-teleoperator systems with interval time-varying communication delays," *Chinese Physics B,* vol. 22, no. 7, p. 070506, 2013.
[68] Q. Chengming, D. Jun, and J. Ming, "Consensus based speed control strategies for multi-agent car with state predictor," in *2013 IEEE 11th International Conference on Electronic Measurement & Instruments*, 2013, vol. 2: IEEE, pp. 536-541.
[69] R. Olfati-Saber, J. A. Fax, and R. M. Murray, "Consensus and cooperation in networked multi-agent systems," *Proceedings of the IEEE,* vol. 95, no. 1, pp. 215-233, 2007.
[70] W. Zhang, J. Zeng, Z. Yan, S. Wei, J. Zhang, and Z. Yang, "Consensus control of multiple AUVs recovery system under switching topologies and time delays," *Ieee Access,* vol. 7, pp. 119965-119980, 2019.
[71] T. Morstyn, B. Hredzak, and V. G. Agelidis, "Distributed Cooperative Control of Microgrid Storage," *IEEE Transactions on Power Systems,* vol. 30, no. 5, pp. 2780-2789, 2015, doi: 10.1109/TPWRS.2014.2363874.
[72] J. W. Simpson-Porco, Q. Shafiee, F. Dörfler, J. C. Vasquez, J. M. Guerrero, and F. Bullo, "Secondary Frequency and Voltage Control of Islanded Microgrids via Distributed Averaging," *IEEE Transactions on Industrial Electronics,* vol. 62, no. 11, pp. 7025-7038, 2015, doi: 10.1109/TIE.2015.2436879.
[73] M. Chen, D. Zhou, and F. Blaabjerg, "Modelling, implementation, and assessment of virtual synchronous generator in power systems," *Journal of Modern Power Systems and Clean Energy,* vol. 8, no. 3, pp. 399-411, 2020.
[74] X. Wan, X. Ding, H. Hu, and Y. Yu, "An enhanced second-order-consensus-based distributed secondary frequency controller of virtual synchronous generators for isolated AC microgrids," *Energy Reports,* vol. 7, pp. 5228-5238, 2021.
[75] W. Yan, W. Gao, T. Gao, D. W. Gao, S. Yan, and J. Wang, "Distributed cooperative control of virtual synchronous generator based microgrid," in *2017 IEEE International Conference on Electro Information Technology (EIT)*, 2017: IEEE, pp. 506-511.
[76] S. Zheng, K. Liao, J. Yang, and Z. He, "Droop-based consensus control scheme for economic dispatch in islanded microgrids," *IET Generation, Transmission & Distribution,* vol. 14, no. 20, pp. 4529-4538, 2020.
[77] Q. Li, D. W. Gao, H. Zhang, Z. Wu, and F.-Y. Wang, "Consensus-based distributed economic dispatch control method in power systems," *IEEE transactions on smart grid,* vol. 10, no. 1, pp. 941-954, 2017.
[78] M. Begum, L. Li, and J. Zhu, "Distributed Secondary Control of Energy Storage Units for SoC balancing in AC Microgrid," in *2020 IEEE Power & Energy Society Innovative Smart Grid Technologies Conference (ISGT)*, 17-20 Feb. 2020 2020, pp. 1-5.
[79] J. Hu and A. Lanzon, "Distributed finite-time consensus control for heterogeneous battery energy storage systems in droop-controlled microgrids," *IEEE Transactions on smart grid,* vol. 10, no. 5, pp. 4751-4761, 2018.
[80] J. Khazaei and Z. Miao, "Consensus control for energy storage systems," *IEEE Transactions on Smart Grid,* vol. 9, no. 4, pp. 3009-3017, 2016.
[81] J. W. Simpson-Porco, F. Dörfler, and F. Bullo, "Synchronization and power sharing for droop-controlled inverters in islanded microgrids," *Automatica,* vol. 49, no. 9, pp. 2603-2611, 2013/09/01/ 2013, doi: https://doi.org/10.1016/j.automatica.2013.05.018.
[82] D. He, D. Shi, and R. Sharma, "Consensus-based distributed cooperative control for microgrid voltage regulation and reactive power sharing," in *IEEE PES Innovative Smart Grid Technologies Conference Europe*, 2015, vol. 2015-January, January ed., doi: 10.1109/ISGTEurope.2014.7028803. [Online].
[83] L. Wu, A. Lei, and X. Hao, "Voltage and reactive power control of microgrids based on distributed consensus algorithm," in *2017 29th Chinese Control And Decision Conference (CCDC)*, 28-30 May 2017 2017, pp. 1403-1408, doi: 10.1109/CCDC.2017.7978737.
[84] M. Andreasson, H. Sandberg, D. V. Dimarogonas, and K. H. Johansson, "Distributed integral action: Stability analysis and frequency control of power systems," in *2012 IEEE 51st IEEE Conference on Decision and Control (CDC)*, 10-13 Dec. 2012 2012, pp. 2077-2083, doi: 10.1109/CDC.2012.6426463.
[85] L. Zhao *et al.*, "A distributed control framework for microgrid with renewables and energy storage systems," in *2017 IEEE Green Energy and Smart Systems Conference (IGESSC)*, 2017: IEEE, pp. 1-5.
[86] S. Bayhan and H. Abu-Rub, "Model predictive droop control of distributed generation inverters in islanded AC microgrid," in *2017 11th IEEE International Conference on Compatibility, Power Electronics and Power Engineering (CPE-POWERENG)*, 4-6 April 2017 2017, pp. 247-252, doi: 10.1109/CPE.2017.7915177.
[87] T.-T. Nguyen, H.-J. Yoo, and H.-M. Kim, "Application of Model Predictive Control to BESS for Microgrid Control," *Energies,* vol. 8, no. 8, pp. 8798-8813, 2015, doi: 10.3390/en8088798.
[88] M. Aminu and K. Solomon, "A Review of Control Strategies for Microgrids," *Advances in Research,* vol. 7, no. 3, pp. 1-9, 2016, doi: 10.9734/air/2016/25722.
[89] O. Palizban and K. Kauhaniemi, "Hierarchical control structure in microgrids with distributed generation: Island and grid-connected mode," *Renewable and Sustainable Energy Reviews,* vol. 44, pp. 797-813, 2015.
[90] S. W. Lin and C. C. Chu, "Distributed Optimal Consensus-Based Secondary Frequency and Voltage Control of Isolated AC Microgrids," in *2021 IEEE 2nd International Conference on Smart Technologies for Power, Energy and Control (STPEC)*, 19-22 Dec. 2021 2021, pp. 1-6, doi: 10.1109/STPEC52385.2021.9718617.
[91] F. Chen, M. Chen, Q. Li, K. Meng, J. M. Guerrero, and D. Abbott, "Multiagent-Based Reactive Power Sharing and Control Model for Islanded Microgrids," *IEEE Transactions on Sustainable Energy,* vol. 7, no. 3, pp. 1232-1244, 2016, doi: 10.1109/TSTE.2016.2539213.
[92] Z. Yu, Q. Ai, J. Gong, and L. Piao, "A Novel Secondary Control for Microgrid Based on Synergetic Control of Multi-Agent System," (in English), *Energies,* vol. 9, no. 4, p. 243, 2016

[93] A. Bidram, A. Davoudi, F. L. Lewis, and J. M. Guerrero, "Distributed Cooperative Secondary Control of Microgrids Using Feedback Linearization," *IEEE Transactions on Power Systems,* vol. 28, no. 3, pp. 3462-3470, 2013, doi: 10.1109/tpwrs.2013.2247071.

[94] Q. Shafiee, C. Stefanovic, T. Dragicevic, P. Popovski, J. C. Vasquez, and J. M. Guerrero, "Robust Networked Control Scheme for Distributed Secondary Control of Islanded Microgrids," *IEEE Transactions on Industrial Electronics,* vol. 61, no. 10, pp. 5363-5374, 2014, doi: 10.1109/tie.2013.2293711.

[95] R. Fu, Y. Wu, H. Wang, and J. Xie, "A Distributed Control Strategy for Frequency Regulation in Smart Grids Based on the Consensus Protocol," *Energies,* vol. 8, no. 8, pp. 7930-7944, 2015, doi: 10.3390/en8087930.

[96] F. Guo, C. Wen, J. Mao, and Y. D. Song, "Distributed Secondary Voltage and Frequency Restoration Control of Droop-Controlled Inverter-Based Microgrids," *IEEE Transactions on Industrial Electronics,* vol. 62, no. 7, pp. 4355-4364, 2015, doi: 10.1109/TIE.2014.2379211.

[97] Z. Lü, C. Su, Z. Wu, X. Dou, and H. Li, "Distributed Secondary Control Strategy and Its Communication Topology Optimization for Islanded Microgrid," *Diangong Jishu Xuebao/Transactions of China Electrotechnical Society,* Article vol. 32, no. 6, pp. 209-219, 2017.

[98] J. W. Simpson-Porco, Q. Shafiee, F. Dorfler, J. C. Vasquez, J. M. Guerrero, and F. Bullo, "Secondary Frequency and Voltage Control of Islanded Microgrids via Distributed Averaging," *IEEE Transactions on Industrial Electronics,* vol. 62, no. 11, pp. 7025-7038, 2015, doi: 10.1109/tie.2015.2436879.

[99] N. Mahdian Dehkordi, N. Sadati, and M. Hamzeh, "Distributed Robust Finite-Time Secondary Voltage and Frequency Control of Islanded Microgrids," *IEEE Transactions on Power Systems,* pp. 1-1, 2016, doi: 10.1109/tpwrs.2016.2634085.

[100] Y. Zhao, Z. Duan, G. Wen, and Y. Zhang, "Distributed finite-time tracking control for multi-agent systems: An observer-based approach," *Systems & Control Letters,* vol. 62, no. 1, pp. 22-28, 2013, doi: 10.1016/j.sysconle.2012.10.012.

[101] R. Halvgaard, L. Vandenberghe, N. K. Poulsen, H. Madsen, and J. B. Jorgensen, "Distributed Model Predictive Control for Smart Energy Systems," *IEEE Transactions on Smart Grid,* vol. 7, no. 3, pp. 1675-1682, 2016, doi: 10.1109/tsg.2016.2526077.

[102] G. Lou, W. Gu, Y. Xu, M. Cheng, and W. Liu, "Distributed MPC-Based Secondary Voltage Control Scheme for Autonomous Droop-Controlled Microgrids," *IEEE Transactions on Sustainable Energy,* vol. 8, no. 2, pp. 792-804, 2017, doi: 10.1109/tste.2016.2620283.

[103] A. Mesbah, "Stochastic Model Predictive Control: An Overview and Perspectives for Future Research," *IEEE Control Systems,* vol. 36, no. 6, pp. 30-44, 2016, doi: 10.1109/mcs.2016.2602087.

[104] N. B. D. Nadai, A. C. Z. d. Souza, J. G. C. Costa, C. A. M. Pinheiro, and F. M. Portelinha, "A secondary control based on fuzzy logic to frequency and voltage adjustments in islanded microgrids scenarios," in *2017 IEEE Manchester PowerTech*, 18-22 June 2017 2017, pp. 1-6, doi: 10.1109/PTC.2017.7981212.

[105] M. S. Golsorkhi, M. Savaghebi, D. D.-C. Lu, J. M. Guerrero, and J. C. Vasquez, "A GPS-Based Control Framework for Accurate Current Sharing and Power Quality Improvement in Microgrids," *IEEE Transactions on Power Electronics,* vol. 32, no. 7, pp. 5675-5687, 2017, doi: 10.1109/tpel.2016.2606549.

[106] T. Qian, Y. Liu, W. Zhang, W. Tang, and M. Shahidehpour, "Event-triggered updating method in centralized and distributed secondary controls for islanded microgrid restoration," *IEEE Transactions on Smart Grid,* vol. 11, no. 2, pp. 1387-1395, 2019.

[107] A. G. Tsikalakis and N. D. Hatziargyriou, "Centralized control for optimizing microgrids operation," in *2011 IEEE Power and Energy Society General Meeting*, 24-29 July 2011 2011, pp. 1-8, doi: 10.1109/PES.2011.6039737.

[108] F. Dorfler, J. W. Simpson-Porco, and F. Bullo, "Breaking the Hierarchy: Distributed Control and Economic Optimality in Microgrids," *IEEE Transactions on Control of Network Systems,* vol. 3, no. 3, pp. 241-253, 2016, doi: 10.1109/tcns.2015.2459391.

[109] C. T. Lee, C. C. Chu, and P. T. Cheng, "A new droop control method for the autonomous operation of distributed energy resource interface converters," in *2010 IEEE Energy Conversion Congress and Exposition*, 12-16 Sept. 2010 2010, pp. 702-709, doi: 10.1109/ECCE.2010.5617936.

[110] C. T. Lee, C. C. Chu, and P. T. Cheng, "A New Droop Control Method for the Autonomous Operation of Distributed Energy Resource Interface Converters," *IEEE Transactions on Power Electronics,* vol. 28, no. 4, pp. 1980-1993, 2013, doi: 10.1109/TPEL.2012.2205944.

[111] J. M. Guerrero, V. Luis Garcia de, J. Matas, M. Castilla, and J. Miret, "Output impedance design of parallel-connected UPS inverters with wireless load-sharing control," *IEEE Transactions on Industrial Electronics,* vol. 52, no. 4, pp. 1126-1135, 2005, doi: 10.1109/TIE.2005.851634.

[112] E. Rokrok and M. E. H. Golshan, "Adaptive voltage droop scheme for voltage source converters in an islanded multibus microgrid," *IET Generation, Transmission & Distribution,* vol. 4, no. 5, pp. 562-578, 2010, doi: 10.1049/iet-gtd.2009.0146.

[113] R. Majumder, A. Ghosh, G. Ledwich, and F. Zare, "Angle droop versus frequency droop in a voltage source converter based autonomous microgrid," in *2009 IEEE Power & Energy Society General Meeting*, 26-30 July 2009 2009, pp. 1-8, doi: 10.1109/PES.2009.5275987.

[114] A. Tuladhar, H. Jin, T. Unger, and K. Mauch, "Control of parallel inverters in distributed AC power systems with consideration of the line impedance effect," in *Applied Power Electronics Conference and Exposition, 1998. APEC '98. Conference Proceedings 1998., Thirteenth Annual*, 15-19 Feb 1998 1998, vol. 1, pp. 321-328 vol.1, doi: 10.1109/APEC.1998.647710.

[115] A. Bidram, "Distributed cooperative control of AC microgrids," 3639639 Ph.D., The University of Texas at Arlington, Ann Arbor, 2014.

[116] C.-H. Lo and N. Ansari, "Decentralized Controls and Communications for Autonomous Distribution Networks in Smart Grid," *IEEE Transactions on Smart Grid,* vol. 4, no. 1, pp. 66-77, 2013, doi: 10.1109/tsg.2012.2228282.

[117] T. Morstyn, B. Hredzak, and V. G. Agelidis, "Control Strategies for Microgrids With Distributed Energy Storage Systems: An Overview," *IEEE Transactions on Smart Grid,* vol. 9, no. 4, pp. 3652-3666, 2018.

[118] A. Cecilia, J. Carroquino, V. Roda, R. Costa-Castelló, and F. Barreras, "Optimal Energy Management in a Standalone Microgrid, with Photovoltaic Generation, Short-Term Storage, and Hydrogen Production," *Energies,* vol. 13, no. 6, 2020, doi: 10.3390/en13061454.

[119] M. Cao, Q. Xu, X. Qin, and J. Cai, "Battery energy storage sizing based on a model predictive control strategy with operational constraints to smooth the wind power," *International Journal of Electrical Power & Energy Systems,* vol. 115, p. 105471, 2020/02/01/ 2020, doi: https://doi.org/10.1016/j.ijepes.2019.105471.

[120] K. Worthmann, C. M. Kellett, P. Braun, L. Grüne, and S. R. Weller, "Distributed and Decentralized Control of Residential Energy Systems Incorporating Battery Storage," *IEEE Transactions on Smart Grid,* vol. 6, no. 4, pp. 1914-1923, 2015.

[121] A. A. Khodadoost Arani, G. B. Gharehpetian, and M. Abedi, "Review on Energy Storage Systems Control Methods in Microgrids," *International Journal of Electrical Power & Energy Systems,* vol. 107, pp. 745-757, 2019/05/01/ 2019, doi: https://doi.org/10.1016/j.ijepes.2018.12.040.

[122] T. Morstyn, M. Momayyezan, B. Hredzak, and V. G. Agelidis, "Distributed Control for State-of-Charge Balancing Between the Modules of a Reconfigurable Battery Energy Storage System," *IEEE Transactions on Power Electronics,* vol. 31, no. 11, pp. 7986-7995, 2016.
[123] O. Palizban, K. J. R. Kauhaniemi, and S. E. Reviews, "Hierarchical control structure in microgrids with distributed generation: Island and grid-connected mode," vol. 44, pp. 797-813, 2015.
[124] Q. Wu, R. Guan, X. Sun, Y. Wang, and X. Li, "SoC Balancing Strategy for Multiple Energy Storage Units With Different Capacities in Islanded Microgrids Based on Droop Control," *IEEE Journal of Emerging and Selected Topics in Power Electronics,* vol. 6, no. 4, pp. 1932-1941, 2018.
[125] P. Yu, C. Wan, Y. Song, and Y. Jiang, "Distributed Control of Multi-Energy Storage Systems for Voltage Regulation in Distribution Networks: A Back-and-Forth Communication Framework," *IEEE Transactions on Smart Grid,* pp. 1-1, 2020.
[126] B. Yu, J. Guo, C. Zhou, Z. Gan, J. Yu, and F. Lu, "A Review on Microgrid Technology with Distributed Energy," in *2017 International Conference on Smart Grid and Electrical Automation (ICSGEA)*, 27-28 May 2017 2017, pp. 143-146, doi: 10.1109/ICSGEA.2017.152.
[127] Q. Shafiee, J. M. Guerrero, and J. C. Vasquez, "Distributed Secondary Control for Islanded Microgrids—A Novel Approach," *IEEE Transactions on Power Electronics,* vol. 29, no. 2, pp. 1018-1031, 2014.
[128] K. De Brabandere, B. Bolsens, J. Van den Keybus, A. Woyte, J. Driesen, and R. Belmans, "A Voltage and Frequency Droop Control Method for Parallel Inverters," *IEEE Transactions on Power Electronics,* vol. 22, no. 4, pp. 1107-1115, 2007, doi: 10.1109/tpel.2007.900456.
[129] X. Lu, K. Sun, J. Guerrero, and L. Huang, "SoC-based dynamic power sharing method with AC-bus voltage restoration for microgrid applications," in *IECON 2012 - 38th Annual Conference on IEEE Industrial Electronics Society*, 25-28 Oct. 2012 2012, pp. 5677-5682.
[130] X. Sun, Y. Hao, Q. Wu, X. Guo, and B. Wang, "A Multifunctional and Wireless Droop Control for Distributed Energy Storage Units in Islanded AC Microgrid Applications," *IEEE Transactions on Power Electronics,* vol. 32, no. 1, pp. 736-751, 2017, doi: 10.1109/TPEL.2016.2531379.
[131] T. Morstyn, B. Hredzak, and V. G. Agelidis, "Distributed cooperative control of microgrid storage," *IEEE transactions on power systems,* vol. 30, no. 5, pp. 2780-2789, 2014.
[132] T. Morstyn, B. Hredzak, and V. G. Agelidis, "Communication delay robustness for multi-agent state of charge balancing between distributed AC microgrid storage systems," in *2015 IEEE Conference on Control Applications (CCA)*, 21-23 Sept. 2015 2015, pp. 181-186, doi: 10.1109/CCA.2015.7320630.
[133] H. Cai and G. Hu, "Distributed Control Scheme for Package-Level State-of-Charge Balancing of Grid-Connected Battery Energy Storage System," *IEEE Transactions on Industrial Informatics,* vol. 12, no. 5, pp. 1919-1929, 2016.
[134] Y. Xu, Z. Li, J. Zhao, and J. J. I. T. o. S. G. Zhang, "Distributed robust control strategy of grid-connected inverters for energy storage systems' state-of-charge balancing," vol. 9, no. 6, pp. 5907-5917, 2017.
[135] T. L. Nguyen, Q. Tran, R. Caire, C. Gavriluta, and N. Van Hoa, "Agent based distributed control of islanded microgrid — Real-time cyber-physical implementation," in *2017 IEEE PES Innovative Smart Grid Technologies Conference Europe (ISGT-Europe)*, 26-29 Sept. 2017 2017, pp. 1-6.
[136] Y. Wang, K. T. Tan, X. Y. Peng, and P. L. So, "Coordinated Control of Distributed Energy-Storage Systems for Voltage Regulation in Distribution Networks," *IEEE Transactions on Power Delivery,* vol. 31, no. 3, pp. 1132-1141, 2016.
[137] C. Huang, S. Weng, D. Yue, S. Deng, J. Xie, and H. Ge, "Distributed cooperative control of energy storage units in microgrid based on multi-agent consensus method," *Electric Power Systems Research,* vol. 147, pp. 213-223, 2017/06/01/ 2017, doi: https://doi.org/10.1016/j.epsr.2017.02.029.
[138] J. Khazaei and D. H. Nguyen, "Multi-Agent Consensus Design for Heterogeneous Energy Storage Devices With Droop Control in Smart Grids," *IEEE Transactions on Smart Grid,* vol. 10, no. 2, pp. 1395-1404, 2019, doi: 10.1109/TSG.2017.2765241.
[139] J. Hu and A. Lanzon, "Distributed Finite-Time Consensus Control for Heterogeneous Battery Energy Storage Systems in Droop-Controlled Microgrids," *IEEE Transactions on Smart Grid,* vol. 10, no. 5, pp. 4751-4761, 2019.
[140] C. Li, E. A. A. Coelho, T. Dragicevic, J. M. Guerrero, and J. C. Vasquez, "Multiagent-based distributed state of charge balancing control for distributed energy storage units in AC microgrids," *IEEE Transactions on Industry Applications,* vol. 53, no. 3, pp. 2369-2381, 2016.
[141] M. Kriegleder, R. Oung, and R. D'Andrea, "Asynchronous implementation of a distributed average consensus algorithm," in *2013 IEEE/RSJ International Conference on Intelligent Robots and Systems*, 2013: IEEE, pp. 1836-1841.
[142] S. Anand, B. G. Fernandes, and J. Guerrero, "Distributed Control to Ensure Proportional Load Sharing and Improve Voltage Regulation in Low-Voltage DC Microgrids," *IEEE Transactions on Power Electronics,* vol. 28, no. 4, pp. 1900-1913, 2013.
[143] K. Meng, Z. Y. Dong, Z. Xu, and S. R. Weller, "Cooperation-Driven Distributed Model Predictive Control for Energy Storage Systems," *IEEE Transactions on Smart Grid,* vol. 6, no. 6, pp. 2583-2585, 2015, doi: 10.1109/TSG.2015.2449760.
[144] F. Zhang, A. Fu, L. Ding, Q. J. I. J. o. E. P. Wu, and E. Systems, "MPC based control strategy for battery energy storage station in a grid with high photovoltaic power penetration," vol. 115, p. 105448, 2020.
[145] Y. Du, J. Wu, S. Li, C. Long, and S. Onori, "Coordinated Energy Dispatch of Autonomous Microgrids With Distributed MPC Optimization," *IEEE Transactions on Industrial Informatics,* vol. 15, no. 9, pp. 5289-5298, 2019.
[146] U. R. Nair and R. J. I. A. Costa-Castelló, "A model predictive control based energy management scheme for hybrid storage system in islanded microgrids," 2020.
[147] T. Morstyn, B. Hredzak, R. P. Aguilera, and V. G. Agelidis, "Model Predictive Control for Distributed Microgrid Battery Energy Storage Systems," *IEEE Transactions on Control Systems Technology,* vol. 26, no. 3, pp. 1107-1114, 2018.
[148] S. Grillo, M. Marinelli, S. Massucco, and F. Silvestro, "Optimal Management Strategy of a Battery-Based Storage System to Improve Renewable Energy Integration in Distribution Networks," *IEEE Transactions on Smart Grid,* vol. 3, no. 2, pp. 950-958, 2012, doi: 10.1109/TSG.2012.2189984.
[149] T. Morstyn, B. Hredzak, and V. G. J. I. T. o. S. G. Agelidis, "Network topology independent multi-agent dynamic optimal power flow for microgrids with distributed energy storage systems," vol. 9, no. 4, pp. 3419-3429, 2016.
[150] T. Morstyn, B. Hredzak, and V. G. J. I. T. o. S. G. Agelidis, "Control strategies for microgrids with distributed energy storage systems: An overview," vol. 9, no. 4, pp. 3652-3666, 2016.
[151] M. Eskandari, L. Li, and M. H. Moradi, "Improving power sharing in islanded networked microgrids using fuzzy-based consensus control," *Sustainable Energy, Grids and Networks,* vol. 16, pp. 259-269, 2018, doi: 10.1016/j.segan.2018.09.001.
[152] A. Rahman, I. Syed, and M. Ullah, "Small-Signal Stability Criteria in AC Distribution Systems—A Review," *Electronics,* vol. 8, no. 2, 2019, doi: 10.3390/electronics8020216.
[153] M. Amin and M. Molinas, "Small-Signal Stability Assessment of Power Electronics Based Power Systems: A Discussion of Impedance- and Eigenvalue-Based Methods," *IEEE Transactions on Industry Applications,* vol. 53, no. 5, pp. 5014-5030, 2017, doi: 10.1109/tia.2017.2712692.

[154] N. Pogaku, M. Prodanovic, and T. C. Green, "Modeling, analysis and testing of autonomous operation of an inverter-based microgrid," *IEEE Transactions on power electronics,* vol. 22, no. 2, pp. 613-625, 2007.
[155] F. Chen *et al.*, "Cost-Based Droop Schemes for Economic Dispatch in Islanded Microgrids," *IEEE Transactions on Smart Grid,* vol. 8, no. 1, pp. 63-74, 2017, doi: 10.1109/tsg.2016.2581488.
[156] G. Chen and E. Feng, "Distributed secondary control and optimal power sharing in microgrids," *IEEE/CAA Journal of Automatica Sinica,* vol. 2, no. 3, pp. 304-312, 2015, doi: 10.1109/JAS.2015.7152665.
[157] M. Begum, L. Li, J. Zhu, and Z. Li, "State-Space Modeling and Stability Analysis for Microgrids with Distributed Secondary Control," in *2018 IEEE 27th International Symposium on Industrial Electronics (ISIE)*, 13-15 June 2018 2018, pp. 1201-1206, doi: 10.1109/ISIE.2018.8433649.
[158] N. M. Dehkordi, N. Sadati, and M. Hamzeh, "Fully Distributed Cooperative Secondary Frequency and Voltage Control of Islanded Microgrids," *IEEE Transactions on Energy Conversion,* vol. 32, no. 2, pp. 675-685, 2017, doi: 10.1109/TEC.2016.2638858.
[159] F. D. Mohammadi, H. Keshtkar, and A. Feliachi, "State Space Modeling, Analysis and Distributed Secondary Frequency Control of Isolated Microgrids," *IEEE Transactions on Energy Conversion,* pp. 1-1, 2017, doi: 10.1109/tec.2017.2757012.
[160] X. Wu and C. Shen, "Distributed optimal control for stability enhancement of microgrids with multiple distributed generators," *IEEE Transactions on Power Systems,* pp. 1-1, 2017, doi: 10.1109/tpwrs.2017.2651412.
[161] X. Chen, C. Zhang, Q. Huang, and M. Ofori-Oduro, "Small-Signal Modeling and Analysis of Grid-Connected Inverter with Power Differential Droop Control," (in English), *Mathematical Problems in Engineering,* 2016, doi: http://dx.doi.org/10.1155/2016/3965945.
[162] J. Sun, "Impedance-Based Stability Criterion for Grid-Connected Inverters," *IEEE Transactions on Power Electronics,* vol. 26, no. 11, pp. 3075-3078, 2011, doi: 10.1109/TPEL.2011.2136439.
[163] N. M. Dehkordi, N. Sadati, and M. Hamzeh, "Fully Distributed Cooperative Secondary Frequency and Voltage Control of Islanded Microgrids," *IEEE Transactions on Energy Conversion,* vol. PP, no. 99, pp. 1-1, 2016, doi: 10.1109/TEC.2016.2638858.
[164] Y. Guan, J. C. Vasquez, and J. M. Guerrero, "Coordinated Secondary Control for Balanced Discharge Rate of Energy Storage System in Islanded AC Microgrids," *IEEE Transactions on Industry Applications,* vol. 52, no. 6, pp. 5019-5028, 2016, doi: 10.1109/tia.2016.2598724.
[165] X. Wu and C. Shen, "Distributed Optimal Control for Stability Enhancement of Microgrids With Multiple Distributed Generators," *IEEE Transactions on Power Systems,* vol. 32, no. 5, pp. 4045-4059, 2017, doi: 10.1109/tpwrs.2017.2651412.
[166] Y. Guan, L. Meng, C. Li, J. C. Vasquez, and J. M. Guerrero, "A Dynamic Consensus Algorithm to Adjust Virtual Impedance Loops for Discharge Rate Balancing of AC Microgrid Energy Storage Units," *IEEE Transactions on Smart Grid,* vol. 9, no. 5, pp. 4847-4860, 2018, doi: 10.1109/tsg.2017.2672882.
[167] M. Zeraati, M. E. Hamedani Golshan, and J. M. Guerrero, "Distributed Control of Battery Energy Storage Systems for Voltage Regulation in Distribution Networks With High PV Penetration," *IEEE Transactions on Smart Grid,* vol. 9, no. 4, pp. 3582-3593, 2018, doi: 10.1109/tsg.2016.2636217.
[168] Y. Cao and W. Ren, "Distributed Coordinated Tracking With Reduced Interaction via a Variable Structure Approach," *IEEE Transactions on Automatic Control,* vol. 57, no. 1, pp. 33-48, 2012, doi: 10.1109/TAC.2011.2146830.
[169] Y. Cao and W. Ren, "Distributed coordinated tracking with reduced interaction via a variable structure approach," *IEEE Transactions on Automatic Control,* vol. 57, no. 1, pp. 33-48, 2011.
[170] D. Shevitz and B. Paden, "Lyapunov stability theory of nonsmooth systems," *IEEE Transactions on Automatic Control,* vol. 39, no. 9, pp. 1910-1914, 1994.
[171] *The Frequency Operating Standard, 2017*, Australian Energy Market Comission, 2017.[Online].Available:http://www.aemc.gov.au.

Appendices

Appendix A

1) Table A1. Fuzzy Rule Set for Inputs and Outputs.

Rule	Fuzzy Parameters					
	f_{ref}	v_{ref}	D_{fi}	D_{Pi}	D_{Qi}	X_{viri}
1	NOTS	NOTS	NOTS	NOTS	NOTS	NOTS
2	NOTS	VLS	NOTS	VLS	VLS	VLS
3	NOTS	LS	NOTS	LS	LS	LS
4	NOTS	NS	LS	LS	LS	LS
5	VLS	NOTS	NOTS	VLS	VLS	VLS
6	VLS	VLS	NOTS	VLS	VLS	VLS
7	VLS	LS	LS	LS	LS	LS
8	VLS	NS	LS	LS	LS	LS
9	LS	NOTS	NOTS	VLS	VLS	VLS
10	LS	VLS	LS	LS	LS	LS
11	LS	LS	LS	LS	LS	LS
12	LS	NS	LS	LS	LS	LS
13	NS	NOTS	NOTS	VLS	VLS	VLS
14	NS	VLS	VLS	LS	VLS	VLS
15	NS	LS	NS	NS	LS	NS
16	NS	NS	NS	NS	NS	NS

2) Table A2. Specifications for Test System.

Names of Parameters	Symbol	Value	Unit
Microgrid Test Model Parameters			
DC Voltage Value	V_{dc}	700	V
Nominal Voltage	v_{ref}	311	V
Nominal Frequency	f_{ref}	50	Hz
Filter Inductor Resistance	R_f	0.1	Ω
Filter Inductor Inductance	L_f	1.35	mH
Filter Inductor Capacitance	C_f	50	μF
Coupling Inductor Resistance	R_c	0.03	Ω
Coupling Inductor Inductance	L_C	0.1	mH

Voltage Controller Specifications			
Proportional Gain	K_{pv}	0.05	-
Integral Gain	K_{iv}	390	-
Feed Forward Gain	F	0.75	-
Current Controller Specifications			
Proportional Gain	K_{pc}	10.2	-
Integral Gain	K_{ic}	$16e^{3}$	-
Power Controller Specifications			
Frequency Droop Gain	$k_{fi}\ (i = 1,2)$	$3.33e^{-5}$	-
	$k_{fi}\ (i = 3,4)$	$6.67e^{-5}$	-
Voltage Droop Gain	$k_{vi}\ (i = 1,2)$	$2.5e^{-4}$	-
	$k_{vi}\ (i = 3,4)$	$5e^{-4}$	-

3) Table A3. Line Data Used in the Test System.

Line Data					
No.	***R* (Ω)**	***L* (μH)**	**No.**	***R* (Ω)**	***L* (μH)**
Line 1,2	0.23	312	Line 5,6	0.12	312
Line 3,4	0.30	318	Line 7,8	0.21	316

4) Table A4. Load Data Used in the Test System.

Line Data					
No.	***R* (Ω)**	***L* (mH)**	**No.**	***R* (Ω)**	***L* (mH)**
Load 1,2	30	50	Load 5,6	20	12
Load 3,4	40	20	Load 7,8	18	50

$$A_{1invi} = \begin{bmatrix} 0 & k_{fi} & 0 & 0 & 0 & 0 & 0 \\ -V_{bD}\sin(\delta_0) + V_{bQ}\cos(\delta_0) & -\omega_c & -\omega_c I_{od} k_{vi} & 0 & \omega_c I_{od} & \omega_c I_{od} & 0 \\ -V_{bD}\cos(\delta_0) - V_{bQ}\sin(\delta_0) & 0 & -\omega_c + -\omega_c I_{od} k_{vi} & 0 & \omega_c I_{oq} & \omega_c I_{oq} & 0 \\ 0 & 2k_{fi}(D_{fi} - D_{Pi}) & 0 & -2D_{fi} & 0 & 0 & 0 \\ 0 & 0 & -2D_{vi} K_P n_{di} k_{vi} & 0 & 2D_{vi} K_P n_{di} & 2D_{vi} K_P n_{di} & -2D_{vi} K_I \\ 0 & 0 & -2D_{Qi} / Q_{imax} & 0 & 0 & 0 & 0 \\ 0 & 0 & -n_{di} k_{vi} & 0 & -n_{di} & -n_{di} & 0 \end{bmatrix}$$

$$A_{2invi} = \begin{bmatrix} 0 & 0 \\ -\omega_c I_{od} R_{viri} + \omega_c I_{od} X_{viri} - \omega_c V_{od} & -\omega_c I_{od} R_{viri} + \omega_c I_{od} X_{viri} - \omega_c V_{od} \\ -\omega_c I_{oq} R_{viri} - \omega_c I_{od} X_{viri} + \omega_c V_{oq} & -\omega_c I_{od} R_{viri} + \omega_c I_{od} X_{viri} - \omega_c V_{od} \\ 0 & 0 \\ -2D_{vi}K_P\left(n_{di}R_{viri} + n_{qi}X_{viri}\right) & -2D_{vi}K_P\left(n_{qi}R_{viri} - n_{di}X_{viri}\right) \\ 0 & 0 \\ n_{di}R_{viri} + n_{qi}X_{viri} & n_{qi}R_{viri} - n_{di}X_{viri} \end{bmatrix} \cdot \begin{bmatrix} \cos(\delta_0) & -\sin(\delta_0) \\ \sin(\delta_0) & \cos(\delta_0) \end{bmatrix},$$

$$A_{3invi} = \begin{bmatrix} 1 \\ 0 \\ 0 \\ 0 \\ 0 \\ 0 \\ 0 \end{bmatrix}$$

$$A_{4invij} = \begin{bmatrix} 0 & 0 & 0 & 0 & 0 & 0 \\ 0 & 0 & 0 & 0 & 0 & 0 \\ 0 & 0 & 0 & 0 & 0 & 0 \\ \sum_{j\in N_i} k_{fj}\left(D_{Pj} - D_{fj}\right) & \sum_{j\in N_i} D_{vj}K_P n_{dj} k_{vj} & \sum_{j\in N_i} D_{fj} & -\sum_{j\in N_i} D_{vj}K_P n_{dj} & -\sum_{j\in N_i} D_{vj}K_P n_{dj} & \sum_{j\in N_i} D_{vj}K_I \\ 0 & \sum_{j\in N_i} {D_{Qj}}/{Q_{jmax}} & 0 & 0 & 0 & 0 \\ 0 & 0 & 0 & 0 & 0 & 0 \end{bmatrix},$$

$$A_{5invi} = \begin{bmatrix} 0 \\ 0 \\ 0 \\ 0 \\ D_{vi}b_i \\ 0 \\ 0 \end{bmatrix}$$

$$M_{invi} = \begin{bmatrix} 0 & 0 & -k_{vi} & 0 & 1 & 1 & 0 \\ 0 & 0 & 0 & 0 & 0 & 0 & 0 \end{bmatrix}, \qquad N_{invi} = \begin{bmatrix} -R_{viri} & X_{vir} \\ -X_{vir} & -R_{viri} \end{bmatrix},$$

$$C_{invωi} = \begin{bmatrix} 0 & -k_{fi}\, b_i & 0 & 0 & 0 & 0 & 0 \end{bmatrix}$$

$A_{sys} = \begin{bmatrix} A_1 & A_2 \\ A_3 & A_4 \end{bmatrix}$, where $A_1 = A_{1inv} + A_{2inv}((Y_1 - Y_2Y_4^{-1}Y_3)^{-1} - N_{inv})^{-1}\ M_{inv} + A_{3inv}\, C_{invω} + A_{5inv}A_{pcc}K_{Pi}IMP_{pcc}((Y_1 - Y_2Y_4^{-1}Y_3)^{-1} - N_{inv})^{-1}\ M_{inv}$, $A_2 = A_{5inv}K_I$, $A_3 = -A_{pcc}IMP_{pcc}((Y_1 - Y_2Y_4^{-1}Y_3)^{-1} - N_{inv})^{-1}\ M_{inv}$, $A_4 = 0$, where $A_{pcc} = \begin{bmatrix} 0\, M_{pcc}\, 0\, 0 \end{bmatrix}$